# Building a light-sheet microscope to study the early development of the polyclad flatworm *Maritigrella crozieri* (Hyman, 1939)

Johannes Girstmair

Research Department of Genetics, Evolution and Environment
University College London

Submitted for the Degree of Doctor of Philosophy

April 2017

## Declaration of ownership

*I, Johannes Girstmair, confirm that the work presented in this thesis is my own. Where information has been derived from other sources, I confirm that this has been indicated in the thesis.*

## Abstract

The Lophotrochozoa is an evolutionary interesting clade comprising many and mostly marine phyla. Despite their diverse morphology, these animals often have a biphasic life-cycle in form of a free-swimming, ciliated larval stage, the trochophore, and seemingly retained a highly conserved developmental pattern called spiral cleavage. This opens the door for comparative studies to better understand the shared mechanisms of the spiralian developmental program, its deviations and the evolution of lophotrochozoan body plans. Here I studied the early development and larva formation in the polyclad flatworm *Maritigrella crozieri* and compared it with other members of this evolutionarily diverse group of animals.

In order to conduct this research, I first built a light-sheet microscope (OpenSPIM) that would allow me to follow the development of the polyclad embryo from the zygote into the larval stage and to acquire sophisticated 3d-reconstructions of fixed embryonic stages. I then used this and other techniques to characterise in detail the early development of *M. crozieri* and its conserved spiral cleavage pattern. Precise volume measurements of 3d-reconstructed early blastomeres and the investigations of associated cleavage patterns indicate that this polyclad worm may not follow a strictly equal spiral cleavage type, as was previously thought. I investigated the cleavage pattern and fate of micromere 4d, which in *M. crozieri* gives rise to mesoderm and generates bilaterally symmetric embryos at a cellular level. A first cell lineage analysis of this organism involved long-term live imaging recordings and point to a conserved fate of blastomeres that, like in other spiral cleavers,

give rise to ectodermally derived structures, specifically the larva's locomotion system (ciliary band) and a sensory organ at the apical point (apical organ). These findings strengthen the idea that these structures may be homologous to those found in other trochophore larvae.

This work increased the current knowledge of the early development of the polyclad flatworm *M. crozieri*, which facilitates evolutionary comparisons of the development of different flatworms and lophotrochozoans more broadly and can contribute to addressing the homology of marine larvae.

## Statement of impact

With so many marine animal phyla that undergo the highly conserved developmental pattern called spiral cleavage, it is of great interest for evolutionary biologists to study the spiralian developmental program in as many representatives as possible. This allows to understand the fundamentals of the evolutionary mechanism that generated an astonishingly diversity of marine invertebrate species in the largest clade of bilaterally symmetric animals: the Lophotrochozoa.

The polyclad flatworms are a member of the Lophotrochozoa and represent an evolutionary particularly important group, as they are the only platyhelminths that have retained the conserved spiral cleavage mode, while embryogenesis in most other flatworms is highly derived. Additionally, many polyclads have a larval stage. Studying the early spiral cleavage mechanism, embryogenesis and polyclad larvae, contributes not only to a better understanding of the evolution of the Platyhelminthes but is interesting for the relationships of the Lophotrochozoa as a whole.

## Acknowledgements

During my time as a PhD student I was surrounded by extraordinary people, and met many more, who were very much interested in my project and contributed to this work. Foremost I would like to thank my supervisor Max Telford, who immensely cared about me and my wellbeing during my time in his lab and who was a constant source of advice, encouragement and new exciting ideas. I am very grateful that the door to his office was always widely open for me and for his optimism and confidence in me and my work.

I also thank Paola Oliveri for her endless advice, which was very helpful and for introducing me to her microinjection setup. It truly is a sacred place.

I cannot thank enough my dear colleagues from the Telford Lab and the Oliveri Lab for being more than just colleagues. It was so much fun to have you around. Particularly I want to thank Anne Zakrzewski, Helen Robertson, Steven Müller and François Lapraz, who all directly contributed to my work in terms of SEM microscopy, WISH and python programming, OpenSPIM microscopy and in many other ways.

I am very grateful to Kate Rawlinson for her advice, reading suggestions and encouraging words throughout my work.

Furthermore, I thank our lab technician, Fraser Simpson, who made my work a lot easier and who joined forces with me on several collection trips to Florida, where his incredible endurance was very much needed to find all the worms.

I want to thank the people involved in the Neptune Marie Curie Initial Training network for their excellent and demanding work that made my life as a Neptune student so much more

enjoyable and allowed me to constantly gain new experience during our conferences and practical courses.

I also take this opportunity to thank the people at the MPI-CBG in Dresden, in particular Pavel Tomancak, for allowing me to visit his lab and learn everything needed to establish an OpenSPIM in the Telford lab; and Peter Pitrone who helped with the design and got me started in terms of laser alignment and all the little tricks. I am especially grateful to Mette Handberg-Thorsager, who is one of the most dedicated researchers I know. Her interest in the spiral cleaving *Maritigrellas* and the initial trials on microinjecting the embryos were crucial for this project.

I also want to thank Bernhard Egger for introducing me to the world of flatworms and the initial time of my PhD we spend together in London, which was full of advice, discussion about flatworms and FTL.

Finally, I want to thank Anna Czarkwiani for being there for me literally all the time and never getting tired of it. It is impossible to imagine the last three years without this extraordinary person and fantastic young researcher on my side, and without her support. I am the luckiest man to have you in my life. Let's continue the fun!

Meiner Familie in großer Dankbarkeit,

besonders meinen lieben Eltern, Elisabeth und Hermann

## Table of Contents

# Table of Figures

## List of Abbreviations

AcTub – Acetylated tubuline

Amp - Ampicillin

ASW – artificial seawater

a/v – animal/vegetal

d - days

DAPI – 4,6-Diamidino-2-phenylindole

DIC – differential interference contrast

DMSO – dimethyl sulfoxide

EdU – ethynyl-2'-deoxyuridine

EMTB - ensconsin's N-terminal MT-binding domain

EtOH – ethanol

FEP - fluorinated ethylene propylene

FSW – filtered seawater

FASW – filtered artificial seawater

GFP – green fluorescent protein

H2A – histone protein H2A

H2B – histone protein H2B

HB – hybridization buffer

Hi – *Hoploplana inquilina*

h – hours

hpf – hours post fertilization

hpo – hours post oviposition/poking of animals

ISH – *in situ* hybridization

IPTG – Isopropyl β-D-1-thiogalactopyranoside, Isopropyl β-D-thiogalactoside

MABT – maleic acid buffer

mCh - mCherry

MeOH - methanol

Mc – *Maritigrella crozieri*

min - minutes

MT - microtubule

PBS – phosphate buffer saline

PCR – polymerase chain reaction

PFA – paraformaldehyde

q – micromere quartet

Q – macromere quartet

S. D. – standard deviation

SEM – scanning electron microscopy

SD – spiral deformation

SI – spindle inclination

SPIM – single plane illumination microscopy

WMISH – whole mount *in situ* hybridization

# CHAPTER 1 Introduction

## 1.1 History of the phylogeny of the Lophotrochozoa

Since the publication of Darwin's 'On the Origin of Species' in 1859, zoologists have tried to devise an evolutionary classification of the animals in order to systematise the animals and as a framework to understand their evolution. Until the adoption of molecular data in recent years, this tree of the animal phyla was based on an understanding and interpretation of their shared morphology. One source of particularly important information came from comparative studies of the embryology of different phyla, which often revealed striking similarities between groups with otherwise unreconcilably different adult body plans. The impact of embryological studies can perhaps be best illustrated by Kowalevski's discovery of the tadpole larva of sea squirts which revealed their link to the chordates rather than to the molluscs as has been suggested by their adult body plans (Raff and Love, 2004). The chordate affinity of the urochordates has, of course, been confirmed by more recent molecular studies which have revolutionised our understanding of the relationships between animal phyla.

In this thesis I focus on comparisons of embryological events between members of one major clade of animals that was similarly ultimately confirmed by molecular studies - the Lophotrochozoa (Aguinaldo et al., 1997; Dunn et al., 2008; Halanych et al., 1995; Hejnol et al., 2009; Pick et al., 2010) (Figure 1.1). This clade contains approximately a dozen very diverse phyla, which, on considering their adult body plans, are not obviously related. It has long been recognised, however, that different members of the Lophotrochozoa share

striking similarities in the earliest events of their embryology, most notably sharing a mode of early blastomere cleavages called spiral cleavage. Development in members of several lophotrochozaon phyla leads to the elaboration of a larval type named a trochophore after the ring of long locomotory cilia (prototroch) typically observed (troch = wheel).

My specific study concerns the early development of one group of lophotrochozoans - the Platyhelminthes or flatworms. Several orders of flatworms have clear signs of spiral cleavage but in only one order - the polyclads - does development result in a ciliated larva. This polyclad Müller's larva is similar to but by no means identical to the trochophore larvae of other lophotrochozoans. It is one aim of my work to study the embryonic development in the polyclad *Maritigrella crozieri* and see if it is possible to discern specific similarities in the way in which Müller's larvae and trochophore larvae are built to see if there is evidence for them being homologous.

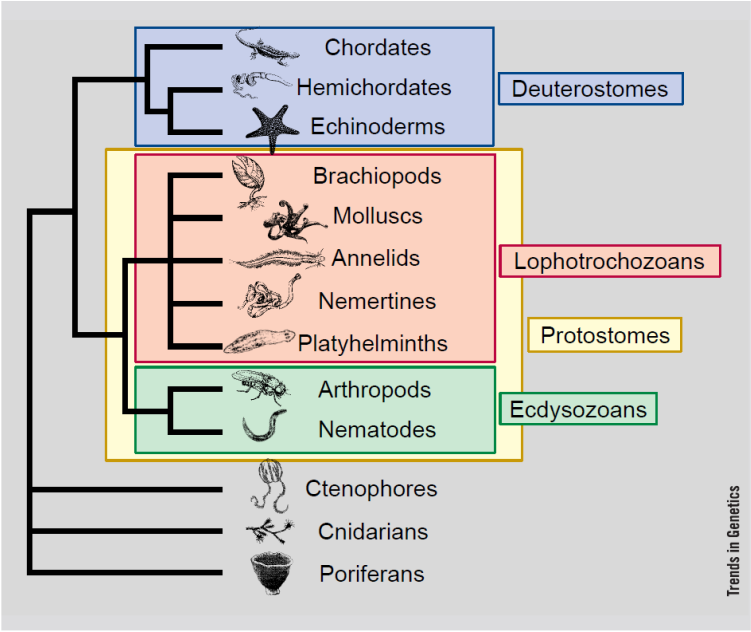


Figure 1.1 - A phylogenetic tree based on 18S rRNA. A consensus of 18S rRNA phylogenies (from Adoutte, Balavoine, Lartillot, & De Rosa (1999)

## 1.2 Phylogeny of the Platyhelminthes

As is true for many phyla, the exact place of the Platyhelminthes within the Lophotrochozoa is still a matter of debate (Laumer et al., 2015a; Struck et al., 2014). But an attempt to resolve the relationships within the phylum Platyhelminthes has recently been advanced by two phylogenetic studies with mostly overlapping consensus using molecular sequencing data (Egger et al., 2015; Laumer et al., 2015b). Previous studies based on morphological characters by Ehlers (1985) and Smith et al. (1986) already suggested a split into the two monophyletic groups within the flatworms: the Catenulida and the Rhabditophora. The latter show various kinds of autapomorphies, for example gland cells called rhabdites which give the group its name (Smith et al., 1982) and two changes to their mitochondrial genetic code (Telford et al., 2000). Also from a classical disposition, it was assumed that the early diverging flatworms Catenulida, Macrostomorpha and Polycladida, all show the plesiomorphic and likely primitive characteristic of endolecithal egg production (yolk incorporated into the embryonic blastomeres) and have at least partially retained spiral cleavage (Martín-Durán and Egger, 2012; Westheide and Rieger, 2013) (although the Catenulida have not been adequately studied yet). The recently published phylogenetic tree of flatworms by Egger et al. (2015) (Figure 1.2) as well as by Laumer et al. (2015) confirmed the relatively early emergence of polyclad flatworms, although the Macrostomorpha emerge before the polyclads. The Lecithoepitheliata are the closest relatives of polyclads suggesting convergent evolution of ectolecithal eggs in the Lecithoepitheliata and Euneoophora (Figure 1.2). While triclads and other euneoophorans show a highly irregular and disperse form of cleavage referred to as blastomere anarchy,

the polyclads have retained a highly conserved form of spiral cleavage pattern during development and are the only flatworms that exhibit a planktotrophic larval stage (Figure 1.2). It is important to point out that if polyclad larvae are homologous to trochophore larvae, then a larval stage must have been lost in some of the other flatworm groups, such as the earlier branching Catenulida (where development needs to be reassessed), Lecithoepitheliata and Macrostomorpha. This point will be discussed in more detail later on.

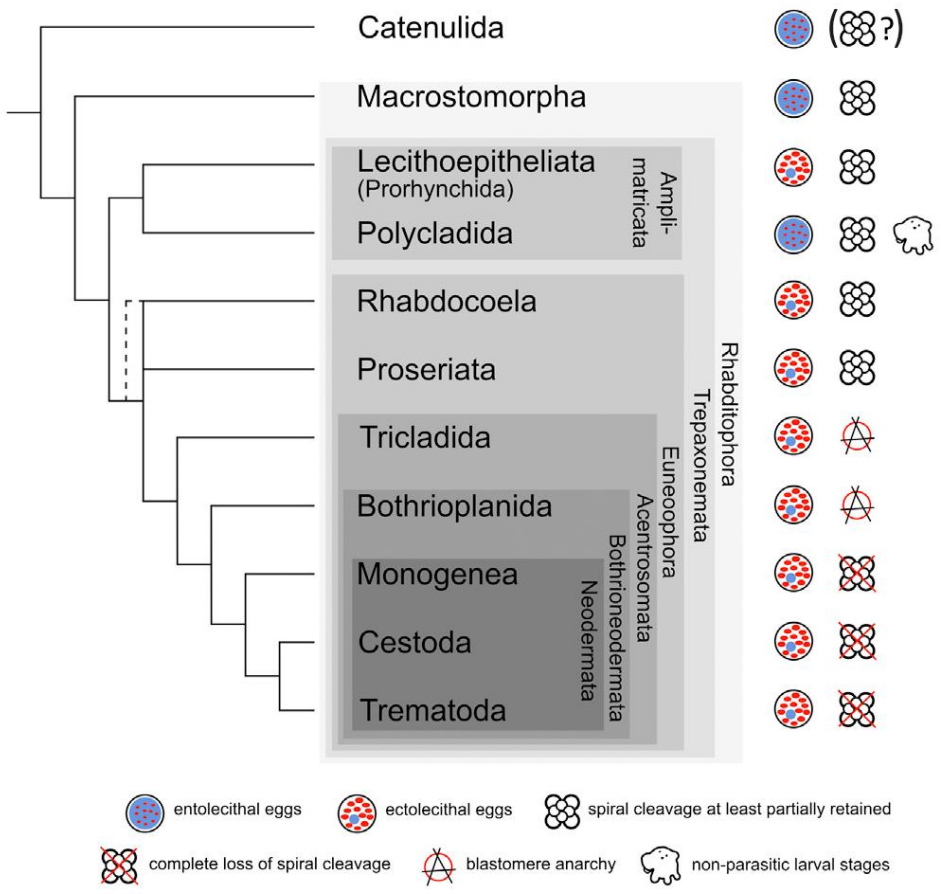


Figure 1.2 - A recently published phylogenetic tree of the flatworms (after Egger et al. 2015) based on transcriptomic and phylogenomic analysis showing the basal position of the Polycladida (with endolecithal eggs) with the Lecithoepitheliata (with ectolecithal eggs) as its sister taxon. A planktotrophic larval stage similar to trochophore larvae found in annelids, molluscs, sipunculids and bryozoans is only present in the Polycladida.

## 1.3 Platyhelminthes: body simplicity with complex life-cycles

The Platyhelminthes, or flatworms, are a highly successful lophotrochozoan phylum with more than 22,500 species found in both marine and freshwater habitats and occasionally on land (Westheide and Rieger, 2013). They are renowned for their remarkable regenerative capabilities. Roughly three-quarters of species described belong to the Neodermata and live a parasitic lifestyle with complex life-cycles that involve highly derived larval types, while the free-living members known as the "Turbellaria" represent a paraphyletic taxon. Platyhelminthes are soft-bodied, non-segmented and acoelomate, meaning that they have no body cavity other than the gut and nearly all flatworms additionally lack a separate mouth and anus. Furthermore, absence of any respiratory or circulatory system is thought to constrain the body size of the free-living flatworms so that most members are ~ 1 mm in size and larger species are dorso-ventrally flattened giving them their name. In many of the free-living flatworms both male and female reproductive organs are present (hermaphrodite) (Figure 1.3). The free-living flatworms can be easily recognised by their characteristic mode of locomotion (gliding along the surface), driven by the coordinated, simultaneous beating of thousands of epidermal cilia (Westheide and Rieger, 2013).

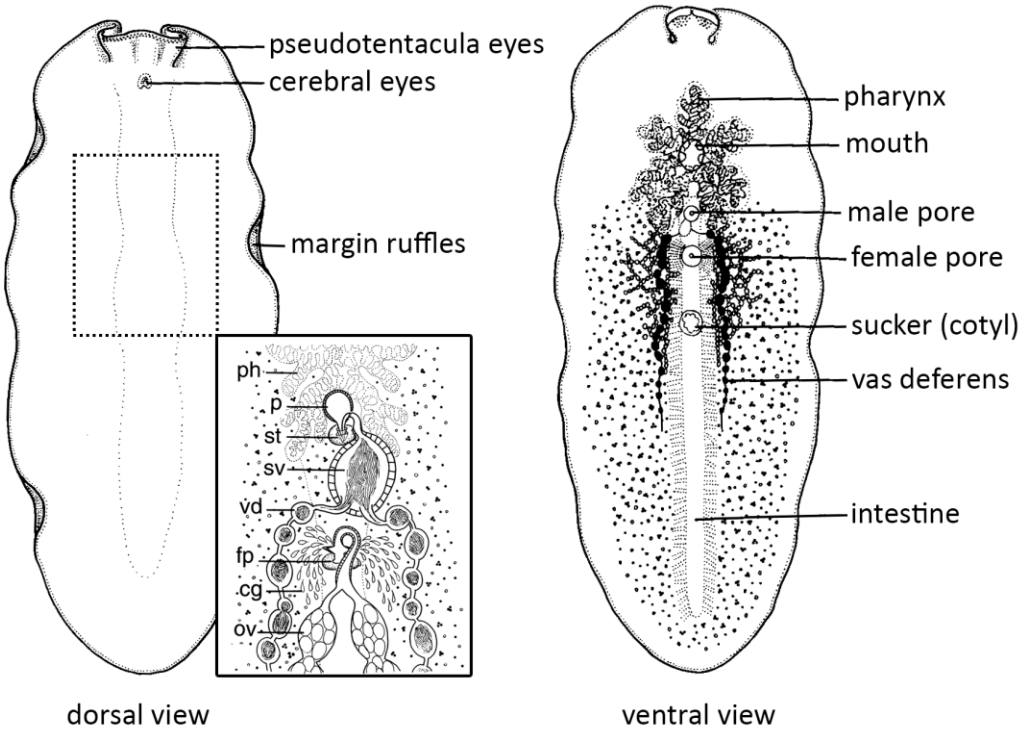


Figure 1.3 - Schematic representation of the cotylean polyclad flatworm *Pseudoceros* from dorsal (left) and ventral (right). **Inset**: Reproductive anatomy; cg = cement glands, fp = female pore, ov = oviducts, p = prostate, ph = pharynx, st = stylet, sv = seminal vesicle, vd = vas deferens, (after Newman & Cannon, 1998). Adult polyclad flatworms are characterised by their leaf-like form and their highly branched intestine (poly = many, clades = branches) and consist of two suborders, the Acotylea and Cotylea, defined by the presence (Cotylea) or absence (Acotylea) of a glando-muscular adhesive organ called a sucker or cotyl.

## 1.4 Summary of spiral cleavage in the Lophotrochozoa

### *1.4.1 Cleavage pattern*

Animals typically start their life as a fertilised egg, the zygote, and develop through one of two recognisable cleavage patterns: radial or spiral cleavage. Polyclad flatworms, like many other lophotrochozoans including annelids, nemerteans, molluscs, undergo spiral cleavage. It begins with two meridional divisions and results in four cells arranged like an equator

around the central animal-vegetal axis and these define four quadrants, A, B, C, D (Figure 1.4).

After the 4-cell stage, a characteristic unequal cleavage takes place that transitions the embryo into an eight-cell stage, consisting of four larger macromeres, positioned vegetally (the first quartet (1Q = 1A, 1B, 1C, 1D)), with four smaller animal micromeres (1q = 1a, 1b, 1c, 1d) sitting above (Figure 1.4). During this division round, the typical spiral deformations (SD) of macromeres are clearly visible in their helical twist towards one side with respect to the animal-vegetal axis. This is best seen if the embryo is viewed from the animal pole (see Figure 1.4, 8-cell stages). The spiral shape taken by all four macromeres can be either clockwise when viewed from the animal pole (dexiotropic) or counterclockwise (laeotropic).

The larger macromeres subsequently undergo further division rounds that sequentially form the second and then the third quartets (tiers) of micromeres. In the course of these divisions the spiral deformations appear in alternating dexiotropic/laeotropic directions up to the fifth cleavage (the rule of alternation). At the same time, the existing micromeres also divide and the embryo, which has so far followed the stereotypic spiral cleavage pattern reaches a 32-cell stage consisting of 8 cells per quadrant (A-D). In each case these are arranged in three distinct quartets (see Figure 1.4).

A fourth and sometimes even a fifth quartet of blastomeres may then be generated by divisions of the macromeres; after this point cleavages become more variable and the divisions less synchronous.

Thanks to the regularity and reproducibility of these early divisions, each cell can be individually recognised across different embryos and indeed across embryos from different phyla. A scheme of blastomere nomenclature, as indicated in Figure 1.4, introduced by (Wilson, 1892) and today mainly based on Conklin's original study on the slipper snail *Crepidula fornicata* (Conklin, 1897) can therefore be reliably used to label each individual blastomere across the spirally cleaving phyla.

### *1.4.2 The presence of animal and vegetal cross-furrow cells*

Intriguingly, in spiral cleaving lophotrochozoans, at the four-cell stage each of the blastomeres represents a quadrant, which typically contribute to the lateral left (A), lateral right (C), anterior ventral (B) and the posterior dorsal (D) body tissues respectively (Henry and Martindale, 1999). A peculiarity often observed at this stage and in emerging macromeres of subsequent embryonic stages is their slight displacement dorsally or vegetally in such a manner that a vegetal and an animal cross-furrow emerges (Figure 1.4, 4-cell stage, vegetal cross-furrow indicated by dashed lines). Cross-furrows yield already the advantage for the observer to readily distinguish A and C blastomeres from B and D blastomeres. The D quadrant is typically observed to be one of the vegetal cross-furrow cells and is of particular interest for three reasons: i) during early development the D quadrant is associated with the future dorsal-ventral axis; ii) it has been shown to function in some species as an embryonic organizer, most notably demonstrated in molluscan embryos (see review by Lambert, 2010) and iii) the D macromere lineage is the sole source of the so-called endomesoderm (giving rise to both endoderm and mesoderm).

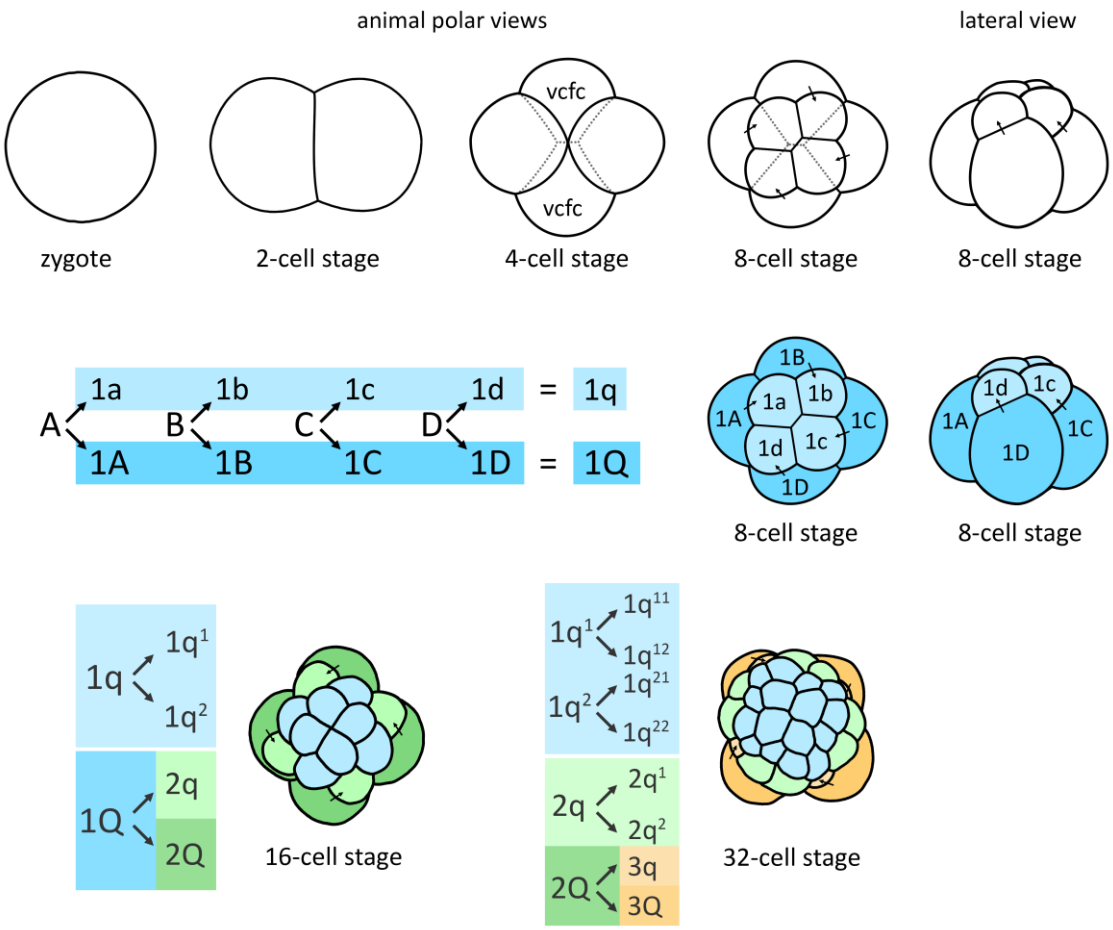


Figure 1.4 - Schematics of the spiral quartet cleavage from zygote to the 32-cell stage. The 4-cell stage consists of two blastomeres, which are positioned more vegetally. These touch each other on the ventral side forming the vegetal cross-furrow (vcfc: B and D). Likewise, there are two animal cross-furrow blastomeres (A and C). The third cleavage is shown as a dexiotropic (clockwise) division as indicated by arrows at the 8-cell stage. The subsequent division of macromeres at the 16-cell stage is shown as laeotropic (counterclockwise) and the 32-cell stage as another dexiotropic division. Q = A, B, C, D; q = a, b, c, d; vcfc = vegetal cross-furrow cell. Four- and eight-cell stages after Kühn (1971) and Robert (1902) respectively.

### *1.4.3 Constancy of blastomere identification and fate*

Because the placement of blastomeres is so similar in the spirally cleaving embryos, individual quartets and their blastomeres can be identified across species. This is of great importance for the comparative study of developmental patterns across Lophotrochozoa. The first detailed comparisons of cell fates of individual blastomeres in lophotrochozoans date back to the late 19th century, in which a striking degree of conservation was revealed (Guralnick, 2002).

The first three quartets of micromeres (1q, 2q, 3q) characteristically give rise to ectodermal structures comprising head (1q), mouth (2q) and most of the trunk (2q), but also form mesoderm, which therefore is referred to as ectomesoderm (2q/3q) (see Figure 1.5). Most endodermal structures derive from the fourth quartet of micromeres and macromeres (4q and 4Q). However, one of the blastomeres of the fourth quartet of micromeres (4q) once again gives rise to endodermal and mesodermal structures (endomesoderm) and is specifically found among the D-quadrant lineage, exemplary in form of a single blastomere 4d (see Lambert (2010) for a minireview and chapter IV for more details). The 4d blastomere, also called mesentoblast, was first described by Wilson in 1892 and became eventually the classic example for a conserved cell fate shared across spirally cleaving lophotrochozoan members.

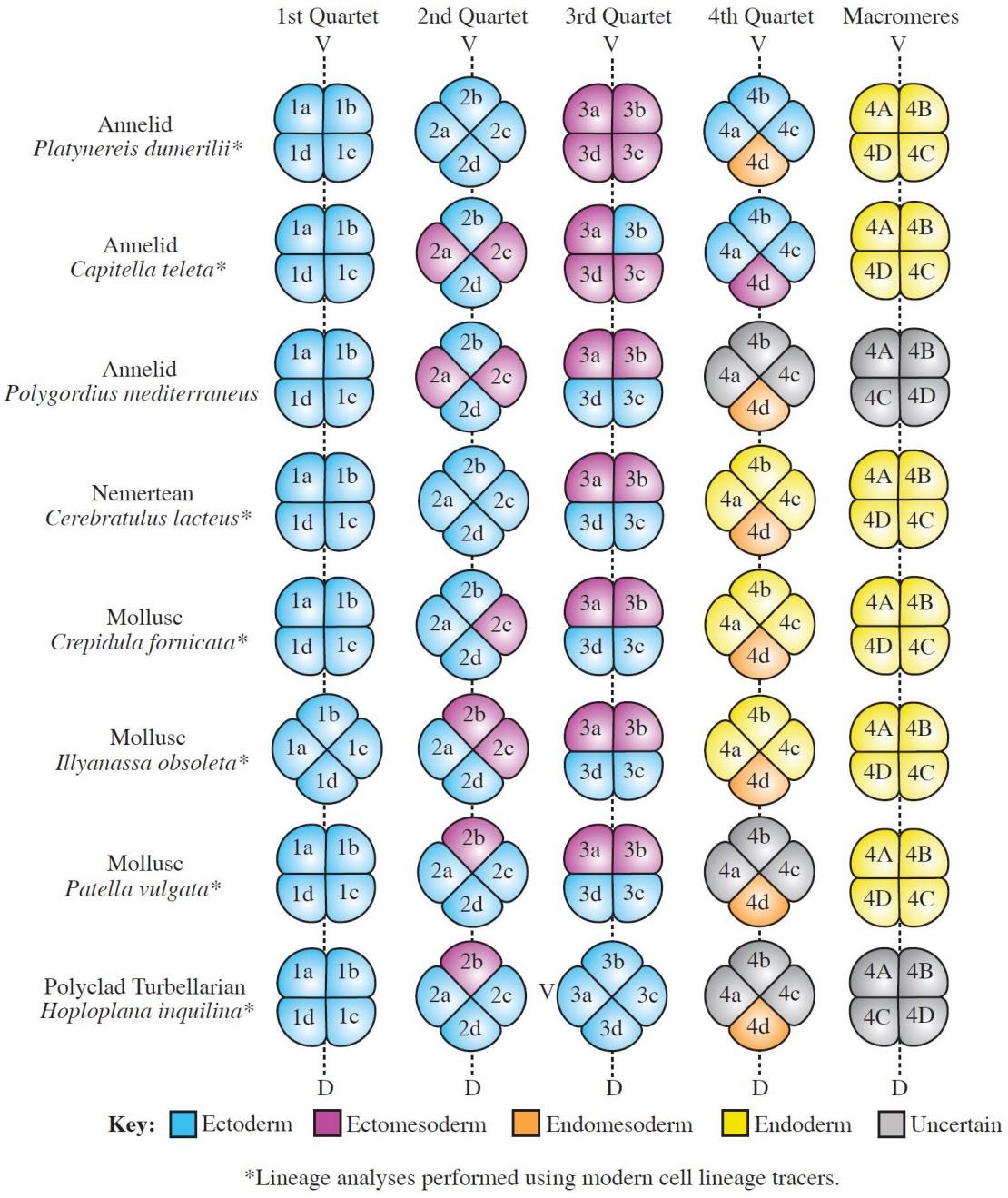


Figure 1.5 - The four quartets of micromeres and the diversity of their cell fates in different members of the Lophotrochozoa from Lyons & Henry (2014) after Henry & Martindale (1999)

### *1.4.4 Equal or unequal spiral cleavage: a way of specifying the D-quadrant*

While the highly conserved spiral early cleavage pattern is widely found in lophotrochozoan embryos, variations exist (Hejnol, 2010). One of the most common ways in which spiral embryos may differ is evident after the first two divisions resulting in a four-cell embryo. At this point spiral cleavage has been categorised into two distinct types, which are thought to represent two ways of specifying the D-quadrant. The first class comprises equal cleavers, whereby 4-cell stage embryos with four indistinguishable blastomeres (A, B, C and D) form. The second class includes all unequal cleavers, in which blastomeres at the 4-cell stage have distinct sizes. In unequal cleavers, the D blastomere, which is usually one of the vegetal cross-furrow cells (vcfc) (Figure 1.1, 4-cell stage) typically is the largest of the four blastomeres (Freeman and Lundelius, 1992; Lambert and Nagy, 2003). The general explanation is that, during their first two cleavages, unequal cleavers differentiate the quadrants by differentially distributing an unknown set of key factors into specific cells. Such a mechanism has been shown for example in the mud snail *Ilyanassa obsoleta* (Render, 1989). The D quadrant is thus specified very early on. In equal spiral cleavers, on the contrary, D-quadrant specification is thought to take place by an inductive interaction, usually between one of the large macromeres and the first quartet of micromeres (for a review see Lyons & Henry (2014)) and therefore the specification of the D quadrant occurs later in development and requires at least five division cycles (Freeman and Lundelius, 1992). The earliest signs of such an inductive specification process have been observed in gastropods around the 24-cell stage (van den Biggelaar and Haszprunar, 1996).

### *1.4.5 The link of a dorsal "organizer" and MAPK activation in the D quadrant of spiral cleavers*

Initially, the spiralian developmental program was seen as a mosaic of determined, self-differentiating cells (Costello, 1945; Wilson, 1904). While this might be partly true, experimental studies on annelids and molluscs have shown that the D quadrant gives rise to a dorsal "organizer", which can determine the fate of adjacent micromeres and is involved in the establishment of the dorsoventral axis (Clement, 1962; Dorresteijn et al., 1987; Henry, 2002; Henry and Martindale, 1987; Render, 1989; Verdonk and Van den Biggelaar, 1983). More recent studies have shown that this organizer activity may be a result of the activation of the MAPK cascade signalling pathway in macromere 3D and might be conserved within the spiralian developmental program (Lambert and Nagy, 2001). This has been investigated so far in ten spiral cleaving animals (six mollusc species (Henry and Perry, 2008; Koop et al., 2007; Lambert and Nagy, 2001; Lambert and Nagy, 2003), 3 annelid species (Amiel et al., 2013; Lambert and Nagy, 2003; Pfeifer et al., 2014)) and one bryozoan species, (Vellutini et al., 2016). In molluscs activation of MAPK in 3D seems to represent the ancestral state. However, in the mud snail *Ilyanassa obsolete*, where a role of the MAPK pathway was first described, the activity was shown to additionally spread to some of the overlying micromeres, which has later been interpreted to be a more derived feature (Lambert, 2009). In the annelid *Hydroides hexagonus* MAPK activity was restricted to micromere 4d and in the bryozoan *Membranipora membranacea* to 3D only. These similarities suggested that a dorsal organiser linked to MAPK activation may be indeed conserved across spiral cleaving animals. More recently however, investigations of the

MAPK cascade in two other annelids (*Capitella sp.* and *Platynereis dumerilii*) showed that the signal is absent during early cleavage and that MAPK might have a different role as shown by its activity in cells around the blastopore during gastrulation (Amiel et al., 2013; Pfeifer et al., 2014). The annelids therefore indicate a high level of variability regarding the link between MAPK activity and a dorsal organizer. More investigations of other spiral cleaving lophotrochozoans will clarify whether this link is conserved or not.

### *1.4.6 The spiral cleavage pattern in Platyhelminthes*

The polyclads are the only flatworms that have retained a highly conserved form of spiral cleavage during early development but a significant deviation that has been observed is the formation of the fourth quartet of micromeres, and the fate of its daughter cells, the yolk-rich and untypically large micromeres 3a-3c, which together with macromeres 4A-4D apparently have a degenerative fate and do not contribute to any embryonic structure (Boyer et al., 1998; Surface, 1907). In the basally branching Macrostomorpha, spirality can be observed only up to the third cleavage (Morris et al., 2004) and in the Lecithoepitheliata to the 20-cell stage (Reisinger and Cichocki, 1974; Westheide and Rieger, 2013). Also in the Proseriata spiral cleavage was described with a typical 8-cell stage of four macromeres and four micromeres that continues at least up to the 12-cell stage and possibly even further (Giesa, 1966). All other Platyhelminthes including the most commonly studied triclads (often called planarians), have a highly modified embryogenesis that cannot be recognised as spiral cleavage. Cell lineage studies in flatworms only exist so far for one polyclad species, *Hoploplana inquilina* (Boyer et al., 1998; Surface, 1907). Preliminarily the fate of spiral quartets during the earliest cleavages have been described in one representative of the

Lecitopeitheliata, *Xenoprorhynchus steinbocki* (Reisinger and Cichocki, 1974). Additionally, in the macrostomorphan flatworm *Macrostomum lignano* the embryonic origins of specialised hull cells have been investigated via a cell lineage study based on 4D microscopy (Willems et al., 2009). These hull cells, which are rich in yolk and start to coat other embryonic blastomeres, do not exist in strictly endolecithal polyclad embryos and represent a significant deviations of the canonical spiral cleavage pattern (Willems et al., 2009), which is highlighted by the fact that they originate from the second quartet of macromeres (2Q), which rules out the possibility of a 3D macromere and then a 4d micromere that classically gives rise to endomesoderm in all other spiral cleaving embryos. However, the fact that the quartet spiral cleavage is found in the earlier branching flatworms, makes it most likely the plesiomorphic cleavage pattern in platyhelminths. Notably, many polyclads have additionally to their spiral cleavage pattern a biphasic life cycle with planktonic larvae that can be compared to the typical lophotrochozoan larva, the trochophore.

### 1.5 The spiralian trochophore larva

The trochophore is the characteristic larval type of lophotrochozoan protostomes and is found in annelids, including sipunculids, molluscs and bryozoans. The larva is equipped with a preoral ciliated band (the prototroch), which separates the anterior region of the larva (the episphere) from the posterior region and is mainly used for locomotion and filter-feeding in the water column (Figure 1.6).

### *1.5.1 Trochophore structures and their origins*

In a typical trochophore the episphere consists of well conserved larval structures derived from the first quartet of micromeres (1q), including apical "sensory" organs and prototrochal cells. The main components of the prototroch originates from specialised founder cells $1q^2$, called trochoblasts (Henry et al., 2007; Nielsen, 2005). While the majority of the primary prototroch is derived from these cells, accessory trochoblasts in form of blastomeres $1q^{12}$ are also often present and contribute to the final prototroch structure. There are other types of ciliated bands which are found in a trochophore larvae from some but not all species. Examples are the metatroch, which is usually associated with the capturing of food particles or a perianal ring, and the terminal telotroch that can provide additional locomotory functions (compare Figure 1.6). Ciliated structures such as the metatroch and telotroch vary significantly among lophotrochozoan larvae and their homology has been questioned (Hejnol et al., 2007; Henry et al., 2007).

### *1.5.2 Apical organs*

The most obvious neural structure of the trochophore is the apical organ (or apical ganglion) which is canonically equipped with long sensory cilia that form an apical tuft. Such apical organs are part of the nervous system and derive from apical rosette cells $1q^{111}$ while other central nervous structures such as the cerebral ganglia in a generalised annelid derive from their sister cells micromeres $1c^{112}$ (right cerebral ganglia) and $1d^{112}$ (Figure 1.6) (Nielsen, 2012a).

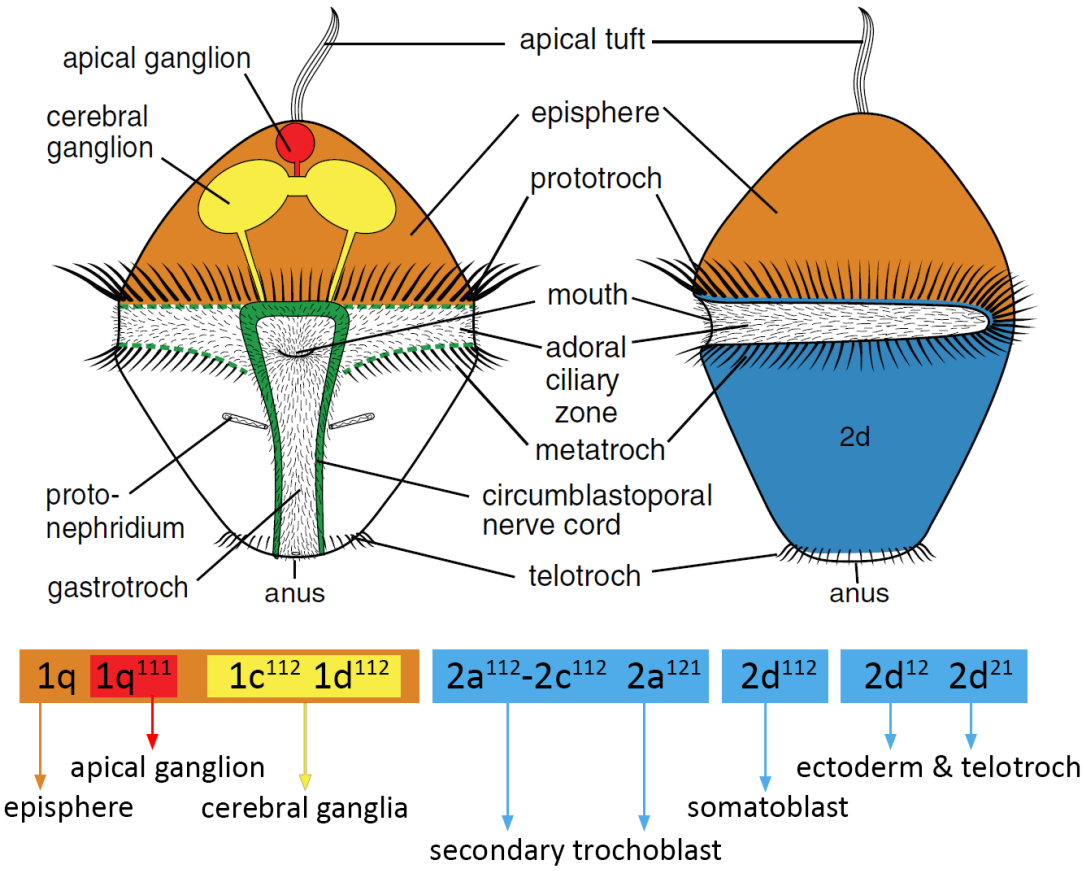


Figure 1.6 - A generalised annelid trochophore larva and contributions of the first and second quartet blastomeres to certain structures (after Nielsen, 2012b)

In most Lophotrochozoa a cell type, commonly found in the apical organ is the large flask-shaped receptor cell with serotonin-like and/or FMRFamide-like immunoreactivity. There are typically four of these flask cells found but sometimes 8-10 cells are present. Other cell types bear long cilia and supplement the apical tuft (Richter et al., 2010) (Figure 1.7). Additionally, peripheral, non-flask shaped cells can be present that surround the flask cells and connect them to the underlying neuropil (Schmidt-Rhaesa et al., 2016) (Figure 1.7). While it is clear that the apical organ serves as a sensory organ, its specific function has

never been fully revealed. Recently it was suggested that apical organs can control larval settlement in molluscs (Hadfield et al., 2000) and annelids (Conzelmann et al., 2013), and could be involved in the coordination of effector organs, such as ciliary fields and musculature. However, it is also known that some larvae without an apical organ can settle and more experimental studies will be needed before an appropriate answer to this interesting question will be found (Schmidt-Rhaesa et al., 2016).

As in polyclad flatworms, ciliated larvae with apical sensory organs are also present in spiral cleaving nemertines (Nielsen, 2012b) and it has been suggested that these nemertean pilidium larvae are homologous to trochophore larvae (see Nielsen (2005) and citations therein).

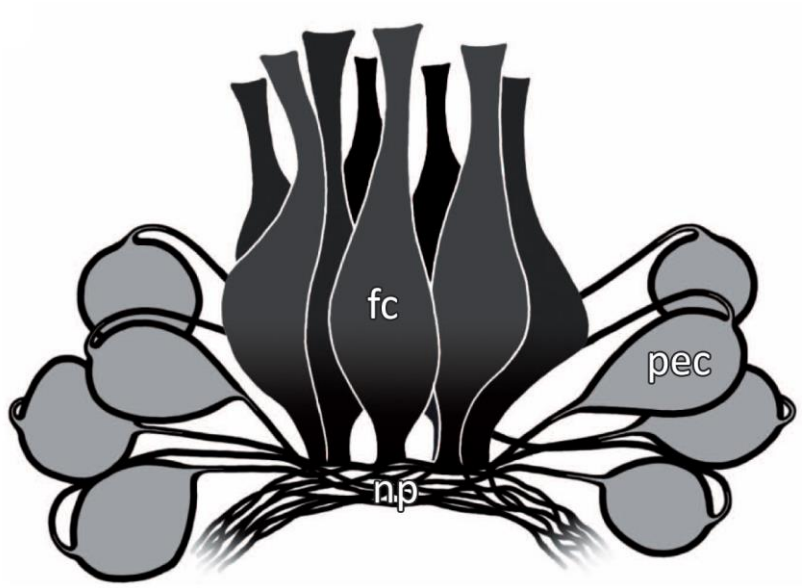


Figure 1.7 - An apical organ from the entoproct *Loxosomella murmanica* with flask-shaped receptor cells (fc) and surrounding peripheral cells (pec) that connect to the neuropil (np). After Richter et al. (2010)

## 1.6 Polyclad flatworms and their larval types

### *1.6.1 Polyclad flatworms*

Adult polyclad flatworms are characterised by their leaf-like form and their highly branched intestine (poly = many, clades = branches) and consist of two suborders, the Acotylea and Cotylea, defined by the presence (Cotylea) or absence (Acotylea) of a glando-muscular adhesive organ called a sucker or cotyl (Figure 1.3). Only 1 mm thick, polyclads can reach relatively large body sizes, typically between 10 to 50 mm in length, and are among the largest of the free-living flatworms. Due to their soft appearance and sometimes beautiful colour patterns the animals are often confused with nudibranch molluscs (Cannon, 2003).

### *1.6.2 Larval types of polyclad flatworms*

In 1850 the first description of several polyclad flatworm larvae characterised by varying numbers of projecting lobes and eyes and their association with an adult animal was published (Müller, 1850). The two most characteristic polyclad larvae are the Müller's larva (Figure 1.9) with (usually) eight projecting lobes and three simple eyes (two cerebral eyes and one epithelial eye) (Figure 1.9, B) and the similar looking four-lobed Goette's larvae (Figure 1.8). A so-called Kato's larva is found in *Pseudoceros reticulata* (Teshirogi et al., 1981; Wang and YU, 2008) with highly reduced lobes and can be interpreted as a transitional stage between larva and juvenile. While the Müller's larva is abundant in both suborders of polyclads (Cotylea and Acotylea) other larval types including Goette's and Kato's larvae together with direct developers are constrained to the Acotylea (Martín-Durán and Egger, 2012). The lobes of the polyclad larvae comprise several rows of ciliary

band cells, which can have distinct numbers depending on the species (Lacalli, 1982) (Figure 1.9, B, C). These cells carry the long cilia and together function as a well-developed locomotory organ, which is also probably used for feeding (Ruppert, 1978). Aside from the number of lobes body shapes can also differ between polyclad larvae. However, all are equipped with an apical sensory organ (previously described as a frontal organ), which bears single long cilia (Figure 1.8) and resembles the apical organs found in other trochophore larvae due to its similar overall structure, and the presence of similar cell-types (Ruppert, 1978).

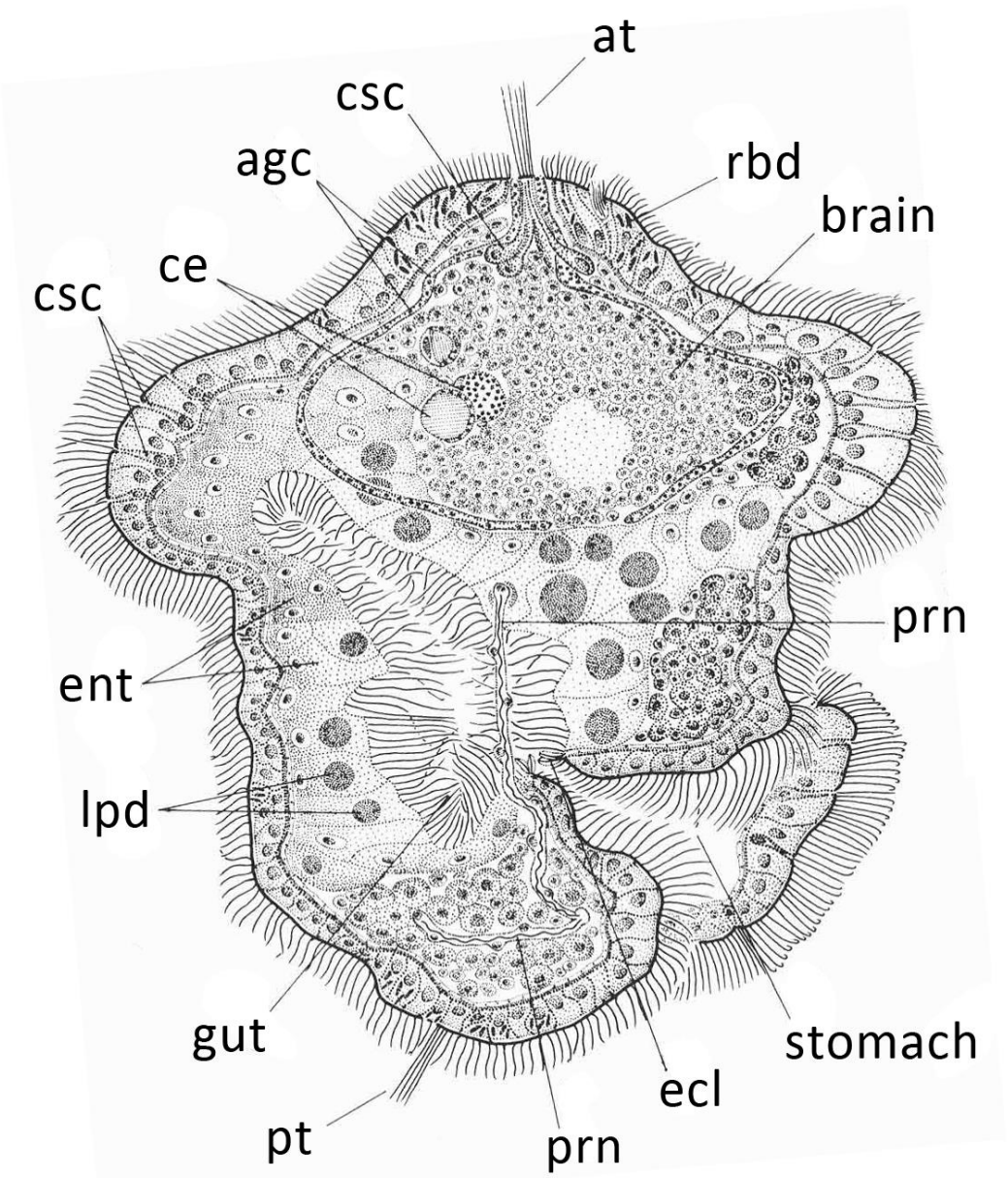


Figure 1.8 - Lateral view of the anatomy of a four-lobed Goette's larva (pelagic stage). The reconstruction is based on serial transverse sections. (at) apical tuft, (agc) apical organ gland cells, (ce) cerebral eyes, (csc) ciliated sensory cell, (ecl) expanded and clubshaped cilia, (ent) entodermal cell, (lpd) lipid droplets, (prn) protonephridium, (pt) posterior tuft, (rbd) rhabdites. After Ruppert 1978.

## 1.7 Larval evolution in polyclad flatworms

The majority of animals are marine organisms and most of them have complex life cycles in the form of at least one larval stage with often completely different body morphologies than their adult stages. This was first discovered during the 19th century, a time when naturalists like Johannes Müller, who also described for the first time the larva of a polyclad flatworm (Müller, 1850), sampled and identified many types of larvae from the plankton. This activity went hand in hand with raising major questions about animal diversity, relationships and origins (Hall and Wake, 1999). For the Lophotrochozoa one fundamental question is still of interest for evolutionary biologists: Whether morphologically similar structures, found in different phyla are homologous or whether they evolved independently.

From the descriptions of the polyclad larvae and the trochophore in the previous sections it becomes clear that both larval types share similar structures such as the apical organ or ciliary bands, which is why the polyclad larva has been previously interpreted as a derived trochophore (Nielsen, 2005). To explore a possible homology of polyclad larvae and the trochophore larva of other lophotrochozoans implies that a primary larva was ancestral in the platyhelminths. The phylogenetic position of Catenulida and Macrostomorpha as earlier branches than the Polycladida mean that a larval stage must have been lost in both these flatworm groups. This is also the case in the sister group of the Polycladida, the Lecithoepitheliata, as well as the Euneoophora and some acotylean Polycladida with direct development. The loss of a biphasic life-cycle in so many flatworm orders has raised some doubts for the existence of a primary larva in the polyclad flatworms (Laumer et al., 2015b)

that can be compared to other trochophore larvae. On the other hand, the complete loss of spiral cleavage in many orders of the Neoophora and its reduced form in the earlier branches of flatworms (see Martin-Duran and Egger, 2012) indicates that flatworms underwent vast evolutionary developmental deviations, while adapting to new environments. It is likely that these evolutionary developmental changes also severely affect the life-cycle or in other words it is perhaps less surprising that the one group of flatworms, in which the spiral cleavage mode has been retained to the highest degree, also retained a biphasic life-cycle with characteristics of other trochophore larvae. The question, however, remains how readily a larval stage can get lost among different orders of flatworms. Intriguingly the Polycladida, which have a Müller's larva in both subgroups, the Cotylea and Acotylea (Ruppert, 1978), demonstrate exactly this case. In some acotylean genera, several types of development can occur. For example, *Hoploplana inquilina* hatches as a Müller's larva, whereas *Hoploplana villosa* is a direct developer (see Martin-Duran and Egger, 2012 and citations therein). Such examples of a complete loss of the larval stage make it, first of all more plausible that a larval stage similar to a Müller's larva is primitive for the Polycladida as a whole (Jägersten, 1972), and secondly demonstrate that a loss of a larva can occur even without reducing or modifying the early spiral cleavage mode, which is also conserved in acotyleans that exhibit direct developing juveniles.

Direct support for putative homology between polyclad Müller's larva and other trochophore-like larvae can be taken from cell-lineage studies, which, in case of the acotylean *H. inquilina,* suggest a close similarity between polyclads and spiral cleaving Lophotrochozoans (Boyer et al., 1998; Surface, 1907). Therefore cell-lineage studies of

larval structures, which are shared across lophotrochozoans, can help to make a strong case for or against a putative homology between polyclad and trochophore-like larvae and is one of the goals we want to achieve in *M. crozieri*.

### 1.8 *Maritigrella crozieri*: a new organism for evo-devo studies

In addition to the acotylean polyclad flatworm *H. inquilina*, in which a Müller's larva is present and which has so far been used for comparative evolutionary studies (Boyer, 1986; Boyer, 1987; Boyer, 1989; Boyer et al., 1996; Boyer et al., 1998; Surface, 1907), the cotylean polyclad flatworm *Maritigrella crozieri* has been recently introduced as a new organism useful for comparisons of development with other lophotrochozoans (Lapraz et al., 2013; Rawlinson, 2010) (Figure 1.9). With its tubular pharynx, marginal tentacles and two cerebral eyespots this polyclad flatworm was placed as a typical euryleptid (Newman et al., 2000). The major advantages of this species are that it can be easily collected in great numbers, due to its specific preference for eating the zooids of the ascidian *Ecteinascidia turbinate* (Herdman), which themselves grow on mangrove roots in plainly visible orange colonies. Maritigrella's stereotypic spiral cleavage pattern can even occur outside the egg-shell in so-called naked embryos making micromanipulations in oocytes and early embryonic stages possible. Its biphasic life cycle results in eight-lobed Müller's larva (Figure 1.9, B and C) and the large mature animals can bear hundreds of eggs. Throughout this work we solely used the polyclad flatworm *Maritigrella crozieri* (Figure 1.9).

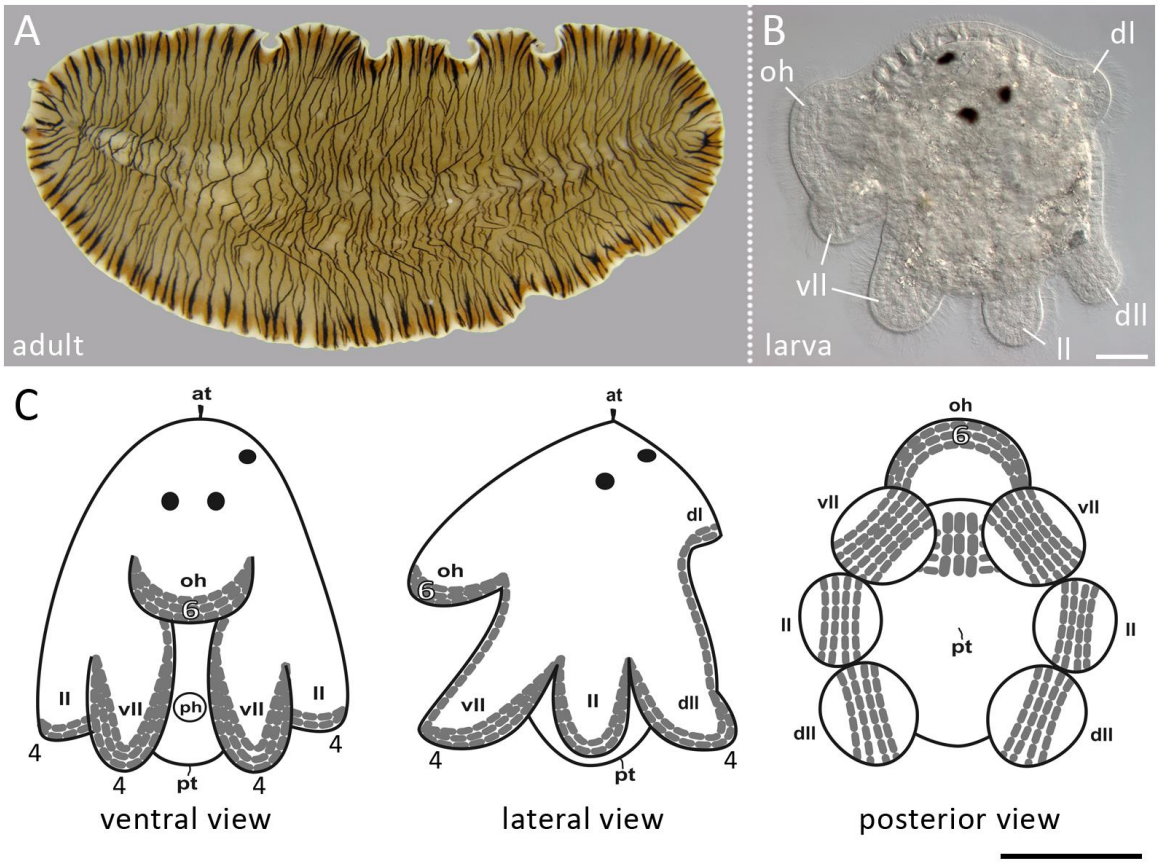


Figure 1.9 - The cotylean polyclad flatworm *Maritigrella crozieri* and its larval stage the Müller's larva. **(A)** Gravid specimen found in the mangroves of the Florida Keys, shown at roughly twice its original size (picture by Fraser Simpson). **(B)** The eight-lobed and three-eyed Müller's larva. **(C)** Schematic drawings of a 1-day-old Müller's larva (from left to right: ventral view, lateral view and posterior view, respectively indicating ciliary band structures in the larva of *Maritigrella crozieri* featuring the ciliary band cells in grey. A broader oral hood that extends over the mouth is opposed by a smaller dorsal lobe (dl). The three paired lateral lobes are referred to as ventro-lateral lobes (vll), lateral lobes (ll) and dorsal lateral lobes (dll). Numbers are related to rows of ciliary band cells. Scale bar of B is 25 µm. Scale bar of C is 100 µm.

### *1.8.1 The Müller's larva of M. crozieri*

The structure of the musculature, nervous system and ciliary band of the Müller's larva from *M. crozieri* (see Figure 1.10) was already previously described in detail (Lapraz et al., 2013; Rawlinson, 2010). In short, the nervous system of *M. crozieri* larvae consists of an apical organ, a brain and several nerve cords beneath the basement membrane (Figure 1.10, A, B). The peripheral nervous system is intra-epithelial and innervates the ciliary band outside of the basement membrane. A lattice of circular and longitudinal muscle fibres cover the overall body wall (Figure 1.10, B) and projections of phalloidin-labelled epidermal cells reveals the ciliary band cells (cbs) (Figure 1.10, inset), which carry the long cilia and are easily recognisable by a slightly elongated shape that narrows significantly between intervals of the projecting lobes.

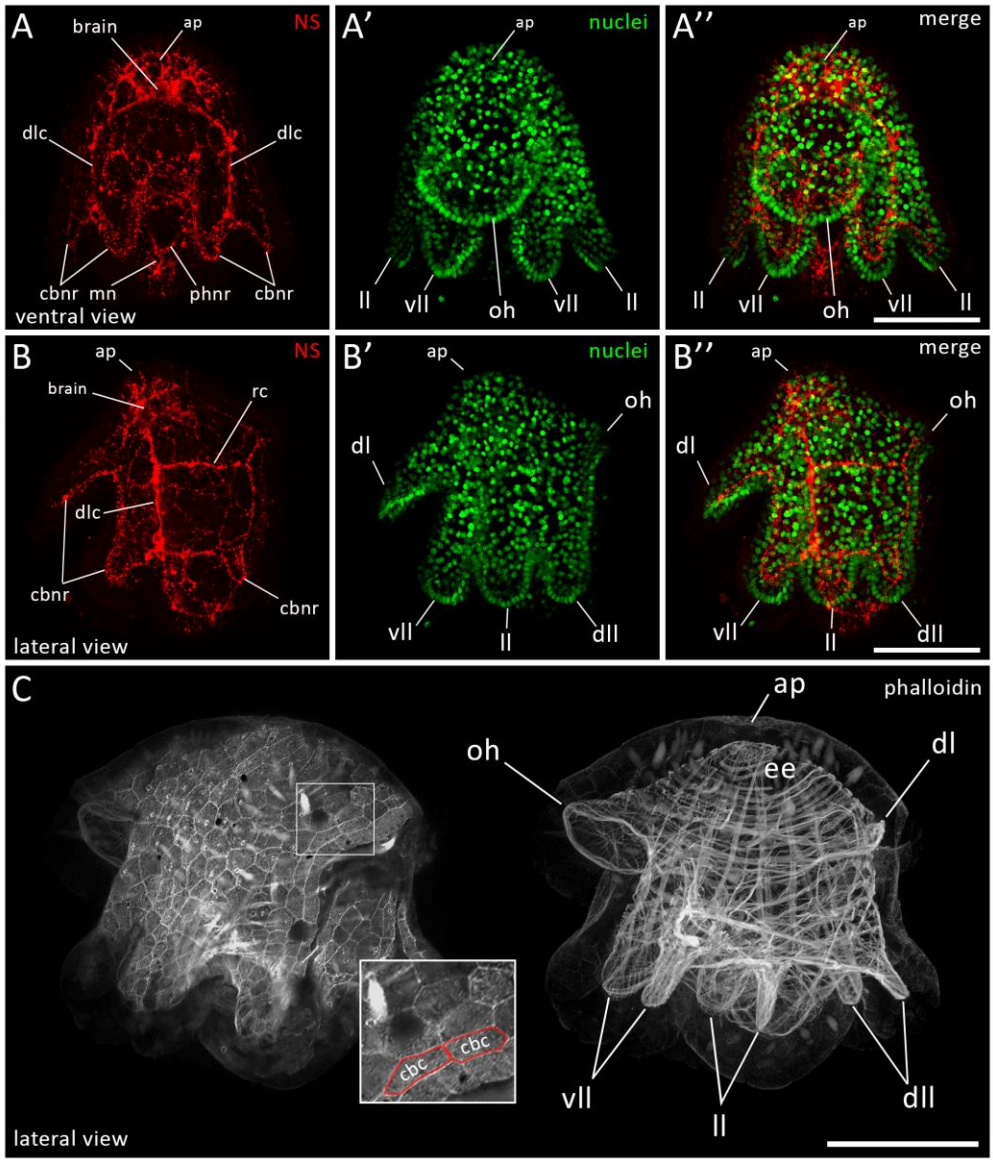


Figure 1.10 - Confocal projection images obtained during this study showing the nervous system (in-house produced neuropeptides in red in combination with the nucleic stain SytoxGreen), epidermis and musculature of the Müller's larva of the polyclad flatworm *Maritigrella crozieri.* **(A)** Frontal view showing the nervous system with arrow indicating area of the cerebral commissure of the neuropile. **(B)** Lateral view of the nervous system with an arrow indicating a dense network of nerves underlying the apical plate. **(C)** Same specimen with phalloidin staining showing the epidermal structures (left) and the underlying musculature (right). Inset shows the specific shape of ciliary band cells highlighted in red. Note the two flask-shaped gland cell and their exit in the top left corner of the inset. (ap) apical plate, (cbc) ciliary band cells, (cbnr) ciliary band ring, (dl) dorsal lobe, (dlc) dorso-lateral connective, (dll) dorsal lateral lobes (ee) epithelial eye, (ll) lateral lobes, (mn) medial nerve, (NS) nervous system, (phnr) pharyngeal nerve ring, (rc) ring connectives, (vll) ventro-lateral lobes. Scale bars are 50 µm

## 1.9 Innovative ways of performing cell lineage studies in polyclad flatworms

Polyclad animals are difficult to maintain in culture and eggs are typically opaque and endolecithal, meaning that they contain yolk, which makes live observations more difficult. The first classical studies of polyclad development have been mostly based on live observations (Girard, 1854; Hallez, 1879; Keferstein, 1868; Lang, 1884; Selenka, 1881; Wilson, 1897), which led to several inconsistencies. Only in 1907 Surface reinvestigated in detail the early embryonic development of *H. inquilina* via careful optical sections (Surface, 1907) which resulted not only into the most comprehensive early developmental study of polyclad flatworms, but also represents the only work, where the cell lineage of a polyclad is followed in detail from the oocyte up to a 100-cell stage. Reconstructing hundreds of embryonic developmental stages is a good deal of work and perhaps explains why nobody after Surface performed a similar cell-lineage study on any other polyclad flatworm.

Modern cell lineage studies are usually based on injecting fluorescent dyes into cells at different stages of the early cleaving embryos. This technique has been used in the last decades on several spiral cleaving lophotrochozoan species to reinvestigate the classical observations in much more detail (see Lyons and Henry, 2014). One example is the cell-lineage study performed on the polyclad flatworm *H. inquilina* (Boyer et al., 1998). One disadvantage of this technique is that the identity of early blastomeres have to be known prior to injections. This can be, however, difficult in spiral developers with equal or equal-like cleavage, where the D quadrant is not immediately obvious due to similar sizes of blastomeres. This is for instance the case in *M. crozieri* and many other polyclad species. Therefore, a high number of embryos need to be microinjected in order to draw satisfying

conclusions, for instance, about the correct origin of initially injected quadrant (A, B, C, D) and so on. For our cell-lineage study in *M. crozieri* we therefore decided to try an original approach. We wanted to develop a microinjections setup, which would allow us to fluorescently tag all the nuclei and combine it with home-built light-sheet microscopy so that nuclei of a single living embryo could be traced over time. This gives us the possibility to follow the fate of early blastomeres simultaneously, while the individual quadrants would reveal themselves by reaching more advanced embryonic stages. The D quadrant, for example, is characterised during spiralian development by asymmetric division timings and for initiating a series of bilaterally symmetric cleavages (Henry, 2014). Therefore light-sheet microscopy represents a major part of this work.

## 1.10 Light-sheet microscopy

Light-sheet illumination for microscopy is an old technology enjoying a dramatic recent renaissance due to introduction of selective plane illumination microscopy (SPIM) (Huisken et al., 2004). The principle of SPIM is to use optics to form a thin sheet of light that passes through the specimen. Unlike a standard microscope in SPIM the objective lens is placed perpendicular to the direction of the light such that the sheet of light illuminates the specimen only at the focal plane of the lens (Figure 1.11).

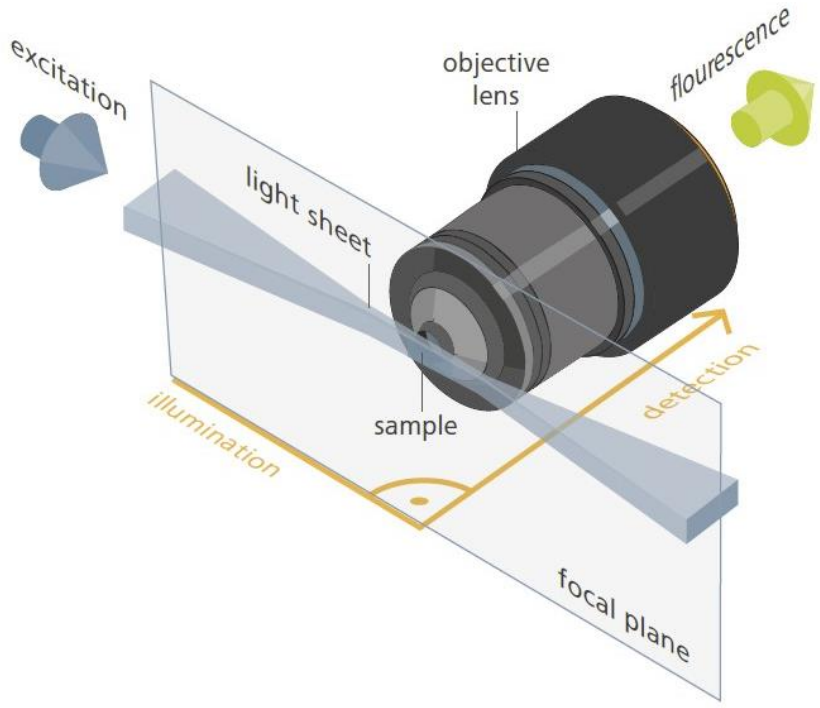


Figure 1.11 - The principle of single plane illumination microscopy (SPIM). A thin laser beam called “light sheet” is formed for instance using a cylindrical lens (not shown) and then gets projected onto a sample perpendicular to the optical axis of the detection lens. While this setup allows the illumination of the entire focal plane the specimen is exposed to a relatively low dose of light (Selchow and Huisken, 2013).

This has two important benefits; it eliminates scattered light from out of focus areas of the specimen providing a natural means of optical sectioning and, because only the imaged area is illuminated, the total amount of light hitting the specimen is orders of magnitude less than in conventional fluorescence microscopy, meaning that photodamage/phototoxicity is enormously reduced and imaging over long periods is possible (Huisken et al., 2004). This latter benefit is of great significance for live imaging. OpenSPIM is an open access light-sheet microscopy design (Pitrone et al., 2013); http://openSPIM.org; see also (Gualda et al., 2013) and Figure 1.12. The OpenSPIM resource gives users step-by-step guidance for building a basic configuration of a SPIM microscope and includes appropriate open source software for image acquisition and processing such as Fiji (http://fiji.sc/Fiji), micromanager (https://www.micro-manager.org/), multiview reconstruction plugins (Preibisch et al., 2010; Schmied et al., 2014) deconvolution (Preibisch et al., 2014) and big data viewer (http://fiji.sc/BigDataViewer). The design can be adapted and upgraded according to the user's specific requirements and budget. We have designed an OpenSPIM microscope capable of dual-sided illumination (a variant of the so-called T-configuration proposed on the OpenSPIM wiki). This technology can be useful for research on organisms such as the polyclad flatworm *M. crozieri* in terms of live-imaging of developing embryos and 3d-reconstructions of both embryos and larva.

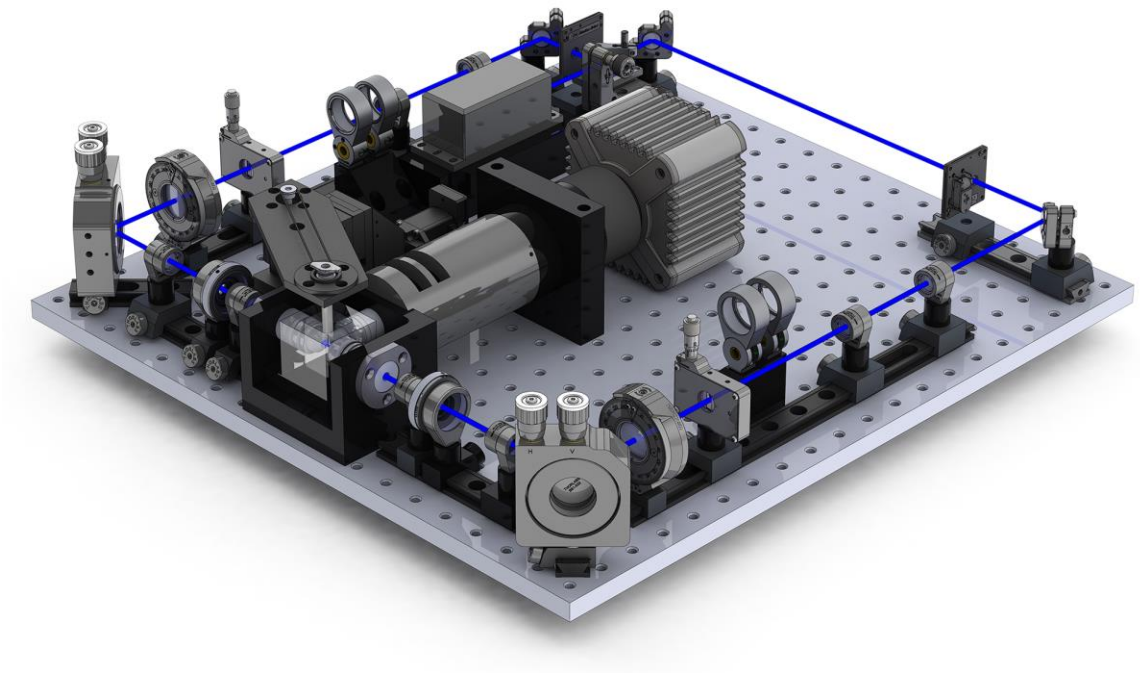

Figure 1.12 - The flexibility of light sheet microscopes such as OpenSPIM allows for different configurations. Here is an example of an OpenSPIM with a double-sided illumination configuration also referred to as a “T-SPIM” (Source: http://openspim.org).

### 1.11 Hypothesis and aims addressed in this thesis

Many members of the Lophotrochozoa have a biphasic life cycle that includes a planktonic larval stage. Despite the morphological diversity, these larvae are usually characterised by at least one band of beating cilia used for locomotion and can therefore be called a trochophore. Additionally, an apical “sensory” organ comprising a tuft of long cilia on the top is often observed among these larvae. One fundamental question is whether these morphologically similar structures, found in larvae of different lophotrochozoan phyla, are homologous or whether they evolved independently. One possible explanation is that a biphasic life cycle including a trochophore-like larva was already present in the last common ancestor of lophotrochozoans. This would imply that the basic body plan of trochophore-like larval stage was fundamentally similar and the shared structures are homologous. During hundreds of millions of years of evolution, the larvae were modified or lost in many lineages.

On the other hand, a very different evolutionary scenario would be that a biphasic life cycle evolved several times in more than one lophotrochozoan lineage by convergent evolution and in such a case complex structures as the ciliary band or apical organ, despite morphological similarities, are not homologous. To better distinguish between these two evolutionary scenarios of homologous versus non-homologous trochophore(-type) larvae, one can study the development of different lophotrochozoans from zygote to their larval stage.

I want to ask specifically whether there is evidence that the ciliated larva of the polyclad flatworms is homologous to the trochophore larvae of molluscs and annelids. While spiral

cleavage clearly points to a developmentally highly conserved beginning in *M. crozieri*, the intriguing question, in terms of homologous larval structures, is how conserved the developmental program has remained throughout the development until the point where a ciliated larva hatches.

The interest in this question is mainly driven by the facts that polyclads represent the only flatworms that i) have a biphasic life cycle with a planktotrophic larval stage, which can be interpreted as a derived trochophore, and ii) show a greatly conserved spiral cleavage mode. Although this has been known for a long time, developmental studies in polyclads are surprisingly scarce and most molecular tools to study the development have not yet been established. I chose the polyclad flatworm *Maritigrella crozieri*, found in the Florida Keys, for a comparative evolutionary study in order to see if it is possible to discern specific similarities in the way in which Müller's larvae and trochophore larvae are built to see if there is evidence for their being homologous.

In order to conduct this research, I first needed to build a microscope that would allow me to follow the development of the polyclad embryo into the larval stage for the longest possible amount of time and to acquire sophisticated 3d-reconstructions of fixed embryonic stages. The building, use and advantages of this microscope are detailed in Chapter III.

The second aim is to take advantage of these newly developed imaging tools together with other established microscopy methods such as scanning electron microscopy and confocal laser imaging, to study in detail the early embryogenesis of *M. crozieri* from zygote up to the point where the bilateral symmetry of the embryo is established (Chapter IV). It will be

interesting to compare the early developmental data of the *M. crozieri* to other polyclad flatworms.

The third major aim is to produce a detailed early cell lineage based on nuclei tracing used to extract information that can be compared to the available data of other polyclad flatworms and also to other lophotrochozoan species. Furthermore, I aim to identify and follow blastomeres, which are known from other spiralian embryos to give rise to apical structures, such as the apical organ, and ciliary bands to determine if their lineage gives rise to similar structures/areas in the developing *Maritigrella crozieri* embryo (Chapter V).

The final aim of this thesis is to treat developing embryos during their third cleavage with agents that specifically inhibit cytoskeletal microtubule and actin polymerization to find out if the spiral cleavage pattern, which is heavily driven on these cytoskeletal components, shows effects similar to those previously described in snails. This can have implications for our basic understanding of the mechanisms of spiral cleavage (Chapter VI).

# CHAPTER 2 Methods

## 2.1 Building a single plane illuminated light-sheet microscope (OpenSPIM)

### *2.1.1 OpenSPIM - Overview*

An OpenSPIM microscope capable of dual-sided illumination (T-configuration) was built on a 600 x 900 x 12.7 mm aluminium breadboard following instructions from the website http://openspim.org/. The principal components of our microscope comprise a multiple wavelength laser system (Stradus VersaLase™ from Laser2000 http://www.laser2000.co.uk/versalase.php) producing two individual wavelengths (λ = 488 and 561 nm); a Zyla 5.5 3 Tap sCMOS camera from Andor (http://www.andor.com/); and a USB 4D-stage from Picard Industries (http://www.picard-industries.com/). The acquisition chamber (designed by Peter Gabriel Pitrone and manufactured by Pieter Fourie Design and Engineering CC; http://www.pfde.co.uk) includes openings for two 10x illumination objectives (Olympus UMPLFLN10xW left and right, N.A. 0.30) and one aperture for a 40x acquisition objective (Olympus; LUMPLFLN40xW, N.A. 0.80). The optical breadboard, rails and rail carriers, optical elements and mirrors were purchased from Thorlabs (http://www.thorlabs.com/), fluorescence clean up and emission filters from AHF (http://www.ahf.de/). The appendix includes a complete list of all purchased parts (see appendix).

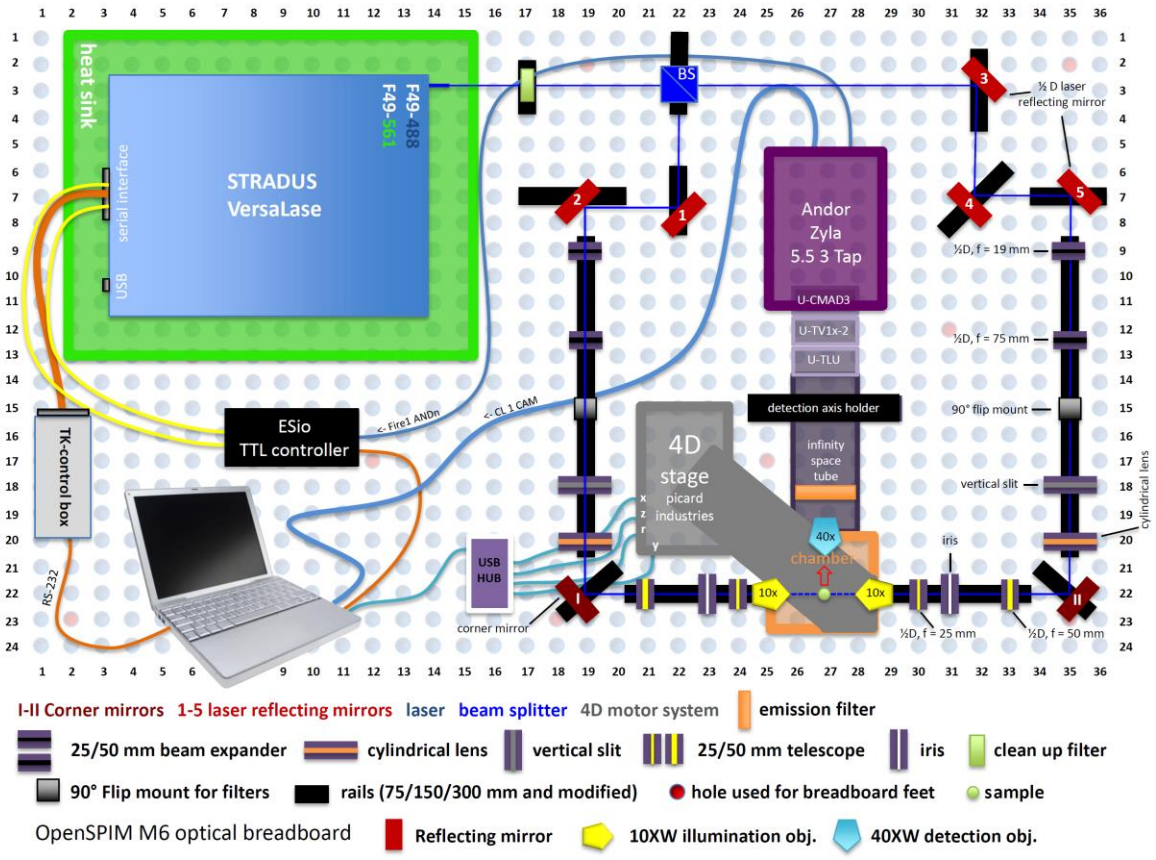


Figure 2.1 – OpenSPIM built for the Telford lab with dual-sided illumination, hardware-controlled laser triggering and all hardware components

### *2.1.2 OpenSPIM - assembly*

Mirror components, optical elements and the acquisition chamber of the OpenSPIM were assembled and mounted on rail carriers as described in the video guide on the OpenSPIM website and is summarized in the following 14 simplified steps schematically represented in Figure 2.2. **Step 1:** Installation of breadboard feet onto the optical breadboard and placing it in its final position; **Step 2:** Installation of laser heatsink on the optical breadboard and fixing the laser system (VersaLase) on top of the heatsink; **Step 3:** Cutting of optical rails for corner mirrors and two reflecting mirrors and installation of the rail system onto

the optical breadboard; **Step 4:** Installation of the pre-assembled acquisition chamber onto the corresponding rail; **Step 5:** Installation of the beam splitter (BS004, Thorlabs), which was placed into a cube adaptor (BS127CAM, Thorlabs), then fixed in place by a cage holder (CM1-4ER/M, Thorlabs) and finally mounted on a rail carrier; **Step 6:** Installation of all corner and laser reflecting mirrors; **Step 7:** Installation of the detection axis holder, infinity space tube, camera and its corresponding connection adapter units to the infinity space tube (U-CMAD3, U-TV1x-2 and U-TLU); **Step 8:** Installation of optical elements (beam expanders, telescope); **Step 9:** Installation of clean-up and emission filters; **Step 10:** Installation of Picard 4D stage in its correct position; **Step 11:** Connecting the controller boxes (Esio TTL controller box & VersaLase control box), VersaLase, Camera, USB 4D-stage and connecting them to the acquisition computer. The Versalase laser system was connected with the help of a controller box and a conventional RS-232 cable to the acquisition computer. ESio's TTL controller box was connected directly to the VersaLase (not to the controller box) via individual SMB connector cables; **Step 12:** Setting up acquisition computer (installation of MicroManager and necessary plugins as well as drivers for VersaLase, Andor camera, Esio TTL controller box and pixel size calibration). The 5 second default security delay of the VersaLase laser system was disabled in the terminal of the Stradus VersaLase GUI software as described on the MicoManager website (https://micro-manager.org/wiki/Versalase); **Step 13:** Hardware configuration with Micromanager and testing for hardware recognition; **Step 14**: Final alignment of light-sheets by illuminating agarose containing fluorescent beads and/or stained specimens.

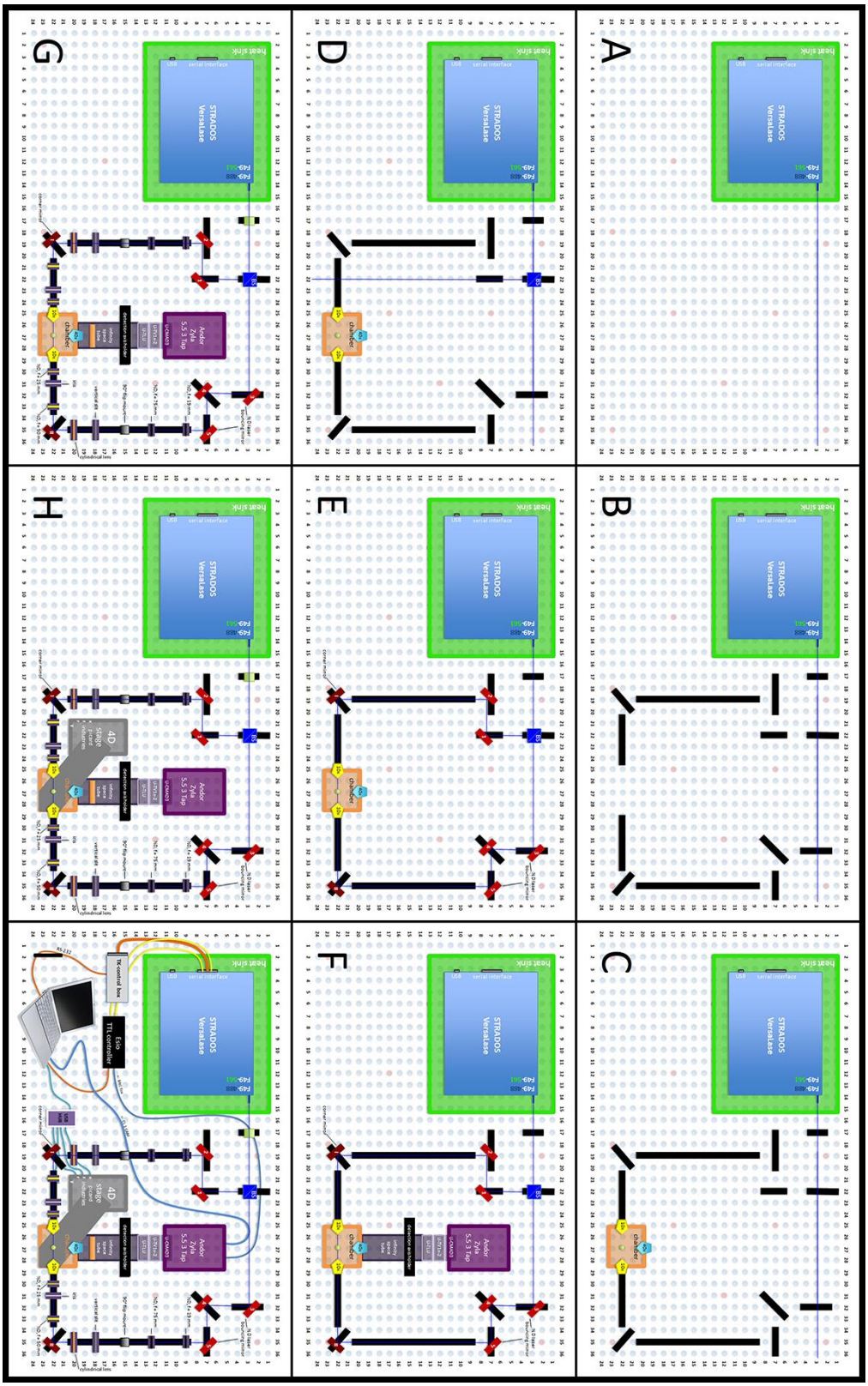


Figure 2.2 - Schematic assembly of the OpenSPIM following step 1-14 (see above).

### *2.1.3 OpenSPIM - alignment of illumination paths along the rails*

The two illumination paths (left and right) were aligned along the optical rails using alignment disks (DG05-1500-H1-MD, Thorlabs) and ring-activated iris apertures (SM1D12D, Thorlabs). Fine-tuning of the light paths was achieved by adjusting the Kinematic Mounts (KM05/M, Thorlabs) of the laser reflecting mirrors. Appropriate laser safety measures were taken during laser adjustments. For example, we use special laser safety eyewear (from laservision) and avoid wearing reflective objects.

### *2.1.4 OpenSPIM - configuration of the acquisition computer*

All necessary hardware component drivers were installed on a HPZ820 workstation computer (see Table A. 2 in the appendix for computer specifications) and the OpenSPIM hardware configured with the open source microscopy software MicroManager (version 1.4.19; November 7, 2014 release; https://www.micro-manager.org/).

### *2.1.5 OpenSPIM - processing of acquired data*

Post-processing of acquired data was performed with the latest version of the freely available imaging software Fiji (Schindelin et al., 2012). For the 3D reconstructions, we took advantage of the bead based registration algorithm and the multi-view deconvolution plugin (Preibisch et al., 2010; Preibisch et al., 2014; Schmied et al., 2014).

## 2.2 Animal culture and embryo collection

Adult specimens of *M. crozieri* were collected in coastal mangrove areas in the Lower Florida Keys, USA in January 2014, November 2014 September 2015 and January 2016 near

Mote Marine Laboratory (24.661621, -81.454496). Animals were found on the ascidian *Ecteinascidia turbinata* as previously described (Lapraz et al., 2013). Eggs without egg-shells (to produce 'naked' embryos) were obtained from adults by poking with a needle (BD Microlance 3) and raised in Petri dishes coated with 2% agarose (in filtered artificial seawater) or gelatin coated Petri dishes at room temperature in penicillin-streptomycin treated Millipore filtered artificial seawater (100 µg/ml penicillin; 200 µg/ml streptomycin; 35-36 ‰). We have successfully maintained adult *M. crozieri* animals for up to six months and longer (Lapraz et al., 2013). However, the best conditions for raising embryos devoid of their egg shell is restricted to a shorter time period (about 2 months) while animals are still large (> 2 cm). While embryos raised in Florida under more natural conditions (natural seawater used and freshly available, extracted from well fed gravid animals) start cleaving approximately 8 hpo (Rawlinson, 2010), embryos poked from gravid worms brought to London and kept in captivity have a similar timing only when they are absolutely fresh. It appears that the longer gravid animals are kept, the more delayed is the first cleavage of extracted embryos, probably due to factors such as the ongoing starvation process, which might influence egg production of adults and may also affect the fertilization of oocytes. Additionally, ciliates parasitizing the adults can multiply over time and also infest naked embryos, which are exposed shortly after the poking. The best developmental conditions for the development of most eggs is therefore shortly after the collection trip. During this time 84% of a normally extracted batch of eggs (n = 106) showed normal spiral cleavage. By poking gravid adults for naked embryos immature and much smaller oocytes are also obtained. Sometimes eggs need to be freed by several washes with artificial sea water on

a mesh from mucus arising from the adult, which can potentially damage some eggs. While we take care to remove those which are too small, slightly damaged or parasitized by ciliates prior to live-imaging it is unavoidable that a few eggs remain in a suboptimal condition, especially those which are not yet mature enough to go through normal development. The two embryos used for the early cell lineage study were compared approximately at 68-cell to the development of fixed embryos from Florida (Figure 2.3). Only embryos, in which nucleic positions looked indistinguishable to embryonic stages fixed in Florida under normal conditions were used for lineage tracing. Additionally, we ensured that the development went through gastrulation (as seen in Figure A. 3) resulting in a ciliated spherical embryo that showed beating ciliary and rotational movements after imaging is completed (see also Figure 5.1).

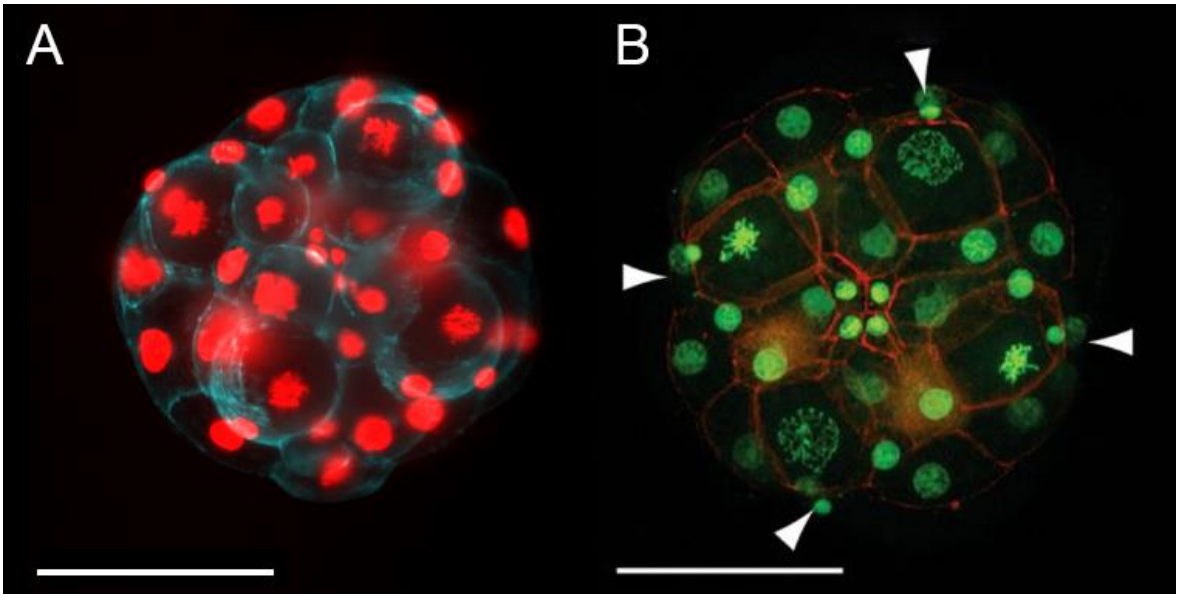


Figure 2.3 - **(A)** Snapshot of a living *M. crozieri* embryo during OpenSPIM image acquisition obtained from lab cultures in London. **(B)** Same cell stage of an embryo fixed freshly in Florida and used for confocal imaging (from Rawlinson (2010)). Scale bars are 100 µm.

## 2.3 Plasmid preparations

### *2.3.1 Transformation and plating*

2 µl of ligation reaction were added to 20 µl of IBA Stargate Top 10 competent cells and then incubated on ice for 30 mins, heat shocked at 42°C in a water bath for 45 secs and immediately transferred back to ice for 2 mins. Then 200 µl of room-temperature S.O.C. medium was added and the tubes incubated on a shaker at 225 rpm at 37°C for 60 mins. Volumes of 20 µl, 50 µl and 120 µl volumes were then spread on pre-warmed LB agar plates (Ampicillin + X-Gal + IPTG) and the plates incubated overnight at 37°C for up to 24 hr.

### *2.3.2 Colony PCR and culture*

The following mastermix was prepared on ice: 17.6 µl water (sterile/nuclease-free); 2.5 µl 10x REDTaq Buffer; 1.575 µl M13 – forward primer (10 pmol/ µl); 1.575 µl M13 – reverse primer (10 pmol/ µl) 0.5 µl dNTPs; 1.25 µl REDTaq Polymerase. Then 10 white colonies from the plates were picked and each briefly dipped into a separate PCR mastermix solution. The reactions were then placed in a in GeneAmp 9700 thermal cycler and run with the following program:

- 94°C - 3:00 mins
- 94°C - 0:45 mins
- 55°C - 0:45 mins
- 72°C - 1:30 mins

x 35 cycles

- 72°C - 7:00 mins
- 4°C - ∞

Pipette tips with picked colonies were placed into culture tubes containing 25 ml of LB Broth (+Amp) and save for later. Finally, 5 µl of each colony PCR product were run on a 1% TAE gel at 90 V for 50 mins. Those culture tubes containing an insert were kept overnight on a shaker at 225 rpm at 37°C.

### *2.3.3 Preparation of Glycerol stocks and purifications of plasmids*

A glycerol stock of each overnight culture was prepared by adding 300 µl to 300 µl of 80% Glycerol and plasmids subsequently purified following the Qiagen Plasmid Midi Kit protocol. For this procedure, bacterial cells were first harvested by centrifugation (6000 x g for 15 min at 4°C) and pellets resuspended in 4ml of Puffer P1. Then the exact procedure was performed as written in the protocol and purified pellets resuspended in 100 µl TE buffer (Ambion pH 8.0) and midi preps send for sequencing.

### *2.3.4 Precipitation and concentration of Midipreps*

20 µl of 3M Sodium Acetate were added to 100 µl of midiprep solution and another 100 µl of Isopropanol. This was incubated overnight at -20°C and then centrifuge at maximum speed for 30 mins at 4°C. The supernatant was then carefully removed and pellets washed with 200 µl of 70% EtOH and centrifuged at maximum speed for 30 mins at 4°C. The washing of the pellet was repeated and the pellet allowed to air dry for 15 mins (and then on heating block at 37°C is necessary). Finally, the pellet was resuspended in 50 µl nuclease-free $H_2O$ and the DNA concentration was measured using NanoDrop.

### *2.3.5 In vitro synthesis of mRNA for fluorescently tagged protein expression*

We synthesised mRNAs for microinjections with Ambion's SP6 mMESSAGE mMACHINE kit. The capped mRNA produced were diluted in nuclease-free water and used for microinjections in order to detect fluorescence signal in early *M. crozieri* embryos. Nuclei were marked and followed using histone H2A-mCherry (H2A-mCh) and GFP-Histone (H2B-GFP). The plasmids carrying the nuclear marker pCS2-H2B-GFP (GFP-Histone) and pDestTol2pA2-H2A-mCherry (Kwan et al., 2007) were transformed, purified and concentrated as described before and then linearized with the restriction enzymes NotI and BglII respectively. To follow live F-actin we used a GFP fusion of the actin-binding domain of utrophin (UTPH-GFP) and for live microtubules a GFP fusion of the microtubule binding domain of ensconsin (EMTB-3XGFP). These clones were the gift of the Bement Lab (University of Wisconsin) (Burkel et al., 2007; Miller and Bement, 2009) or were commercially ordered from http://addgene.org (GFP-UtrCH: https://www.addgene.org/26737/; EMTB-3XGFP: https://www.addgene.org/26741/).

## 2.4 Microinjections

Microinjections of synthetic capped mRNAs (~400-500 ng/µl per mRNA in nuclease-free water) into 100-200 *M. crozieri* oocytes per session were carried out under a Leica DMI3000 B inverted scope with a Leica micromanipulator and a Picospritzer® III at room temperature prior to first cleavage. The fine-tipped microinjection needles were pulled on a Sutter P-97 micropipette puller (parameters: P=300; H=560; Pu=140; V=80; T=200.). Fluorescent signal

was detected 3-4 hours later at the earliest in two- to four-cell stage embryos. Embryos increased their fluorescent signal significantly during their transition into an 8-cell and 16-cell stage and fluorescence was detectable in larval stages more than 10 days later (see Video 1).

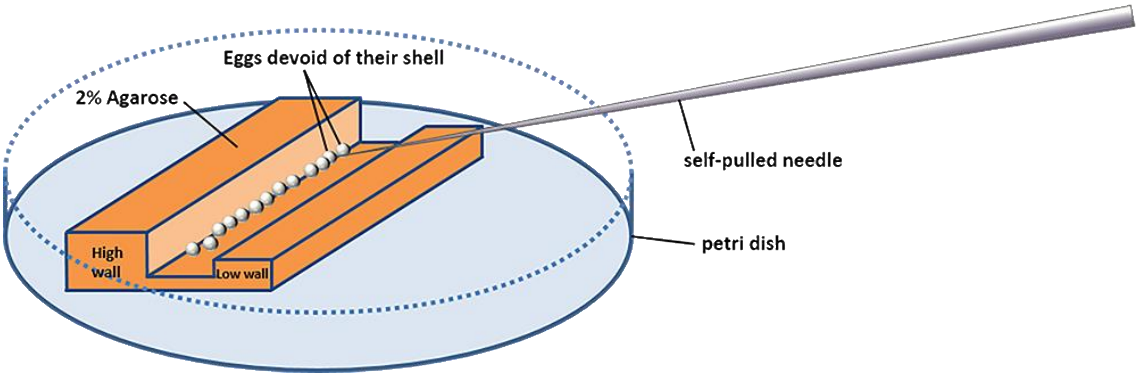


Figure 2.4 - Schematic drawing of the microinjection setup for the polyclad flatworm *M. crozieri*. The stage is 2% agarose poured into a mold, which is then transferred into a 60 mm Petri dish lid. This is filled up with artificial seawater prior to injections. The cleaned eggs are devoid of an eggshell and are arranged in a single row.

### 2.5 Standard fixation and immunohistochemistry procedure

Embryos were fixed for 1 hour in 4% formaldehyde (diluted from 16 % paraformaldehyde: 43368 EM Grade, AlfaAesar) in 0.1 M phosphate buffered saline (PBS) at room temperature or at 4°C overnight, followed by a 5-times washing steps of min 5 min each in PBS. 1-day old larvae were relaxed for 10 to 15 min in 7.14% MgCl2 * $6H_2O$ prior to fixation. The larvae were subsequently stepwise transferred into 100% methanol (25%, 50%, 75%, 2x 100%) and stored at -20°C. Embryos were fixed in the same way but without the $MgCl_2$ relaxation step.

Larvae and embryos were rehydrated from methanol to 0.1% Triton X-100 in 0.1 M phosphate-buffered saline (PBST) by four PBST washing steps, each reducing the concentration of methanol in PBST by 25%. Larvae (not embryos) were subsequently treated with proteinase K (0.1 mg/ml in PBST) for 5-8 minutes and quickly rinsed several times in PBST. Two drops of Image-iT™FX Signal Enhancer (Molecular Probes) were added to specimens, followed by four PBST washes (5 min each) and a 2-hour blocking step in 1% bovine serum albumin diluted in PBST (BSA solution). Primary antibody (1:250 monoclonal Mouse anti-Acetylated Tubulin antibody from Sigma, which labels stabilised microtubules and ciliated cells) and a secondary antibody (1:500 Alexa Fluor® 568 Goat anti-Mouse from Invitrogen™) were diluted in BSA solution. Primary antibody incubation took place at 4°C overnight in the dark, followed by several washes of PBST. Then secondary antibody incubation took place at 4°C overnight in the dark, followed by several washes of PBST. Additionally, 0.1 uM of the nuclear stain SytoxGreen (Invitrogen) was added during the final wash to specimens for 30 min and rinsed with PBST for 1 hour.

### 2.6 Chromogenic whole mount *in situ* hybridization

Fixed larvae (fixed using our standard fixation protocol) were first re-hydrated with graded methanol washes (70% MeOH/40% PBST, 30% MeOH/70% PBST and 30%). Specimens were then washed four times in PBST and digested with 0.05 mg/ml Proteinase K in PBST for 3 min at room temperature. Digestions was stopped with two quick washes of 2x Glycine (2 mg/ml in PBST), followed by two more 5 min washes with 1x Glycine solution. Larvae were then rinsed with a 1% triethanolamine (TEA) solution in PBST followed by two washes of

acetic anhydride in TEA (1.5 µl per ml TEA). This was followed by two washes of PBST prior to a refixation step in 3.7% formaldehyde (from 16 % paraformaldehyde: 43368 EM Grade, AlfaAesar) in PBST for one-hour rocking. After fixation, larvae were washed five times in PBST (fourth wash in a heating block at 80°C for ten min), then washed twice for 10 min each in hybridization buffer (50% Formamide, 5x SSC (pH4.5), 2 mg/ml heparin, 0.1% Tween-20, 1% SDS, 100 mg/ml salmon sperm DNA, diluted in DEPC treated water) at room temperature. Pre-hybridization took place in a humidified chamber at 65°C for 72 hours. Probes were added with a concentration of 1 ng/µl and larvae hybridised for one week at 65°C. This step was followed by two washes in hybridisation buffer at 65°C (10 in and 40 min respectively) and half hour washes of graded hybridization buffer solution in 2x SSC (pH 7) (75% hybridization buffer/25% 2x SSC, 50% hybridization buffer/50% 2x SSC, 25% hybridization buffer/75% 2x SSC, 100% 2x SSC). Next larvae were washed three times for 20 min in 0.05x SSC still at 65°C followed by several washes of a SSC/PBST gradient at room temperature, on a rocker (75% SSC/25% PBST, 50% SSC/50% PBST, 25% SSC/75% PBST, 100% 2x SSC). Then after five additional washes of PBST at room temperature the larvae were blocked for 1 hour at room temperature (1:10 of 1x Boehringer-Mannheim Blocking buffer solution in 1x maleic acid buffer) and subsequently incubated with an anti-DIG AP antibody solution overnight at 4°C. Next larvae were incubated into the chromogenic staining reaction (100 mM NaCl, 50 mM $MgCl_2$, 100 mM Tris (pH 9.5), 0.5% Tween-20, diluted in DEPC treated water) solution containing 5 µl of NBT/BCIP solution in PBST. The staining reaction was stopped with several washes of PBST and specimens cover slipped and

## 2.7 OpenSPIM 4D microscopy of live embryos

Embryos showing fluorescent signal were selected under an Axioimager M1 Epifluorescence and Brightfield Microscope (Zeiss). Live embryos were briefly incubated in 40 °C preheated and liquid low melting agarose (0.1%) and immediately sucked into fluorinated ethylene propylene (FEP) tubes (Bola S1815-04), which were mounted in the OpenSPIM acquisition chamber which was filled with filtered artificial seawater and antibiotics via a 1 ml BD Plastikpak (REF 300013) syringe. The use of FEP tubes has been previously described (Kaufmann et al., 2012) and allows the specimen to remain inside the tube during image acquisition without causing any blurring to the acquired images, as would be the case with other mounting materials such as glass capillaries. Using FEP tubes enables us to mount specimens in lower percentage agarose (0.1%), thus lessening the perturbation of embryo growth and development. The interval between images depends on the user's intention. For long-term imaging single timepoints, which can consist of 40-70 optical slices and were captured every 1-3 mins and the interval was increased during later developmental stages sometimes up to 7 min per time point.

Finding the samples with high magnification objectives (40x and higher) can be a time-consuming process. We therefore adjust the color-coded markings of our glass capillaries to the same calibration number of the mounting syringe and use FEP tubes of similar lengths to standardize the mounting procedure. Additionally, we bring the USB 4D stage to its home position before mounting. When a conventional LED lamp beam is directed against the chamber, FEP tubes and glass capillaries, as well as specimens become clearly visible as soon as the agarose is in focus. In our experience, the easiest way of finding the

sample is by going initially to the tip of the FEP tube or capillary, then by focusing on the agarose and screening for the specimen from bottom upwards.

## 2.8 4D microscopy of live embryos under an AxioZoom (Zeiss)

Several embryos in which fluorescent signal could be detected were centered within a 90 mm petri dish containing penicillin-streptomycin (100 µg/ml penicillin; 200 µg/ml streptomycin) treated Millipore filtered artificial seawater (35-36 ‰) for simultaneous live imaging. To avoid evaporation and make fluorescent imaging possible a tiny hole was made in the middle of the lid and artificial seawater containing fresh antibiotics carefully exchanged from the side when evaporation became apparent. Brightfield, green and red fluorescence was acquired every 7 min.

## 2.9 3D reconstruction of embryos imaged with the OpenSPIM

### *2.9.1 Imaging of embryos for 3D-reconstructions*

For 3D reconstructions of fixed embryos, glass capillaries were mounted into the OpenSPIM chamber via a 1 ml BD Plastikpak (REF 300013) syringe and embryos embedded in 1% agarose containing 0.5 µm sized fluosphere beads (F-Y 050 Fluorescent Microspheres from Estapor with a 1:1500 concentration) to enable registration of images taken from different angles. For imaging, agarose was pushed out of the glass capillary once mounted onto the OpenSPIM chamber filled with water, to a point that the embryos were visible outside the capillary.

### *2.9.2 Fixation and staining of embryos for 3D reconstructions*

Embryos were either directly extracted from gravid adults at the Keys Marine Laboratory (Florida) by poking and allowed to cleave until the desired stage was reached or in the same way from animals kept in culture in London. Embryos were then fixed as described previously for immunostaining but without transferring to methanol (which is not compatible with phalloidin staining).

In order to image specimens from 5 angles to perform volume measurements of early blastomeres, embryos were washed to remove sodium azide with 0.1 M phosphate-buffered saline containing 0.1% Triton X-100 in (PBSTx) by four washing steps and stained with 1:300 Rhodamine Phalloidin (ThermoFisher Scientific R415) for 2-3 h at room temperature or overnight at 4°C. Following several washes of PBST or PBSTx 0.1 µM of the nuclear stain SytoxGreen (Invitrogen) was added for 30 min and the embryos then rinsed with PBST for another hour.

## 2.10 Fixation and imaging of embryos used for scanning electron microscopy (SEM)

Batches of embryos were raised until development reached the desired stage (1-cell, 2-cell, 4-cell, 8-cell, 16-cell, 32-cell, 64-cell, 128-cell and intermediate phases). Fixation was done at 4°C for 1 hour in 2.5% glutaraldehyde, buffered with phosphate buffered saline (PBS; 0.05 M PB/0.3 M NaCl, pH 7.2) and post-fixed at 4°C for 20 min in 1% osmium tetroxide buffered with PBS. Fixed specimens were dehydrated in an ethanol series, dried via critical point drying, and subsequently sputtered coated with carbon or gold/palladium in a Gatan

681 High Resolution Ion Beam Coater and examined with a Jeol 7401 high resolution Field Emission Scanning Electron Microscope (SEM).

### 2.11 Confocal imaging of fluorescently labelled samples

Confocal images of fluorescently labelled samples were imaged either on a Leica SPE2 or a Leica TCS SP8 MP confocal laser scanning microscope. The LAS-AF software implemented to capture the image stacks was used.

### 2.12 EdU pulse staining

Labelling of EdU positive cells was carried out using the Click-iT® EdU HCS Assay (Invitrogen). Pulse experiments reveal a snapshot of all cells going through S-phase during which EdU gets incorporated into the DNA of cells. Larvae were incubated in 10 µM EdU dissolved in filtered artificial seawater for 1 h (first test on larvae) or 2 h (4d-injection experiment) followed by 10 min relaxation step in 7% $MgCl_2$. Relaxed larvae were then fixed following the standard fixation method. Larvae were then washed 6x with PBST and permeabilized for 1h in PBSTx (1x PBS with 0.1% Triton X-100). After two more PBST washes 100µl of the reaction cocktail was added to the samples for 30 min (made according to manufacturer's instructions and using kit reagents). The solution was then removed and the samples were washed for 30 min in Click-IT reaction rinse buffer. The buffer was then also removed followed by two PBST washes and finally DAPI was added to counterstain all nuclei.

### 2.13 Drug treatments, fixation and visualization of spindles and actin cytoskeleton

To inhibit microtubule assembly Cholchicine (Sigma) was diluted from a previously prepared 1% stock solution (diluted in EtOH) to the desired concentrations in 50 ml filtered artificial seawater containing antibiotics (100 µg/ml penicillin; 200 µg/ml streptomycin). For the inhibition of actin polymerization, the same procedure was followed and desired final concentrations were prepared from a 1mM stock solution of Latrunculin A (Sigma).

All drug treatments were performed on embryos obtained by poking several gravid *M. crozieri* adults and were therefore devoid of any egg-shell. Subsequently embryos were allowed to develop into 4-cell stages and about one hundred embryos quickly transferred into petri-dishes coated with a thin layer of 2% agarose (to avoid adhesion of embryos) containing 20 ml of drug solution buffer. Control embryos were similarly transferred into petri dishes containing control solution buffer (artificial seawater containing antibiotics and the same percentage of EtOH as used in inhibitor experiments). Every hour about 30 embryos of every experimental condition, including controls, were fixed for 1 hour with 4% formaldehyde (diluted from 16 % paraformaldehyde: 43368 EM Grade, AlfaAesar) diluted in one quarter filtered artificial seawater and two quarters nuclease free $H_2O$, followed by several washes of PBST every 5 min. The fixed embryos exposed to the same drug concentrations but fixed at different time points were eventually pooled together and stored in PBS at 4 °C containing Na-Azide for several weeks.

Embryos were stained with anti-alpha-Tubulin antibody (Sigma), 568-Rhodamine Phalloidin (Life Technologies Limited) and DAPI, following our standard immunostaining protocol and

eventually observed under an Axioimager M1 Epifluorescence and Brightfield Microscope (Zeiss) or selected for confocal laser imaging (Leica TCS SPE system).

# CHAPTER 3 OpenSPIM microscopy

## Introduction

In the previous chapter, I described in detail how we built and test a light-sheet microscope (OpenSPIM) to study the embryonic development of the polyclad flatworm *M. crozieri*. In this chapter, I show how the microscope performs in terms of 3d-reconstructions and live-imaging. Eggs of polyclad flatworms are opaque and contain copious amounts of yolk. For this reason, imaging is much more difficult than in other, more transparent specimens (e.g. sea urchin pluteus larvae). The results presented here focus on both embryonic stages (fixed and *in vivo*) and larval stages (fixed) and demonstrate what can be achieved to overcome these difficulties, why we chose a certain configuration (e.g. dual-sided illumination) and their advantages and how the microscope performs in comparison to the more commonly used confocal microscopy. Due to the fact, that we learned a lot during this process, we decided to publish the experience and would like to point out that the following chapter can be read also in published form:

Girstmair et al., 2016. Light-sheet microscopy for everyone? Experience of building an OpenSPIM to study flatworm development. *BMC Developmental Biology*, 1–16. https://doi.org/10.1186/s12861-016-0122-0

# Results

## 3.1 Necessary steps for achieving an optimal alignment for both excitation light-sheets

The light-sheets emerging from each illumination path (left and right) were initially aligned using the 25 mm and 50 mm telescope lenses and the adjuster knobs of the two gimbal mounts of each corner mirror (Horizontal & Vertical). The light-sheets were visualized in a column of agarose within the water filled acquisition chamber and using the lowest laser power (1mW) (Figure 3.1, A-B). Additionally, during the alignment emission filters and cylindrical lenses were removed. By adjusting the distance between the 25 and 50 mm telescope lenses and their distance to the illumination objective, the light-sheet first appears as an indistinct broad fuzzy beam crossing the field of view horizontally from left to right (Figure 3.1, A and C, orange arrows). The telescope lenses can then be further adjusted to increase the sharpness of the beam (step 1 in Figure 3.1, A) and to centre its focal point (step 2 in Figure 3.1, A). Next the horizontal gimbal mount adjuster knob is adjusted to bring the light-sheet in focus with the detection objective up to the point where it then is seen as a very thin stripe instead of a coarse beam. Finally the vertical gimbal mount adjuster knob is adjusted to center the light-sheet (step 3 in Figure 3.1, B). In this way both illumination paths are aligned and carefully centered until they overlap each other (Figure 3.1). By putting the cylindrical lenses and the emission filter back, the alignment of both excitation light-sheets can now be tested on fluorescent beads, which ideally homogenously cover the field of view and/or on a specimen embedded in agarose

(Figure 3.1). Usually additional fine-tuning by adjusting the horizontal gimbal mount knob is necessary to achieve best imaging results.

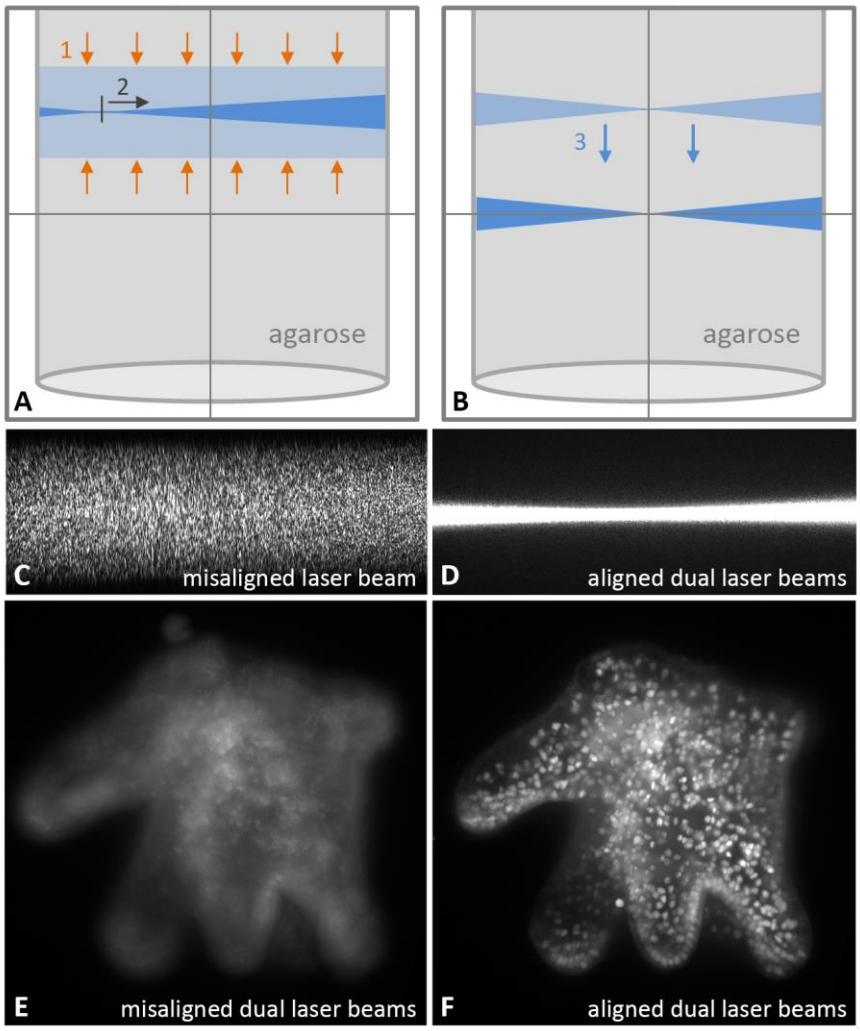


Figure 3.1 – **(A - B)** Schematic drawing of laser beam visualised on agarose hanging from above into the water filled acquisition chamber, Also seen in A and B are three alignment steps of the laser beam (1-3); **(C - D)** Actual misaligned and aligned laser beams visualised on agarose by removing emission filters and cylindrical lenses; **(E – F)** SPIM images (maximum projections) acquired with misaligned and aligned laser beams. The initially visible fuzzy beam is indicated by a bright blue horizontal stripe in between orange arrows. This coarse beam is then brought into focus with the detection objective (step1) and therefore appears as a much thinner laser beam indicated by a blue horizontal stripe in an hourglass-like shape. Note that in this example the focal point of the beam is at this point still shifted to the left (vertical grey line) and needs further adjustments (step2). B The laser beam is shifted from the top to a central position within the field of view (step3).

## 3.2 Our OpenSPIM produces high quality images which we compare to scanning electron micrographs (SEM)

To test whether the OpenSPIM microscope can produce high quality images, 1 day old Müller's larvae were stained with a monoclonal Mouse anti-Acetylated Tubulin antibody (Sigma) and used a secondary antibody conjugated to Alexa Fluor® 568 Goat anti-Mouse (Invitrogen™). Our OpenSPIM images (shown as maximum projections) show cilia covering the whole epidermis of the polyclad larva (Figure 3.2, A-E). This dense film of short cilia can easily be distinguished from longer cilia comprising the ciliary band along the eight lobes (Figure 3.2, E). Our OpenSPIM images show a clear resemblance to scanning electron microscopy images (Lapraz et al., 2013) of similar stage larvae (Figure 3.2 D, E and F) confirming reliable image acquisition with OpenSPIM at the level of embryo morphology.

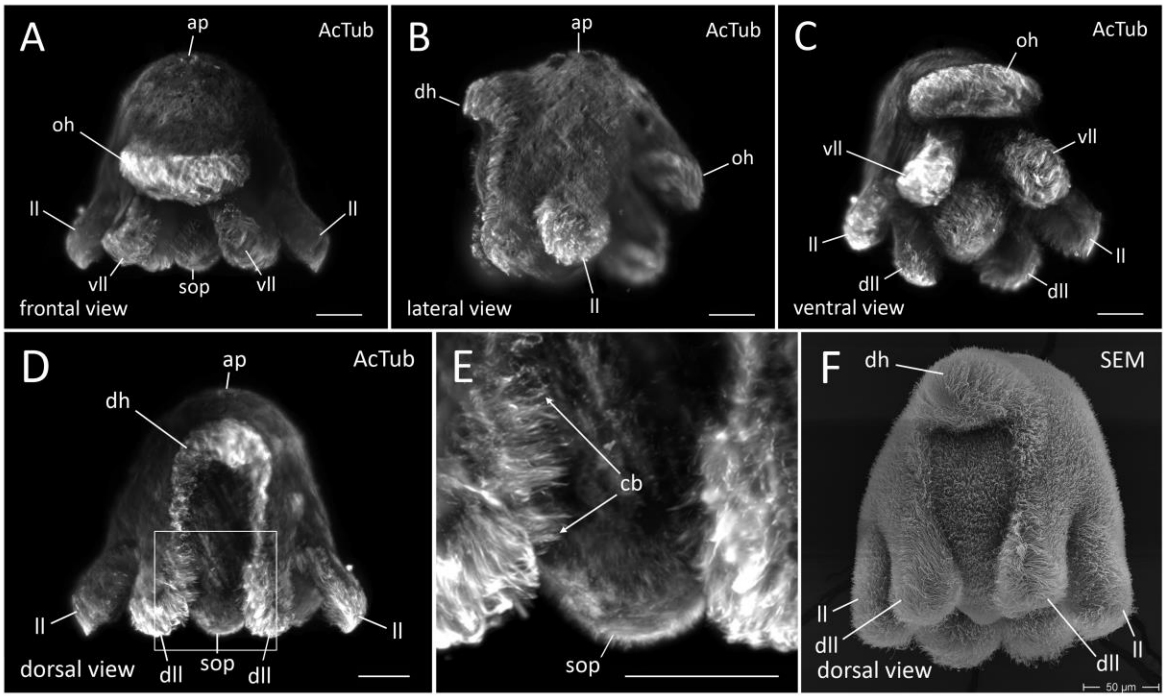


Figure 3.2 - Maximum projections of fixed Müller's larvae stained with Acetylated tubulin and imaged with OpenSPIM **(A-E)** (A) Anterior view (B) Lateral view (C) Ventral view (D) Posterior view (E) magnified view of area boxed in D. **(F)** Posterior view of a *M. crozieri* larval stage obtained with scanning electron microscopy for comparison with imaging acquired by our OpenSPIM. Ap, apical plate; oh, oral hood; vll, ventro-lateral lobe; ll, lateral lobe; dll, dorso-lateral lobe; sop, sub-oral plate; cb, ciliary bands (long cilia). All scalebars are 50 µm

### 3.3 The advantage of OpenSPIM multi-view reconstructions over confocal microscopy and single image in *M. crozieri*

Standard confocal microscopes lack the possibility of multi-view imaging and reconstruction. This is important for the study of *M. crozieri* larvae and embryos due to the attenuation of light intensity caused by the opaque yolk meaning than only one side of the embryo can be visualized. It was found that the opacity causes significant signal loss, which becomes especially obvious in *Maritigrella* when the confocal z-stack of an imaged

specimen is rotated. This is demonstrated here in a fixed larva labeled with the nucleic-stain SytoxGreen (Figure 3.3, right).

The second drawback of a confocal is the necessity of using a slide with coverslip, which tends to cause deformation of our topologically complex larvae. The rotation of a confocal imaged larva reveals the slightly squeezed body shape of the larva. Such confocal z-stacks are not always suitable for further image processing (e.g. image pattern registration as described by Asadulina et al. (2012) and Tomer et al. (2010), for which consistent anatomical structures of whole-body scans are required).

In contrast to confocal imaging, OpenSPIM offers a multi-view reconstruction method, whereby different angles of the same specimen can be fused into a single z-stack as shown in Figure 3.3 (left side). The reconstructed larva not only keeps its natural shape, but also includes the information obtained from each individual angle, resulting in a whole-mount containing high-resolution signal from all sides. For *Maritigrella* larvae and embryos multi-view reconstructions achieved with OpenSPIM create a crucial advantage over confocal microscopy.

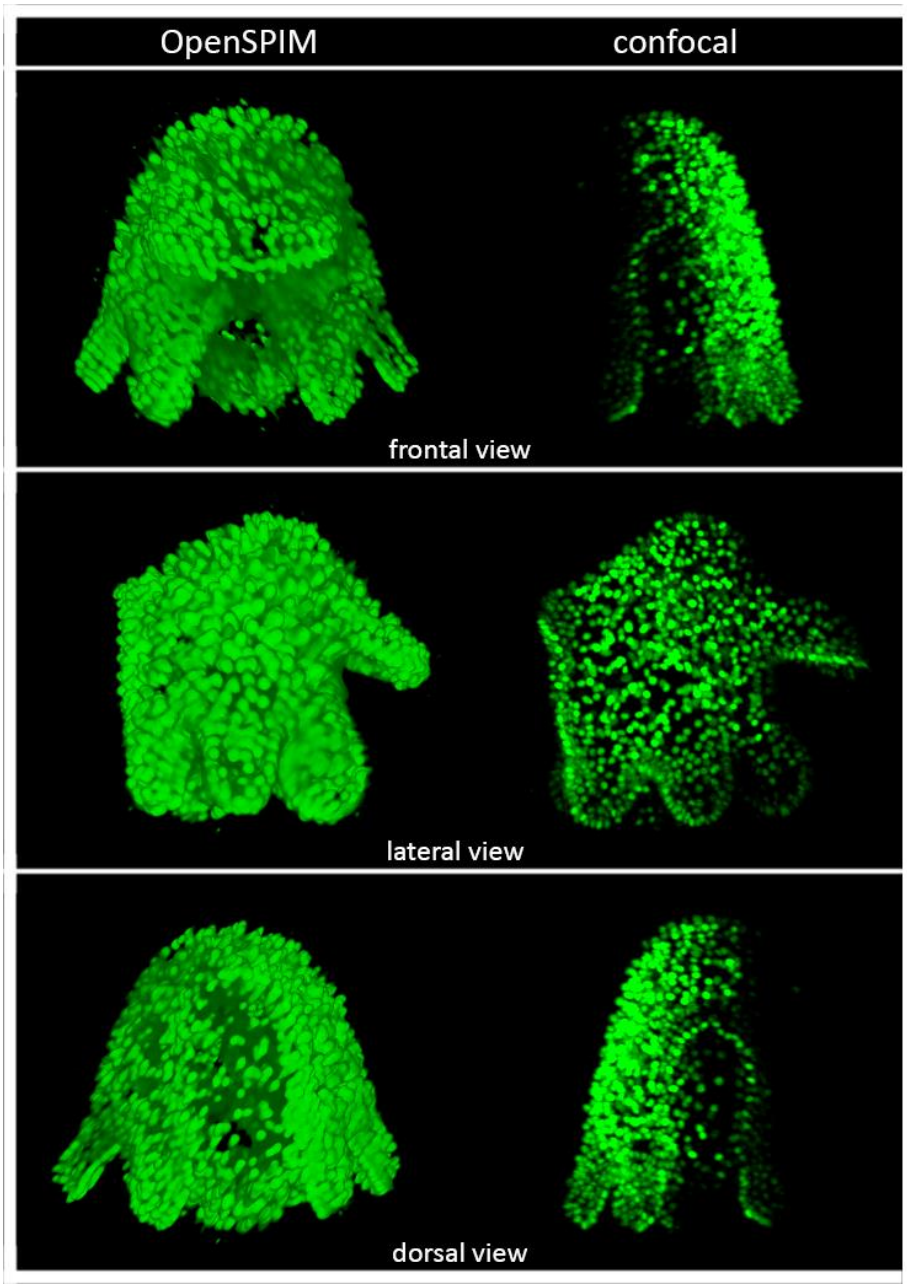


Figure 3.3 - A comparison of a multi-view reconstructed larva (multi-view deconvolution of several angles) stained with the nucleic marker SytoxGreen (left side) with a larva with the same staining captured with a Leica TCS SP8 confocal laser microscopy (right side)

### *3.3.1 Multi-view deconvolution*

When emitted light of a single point source is collected and then focused by an objective lens, light waves converge and interfere due to an optical effect called spherical aberration. As a result, a three-dimensional diffraction pattern of concentric rings of light emerges from the point source, with a central bright disk in the middle. This diffraction pattern can be described as a point spread function (PSF) in which the disk's size strongly depends on the numerical aperture of the objective. In 3D microscopy, the PSF is typically measured by acquiring a z-stack of a fluorescent bead, which can then be used to determine the resolution performance of the objective or for reducing out of focus light (blur) by a mathematical transformation of the image data called "deconvolution". Thereby an algorithm based on the PSF can significantly improve the effect of spherical aberration (typically seen as blur) in acquired images produced e.g. by light-sheet or confocal microscopy. More detailed information on this topic is available e.g. on the Zeiss website (http://www.zeiss.com).

It is interesting to find out to what extent average fusion and deconvolution (Preibisch et al., 2014) can improve results over a single view in an *M. crozieri* embryo when imaged with our OpenSPIM. This is relevant e.g. for early cleavage observations, when nuclei of the macromeres shift from the animal pole towards the vegetal pole of the embryo and are thus difficult to see.

In terms of imaging the entire embryo, it is not surprising that again a clear benefit gained by applying multi-view imaging (average fusion or multi-view deconvolution of 5 angles) over a single one angle view was found. The differences are shown in Figure 3.4 (A-C); in

the single angle view the small macromeres (cells A-D) at the vegetal extreme of the embryo are not visible (Figure 3.4, A). The acquisition of several angles (Figure 3.4 4, B and C) reveals the missing cells and makes clear that embryonic 3D reconstructions, which should include all nuclei information, depends on multi-view imaging. A slight improvement of multi-view deconvolution with 12 iterations over average fusion could be achieved (Figure 3.4, B and C), but appears to be less critical for nuclei staining in early staged *M. crozieri* embryos.

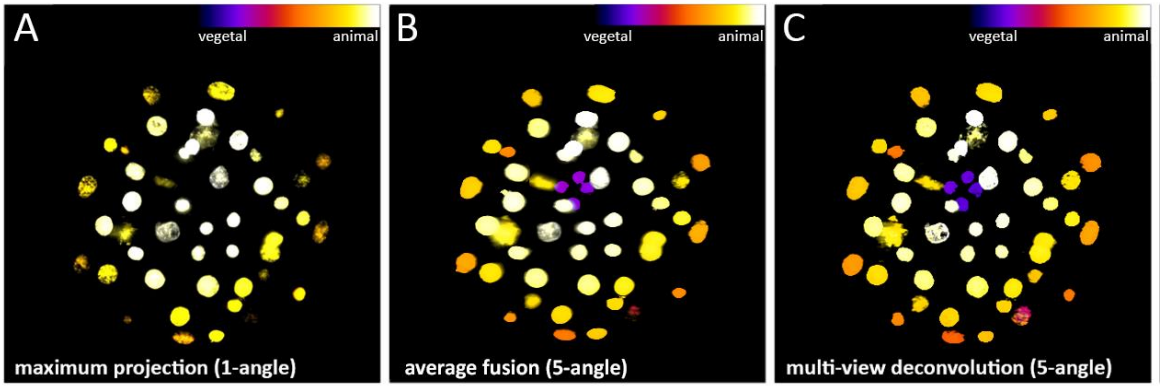


Figure 3.4 - The benefit gained by applying the multi-view deconvolution method (5-angles used) vs. simple maximum projections of an acquired stack (1-angle) on an early staged *M. crozieri* embryo. **(A)** Depth color coding (Fire) of all nuclei after maximum projection of a raw z-stack (1-angle) **(B)** Depth color coding (Fire) of all nuclei after a maximum projection of a raw z-stack (1-angle) **(C)** Maximum projection of all nuclei after multi-view deconvolution. Additionally, all nuclei missing in the single angle maximum projection (from b) have been coloured in red.

### 3.4 Dual-sided illumination efficiently compensates axial intensity attenuation in semi-transparent specimens

Dual-sided illumination for OpenSPIM microscopy can be achieved by building a so-called T-configuration, whereby the laser beam gets split into two beams and a second optical path is installed on the optical breadboard. This allows the illumination of specimens from two sides, instead of one, as demonstrated originally by (Huisken and Stainier, 2007), and was also suggested as a potential extension in the original OpenSPIM publication (Pitrone et al., 2013). The benefit of having dual-sided illumination in our OpenSPIM was tested on fixed *M. crozieri* embryos stained with the nucleic acid marker SytoxGreen. In single-sided illumination images (where one of the two illumination paths has been completely obscured - left or right respectively), a significant loss of signal during acquisition on the side of the missing illumination path becomes obvious due to axial intensity attenuation caused by our opaque and yolky specimens (Figure 3.5, A and C). The light attenuation is especially apparent when single nuclei from opposed illumination sites (left and right) are directly compared to each other (Figure 3.5, A and C, insets). In contrast, a more complete picture of the stained nuclei is achieved by using both illumination paths simultaneously (Figure 3.5, C, insets). This simple test clearly demonstrates the benefit of using dual-sided illumination for our slightly opaque endolecithal polyclad embryos.

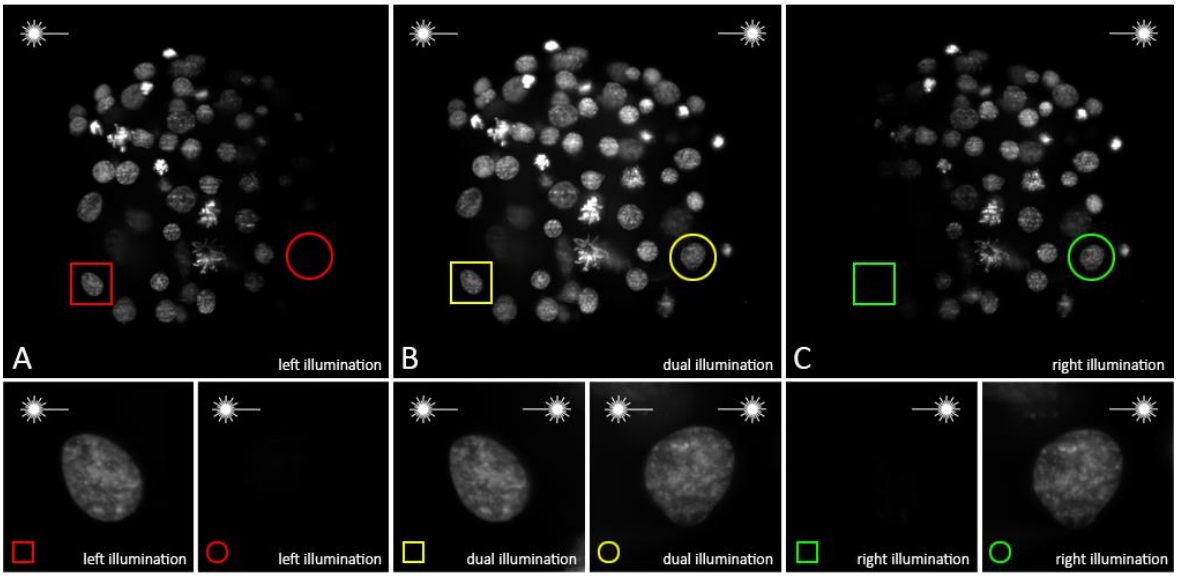


Figure 3.5 - A single and dual-sided illumination, imaging test showing maximum projections of nuclei stained with the nucleic acid marker SytoxGreen. **(A)** Maximum projections of embryonic nuclei using left illumination path of the OpenSPIM microscope, **(B)** Both illumination paths and **(C)** Right illumination paths respectively. Image stacks were acquired in the following order: left illumination, right illumination, dual-sided illumination (A following C following B). All stacks and related insets have been processed identically

## 3.5 Two laser lines allow the visualization of two detection channels

The OpenSPIM is equipped with two individual lasers (λ = 488 nm and 561 nm). The twin laser system was tested on fixed 1-day old *M. crozieri* larvae stained with the nucleic marker SytoxGreen (488). The 561 laser was used in the same specimens to visualize auto-fluorescence of gland cells (rhabdites). The larvae have gland cell scattered mostly around the apical plate and on the ventral side of the animals, which is shown in Figure 3.6 in a single specimen, in which both channels (green and red) have been combined. Here I simply demonstrate the use and precise alignment of the twin laser beams (488 nm and 561 nm). Precise alignment is required during multi-color imaging to obtain good quality images from

both channels. The initial laser beam alignments in a multiple laser system (in our case VersaLase) is done by the manufacturer and an OpenSPIM user can later only align one wavelength, e.g. 488 nm, while the other wavelength(s) (in our case the 561 nm) is presumed to coincide. It is worth noting that I have transported the OpenSPIM by train and car and that the default alignment of our laser system alignment has proven robust during travelling.

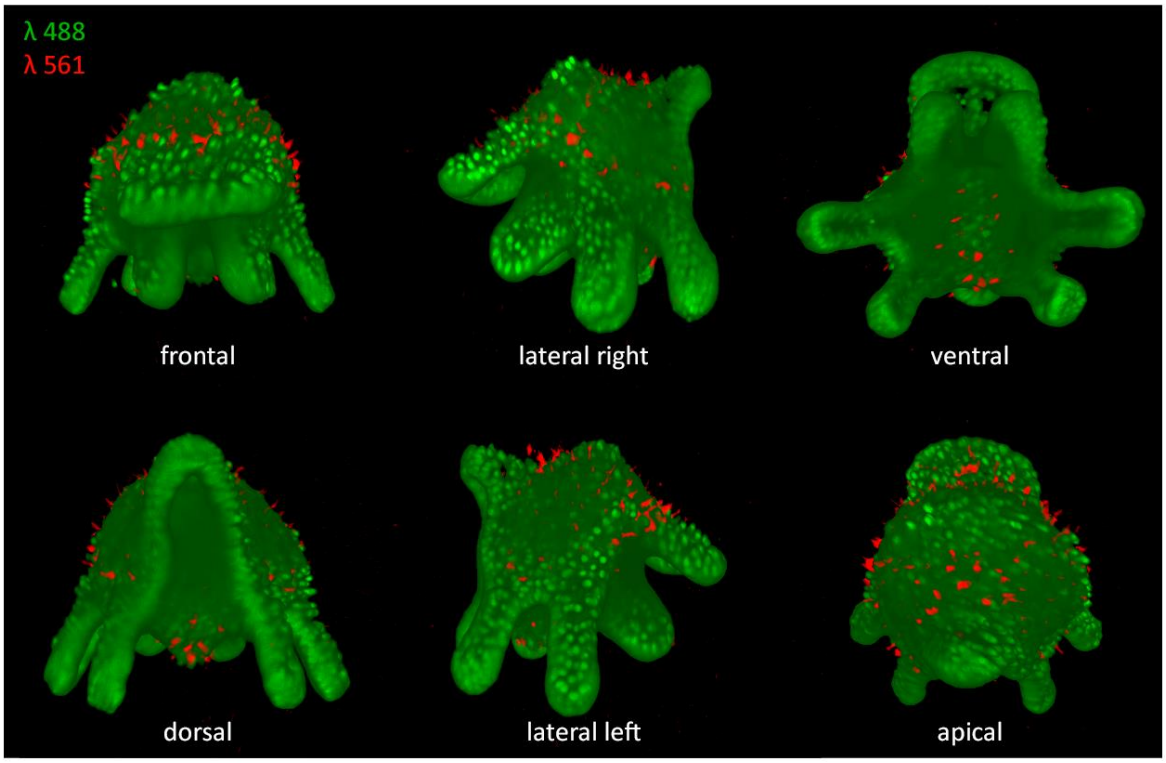


Figure 3.6 - Several angles of a 3D-rendered Müller's larva showing nuclei in green (captured with the 488 laser detection channel) and gland cells in red (captured with the 561 laser detection channel).

### 3.6 OpenSPIM image acquisition with hardware controlled laser triggering is more than twice as fast

With the aim of reducing image acquisition time, we incorporated ESio's TTL controller box (http://www.esimagingsolutions.com/) into our OpenSPIM microscope; this enables hardware-controlled synchronization of the timing of camera exposure and laser triggering. To test our ESio TTL controller, a 100 µm thick single-color stack was imaged (1280x1080 resolution in 16-bit and an exposure time of 32 ms) with a constant step size of 1.5 µm. In this test, the software-controlled image acquisition (by MicroManager without the TTL controller box) completed the acquisition in 43.5 sec. In comparison, when hardware-controlled imaging is used, where lasers are triggered with the TTL controller box from ESio, image acquisition took 17.5 sec demonstrating a significant reduction of image acquisition time without compromising image quality.

## 3.7 Fiji's bead based registration algorithm and multi-view deconvolution is essential to visualize all nuclei in *M. crozieri* embryos along the animal-vegetal axis

Having the possibility to 3D rotate the specimen and using a faster image acquisition method opens up the possibility of carrying out whole-embryo time-lapse videos of the development of an embryo. Fiji's bead based registration algorithm and multi-view deconvolution plugins (Preibisch et al., 2010; Preibisch et al., 2014) make it possible to fuse and deconvolve z-stacks imaged at multiple angles, acquired sequentially at any given time-point. As a first test, this was done for the early development of *M. crozieri* covering the spiral cleavage and the formation of the four quadrants (Figure 3.7 A-J'). To compare our live-imaging videos during early development, I fixed specimens from series of cleavage stages, for which both 3D reconstructions of immunostained OpenSPIM imaged embryos and SEM imaged embryos were performed (Figure 3.7 A-J & A-J''). The 3D-reconstructed series of fixed embryos of several stages are also available as 3D models (Video 2).

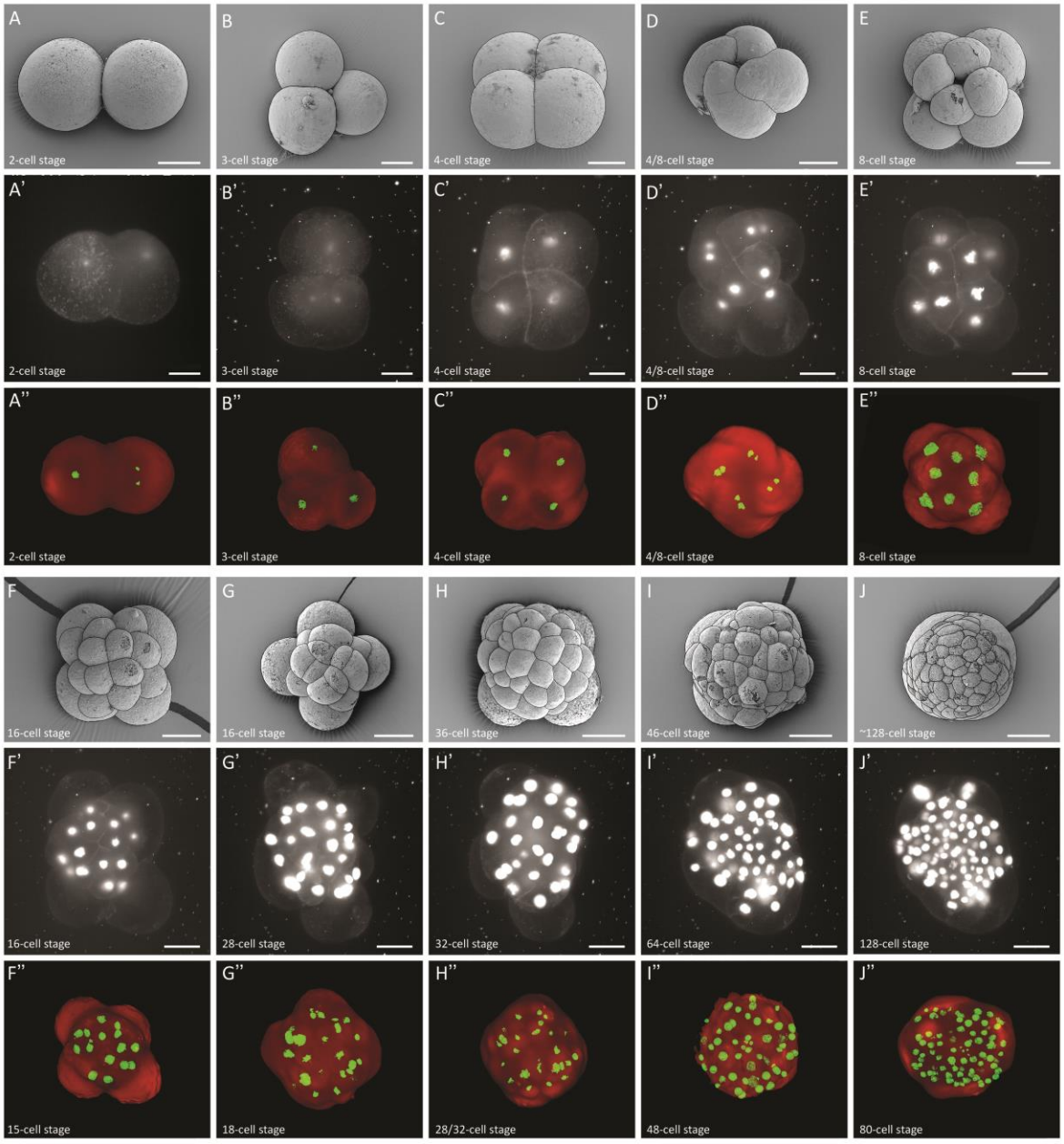


Figure 3.7 - Summary figure of the early embryonic development of the polyclad flatworm *M. crozieri* (1–128-cell stages) (A-J); SEM pictures (A-J) have been captured for comparison, stills from time-lapse sequences (A-J'), multi-view 3D reconstructions (A-J"); all embryos are shown from animal side. Note that time-lapse images (A-J') are presented as captured by the OpenSPIM (mirror images) and therefore cleavage direction is opposite to 3D and SEM images. All scale bars are 50 µm

## *3.8* Rapid *in vivo* time-lapse sequences captured with OpenSPIM show the dynamic early embryonic development of *M. crozieri*

With the OpenSPIM equipped with two illumination paths and capable of rapidly producing, high-quality image stacks, the aim became to visualize the embryonic development in *M. crozieri* up to the 128-cell stage to further test the potential of OpenSPIM for live-imaging and, ultimately, for lineage tracing. We created a time-lapse sequence of a developing embryo injected at the one cell stage with a nuclear marker (H2B:GFP) and a membrane marker (CAAX:GFP). Our time lapse covers 18 hours and shows the stereotypical spiral cleavage and formation of four quartets and further development in *M. crozieri*. The sequence visualizes the embryo from the animal pole (Figure 3.7 A-J′ and Video 3) and consists of 273 individual time-points. During early cleavage, the live specimens had similar morphology at specific time points when compared with fixed specimens (SEM and 3D reconstructions) at the same developmental stages.

## 3.9 Discussion of OpenSPIM

### *3.9.1 New modifications tested for OpenSPIM*

When designing microscopes for *in vivo* imaging with the purpose of tracing cells, one of the goals is to have a high imaging speed in order to have the best time resolution. One of our own modifications included hardware-controlled imaging that appears to be an elegant way of removing unwanted delays during image acquisition. Another relatively new implementation, at least in the context of OpenSPIM, is the use of dual-sided illumination,

which we tested on our specimens. We demonstrated that bringing the light-sheet simultaneously from two sides to our opaque and yolky samples results in a significant increase in signal across the sample as shown for the nucleic markers of stained embryos (Figure 3.5).

### *3.9.2 Limitations of our self-built OpenSPIM*

It is worth mentioning that simultaneous dual-sided illumination can lead to the light-sheet widening and a reduction in image quality due to additional light scattering effects and shadowing (Huisken and Stainier, 2007). In our sample, these issues do not outweigh the benefits gained by dual-sided illumination in comparison to the otherwise much more severe attenuation effect observed, but it is assumed to have an impact on the final image quality.

Another limitation of conventional light-sheet microscopy concerns the thickness of the light-sheet. Thinner light-sheets are governed by the illumination objective and the thickness depends in particular on their numerical aperture. Ideally the thickness of the light-sheet is uniform across the field of view. In reality, it widens on each side of view and its narrowest point resides in the middle. Fortunately, that is where the sample is normally located. When a static light-sheet is created by passing a pencil beam through a cylindrical lens, the ratio of the light-sheet thickness between the center and the side of the field of view depends on the numerical aperture of the illumination objective and the size of the field of view, i.e. the magnification of the detection objective. OpenSPIM as described presents a good compromise, however the sample should be positioned as centrally as possible for optimal sectioning.

To address these problems in light-sheet microscopy, and of particular importance for specimens larger than our embryos, more advanced light-sheet microscopes illuminate the sample from left and right sides sequentially (rather than simultaneously as presented here (see Figure 3.5) and also take advantage of pivoting (scanning) the light-sheet as described for the mSPIM (Huisken and Stainier, 2007). This significantly reduces scattering and attenuation across the field of view. Alternatively, a light-sheet can be generated by scanning a Gaussian beam up and down across the field of view (Keller et al., 2008). Thus, the light-sheet that is created can be further modified in various ways (Fahrbach and Rohrbach, 2010; Huisken, 2012). However, such a light-sheet formation paradigm goes beyond the original OpenSPIM design. Nevertheless, it can be implemented on the OpenSPIM platform and it is expected that the community of users forming around OpenSPIM will do so.

### *3.9.3 Points for consideration before purchasing and building an OpenSPIM*

There is little doubt that a self-built light-sheet microscope is significantly more affordable than existing commercially available alternatives. The question that a laboratory considering whether to embark on building one ought to consider rather depends on two factors. First is the question of whether the finished microscope will be an adequate alternative in terms of image quality and ease of use for the specific task. Second, it is essential when considering an OpenSPIM to factor in the hidden costs involved, most obviously, the costs implied by the time spent building the microscope, learning to use it and learning to use the open source software required to run the microscope and to process the data acquired.

For our purposes, the quality and speed of acquisition that we were able to achieve with our home-built OpenSPIM device provides valuable, high quality data that suit our requirements. However, despite the fact that the assembly of an OpenSPIM is indeed quite straightforward, this step remains only one of the many challenges to overcome. Here we summarize various steps we feel are worth considering before building an OpenSPIM in order to avoid assembling an expensive toy that will be forgotten shortly after (Figure 3.8).

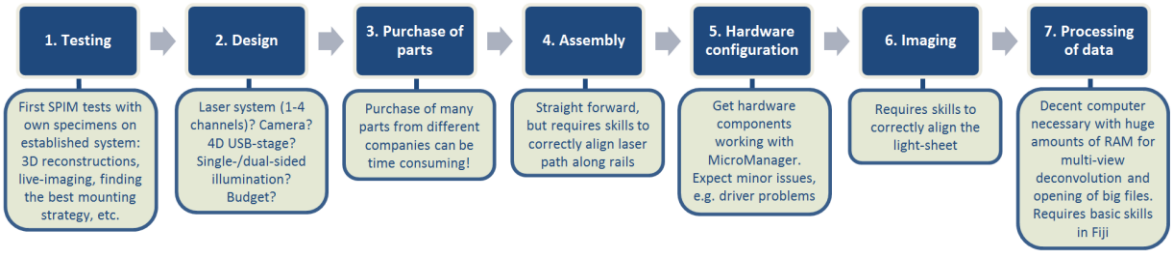


Figure 3.8 - Flow chart illustrating steps necessary for establishing a home-built OpenSPIM

### *3.9.4 Before you begin.*

Before beginning we would recommend prospective OpenSPIM users to image your own specimens on an established OpenSPIM system. This will provide valuable information on whether the system will be suitable for your purposes as well as show what is required in terms of hardware for capturing high-quality images of your particular specimens. This is also an opportunity to gain skills such as correctly aligning the light-sheets, getting familiar with the acquisition software, finding the optimal mounting strategy for the specimens and will inform decisions for the OpenSPIM design selected, as discussed in the next section. There are many OpenSPIM systems around the world; the current estimate is 70. The system from Tomancak lab also regularly travels to practical courses and was extensively used during the EMBO course on Light-sheet Microscopy in Dresden (2014

http://openspim.org/EMBO_practical_course_Light_sheet_microscopy and upcoming August 2016).

### *3.9.5 Designing an OpenSPIM*

The basic design of an OpenSPIM can be taken from the open access platform (http://openspim.org). However, modifications, which might meet more specific needs of individual users, require well thought-through decisions especially considering that most divergences from the basic plan will involve higher costs and, very likely, additional trouble shooting.

We have discussed the most significant amendments we have made in building our own OpenSPIM. Dual sided illumination allows us to image our relatively opaque, yolky embryos optimally and we have shown the benefits of this. Twin lasers allow us to observe more than one labelled molecule per sample. As the most expensive component, the laser system is of particular importance, especially when it comes to multi-channel acquisition. Our OpenSPIM can be easily upgraded up to as many as 4 different laser wavelengths whose beams are aligned within the laser system itself. This alignment of two lasers has proven robust even when travelling, meaning the microscope is fairly portable.

As our embryos are extracted from animals living in tropical waters they can be left at room temperature (23 degrees) during development. Therefore, our OpenSPIM chamber temperature is currently not temperature regulated, but depending on the experiment or the specimens used for imaging a more sophisticated control of the chamber temperature might often be advantageous or even a requirement. While we have no experience of controlling variables in the acquisition chamber, we think that temperature control could

be achieved easily by simply placing the chamber on top of a heating/cooling plate. Additional regulations such as pH or $CO_2$ controls, although feasible, would require more elaborate chamber modifications to avoid, for example, bubbling or flow disturbance of the chamber water created by the connected gas supply and reliable measuring systems.

### *3.9.6 Time taken for Purchasing*

While this might sound trivial, we found that purchasing elements occupied a significant time. There were three reasons for this, first that there is a multitude of suppliers to be negotiated with. Second, as some of the parts are expensive we (like many institutions) were required to obtain multiple quotes for each item. Third, the choices made regarding some parts had knock-on effects regarding the choice or specification of other parts. Finally, it should not be forgotten that some of the parts of the OpenSPIM are bespoke and require a workshop or manufacturer for their production.

### *3.9.7 Assembly*

The assembly of all parts can be considered fairly easy, also thanks to the information provided from the http://openspim.org website. Usually this should be the least time consuming (and the most fun) task.

### *3.9.8 Software and hardware integration*

The MicroManager software and information provided on the OpenSPIM website makes correct hardware configuration relatively easy. However - at least in our experience - establishing the correct links between hardware components and the acquisition computer

causes time consuming problems. Additional time for hardware testing and configuration should be allowed. As an example, we experienced a major issue installing a simple FTDI chip driver, which is necessary for the ESio's TTL controller box to communicate with the acquisition computer. Solving this problem required additional testing of the hardware and interaction with the original suppliers. Moreover, we strongly recommend interacting with the growing OpenSPIM online community via the mailing list, since many users are experiencing the same problems and it is the power of this community that will help you overcome them. Besides, hardware software integration is not something that a typical biologist can master with ease. Involving computer scientists or engineers on the undergraduate level, which should be relatively easy at any large University, is likely to smooth many integration problems. It will also give the students valuable experience with open access hardware and electronics and connect them with the active online communities in these areas.

### *3.9.9 A fast way to correctly align the OpenSPIM*

Learning how to correctly align the light-sheet is a skill that might require some help, but it is not particularly difficult to learn. Within the materials and methods, we describe what we learned and how we currently align our two excitation light-sheets by simply adjusting the 25 mm and 50 mm telescope lenses and the two adjuster knobs (Horizontal & Vertical) of the Gimbal mounts of each corner mirror. It is a relatively fast approach (and certainly not the only one), but in our experience the results achieved in terms of image quality are more than satisfying.

### *3.9.10 Time needed to complete building the OpenSPIM*

Altogether it took us about 7 months from ordering the OpenSPIM parts to acquiring a first image. This time span is surely highly variable and some delays we experienced and mentioned above (see time taken for purchasing) can probably be improved or avoided at all.

### *3.9.11 Image processing*

Imaging and processing and the challenge of multi-view 4D microscopy of acquired data can be straightforward or become a major issue depending on the operator's ambitions. Acquisition of z-stacks of fixed specimens and subsequent processing with Fiji can be easily learned and more sophisticated processing such as multi-view deconvolution can be learned, using online Fiji tutorials on how to use the necessary plugins.

Considerably more challenging, in our experience, is long-term multi-view 4D microscopy of live embryos. This live-imaging setup (keeping the embryo alive and developing normally during acquisition for example) is clearly important. It is also essential to consider the challenge of post-processing the huge amount of data that are generated. Home-built OpenSPIMs are in principle capable of creating elaborate multi-view 4D microscopy videos on difficult specimens (e.g. opaque embryos with scattered emission-light). This was successfully demonstrated on *Drosophila* embryos, where data from six angles per time point have been acquired and the OpenSPIM data generated were subsequently successfully reconstructed using Fiji's bead based registrations algorithm and fused via multi-view deconvolution (Preibisch et al., 2010; Preibisch et al., 2014). However, multi-

view 4D microscopy requires an efficient work flow saving the produced data onto hard drives. The second major requirement is a precise 4D motor system to keep the positional information of the specimen over time as exact as possible in concert with acquisition software that allows the correction of minor drifting of the specimen. Finally major computational resources are needed for processing the data generated, especially if multi-view deconvolution of hundreds of time-points is intended. In our opinion, multi-view 4D microscopy is one of the most demanding and challenging experiments one can undertake with a home-built OpenSPIM and will thus be discussed further in the following section.

### *3.9.12 Inefficient data saving can prolong time-point intervals during imaging*

Multi-view 4D microscopy requires software that reliably saves large amounts of data on hard-drives without running into the problem of a data bottleneck. In single-view time-lapse videos, we observed that the creation of closely spaced time-points (intervals from about 90 sec / time-point) with the MicroManager SPIMacquisition plugin (available at OpenSPIM.org) can cause delays after a certain amount of time has passed. The interest here is, perhaps, less in the specifics of this issue and more in the observation that running an OpenSPIM (as opposed to a commercial system) will require the operator to get involved in many such technical challenges. Alternatively, as this is clearly a solvable issue, one could invest in collaboration with software engineers to identify the problem and adjust the open source software accordingly. Expert help from microManager, Fiji and OpenSPIM communities is expected and required. To ensure the problem is solved one has to invest in the solution. These communities are not compensated for developing the resources and their ability to fix specific problems is limited.

### *3.9.13 Combining multi view acquisition with long term in vivo experiments*

In our experience, long term *in vivo* multi view experiments with the aim of acquiring many time-points with several angles is not an easy task. Our living embryos occasionally undergo dynamic developmental processes, which can cause minor drifts during imaging. Additionally, the automated correct positioning for each angle relies on the smooth and precise running of the USB-4D stage motors system (x, y, z, and twister motors) and on advanced acquisition software. Recently anti-drift plugins have been developed and implemented into MicroManager (see http://openspim.org/Anti-Drift) and are currently being further improved. We anticipate that these developments will bring major benefits for multi-view multi time point acquisition with an OpenSPIM.

### *3.9.14 Processing of acquired multi-view data is challenging*

The creation of multi-view 4D videos with an OpenSPIM has many interesting challenges. One important question that remains is how to deal with the huge amount of data generated. The processing of single time-points is feasible on a decent desktop computer (our system information can be found in the supplementary files), keeping in mind that SPIM registration processes such as multi-view deconvolution can require up to 128 GB of memory to successfully deconvolve a single time-point without compromising image quality and depending on parameters such as z-stack size, resolution, bit-rate, etc. To handle hundreds of time-points, even when imaging quality standards are lowered, a cluster computer with a sophisticated pipeline to organise the processing becomes a necessity. Cluster processing will certainly get more accessible in the future and an

automated workflow for multiview SPIM recordings, see (Schmied et al., 2015), but the need to set up such a pipeline and to have access to a cluster computer should also be borne in mind if OpenSPIM multi-view 4D microscopy is required. Different laboratories have currently already developed a range of increasingly user-friendly tools to visualize, handle and automatically extract information from large-scale light-sheet data (Amat et al., 2015; Peng et al., 2014; Pietzsch et al., 2015; Stegmaier et al., 2016).

# CHAPTER 4 Early development of *M. crozieri*

## Introduction

Despite fundamental similarities between spiralian developmental programs, some major distinctions have also been pointed out. Variations include whether the formation of polar lobes takes place or not, differences in sizes of micromeres and macromeres during early cleavage, blastomere arrangements and cell fates (Hejnol, 2010).

Another distinction, relevant for this chapter, is whether the embryo represents an equal or an unequal cleaver. Which of the two classes of early cleavage an embryo follows is evident by looking at blastomeres sizes at the 4-cell stage. In equal cleavers, the first two divisions give rise to four blastomeres of equal size. Each blastomere is considered equipotent and can give rise to the future D quadrant. In contrast to this, unequal cleavers form four blastomeres of which one can be identified as the largest cell that contains (still unknown) key factors that cause this blastomere to give rise to the future D-lineage. Thus, the D quadrant in unequal cleavers is specified early on, while the mechanism for D quadrant specification in equal cleavers is likely based on an inductive signal, whereby one of the macromeres (3D) contacts the first quartet of micromeres (see detailed discussion in Chapter I). Other examples of differences between spiralians concern the timing of cleavages (in particular, the relative division timing of the 4d blastomere), the arrest or degeneration of certain blastomeres (the latter is known to be the case in polyclad flatworms), the sizes of blastomeres (e.g. the untypically large first quartet in nemerteans) and so on. Such differences in the highly conserved spiral cleavage patterns in different

lophotrochozoan phyla may be explained by a combination of history (phylogenetic relatedness) and adaptation and so studying these can aid our understanding of the evolutionary patterns. It is thus important to gather detailed, in-depth information about the mode of development of these diverse animals.

Previously *M. crozieri* has been described as an equal cleaver (Lapraz et al., 2013; Rawlinson, 2010). Macromeres at the 4-cell stage are therefore expected to be indistinguishable by their size and the specification of the D quadrant lineage is thought likely to follow an inductive mechanism. An observation, which on the other hand would be characteristic for unequal cleavers and point towards this specific cleavage type, is an enlarged D-macromere at the 4-cell stage.

To differentiate whether the blastomeres are of equal size at the 4-cell stage, precise volume measurements are necessary to find potential subtle differences between their sizes. To observe such developmental patterns, we take advantage of our live-imaging/3d-reconstruction set-up and microinjection techniques, which allow us to identify specific blastomeres early on and to observe their cellular behaviour during embryogenesis. These techniques were established specifically for the polyclad flatworm *M. crozieri* (see Chapters 2 & 3).

Detailed descriptions of the early development of polyclad flatworms are generally scarce and it will be interesting to compare embryogenesis of *M. crozieri* not only to stereotypic developmental patterns known in other spiralian phyla but also to the existing developmental literature of polyclad flatworms. For example, it has been described that, during polyclad development, the cytoplasm of blastomeres can show peculiar activities

during early development (see Gammoudi, Noreña, Tekaya, Prantl, & Egger, 2012), which we here refer to as cytoplasmic perturbations. Although there is little knowledge of this peculiar phenomenon and the role of cytoplasmic perturbations during early embryogenesis, our live imaging setup is able to capture these dynamic processes in *M. crozieri* and allows us to compare them to previous descriptions of other polyclad flatworms.

Another open question concerning early polyclad flatworm development is the exact cleavage pattern of micromere 4d. This blastomere is famous for producing endomesoderm (endoderm and mesoderm) in all spiralian embryos and as well as being especially notable for breaking the embryo's radial symmetry by initiating a series of bilateral symmetric cleavages (see Lyons & Henry, 2014). Our live imaging recordings of this particular cell and its progeny in living embryos of *M. crozieri* will contribute to a better understanding of the behaviour of this particularly important blastomere. Finally, the mesodermal fate of blastomere 4d will be investigated by injections of micromere 4d and their descendants followed for 11 days into mature Müller's larvae. Some of these 4d-injected larvae were subsequently stained for an EdU (5-ethynyl-2'-deoxyuridine) pulse experiments, whereby EdU positive cells were used as an indicator for an area comprising mesodermal cells in order to ask the question if descendants of micromere 4d will be located in an overlapping territory.

It is the goal of this chapter to describe the embryonic development of *M. crozieri*, starting from zygote up to the ~100-cell stage and to discern the developmental patterns in this species, in particular equal versus unequal cleavage, and to carry out a comparison of the observed cleavage patterns within the Lophotrochozoa as a whole.

# Results

## 4.1 Oocytes and first cleavage

When eggs are obtained from gravid adults by poking, they first show an elongated, slightly bent shape before turning into a spherical egg, which is covered by a layer of mucus (Figure 4.3, A-B). Some have been observed to be infested by parasitic ciliates (Figure 4.3, B-C) that are usually attached to the adult worms.

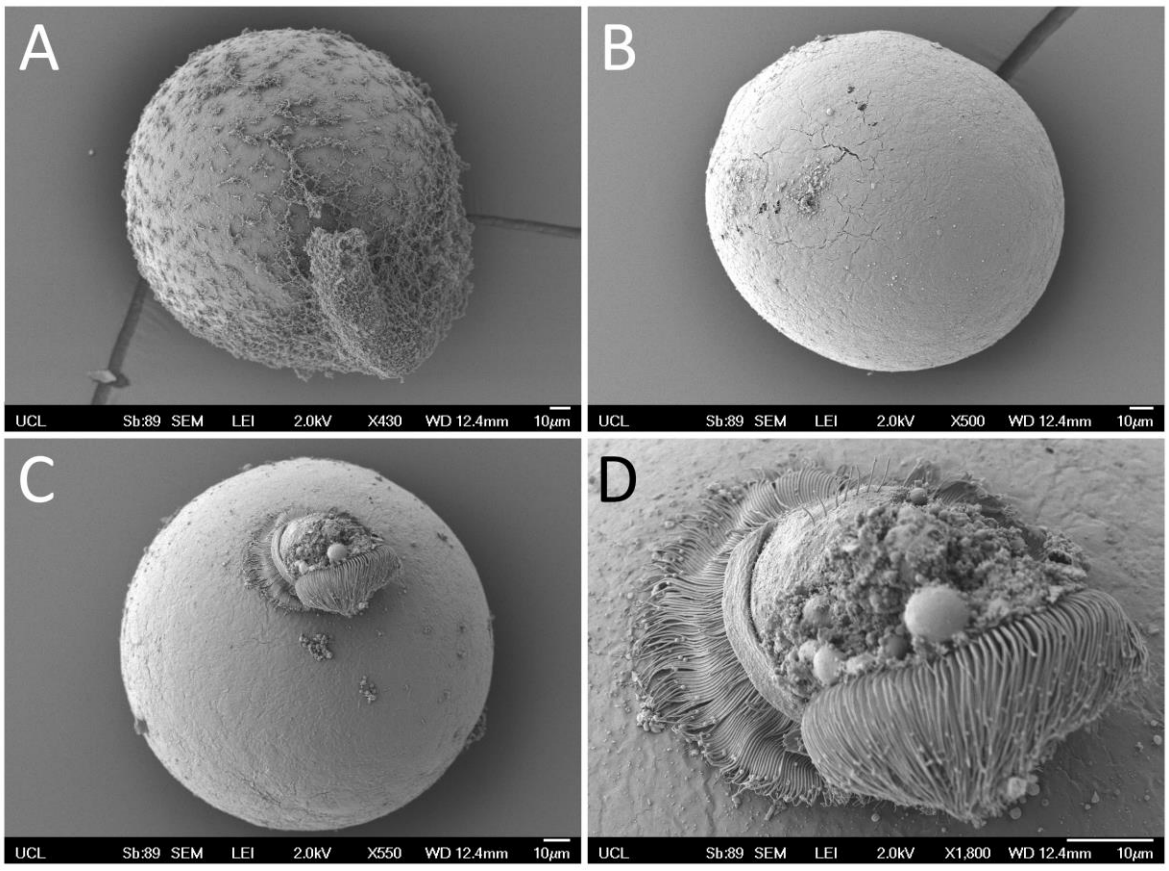


Figure 4.1 - SEM pictures of the 1-cell stage in *M. crozieri*. **(A-B)** Oocyte extracted from a gravid animal. The egg in A is still covered by a layer of mucus. **(C-D)** Same eggs infested by a parasitic ciliate. All scale bars are 10 µm.

During egg maturation, we observe prominent cytoplasmic perturbations in oocytes (Figure 4.2, A-D). This event is known as cell blebbing, which in *M. crozieri* closely resembles observations of other polyclad species (Hallez 1879; Selenka 1881; Goette, 1882; Wheeler 1894; Surface 1907; Kato 1940; Teshirogi et al. 1981; Anderson, 1977; Trubitsina, 1997; Malakhov and Trubitsina 1998; Younossi-Hartenstein and Hartenstein, 2000**;** Rawlinson et al. 2008; Gammoudi et al. 2012; see also Duran and Egger 2012). Similar to these descriptions, in *M. crozieri,* egg maturation involves firstly a depression of the oocyte at the animal pole (Figure 4.2, A) and secondly the emergence of amoeboid/pseudopodia-like irregularities all over the cell membrane (Figure 4.2, C and insets). Older literature provides detailed descriptions, including drawings of blebbing polyclad oocytes, see for example Surface (1907) and Kato (1940).

Kato's detailed drawings of egg maturation and oocyte blebbing based on different Japanese polyclad species, fit very well with our observations made in *M. crozieri*.

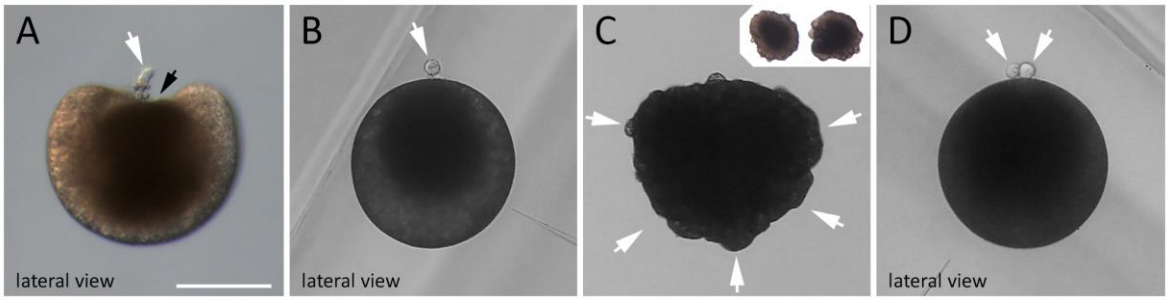


Figure 4.2 - **(A-D)** Cell blebbing during egg maturation in *M. crozieri* oocytes. **(A)** Extrusion of first polar body (white arrow) and depression of oocyte at the animal pole (black arrowhead). **(B)** Egg cell with one polar body and darkish pigment accumulated at the animal pole **(C)** Cell blebbing recognisable by the formation of amoeboid/pseudopodia-like irregularities all over the cell membrane. **(D)** Egg cell with two polar bodies and darkish pigment accumulated at the animal pole. Scale bar is 100 µm.

During the transition into a 2-cell stage (Figure 4.3, A-B) the formation of a cleavage furrow is occasionally more pronounced towards one side of the egg (the animal pole). Sometimes one of the two blastomeres is distinctly larger (Figure 4.3, C-D). In the 2-cell stage, both nuclei are located at the animal pole and pigmented cytoplasm accumulates around the nuclei (n=15/15) ( Figure 4.3, inset of D). These signs indicate the animal hemisphere of the embryo at an early stage.

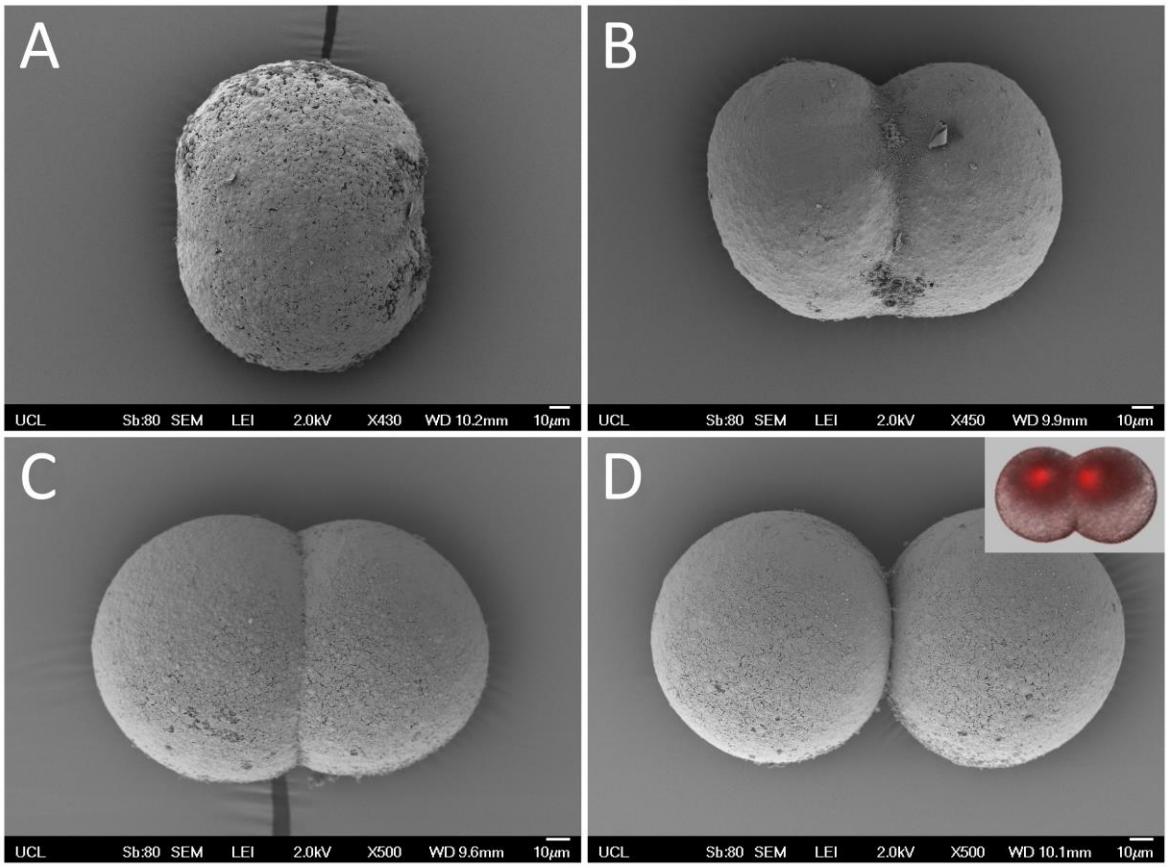


Figure 4.3 - **(A-B)** SEM of two eggs during first cleavage. **(C-D)** 2-cell stages. In C the left blastomere is clearly slightly larger than the right. Note that in B the cleavage furrow appears more pronounced on one side, presumably the animal pole. D shows a different embryo where both blastomeres look very similar in size. Inset shows a microinjected 2-cell stage with fluorescently labelled histone H2A-mCherry surrounded by darker pigments. All scale bars are 10 μm.

Pigmented cytoplasm in micromeres surrounding the nuclei is also visible in embryonic stages during early cleavage (n=73/73). Similar observations of pigmented cytoplasm have been made e.g. for the acotylean polyclads *Thysanozoon brocchii* (Lang 1884, Gammoudi 2011) and *Pseudoceros japonicus* (Malakhov & Trubitsina, 1998).

## 4.2 Second cleavage

### *4.2.1 The formation of 3-cell stages and putative polar lobe structures in M. crozieri*

The second cleavages can be slightly asynchronous, which explains the occasional observation of embryos in a 3-cell stage before the formation of four similar blastomeres takes place. This is the most common explanation for the 3-cell stages occasionally observed. In at least two other descriptions of polyclad early development, however, noticeable lobe-like structures have been observed at the vegetal pole of each blastomere (Teshirogi et al., 1981; Malakhov & Trubitsina, 1998). Interestingly we once captured a polar lobe-like structure at the 2-cell stage in *M. crozieri* (Figure 4.4).

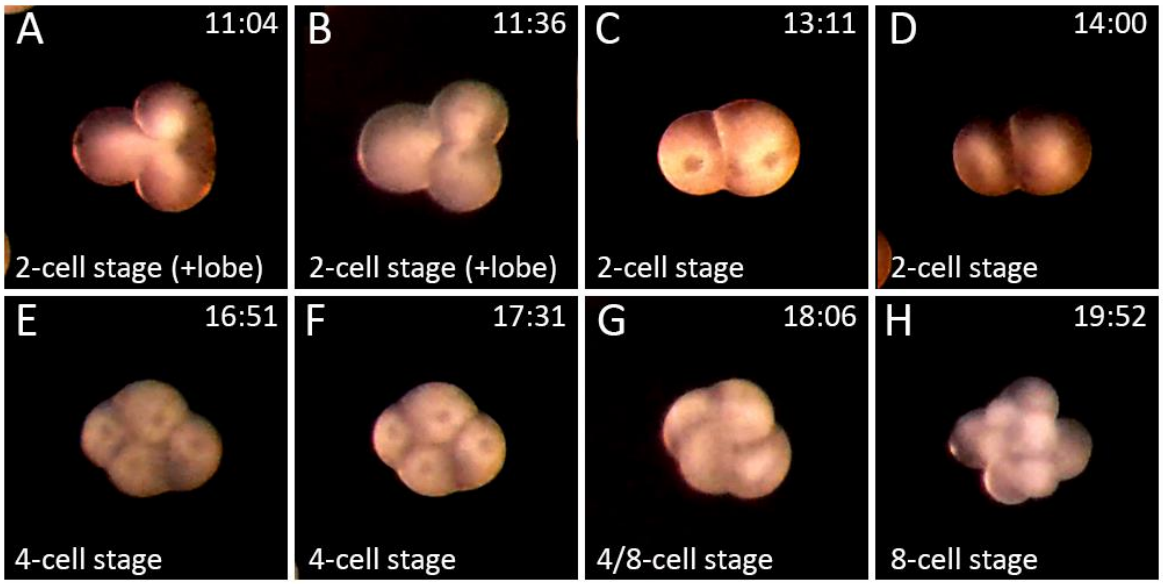


Figure 4.4 – **(A-H)** A series of images of a *M. crozieri* embryo between 2-cell stage and 8-cell stage **(A-B)** A polarlobe-like structure appears during the transition from 2- to 4-cell stage in this embryo. **(G)** Spiral arrangements of blastomeres **(H)** 8-cell stage has formed. Hours post ovipositione (hpo) are shown in the top right corner.

From snapshots of a total of 435 embryos, all of them passing from a 2-cell stage into a 4-cell stage, 20 embryos showed a transient stage of 3-cell cells (see Figure 4.5). As we only looked at snapshots, it is possible that more or perhaps even most embryos pass through a brief 3-cell stage. In these pictures, a 2-cell stage with a potential lobe-like structure cannot be distinguished from a true 3-cell stage, which contains three nuclei, therefore we can only infer that either lobe-like structures or transient 3-cell stages or both show up frequently during the early development of *M. crozieri*.

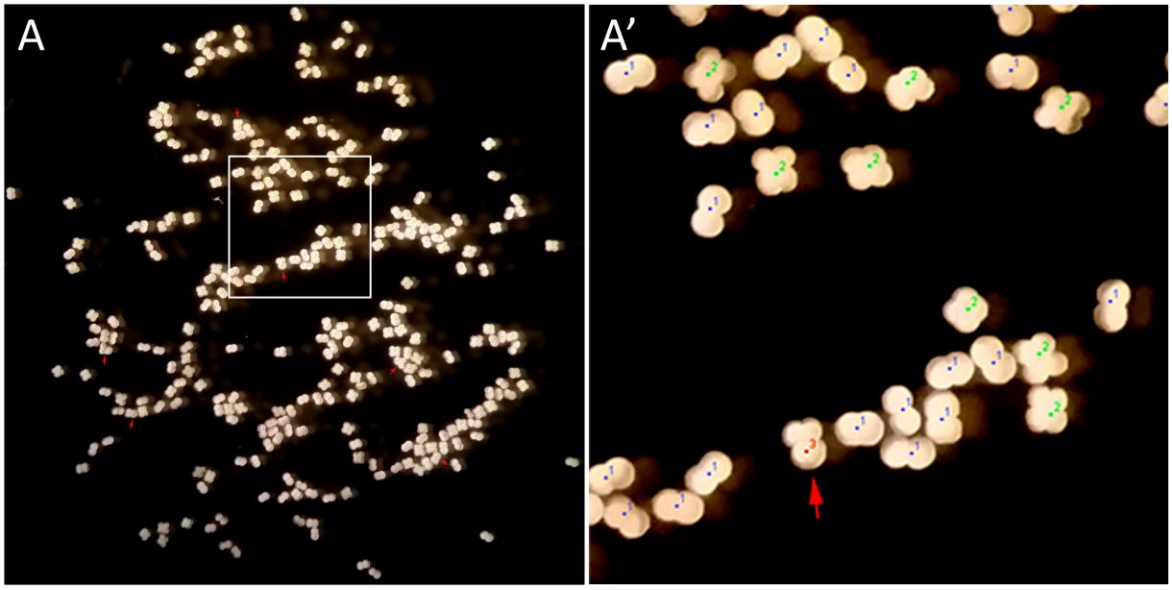


Figure 4.5 – **(A)** A snapshot of developing embryos between 2-cells and 4-cells. Red arrows indicate 3-cell-like stages. **(A’)** Inset of A. In such snapshots 3-cell-like stages (as depicted by red arrow) are readily found, but it is not clear whether they represent embryos consisting of 3-blastomeres or of two blastomeres and an additional lobe-like structure.

### *4.2.2 Blastomeres A-B and C-D are related sister cells*

OpenSPIM live imaging as early as the 2-cell stage can be difficult due to the slow development of the fluorescent signal, which only starts intensifying during the third division. However, in one embryo, live-imaging observations captured from the 2-cell stage were possible and allowed us to follow the relationships between cells into the 4-cell stage (Figure 4.6). At the 4-cell stage, two opposing blastomeres are positioned more towards the vegetal side of the embryo and the other two more towards the animal side. The original identities of these blastomeres were then determined in this embryo by recording development up until the time when the bilaterally symmetric embryo is evident and the

D-quadrant is unambiguously identifiable and then reverse tracing the cells back into the 4-cell stage. Tracing the 4d cell back further into the 2-cell stage showed that the sister cell of vegetal blastomere D is the animal blastomere C and the sister cell of vegetal blastomere B is animal blastomere A (Figure 4.6, A-I). This observation is in accordance with Surface's description of the second cleavage in *H. inquilina* (Surface, 1907). At the 4-cell stage the typical vegetal and animal cross-furrows (where the two cells touch each other) are clearly visible, with blastomeres B and D in touch with each other on at the vegetal pole and blastomeres A and C touching towards the animal pole (Figure 4.6, I).

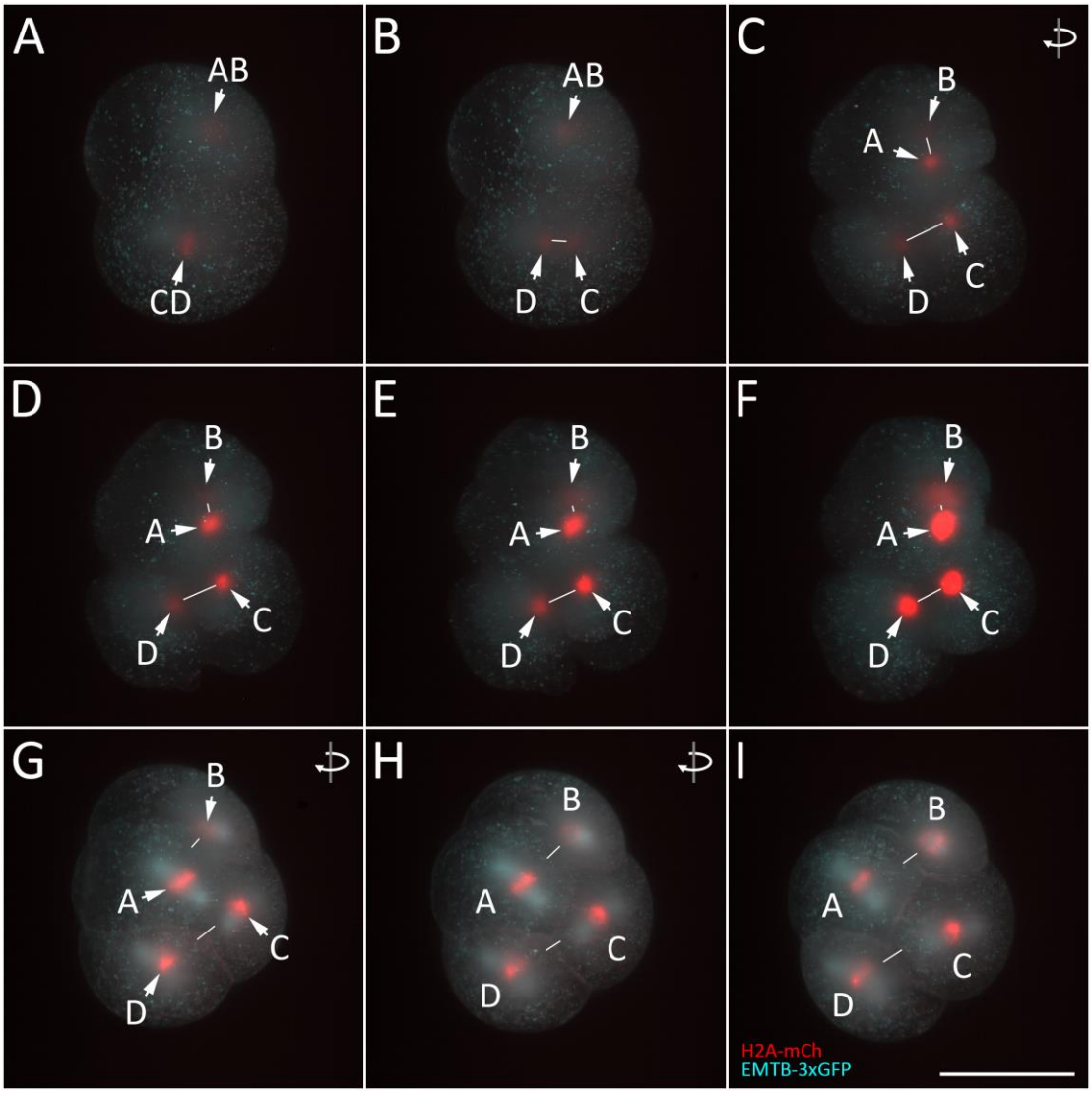


Figure 4.6 - The transition from 2-cell to 4-cell stage in *M. crozieri.* Embryo viewed from animal pole. Oocytes were microinjected with nuclear marker H2A-mCherry (red) and microtubule marker EMTB-3xGFP (cyan). Individual blastomeres could be identified by reverse tracing the D quadrant back into the 4-cell stages. The rotational symbols indicate slight adjustments made during the live-imaging to correct for a better animal view. **(A)** 2-cell stage showing blastomere AB and CD. Note that nuclei have a slightly oblique position relative to each other. **(B)**. Asynchronous division with blastomere CD being slightly more advanced. At this point for a short time a 3-cell stage can often be observed. **(C-E)** Nuclei of blastomere AB have now also separated, revealing the oblique spindle orientations that can be called a spiral arrangement. **(F)** At this stage, the vegetal position of blastomere B and D and animal position of blastomere A and C becomes more obvious. **(G-I)** Once more nucleic condensations become visible and each blastomeres cell border can be distinguished it becomes easy to see the animal cross-furrow border between blastomeres A and C at the animal pole. Scalebar is 100 µm.

Therefore, it can be said that blastomeres B and D carry the more animally positioned vegetal cross-furrow cells A and C, which is also reflected by a height difference of nuclei as can be seen in a 3d reconstruction from a lateral view (Figure 4.7 and Video4).

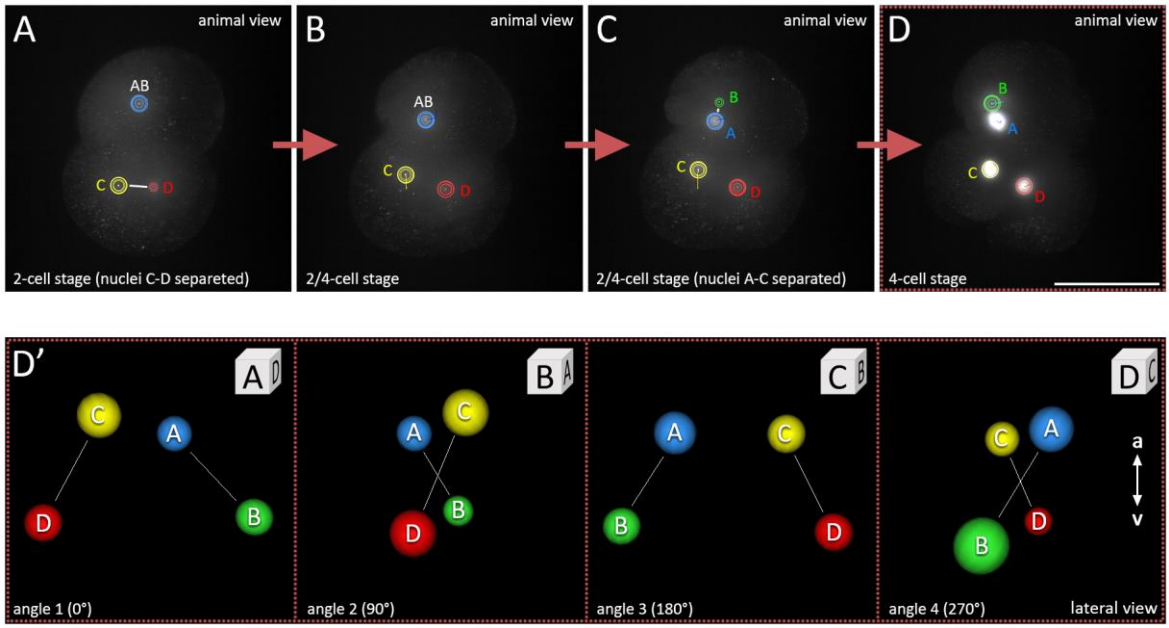


Figure 4.7 - **(A-D)** Animal view of an embryo going from the 2- to the 4-cell stage. **(D')** Schematic four-angle (A, B, C, D) 3d reconstruction of same embryo as shown in D but instead of an animal view depicted here always from a lateral. The correct spatial nucleic positions relative to each other were extracted from the embryos z-stack. The nuclei of blastomere B/D are clearly more vegetally positioned than nuclei of blastomeres A/C.

### 4.3 Formation of first, second and third blastomere quartets

The third cleavage (4- to 8-cell stage) is clearly asymmetric giving rise to the smaller first micromere quartet (1a, 1b, 1c, 1d = 1q) at the animal pole and the larger first macromere quartet (1A, 1B, 1C, 1D = 1Q) vegetally (Figure 4.8, A). When viewed from the animal pole, the uppermost micromeres bud off on the clockwise side of the vegetal macromeres, and the cleavage is designated as dextral (or dexiotropic). A sinistral cleavage type during the third cleavage was not observed in any live imaging recording, in which this could be tested

(n = 22). The quartet of larger macromeres subsequently gives rise to the second and third quartets of micromeres (2q and 3q respectively). These cleavages alternate from counter-clockwise (sinistral for 2q) back to clockwise (dexiotropic for 3q) (Figure 4.8, A, B and E). The cleavage pattern of blastomeres up to the third quartet is shown in our SEM images, with sister blastomeres joined by a white line (Figure 4.8, A-E). Note that an intermediate 12-cell stage forms (Figure 4.8, B), because the division of the first micromere blastomeres (1a-1d) is slightly delayed relative to the division of their sister macromeres (1A-1D) (Figure 4.8, C and D). Until the formation of the fourth quartet, *M. crozieri* illustrates a classic example for the highly stereotypic lophotrochozoan spiral cleavage pattern. During the formation of the fourth quartet (Figure 4.8, F), however, which occurs shortly after the 32-cell stage has been reached, macromeres (3A-3D) begin to deviate from canonical spiral cleavage in their division pattern.

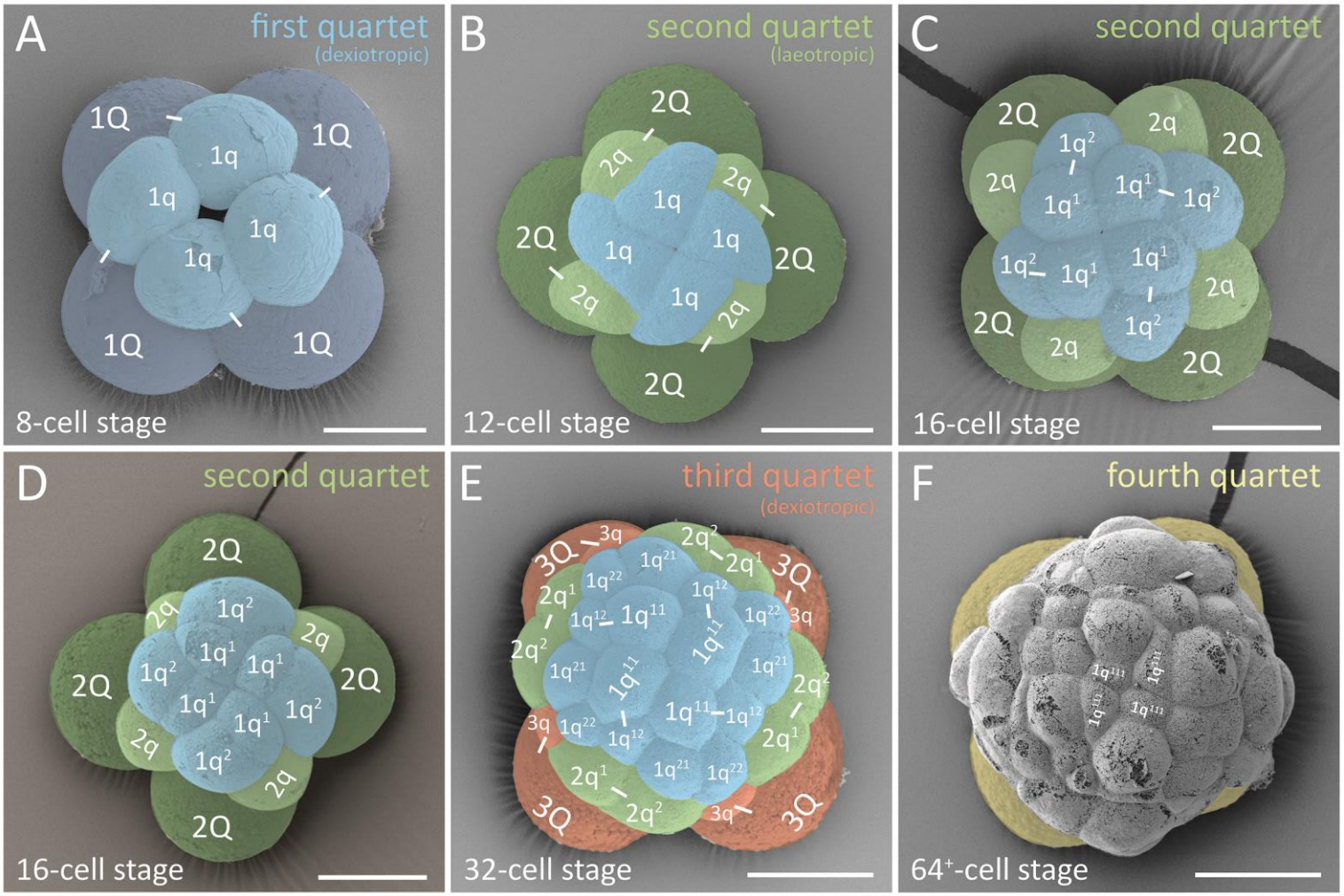


Figure 4.8 Formation of the four quartets in *M. crozieri.* **(A-D)** SEM pictures coloured according to micromere quartets. **(A)** First quartet (1Q and 1q indicated in blue). **(B-D)** Second quartet (2Q and 2q) indicated in green. **(E)** Third quartet (3Q and 3q) indicated in orange. **(F)** Large fourth micromere quartet (4q) indicated in yellow. Scalebar in A-F = 50 µm.

## 4.4 Formation of the fourth quartet

The fourth quartet formation is different from the typical spiral cleavage pattern. For the previous three divisions, the macromere nuclei are towards the animal pole. In the divisions that gives rise to the fourth quartet the mitotic spindles formed by the third quartet, macromeres move the nuclei from an animal position (Figure 4.9, B-D) to a vegetal one (Figure 4.9, E, blue arrows). As a consequence of this, the nuclei of 3A-3D are seen close together at the vegetal pole of the embryo, where each cell divides along the a-v axis (Figure 4.9, F-H). Rather than producing four small animal micromeres and four large vegetal macromeres, the reverse is true; the smaller cells are the most vegetal products of this division (compare previous Figure 4.8) but, due to their vegetal position, the four very small blastomeres are nevertheless designated as the fourth quartet 'macromeres' (4A, 4B, 4C, 4D = 4Q). The four larger animal cells, which still contain most of the yolk, are designated as the fourth quartet 'micromeres' (4a, 4b, 4c, 4d = 4q) (Figure 4.9, F).

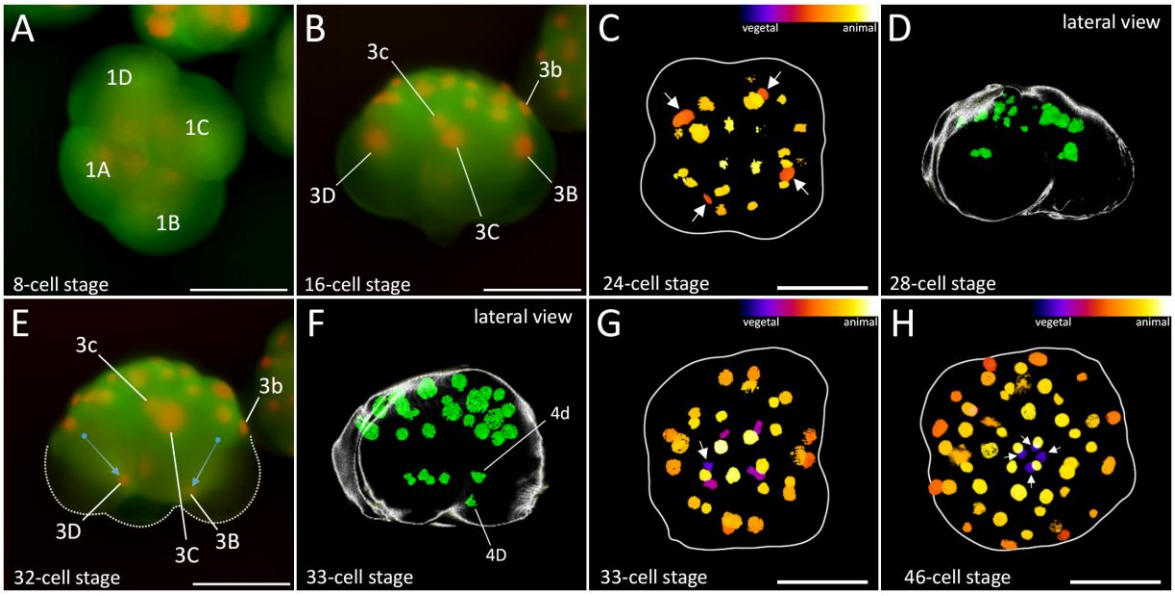


Figure 4.9 – Formation of the fourth quartet in *M. crozieri*. **(A-B)** Same embryo first at 8-cell stage (A) and then at 16-cell stage (B). The 16-cell stage shows macromeres 3B-D and their nuclei at an animal position within the large blastomeres. **(C)** 24-cell stage of a 3d-reconstructed embryo with nuclei 3A-3D also clearly at a more animal position (Their depth in the embryo is coded by colours as seen in top right part of the panel. They are coloured orange and their position is indicated by white arrows). **(D)** Lateral view of a 3d-reconstructed embryo. Macromeres 3A-3D are positioned in the centre of the embryo. **(E)** Same embryo as in A-B at the 32-cell stage. Nuclei of 3B and 3D are now positioned at the vegetal pole of the macromeres. **(F)** Division of one of the macromeres, believed to be 3D (into 4D and 4d), has taken place. **(G)** Same embryo as in F but from an animal view indicating that the division was dexiotropic. The white arrow indicates the newly formed small macromere of the fourth quartet coloured purple indicating it is close to the vegetal pole. **(H)** 3d-reconstructions showing that all four macromeres of the fourth quartet are now positioned at the most vegetal pole of the embryo (coloured purple and indicated by arrows).

### *4.4.1 The precocious division of 3D is followed by an asynchronous division pattern during fourth quartet formation*

In most cases (n=4/5), the third generation of macromeres (3Q) shows the following asynchronous division pattern: Macromere 3D cleaves first and is immediately followed by the division of macromere 3B (Figure 4.9, E-G; Figure 4.10, F). The cleavage of both macromeres 3A and 3C is then slightly delayed by several minutes but both then happen almost simultaneously. This division pattern is interesting, as similar observations have been noted in also in molluscs (Van den Biggelar 1996). Surface (1907) also states that macromeres 4B and 4D in the polyclad flatworm *H. inquilina* form first, followed by 4A and 4C. Furthermore, in the acotylean *Discocelis tigrina* (Lang 1884) macromere 3D – very much as in *M. crozieri* - divides first, followed shortly by 3B and subsequently by macromeres 3A and 3C. In general, such division timing patterns with macromere 3D dividing earlier than macromeres 3A, 3B, and 3C is a common pattern in spiral cleaving lophotrochozoan embryos. In gastropods, however, macromere 3D has been shown to divide either first or later (Van den Biggelar 1996).

## 4.5 Cytoplasmic perturbations found on macromeres

Prior to the highly asymmetric cleavage of the third generation of macromeres (3A-3D) the formation of protuberances have been observed on the surface of all four macromeres. These protuberances appear during the divisions of macromeres 2A-2D in form of vesicle-like protrusions (Figure 4.10, A-D) (n = 17/18). Their function is unclear but mitotic

cytoskeletal activity during anaphase seems to correlate with the observed protrusions (Figure 4.11). During the formation of the fourth quartet (3A- 3D), we also observed cytoplasmic perturbations in form of waves of contractile activity in all four macromeres (n=18/18). In this case the macromeres attain an elongated shape (Figure 4.10, F-H) at the onset of the formation of micromeres 4a-4d. More detailed time-lapse sequences of these peculiar cytoplasmic perturbations are shown in Figure 4.12).

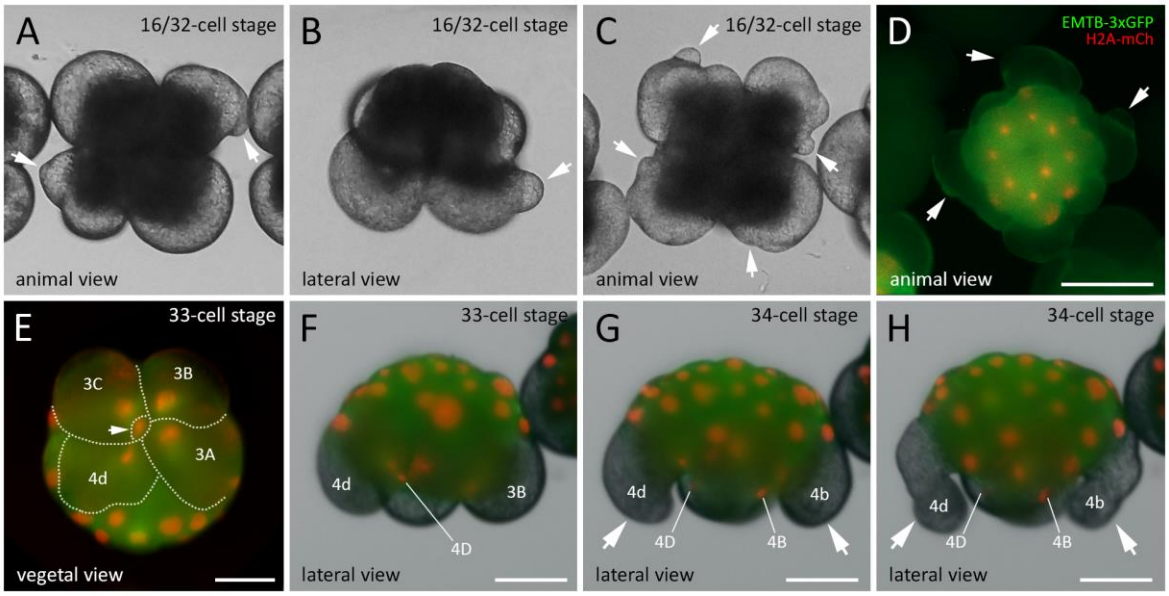


Figure 4.10 - Protuberances and cytoplasmic perturbations during third and fourth quartet formation (A-D) Cytoplasmic perturbations and the formation of extracellular vesicle-like structures appear prior to third quartet formation (16-32 cell stage) among all four macromeres. **(D-H)** Embryos microinjected at one cell stage with microtubule marker (EMTB-3xGFP) and histone nuclear marker (H2A-mCh). **(E-F)** Vegetal (E) and lateral view (F) of the division of macromere 3D into tiny macromere 4D (white arrowhead) and mesentoblast precursor 4d, which is the starting point for cytoplasmic perturbations during fourth quartet formation in all macromeres. **(F-H)** Cytoplasmic perturbations in form of clear deformations of (large) micromeres 4b and 4d. Live imaging was performed under a Zeiss Axio Zoom Stereo Microscope. All eggs were extracted from adults prior to shell formation. Scalebar is 100 µm in A and 50 µm in H-L.

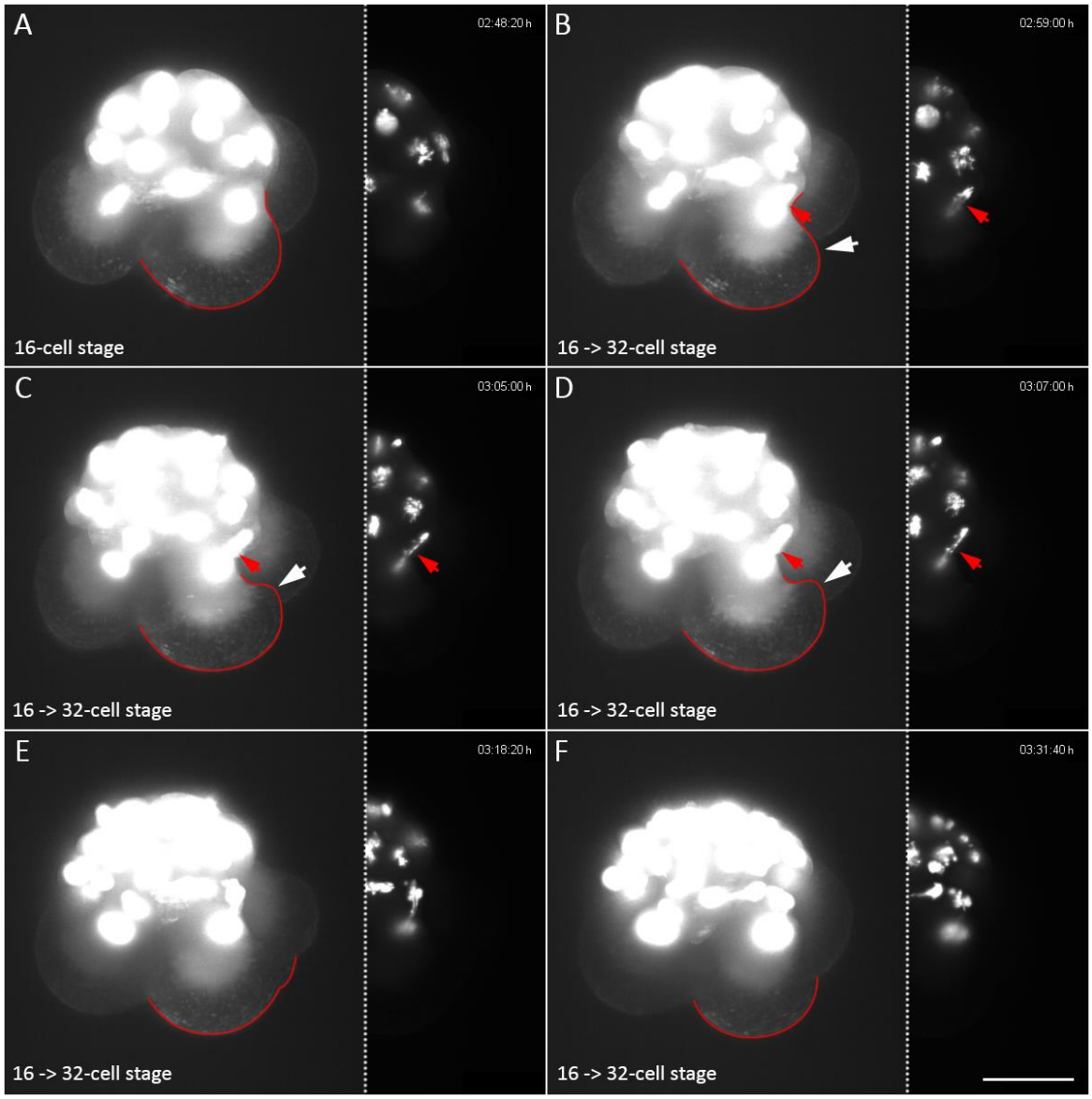


Figure 4.11 – Cytoplasmic perturbations imaged with the OpenSPIM in one of the second quartet macromeres shown during mitosis. The whole embryo is shown over-exposed to better visualize the membranous outlines of the macromeres. Right of each embryo its nuclei are depicted with normal exposure. Red arrows point to the same nuclei of the embryo. A red line highlights the outline of the corresponding macromere. The shape deformations caused by the cytoplasmic perturbations of the macromere correlate precisely with the mitotic anaphase and reach a maximum in panel D. Scalebar = 50 µm.

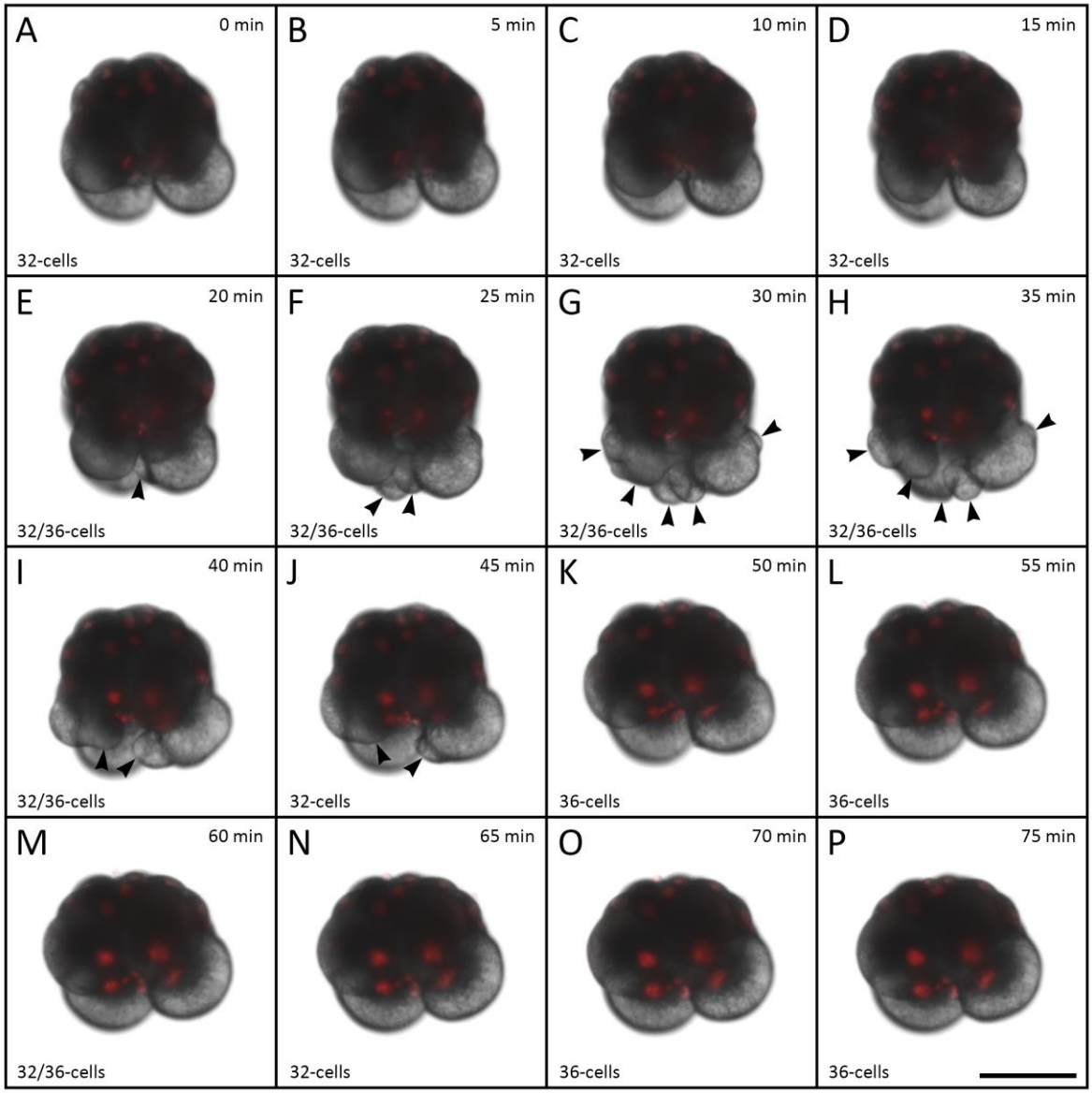


Figure 4.12 – **(A-P)** Time-lapse recording showing the formation of the small macromeres (4Q) and large micromeres (4q) of a single *M. crozieri* embryo in 5 min intervals showing striking cytoplasmic perturbation activity at the vegetal pole of the embryo (indicated by black arrows). **(F-K)** 25 min of cytoplasmic perturbations are clearly visible in macromeres 3A-3D. Live imaging was performed under a Zeiss Axio Zoom Stereo Microscope. Scale bar is 100 µm.

## 4.6 Micromere 4d is responsible for the symmetry breaking at a cellular level

In most spiral cleavers the direct progeny of macromere 3D (i.e. micromere 4d) typically divides into left and right daughters thus breaking the embryo's radial symmetry producing a bilaterally symmetrical embryo with a left and right side.

From our light-sheet live-imaging data it becomes clear that the *M. crozieri* 4d blastomere does not immediately divide laterally but first divides along the anima-vegetal (a-v) axis into a smaller and animally positioned cell, which we designate as $4d^1$ and a large, vegetally positioned cell, namely $4d^2$ (Figure 4.13, A-B). This happens on average 196 min (n = 8; ±34.8 S.D.) after the apical rosette cells ($1q^{111}$) have formed. Following this additional division of micromere 4d the symmetry is broken by the horizontal (left-right) division of both sister cells, $4d^1$ and $4d^2$. Interestingly, the metaphase of dividing micromere 4d initiates a brief period of obvious cytoplasmic movement, during which a number of amoeboid irregularities of the membrane becomes visible (n = 16/16) (Figure 4.13, B). The horizontal divisions of $4d^1$ and $4d^2$ appear equal and this is particularly obvious in $4d^2$ due to its large size and exposed external position (Figure 4.13, C).

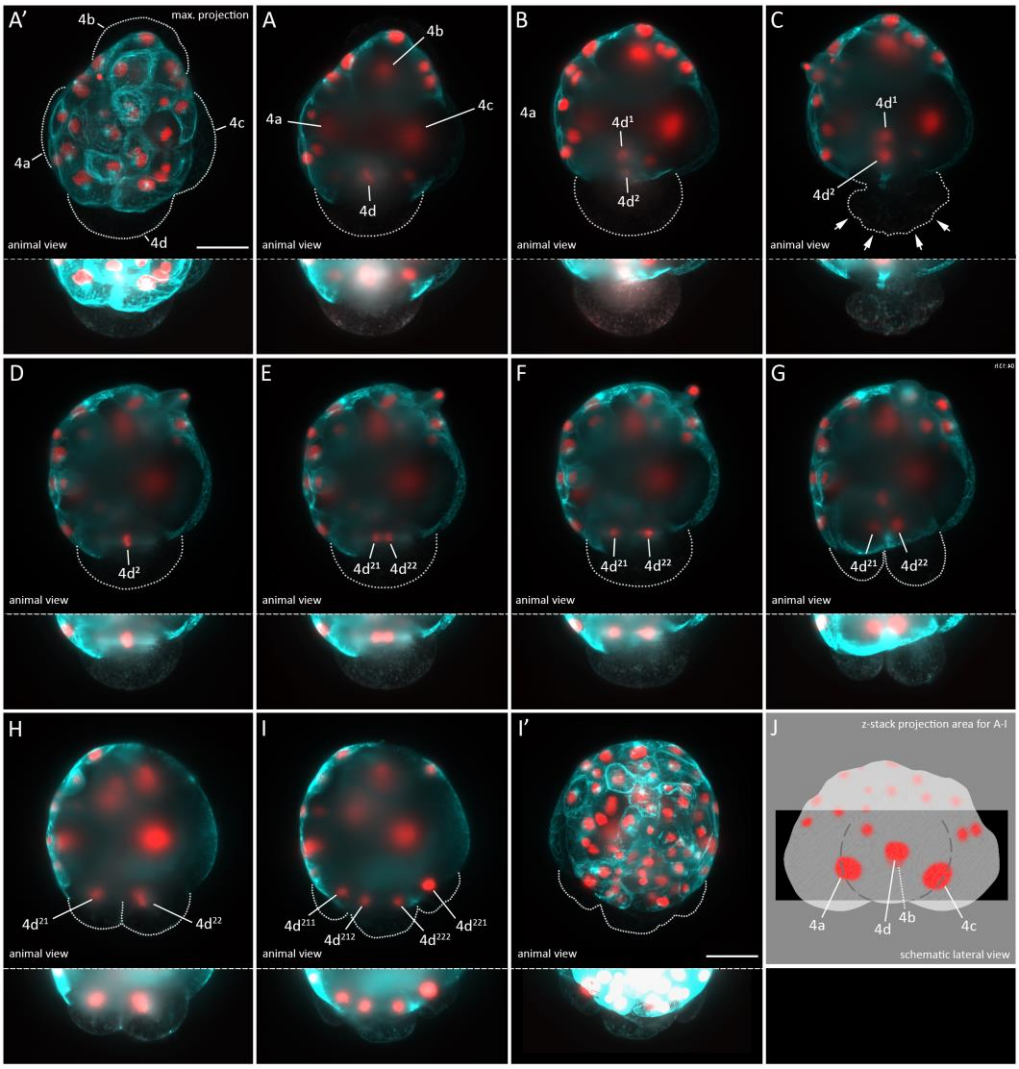


Figure 4.13 - **Animal view of the cleavages of the endomesoderm precursor 4d in *M. crozieri*.** Oocytes were microinjected with nuclear marker H2A-mCherry (red) and microtubule marker EMTB-3xGFP (cyan) and the embryo used for 4d microscopy with OpenSPIM. **(A-I)** Partial maximum projections of different time points of the same embryo breaking its radial symmetry by divisions of micromere 4d. Only a part of the z-stack has been used for the projections to better visualise the cleavage pattern of 4d indicated as the darker rectangle in **J** (lateral view). **(A)** Chromosome condensations only visible in 4d, not in 3a, 3b and 3c. (**A'**) maximum projection of the embryo seen in A. **(B)** Division of 4d along the animal-vegetal (a-v) axis of the embryo. At this point the radial symmetry of the embryo is broken. **(C)** Cytoplasmic perturbations (white arrowheads), observed during the cleavage of 4d. **(D-H)** The horizontal division of $4d^2$ give the embryo a bilateral morphology. **(I)** The next horizontal division of the daughter cells of $4d^2$ is depicted; The 4d cell and its progenies have been depicted separately below each figures' whole embryo but with increased levels to better visualize membrane dynamics. (**I'**) maximum projection of the embryo seen in I. Scalebar = 50 µm.

Both descendants of $4d^1$ and $4d^2$ ($4d^{21}$ and $4d^{22}$ and $4d^{11}$ and $4d^{12}$) then undergo another round of horizontal cleavages, similar to Surface's descriptions on *H. inquilina* (1907).
Of all embryos that follow the stereotypical spiral cleavage pattern with quartet formations the described first division of 4d along the animal-vegetal (a-v) axis and the subsequent horizontal divisions of both daughter cells has so far been only found in the Polycladida.

### *4.6.1 Injections of the 4d blastomere in M. crozieri indicate a mesodermal fate*

To investigate if the 4d cell in *M. crozieri* can form mesoderm as has been described and demonstrated for the polyclad flatworm *H. inquilina* (Boyer et al., 1998; Surface, 1907) we microinjected macromere 3D or its large descendant micromere 4d. During injections of embryos (32- to 36-cell stage) the vegetal cross furrows were still present and helped to discern D and B quadrants from A and C quadrant. If macromere 3D was successfully injected, GFP signal should also be present in small macromere 4D, which will be always located at the most vegetal pole of the embryo and which does not undergo any further divisions and so represents a good landmark. Injections of any of the cells 3A-C can be easily distinguished since their daughter cells 4A-C and 4a-c do not undergo any further divisions (Boyer et al., 1998; Surface, 1907). In 3D-4d injected embryos observed during development, after one or two days we can see a mostly bilateral symmetric pattern of fluorescence (see Figure 4.14, A-F).

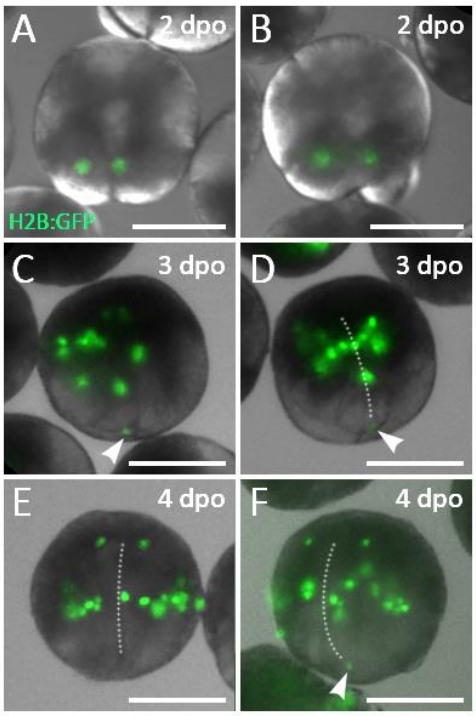


Figure 4.14 - GFP expression showing the descendants of 4d, which was initially microinjected with the nuclear marker H2B-GFP. Embryos are seen from a lateral view. Animal pole is up. **(A-B)** 2 days after the egg was injected the bilateral symmetry of the embryos is established. The horizontal division of the large cell $4d^2$ has taken place (left and right daughter cells depicted by their green nuclei). $4d^1$ and descendants are not visible. **(C-D)** 4d descendants continue to divide. Most vegetally seen is the small macromere 4D (white arrowhead) indicating that macromere 3D was initially injected. This cell (4D) can be used as a landmark for the vegetal side. **(E-F)** Bilateral symmetry of the bands of mesoderm is visible (left and right side of white dashed band). Scale bars are 100 µm. Dpo = days post oviposition.

One of these embryos was fixed at a much more advanced stage (7 dpo) and used for 3 dimensional reconstructions and deconvolution. The GFP signal present in descendants of 4d was also counterstained with Rhodamine-Phalloidin to visualise F-actin of newly forming musculature (Figure 4.15) (see Video 5). From this it was seen that in this embryo, none of the cells deriving from 4d was present in the epidermis in line with the expectation that 4d is forming mesoderm.

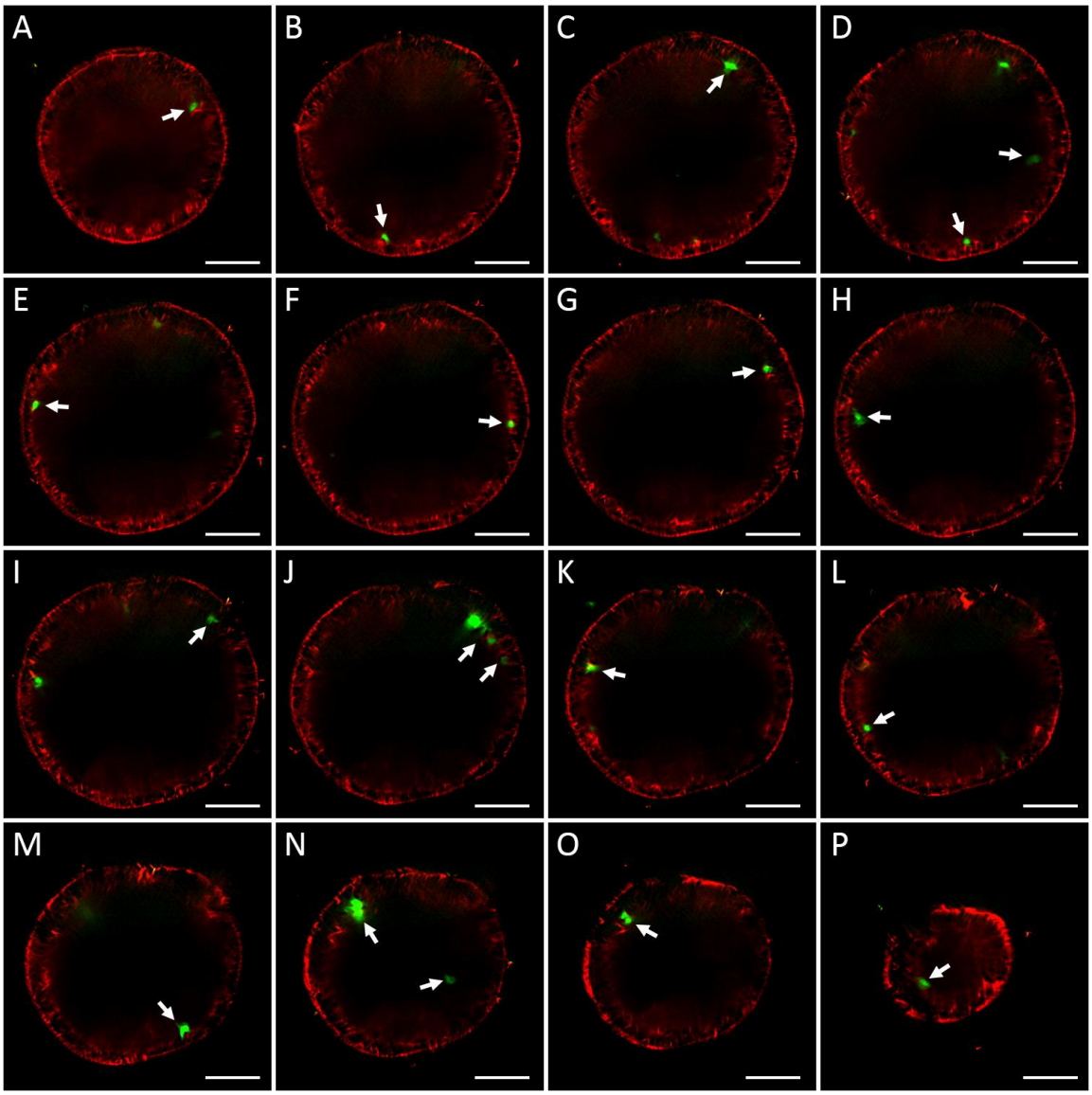


Figure 4.15 – Slices through a 3d-reconstructed z-stack of a 7-day old *M. crozieri* embryo post gastrulation, which was initially injected 25 hpo into the 4d blastomere (A-P). The nuclei of its descendants can be seen marked green (GFP) and are also indicated by white arrows. None of the nuclei acquired an epidermal fate. Labelled F-Actin is shown in red. Scale bars are 50 µm.

Notably a few nuclei of this embryo were specifically found in close proximity to cells of the dorsoventrally-forming musculature, suggesting that some descendants of 4d gave rise to mesoderm by differentiating into mature muscle cells (Figure 4.16). This also suggests that micromere 4d fulfils its expected fate as a mesoderm precursor cell. All other embryos developed by day 11 into swimming 8-lobed Müller's larvae, where they were subjected to a 1-2 hour EdU pulse before fixation.

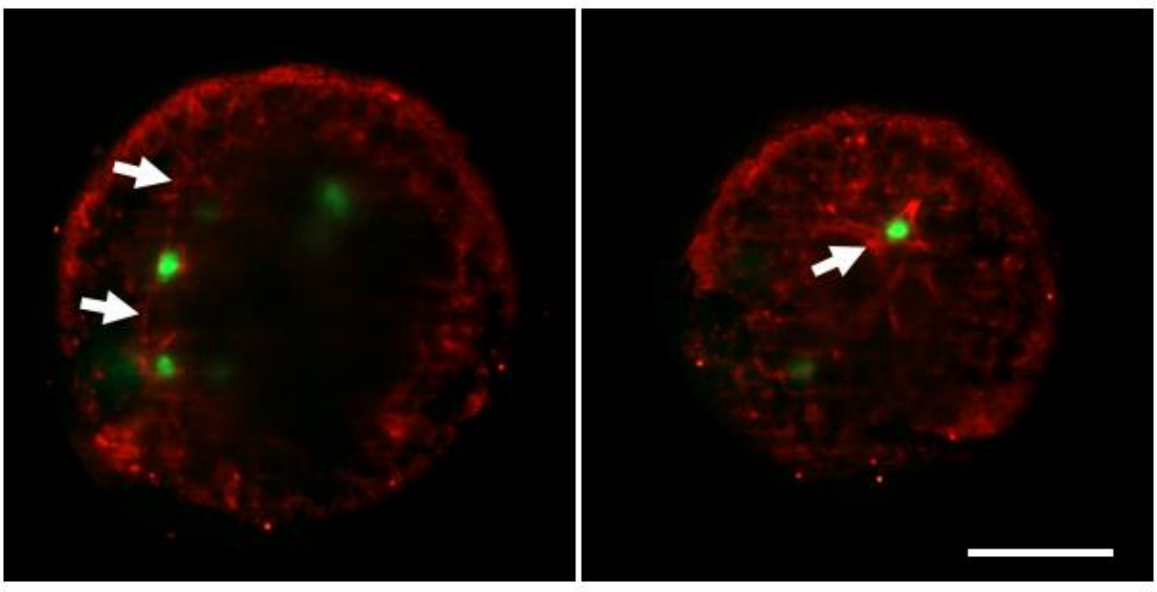

Figure 4.16 - Same embryo as in Figure 4.15 with focus on a few derivatives of the injected 4d blastomeres in form of GFP positive nuclei, which are nested within muscle fibres stained with phalloidin for F-Actin (red). Scale bar is 50 µm.

### *4.6.2 EdU pulse experiments in combination with 4d injections*

In adult flatworms, EdU staining reveals a continuously proliferative pool of so called neoblasts, which are distributed throughout the mesenchymal tissue. Neoblasts are the only proliferating cells in flatworms, and therefore can incorporate EdU into the DNA during their S-phase. Neoblasts have the remarkable capability to differentiate into any cell type

including the germ line. This unique stem cell system of neoblasts is thought to be the key for the remarkable regenerative capabilities found in so many different flatworms. Rhabditophoran flatworms renew their epidermal tissue exclusively from the previously described mesodermal neoblasts (Egger et al., 2009 and citations therein). The epidermis itself is, however, always free of neoblasts. Therefore, any EdU pulse experiments, which stain neoblasts during their S-phase, should not show any positive signal within the epidermis of the flatworm but rather should indicate the mesenchymal tissue located between the epidermis and the gastrodermis. For this reason, we expect EdU positive cells also in polyclad larvae to indicate mostly mesodermally derived tissue. Therefore, if GFP-positive signal of 4d-injected derivatives are not visible within the epidermis of the larvae, but are rather distributed in areas where EdU-positive cells frequently show up, this observation would indicate also a likely mesodermal fate of the 4d blastomere.

We first tested EdU staining on a series of Müller's larvae to determine if the pattern is similar to the distribution of neoblast stem cells found in juvenile or adult flatworms (Figure 4.17). Similar to a preliminary test on Müller's larvae performed with BrdU instead of EdU (Lapraz et al., 2013), epidermal cells were devoid of any positive EdU labeled nuclei (n=20), which can be particularly well seen in lobes and the oral hood (Figure 4.17). When looking at Müller's larvae from the ventral or anterior view, we noticed that EdU positive cells appear to be distributed in two main lateral stripes, an observation which is similar to descriptions of adult flatworms, e.g. the basal branching flatworm *Macrostomum lignano* (Ladurner et al., 2000; Rieger, 1994).

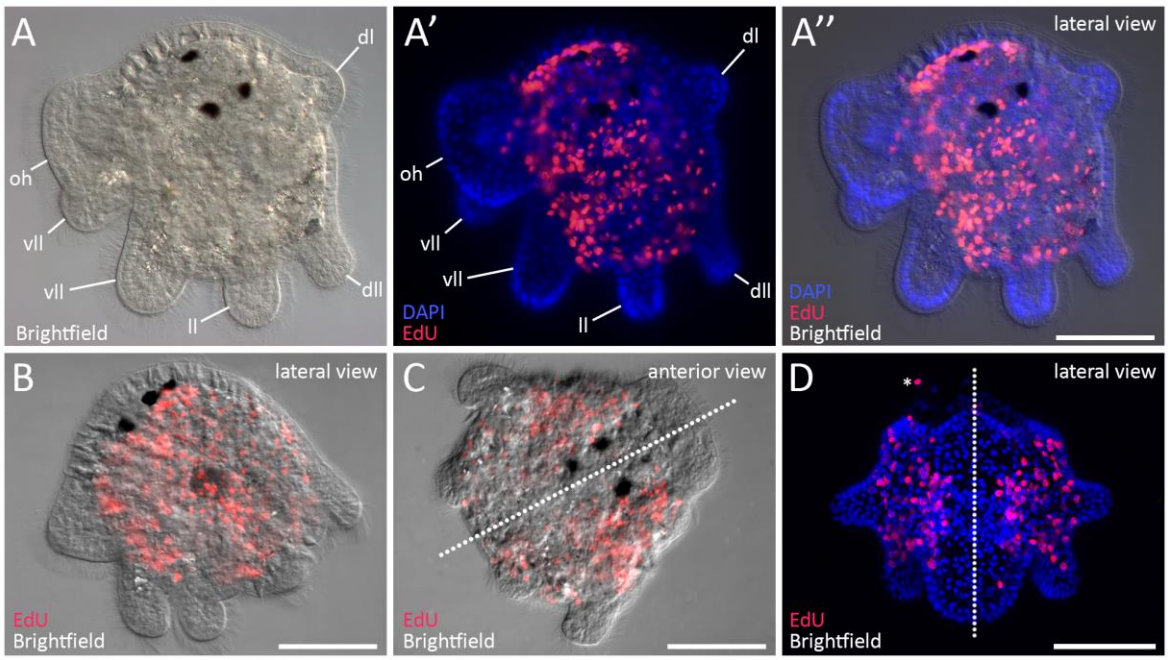


Figure 4.17 - Fixed and stained 8-lobed Müller's larvae, which were previously labeled for S-phase cells with a 1 hour pulse of 10 µM EdU. **(A)** Brightfield image showing the lateral view of a Müller's larvae. **(A')** Same larvae visualised for DAPI staining and EdU positive cells **(A'')** merge of all three channels. It is obvious that cell proliferation does not take place in ectodermal tissue thus lobes and epidermis completely lack any EdU positive signal. **(B)** Further examples of an EdU stained Müller's larva showing the same result. **(C-D)** apical view of a Müller's larvae showing the bilateral distribution of EdU positive cells. D is the only picture acquired by confocal imaging. Next to the asterisk is a EdU labelled cell, which is detached from the rest of larval body, perhaps due to the squeeze preparation. (oh) oral hood, (dl) dorsal lobe, (vll) ventro-lateral lobe, (ll) lateral lobe, (dll) dorso-lateral lobe. Images captured with an Axioimager M1 Epifluorescence and Brightfield Microscope (Zeiss). Scale bar = 100 µm.

4d-injected 11 day old Müller's larvae neither EdU positive cells nor 4d descendants were present within the epidermal layers of the larvae, however an overlap between the EdU positive cells and GFP positive nuclei could never be determined, even when looking at z-stacks of confocal imaging Figure 4.18, A-C). Notably, this is also true for control larvae, where the one-cell stage was injected instead of micromere 4d. In these control injections, the GFP signal only partially overlaps with the nuclei stained with DAPI (Figure 4.18, D) and no overlap between EdU positive cells and cells containing GFP positive nuclei is visible. This suggests that the high proliferation rate of non-ectodermal larval tissue (presumably mostly mesoderm) has diluted the GFP signal initially present in nuclei of cells to an extent where an overlap of initially GFP positive cells with later stained EdU positive cells is not detectable anymore.

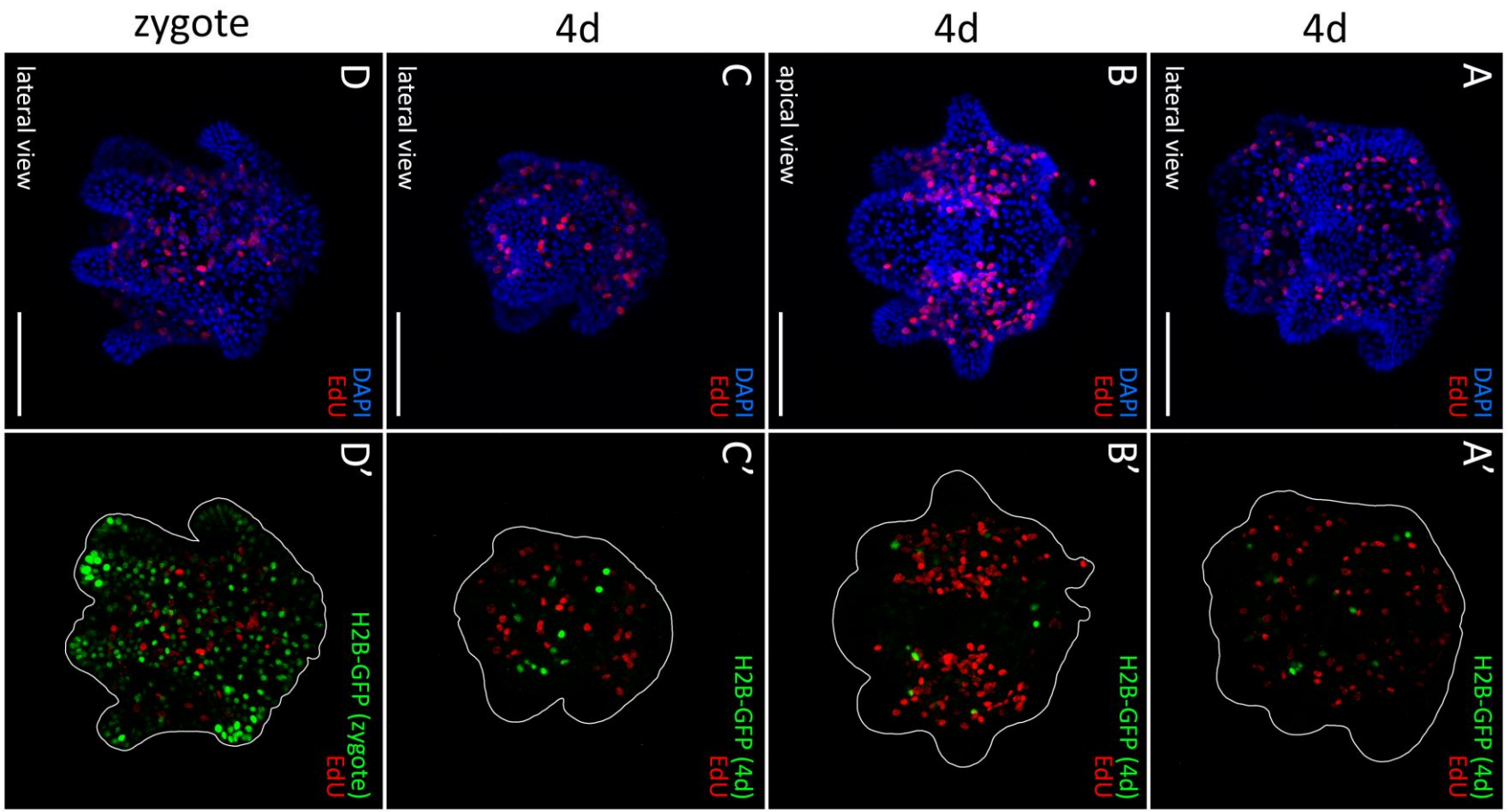


Figure 4.18 - EdU positive cells after a 10 µM 2-hour pulse in Müller's larva, which were microinjected 11 days earlier either in micromere 4d or 1-cell stage zygote **(A-C)** EdU staining in larvae counterstained with DAPI and microinjected for micromere 4d. **(A'-C')** Same larvae showing EdU positive cells merged with GFP positive after microinjections with histone marker H2B-GFP into micromere 4d and followed through embryogenesis for 11 days into the Müller's larva. **(D)** A larva from same batch of embryos showing EdU positive cells microinjected with histone marker H2B-GFP into the zygote. **(D')** Same larvae showing EdU positive cells and GFP signal descendants microinjected into the zygote. Images acquired with a Leica TCS SP8 MP confocal laser scanning microscope. Scale Bars are 50 µm.

### 4.7 Embryonic vegetal cross-furrow cells give rise to the D quadrant

Embryos with typical spiral quartet cleavage will at some point during early development specify the so-called D-quadrant. In unequal cleavers at the 4-cell stage the D-quadrant would be the largest of the four cells and also one of the vegetal cross-furrow cells (i.e. one of the pair of opposing cells which make contact at the vegetal poles), which acquires a D quadrant specific fate. We wanted to find out if one of the vegetal cross-furrow blastomeres seen in the 4-cell stage of *M. crozieri* is consistently destined to become the D-quadrant. This can be achieved using our live-imaging data by ascertaining which of these cells becomes the definitive D quadrant in bilaterally symmetric *M. crozieri* embryos. In those embryos where radial symmetry breaking divisions of micromere 4d have already occurred, we can follow the quadrant back to its ancestral cell at four/eight cell stage. Micromere $4d^2$ is easily identified due to its horizontal division plane and large size (indicated in Figure 4.19 A by the pair of white arrowheads in embryo i-iv). We manually traced $4d^2$ back to its vegetal macromeres at the 8-cell stage (n=7; indicated by a white asterisk in Figure 4.19, B). At this stage the correct identification of vegetal and animal cross furrow cells can be identified (Figure 4.19, indicated by dashed lines). Our reverse tracking approach reveals that without exception (n=7/7) $4d^2$ originates from one of these vegetal cross-furrow cells. (Figure 4.19, B marked by white asterisk). Since cleavage furrows of 4- and 8-cell stages are identical at this early stage it becomes clear that one of the vegetal cross-furrow cells is already determined to become the D quadrant at the 4-cell stage.

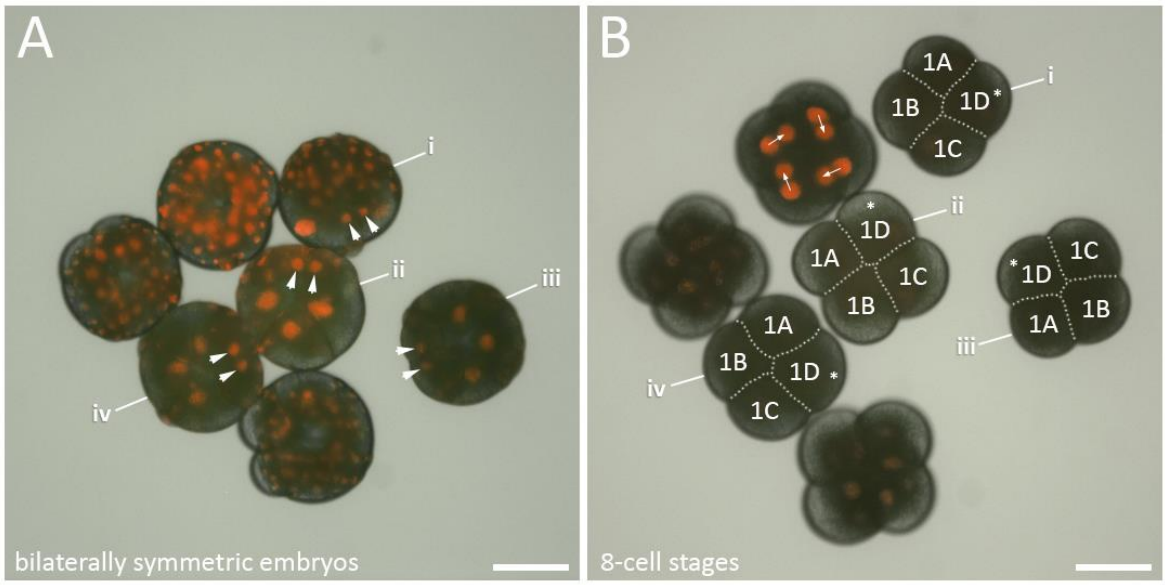


Figure 4.19 - Identification of the D quadrant in 8-cell stages of *M. crozieri* via reverse tracking of the bilateral dividing $4d^2$. **(A)** Embryos after they have acquired a bilaterally symmetric shape following the division of 4d. Both daughter cells of $4d^2$ are highlighted by white arrowheads in embryos i-iv and clearly indicate the D quadrant of the embryo. This information has been used to identify the origin of the D quadrant in 8-cell staged embryos of A by reverse tracking of these cells. **(B)** 8-cell stages of the same *M. crozieri* embryos as seen in A. Embryos labelled i-iv are seen from the vegetal side and cross-furrows have been highlighted with a white, dashed line. All other embryos are seen from the animal side with one embryo in which its dexiotropic cleavage pattern has been indicated by white arrows. The white asterisk in each embryo seen from the vegetal pole indicates the end of the reversed tracking and thereby identifying macromere 1D, which is connected via the vegetal cross-furrow to the B blastomere (positioned opposite). Blastomeres A and C are in touch with blastomere D and B but not with each other. Scalebar = 100 µm.

### 4.8 All blastomeres are equal, but some blastomeres are more equal than others

*M. crozieri* has previously been described as an equal cleaver (Rawlinson 2010; Lapraz 2013) been. Rawlinson already pointed out that the similar sizes of blastomeres at the 4-cell stage makes D quadrant identification difficult. What most clearly separates an unequal cleaver from an equal cleaver is the presence of an enlarged D blastomere. To clarify whether *M. crozieri* is indeed an equal cleaving embryo or might have inconspicuously

different blastomere sizes we performed a series of precise blastomere volume measurements during the first and second cleavages. These allowed us to explore the possibility of an early D quadrant specification, similar to unequal cleavers, in *M. crozieri* 4-cell stages using SPIM microscopy.

For this purpose, we 3D reconstructed 25 fixed embryos between the 2- and 4-cell stages. Interestingly, a significant difference of 6% in volume size could on average be discerned even at the 2-cell stage (n=13/13) (Figure 4.20, C and Figure 4.21). In two embryos, which went through a 3-cell stage, the volumes of the two smaller cells also differ slightly (Figure 4.20, D and Figure 4.21). The volume of the remaining larger blastomere, which is still in a state before its second cleavage, is smaller than the combined volume of the two smaller cells.

Individual blastomeres of 4-cell stage embryos showed that one cell was always significantly larger than all other three blastomeres (Figure 4.20, E and Figure 4.21). Interestingly, whenever the cross-furrow of 4-cell stage embryos was clearly recognisable (in 8/10 cases) the largest cell is invariably one of the vegetal cross-furrow cells consistent with this being the D quadrant (see above).

This finding clearly resembles the type of unequal cleavers as seen in other spiralian embryos and one could conclude that precise volume measurements are a necessity to reveal the unequal size of blastomeres as we have demonstrated here via multi view 3d reconstructions.

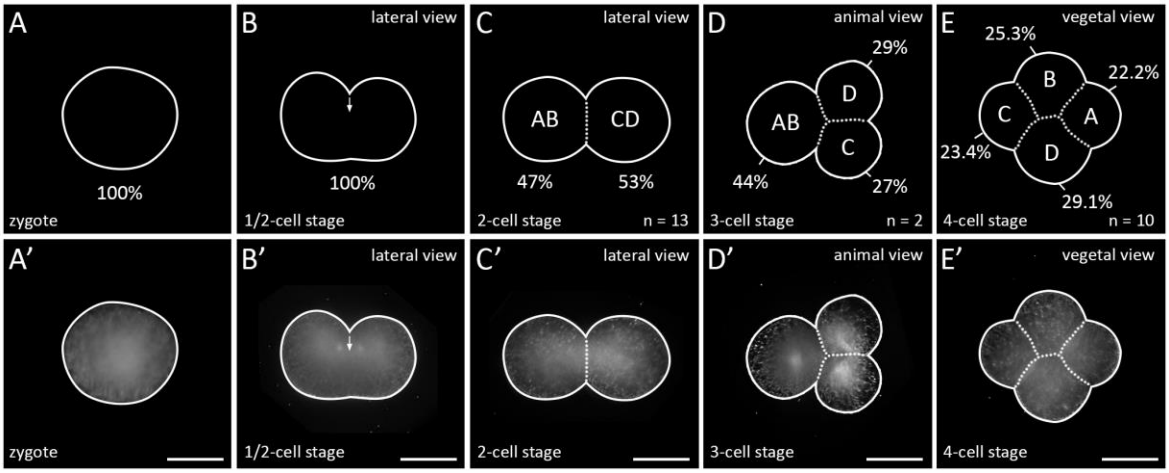


Figure 4.20 - Averaged volume measurements in *M. crozieri* blastomeres of embryos going through the first and second cleavages. **(A-E)** Volumes are given as a percentage of the volume of the total embryo, which is 100%. **(C)** At the 2-cell stage the larger cell is assumed to represent blastomere CD and the smaller cell blastomere AB. **(D)** At the 3-cell stage blastomere CD most likely precedes the division of blastomere AB. **(E)** At the 4-cell stage the largest blastomere is always one of the vegetal cross-furrow cells and is interpreted as the D blastomere. **(A'-E')** All volume measurements come from 5-angle 3D-multiview reconstructions and have been orientated with a view from their vegetal side. Only a single plane of the 3D reconstructed stack is shown. Scalebar = 100 µm.

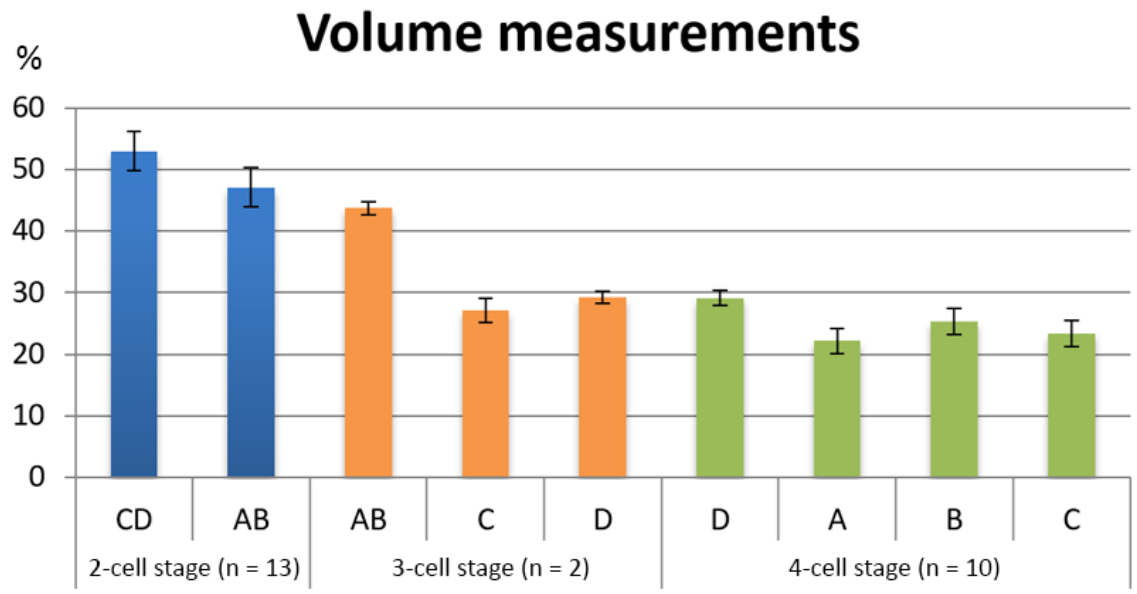


Figure 4.21 - An average of the volume measurements of 3D-reconstructed blastomeres in *M. crozieri* embryos of the 2-cell, 3-cell and 4-cell stages. The data are based on measurements of individual blastomeres. To provide the data as percentages makes sense as each individual embryo can vary in size. The 2-cell stages are indicated as blue columns (n=13), 3-cell stages as orange (n=2) and 4-cell stages as green columns (n=13). Volumes are given as a percentage of the total volume of the embryo which is 100%. Standard deviations are indicated for smaller blastomeres only. In two cell stages a 6% difference was noted between the two cells on average. In 3-cell stages the two sister blastomeres (C and D) show on average a 2% difference. In 4-cell stages the largest blastomere (indicated as D) is almost 5.8% larger compared to its sister cells (indicated as C). Of the two remaining sister blastomeres, the size difference is only 3.3% (with the larger one indicated as blastomere B).

# Discussion

## 4.9 Cytoplasmic perturbations are common during the early development of M. crozieri

During egg maturation and after fertilisation, animal oocytes typically undergo obvious changes. Examples are the fusion of sperm and egg pronuclei, the addition of centrioles to the ooplasm, the activation of metabolic pathways and the localisation of important materials in specific parts of the oocyte. An increased activity of the cytoskeleton resulting in deformations of the egg's cytoplasm and increased egg contractility is often observed during this period. This is usually thought to be a sign of the oocyte segregating cell content (Wall, 1990). In polyclad flatworms, *M. crozieri* included, similar changes have been observed several times during egg maturation, where this process is best known as cell blebbing and is linked to the extrusion of the polar bodies. Our current knowledge of such cytoplasmic perturbations in polyclads was recently summarised by Gammoudi (2012).

In several animal phyla, including other lophotrochozoans such as gastropods and annelids, oocytes also undergo cytoplasmic changes (usually after fertilization and during meiosis) (Dettlaff and Vassetzky, 1991; Henry et al., 2006; Lehmann and Hadorn, 1946). In *Platynereis dumerilii* cytoplasmic movements have been described to induce a flow of clear cytoplasm starting from the centre of the egg towards the animal pole, while at the same time granules and lipid droplets accumulate at the vegetal pole of the zygote (Costello, 1945; Dorresteijn, 1990; Dorresteijn and Fischer, 1988). Outside the Lophotrochozoa, amoeboid movements have been found for instance in the eggs of nematodes (Spek, 1918).

In amphibians so called surface contraction waves (SCW) have been described first in axolotl eggs (Hara, 1971) and later also in *Xenopus laevis* ((Yoneda et al., 1982). Several other animal models have eggs that undergo a process called cytoplasmic streaming, described in *Caenorhabditis elegans*, *Drosophila melanogaster*, ascidians, zebrafish and also mice. Cytoplasmic streaming happens either during late oogenesis or at meiosis (Li and Albertini, 2013). It appears that cytoplasmic perturbations are common in many animal oocytes, especially after fertilization or egg maturation, and often noticeable by cytoplasmic changes based on an in increased cytoskeletal activity.

In *M. crozieri* and a few other cases it has been demonstrated that such cytoplasmic perturbations are not restricted to egg maturation alone but sometimes can return frequently during early cleavage (Gammoudi et al., 2012; Malakhov & Trubitsina, 1998; Teshirogi et al., 1981; this study). In *M. crozieri* we noted that the cleavage of macromeres that bud off the micromere quartets as depicted in Figure 4.8 are dynamic divisions (deforming the cell shape), possibly due to the large size of macromeres and the large amount of yolk contained within them. The formation of vesicle-like protuberances in all four macromeres are noticeable during the more or less synchronous 5th cleavage divisions of 2A-2D (at the transition from the 16- to 32-cell stage). Additionally, the appearance of cytoplasmic perturbations becomes especially clear during the formation of the fourth quartet (Figure 4.10). Conspicuously, when we mounted embryos in high concentrations of agarose (>0.6%), we observed severely abnormal development beyond the point where the fourth quartet formed (n=5). We speculate that cytoplasmic movements are severely restricted by the solidity of higher concentrations of agarose and the defects observed

suggest these movements are essential for normal development. In general, their appearance can be difficult to observe without live-imaging due to their short persistence and this might be one reason why such descriptions are scarce. However, very similar perturbations as observed in *M. crozieri* during divisions of macromeres 2A-2D have also been depicted in a second polyclad species, *Pseudostylochus intermedius* (Teshirogi et al., 1981), but one division round earlier (8- to 16-cell stage). In the common pond snail *Lymnaea stagnalis*, so called RNA-containing ectosomes have been described. In this case, ectosomes are extracellular vesicles, which appear likewise on the third-generation macromeres in the snail, where they interact with micromeres of the animal pole via gap junctions. The vesicles in the snail behave differently in macromere 3D when compared to its counterpart macromeres 3A-3C - ectosomes of the latter three macromeres become much more compact, while the ectosomes of macromere 3D are ultimately dispersed (Dohmen and Van de Mast, 1978; van den Biggelaar, 1976). A similar function of the vesicle-like protuberances observed in *M. crozieri* macromeres 2A-2D is possible but their presence during macromere divisions make a cytoskeletal rather than ectosomal cause more likely (Figure 4.11). The same might be true for the even more pronounced cytoplasmic perturbations during the divisions of macromeres 3A-3D. We have also shown some preliminary evidence that polar lobes might occur during the early cleavages in *M. crozieri* (2-cell to 4-cell stages), however this finding needs to be further investigated. In general, only few observations of cytoplasmic protuberances accompanying the early cleavage pattern of polyclad flatworms are available.

A model to better understand the mechanism of cytoplasmic perturbations in cells such as blebbing, and other cellular forces like cell migration or cell division, is based on the idea of local breakage of the cortical actomyosin meshwork (Paluch 2005). Rapid cell shape changes, cell movements, the resistance to external mechanical stress, the capability to oppose intracellular osmotic pressure and other dynamic cellular forces all depend on the actomyosin cortex of animal cells. This thin layer is located underneath the plasma membrane and can be seen as a highly dynamic cross-linked gel comprised of actin, the main component that gives stiffness to the cell, myosin motors, which add contractile forces to the meshwork and keep the actin under tension, as well as a variety of actin-binding proteins (see Paluch 2005 & Guillaume 2012). In short, the mechanism leading e.g. to blebbing can be triggered by spontaneous raptures within the actomyosin gel driven by increased localized activity of myosin II. Cytoplasm is then extruded through the resulting cortical hole and a protrusion grows, which is reversed during the process of the formation of a new actin network within the bulge that subsequently serves as a substrate for the myosin motors to attach. This phenomenon is described as cortical oscillations and underlines an intrinsic instability of the cortical actomyosin system. Such a mechanism might be involved also in the observed cytoplasmic perturbations of polyclad flatworms, which in Figure 4.22 are summarised as described previously in polyclad flatworms, together with our own observations of the early development of *M. crozieri*.

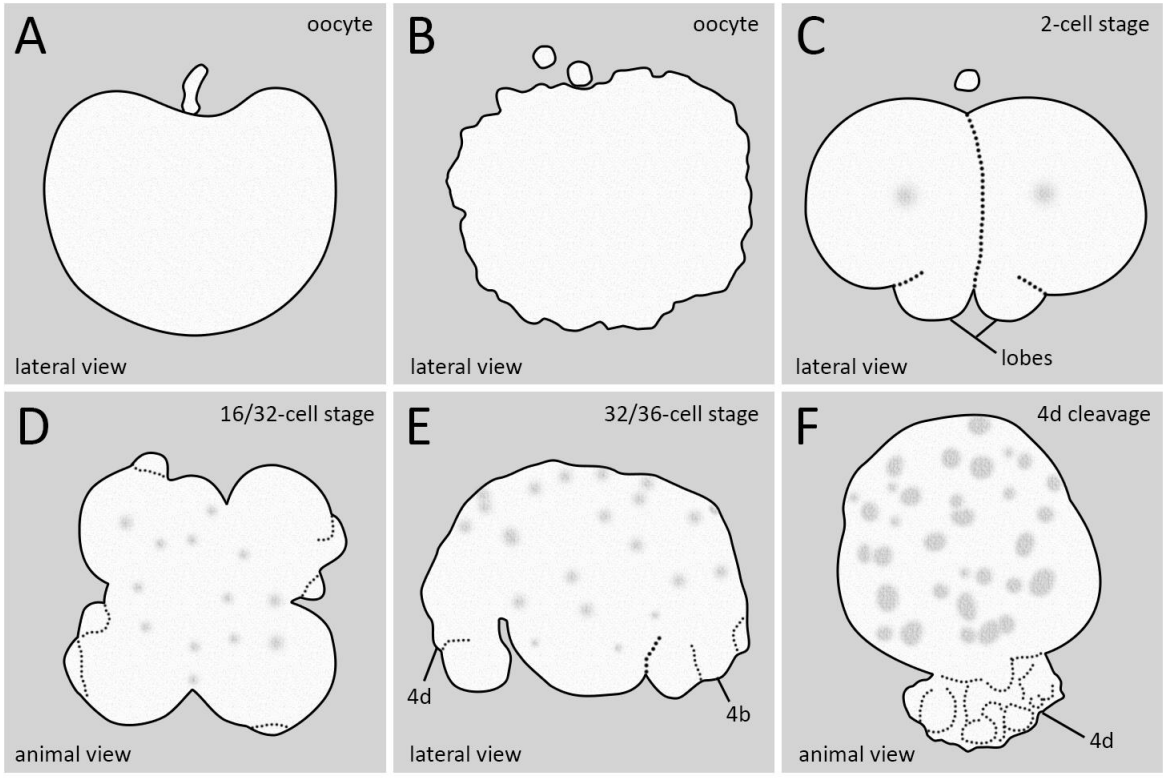


Figure 4.22 - Summary of cytoplasmic perturbations found in different polyclad flatworm species. **(A)** Depression of the animal pole during the formation of the first polar body described by Kato (1940) for some Japanese polyclad species and for *Maritigrella crozieri* (this study). **(B)** Cell blebbing in oocytes as described for most polyclads during the first and second meiotic divisions (see Gammoudi et al. 2012). (**C)** Vegetal lobe like structures found in *Pseudostylochus intermedius* (Teshirogi & Sachiko, 1981) and *Pseudoceros japonicus* (Malakhov and Trubitsina, 1998). Drawing taken from *P. intermedius* **(D)** Cytoplasmic perturbations seen in *Pseudostylochus intermedius* (8- to 16-cell stage) (Teshirogi & Sachiko, 1981) and *Maritigrella crozieri* (16- to 32-cell stage, this study). **(E)** Waves of contractile activity in all four macromeres of *Maritigrella crozieri* (this study) whereby macromeres attain an elongated shape. **(F)** Similar cytoplasmic perturbations seen during the highly asymmetric cleavage of micromere 4d found in *Maritigrella crozieri* (this study).

## 4.10 Volume measurements of macromeres A, B, C and D suggest an unequal cleavage mechanism for *M. crozieri* embryos

As discussed in the introduction of this Chapter and also in Chapter I, unequal cleavers are characterised by an enlarged cell volume in one of the four macromeres, which is already specified to give rise to the D quadrant lineage and is therefore referred to as the D macromere. In such a case, an inductive mechanism (cell-cell contacts), in order to specify the D-quadrant, is usually not observed, as (still unknown) determining factors have already been shunted into the D macromere at the 4-cell stage.

Slight size differences at 4-cell stages have been reported several times in polyclad flatworms (Anderson, 1977; Kato, 1940; Lang, 1884; Surface, 1907; Teshirogi et al., 1981). Despite these descriptions, polyclad flatworms are often considered more or less equal cleavers (Martín-Durán and Egger, 2012). This implies conditional specification of the D quadrant via an inductive cell-cell interaction, known from other equal cleavers.

This uncertainty of being an equal or unequal cleaver is also true for the polyclad *H. inquilina*, where Surface (1907) already mentions a slightly enlarged D blastomeres in 2 and 4-cell stages and later Boyer stated – despite having difficulties identifying a definitive D blastomere – that at least the two vegetal cross-furrow cells are larger compared to their two counterpart animal blastomeres. Our 2- and in particular our 4-cell stage volume measurements suggest that in *M. crozieri* embryos a mechanism exists that actively produces vegetal cross-furrow blastomeres, namely B and D, which have a larger volume on average (Figure 4.20; Figure 4.21). Therefore, it appears that one macromere, most likely macromere D, receives the largest amount of cytoplasm, as has been suggested for

*H. inquilina* by Surface (1907). This suggests that *M. crozieri* tends to follow an unequal D quadrant specification mechanism.

This being said, the precise mechanism for the D blastomere specification in unequal cleavers is still only poorly understood and based on the idea of obvious, asymmetric distribution of inheriting key determinants, which are eventually shifted into the D macromere at the 4-cell stage. Unfortunately, these determinants are not known yet and there is also the possibility many of them might get segregated during the first two cleavages without concomitants in terms of unequal cell sizes (or e.g. the production of obvious structures such as polar lobes). At least in polyclad flatworms it seems that asymmetric cleavages do play a role during the first two cleavages as shown by our volume measurements. These differences are, however, very subtle and cannot be detected by traditional microscopy. This might explain why it comes so often to conflicting statements regarding the true size of blastomeres in polyclad flatworms.

## 4.11 Unequal cleavage in *M. crozieri* does not rule out the possibility of an inductive mechanism to specify the D quadrant

In *M. crozieri*, our reverse tracking approach revealed that $4d^1$ and $4d^2$ originate from one of the vegetal cross-furrow cells already in the 4-cell stage (Figure 4.19). This finding matches Boyer's observations in embryos of the polyclad *H. inquilina* where deletion experiments in 8-cell stages showed the importance of vegetal cross-furrow blastomeres for establishing bilateral symmetry during development (Boyer, 1989). In the polyclad *H.*

*inquilina* Boyer noted that a loss of two micromeres at the 8-cell stage results in problems for a correct establishment of bilateral symmetry and as an explanation pointed out that an early cell-cell interaction mechanism between at least one of the first quartet macromeres (1Q) and the first micromere quartet (1q) (Boyer, 1989) might exist. Such an inductive D quadrant specification has never been shown in any other spiralian embryo at such an early stage. The possibility of an inductive scenario should nonetheless be taken seriously as we know from experiments on equal and dextral cleaving *L. stagnalis* snail embryos, where an inductive mechanism specifies the D-quadrant (Freeman and Lundelius, 1992), their left-right asymmetry is also dictated by a macromere-micromere contacting geometry at the 8-cell stage (Kuroda et al., 2009). If the left-right asymmetry can be established via cell-cell interactions already during the third cleavage, similarly an early specification of the D quadrant lineage is conceivable.

However, the fact that one of the two vegetal cross-furrow macromeres at the 4-cell stage is already determined to give rise to the D quadrant lineage, does not necessarily suggest that *M. crozieri* embryos behave strictly as unequal cleavers, where the D quadrant lineage is already specified at the 4-cell stage.

One example, why we cannot jump to such a conclusion, can be taken from equal cleaving gastropods. In the pond snail *L. stagnalis*, blastomeres of the 4-cell stage are of equal size and similarly to *M. crozieri,* both sister cells, A/C and B/D, can be distinguished from their cross-furrow position. It could be shown in *L. stagnalis* that one of the vegetal cross-furrow macromeres at the 4-cell stage will give rise to the D quadrant lineage. The embryo, however, clearly uses an inductive mechanism for specifying its D quadrant later on

(Freeman and Lundelius, 1992). This example makes clear that early determination of one macromere is not equal to true specification as seen in unequal cleavers.

### 4.12 4d cleavage: another example of the onset of bilateral symmetry in polyclad flatworms

In spiral cleavers, the direct progeny of macromere 3D (i.e. micromere 4d), which typically divides into left and right daughters thus breaking the embryo's radial symmetry, often gives rise to the mesoderm and often also to parts of the endoderm (see Lyons & Henry, 2014). In such cases 4d is referred to as the mesentoblast. In the polyclad *H. inquilina* 4d also gives rise to mesodermal structures such as longitudinal, diagonal, and oral hood muscles as well as mesenchyme and some endoderm (Boyer et al., 1998). This agrees with Surface's observations of $4d^1$ giving rise to the mesoderm and entoblast (Surface, 1907). Additionally, Surface and later van den Biggelaar (1996) noted that in polyclads the cleavage pattern of 4d differs from its canonical fate of an immediate horizontal, equal division into a left and right descendant, $4d^1$ and $4d^2$. According to van den Biggelaar – taking also the descriptions of Surface into account – this division is delayed in the polyclad *Hoploplana inquilina* and in *Prostheceraeus* by one cell cycle. In such cases 4d first undergoes an approximately animal-vegetal (a-v) division into $4d^1$ and $4d^2$ which is then followed by horizontal cleavages of both $4d^1$ and $4d^2$. Van den Biggelaar suggested that the animal positioned cell $4d^1$ corresponds to the molluscan and annelid mesentoblast (also reviewed by Martin-Duran & Egger, 2012). However, in more recent descriptions of polyclad flatworms (Malakhov and Trubitsina, 1998; Rawlinson, 2010; Teshirogi et al., 1981;

Younossi-Hartenstein and Hartenstein, 2000) it appears that this additional division of $4d^1$ remains un-noted, suggesting that either some polyclad flatworms lack the a/v division of $4d^1$ or, as seems more likely, careful serial sectioning or the use of live imaging, with optical sections, is necessary to reveal it. *Maritigrella* and *Prostheceraeus* are members of the large order of polyclads, the Cotylea; together with the observations made by Surface (1907) in an acotylean polyclad flatworm, the common conservation of the a/v cleavage of 4d suggests this it is the primitive state of the Polycladida.

### 4.13 The 4d blastomere in *M. crozieri* shows signs of mesodermal formation

In the last few decades studies in annelids, molluscs, nemertines and polyclad flatworms (Ackermann et al., 2005; Anderson, 1973; Chan and Lambert, 2014; Damen, 1994; Damen and Dictus, 1994; Fischer and Arendt, 2013; Hejnol et al., 2007; Henry and Martindale, 1994; Henry and Martindale, 1998; Meyer and Seaver, 2010) were performed using cell lineage tracers and the derivatives of individual quartets were followed more precisely and in higher resolution than was possible in classical studies of the late 19$^{th}$ century. The consensus of these reinvestigations is that the first three quartets of micromeres form ectodermal structures of which the second and/or third quartet usually provides a second source of mesoderm called the ectomesoderm. Endoderm is restricted to fourth quartet micromeres and macromeres and essentially in all species the 4d blastomere gives rise to mesoderm (and some endoderm) and is therefore often referred to as the mesentoblast. This specific endomesodermal fate of 4d also appears to be the case for polyclad flatworms, although the cleavage behaviour of cell 4d deviates slightly from the canonical division

pattern. In polyclads, the mesentoblast is not 4d as such but one or both of its daughter cells, and therefore delayed by one generation of cell divisions (see Martin-Duran & Egger, 2012; van den Biggelaar, Dictus, & van Loon, 1997). In the polyclad flatworm *H. inquilina,* Surface (1907) has shown that the descendants of 4d form mesodermal bands resembling those found in annelids and molluscs and Boyer et al. (1998) showed that mesoderm is derived from ectodermal blastomere 2b and the 4d blastomere. *H. inquilina* is the only flatworm species where the origin of mesoderm has been described.

### *4.13.1 4d blastomere injections give rise to bilaterally symmetric bands and 4d descendants show a mesodermal, neoblast-like distribution pattern*

Regeneration in flatworms is based on pluripotent stem cells (Wagner et al., 2011) called neoblasts, which are the only proliferative cells, distributed throughout parenchyma, which typically indicates the mesodermal tissue between epidermis and gut in Platyhelminthes. In general neoblast stem cells are also not present in the anterior most head region above the eyes and are absent from the pharynx (Baguñà, 1976).

So far it is unknown whether Müller's larvae of polyclad flatworms can regenerate or not. If so, one assumption would be that the regenerative process will be based on a stem cell population called neoblasts that are well known to drive the remarkable regenerative capabilities in adult flatworms. In Müller's larvae BrdU staining (Lapraz et al. 2013) as well as EdU staining consistently showed an absence of EdU positive pulsed cells from ectoderm derived epidermal tissue. The same is true for EdU positive neoblast stem cells of other rhabditophoran flatworms, where the epidermis is known to be exclusively renewed by

mesodermally located neoblasts (Drobysheva, 1988; Gustafsson, 1976; Ladurner et al., 2000; MacKinnon et al., 1981; Newmark and Sánchez Alvarado, 2000).

Notably we also observed lateral distribution of EdU-positive nuclei along the anterior-posterior axis of the larvae with EdU positive cells absent from the primitive mouth and midline (Figure 4.17, B). It is interesting that similar observations for distributions of neoblast stem cells have also been made in another early branching flatworm, *Macrostomum lignano* (Ladurner et al., 2000; Rieger et al., 1994).

Additionally, a single study on embryos and larvae of the polyclad flatworm *Cycloporus japonicus* has shown that in embryos at the stage of organogenesis and in later larval stages, no mitosis was detected in the intestine, but occurred in mesodermal (mesenchymal) cells (Drobysheva and Yurij, 2001). Together with our observation that proliferating cells are absent within the epidermis of *M. crozieri* larvae this would constrain mitosis exclusively to mesodermal tissue. Therefore, it seems that the use of BrdU/EdU staining performed in several day old polyclad larvae seems to be a suitable marker for mesodermal tissue and that a potential overlap of the area where GFP-positive nuclei derived from the 4d blastomere are detected would be another indicator for the 4d blastomere giving rise to mesodermal tissue.

Our observations on the distribution of the early descendants of the 4d blastomeres show they are first formed in bilaterally symmetric bands, which can vary slightly in shape (Figure 4.14). Similar observations were also made by Surface (1907) on *H. inquilina*.

Embryos, in which histone-GFP had been injected into 4d and which were raised for 11 days into free swimming, 8-lobed Müller's larvae show that GFP-positive nuclei are distributed

throughout the inner tissues, similarly to EdU positive cells. At this stage no GFP or EdU signal could be observed within ectodermal structures such as lobes or epidermis (Figure 4.18) and further supports the assumption that many of the 4d derived cells have acquired a mesodermal fate.

But the strongest evidence in *M. crozieri* of a mesodermal fate for at least a subpopulation of 4d injected cells comes from an embryo, which was 3d-reconstructed with muscle cells counterstained for F-Actin. The fact that some muscle cells showed a clear GFP-positive signal (Figure 4.16) clearly indicates their origin from micromere 4d and thereby points to its mesodermal fate.

# CHAPTER 5 Cell lineage study of *M. crozieri*

## Introduction

In the Lophotrochozoa the conserved spiral cleavage developmental program allows us to identify individual homologous blastomeres across phyla. The specific cell lineages of a given spiral cleaving embryo can therefore be studied and the question asked if the fates of those homologous blastomeres are conserved during embryonic development. It is striking that classical as well as recent cell lineage studies have revealed a strong conservation of several of these lineages and their fates, while deviations from these stereotypical patterns allow us to identify evolutionary changes between spiralian embryos and perhaps to speculate as to the adaptive as to the adaptive explanation for the changes. In this chapter, I focus on the lineage of the first quartet of micromeres (1q), which, in almost all spiral cleavers gives rise to ectodermal structures of the head including eyes, nervous system and apical organ (typically derived from apical rosette cells $1q^1$ (Nielsen, 2004; Nielsen, 2005) as well as anteriorly located parts of the ciliary band. In annelids, molluscs and nemerteans these morphological features originate from similar blastomeres (Damen and Dictus, 1994; Henry et al., 2007; Maslakova et al., 2004a; Maslakova et al., 2004b). Conserved cell-lineages and fate maps of these structures, if present, would be perhaps the strongest indication for homology of polyclad Müllers larvae with trochophore(-like) larvae of other lophotrochozoan phyla.

A major part of this chapter is dedicated specifically to study specifically this question in embryos of the polyclad flatworm *M. crozieri*. We aim to identify homologous blastomeres

giving rise to the apical organ (putatively the apical rosette cells $1q^{111}$) and ciliary band cells (putatively the primary trochoblast $1q^{2}$) in order to find conserved developmental patterns during early embryogenesis. It will be interesting to see if a conservation of other patterns emerges, such as order of spindle orientations (laeotropic versus dexiotropic), relative blastomere sizes and timing of cell divisions, and if so whether they resemble observations among other spiral cleavers. It has been shown that such data sets can be used to for comparative analysis and even to create phylogenies (Guralnick and Lindberg, 2001). We will mainly use it for a comparison with the polyclad flatworm *H. inquilina*, the only flatworm species where a comparable data-set of relative division timings exist.

Ultimately, we aim to follow lineages of different blastomeres for the longest possible time span to determine if they could give rise to similar complex structures in *M. crozieri* as in other lophotrochozoans. To achieve these aims, we use long-term, live-imaging OpenSPIM recordings where blastomeres can be identified early on and lineages of interest adequately traced for a long time. A single particle tracking algorithm is used to automate the tracing of nuclei during most of the first day of development.

## Results

Cell-lineages based on two OpenSPIM 4D live-imaging videos (Video 6 and Video 7) were created and analysed. Due to their size both detailed lineages are accessible as a digital '.svg' file (see CD-ROM). Lineage information obtained by automatic nuclei tracking with the Fiji plugin TrackMate (Tinevez et al., 2016) was extracted up to the 100-cell stage, which allowed us to identify each cell during this period, follow its fate over time and determine its precise timing of division and the spatial orientation of its spindle during mitosis. We decided to only use embryos for our cell-lineage study, that successfully completed epiboly during gastrulation, formed a mouth and showed epidermal cilia activity as well as signs of ciliary band activity (see Figure 5.1 and Video 8). Although an automatic way to detect and even trace nuclei could be used, the position of each individual nuclei at each time-point was manually confirmed and in some cases the nuclei position had to be corrected. Both, the recording of these very long time-lapse recordings at a quality that would allow us to take advantage of Fiji's TrackMate plugin, as well as the manual verification of all time-points, limited our cell-lineage study to only two embryos. Further challenges using this technique on live-embryos in *M. crozieri* are given in Chapter VII.

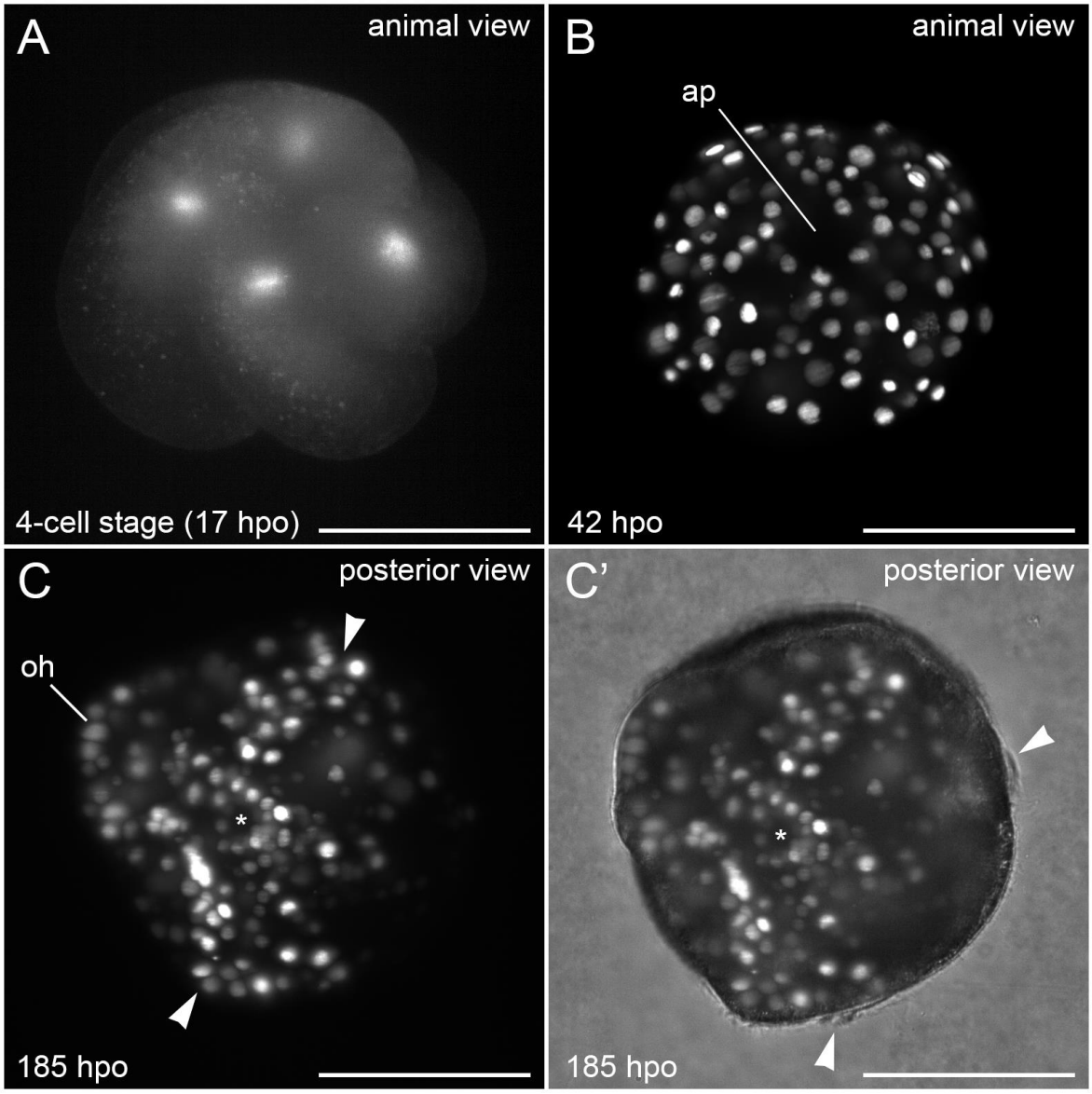


Figure 5.1 - Embryo microinjected with the nuclei marker H2B-GFP and used for cell-lineage tracing. **(A)** Advanced 4-cell stage with signal coming up in all four nuclei about 17 hpo. **(B)** Same embryo as depicted in A, 25 hours later. **(C)** Same embryo as depicted in A and B shown 185 hpo from the posterior view. At this stage larval features, such as lobes (white arrowheads) an oral hood and a mouth (white asterisk), can be seen. **(C')** Brightfield image of the same embryo with arrowheads pointing at ciliary band cells identified by their long cilia. The beating of this cilia and embryonic movements can be seen in Video 8. (ap) apical plate, (oh) oral hood, (hpo) hours post oviposition. Scale bar is 100 µm.

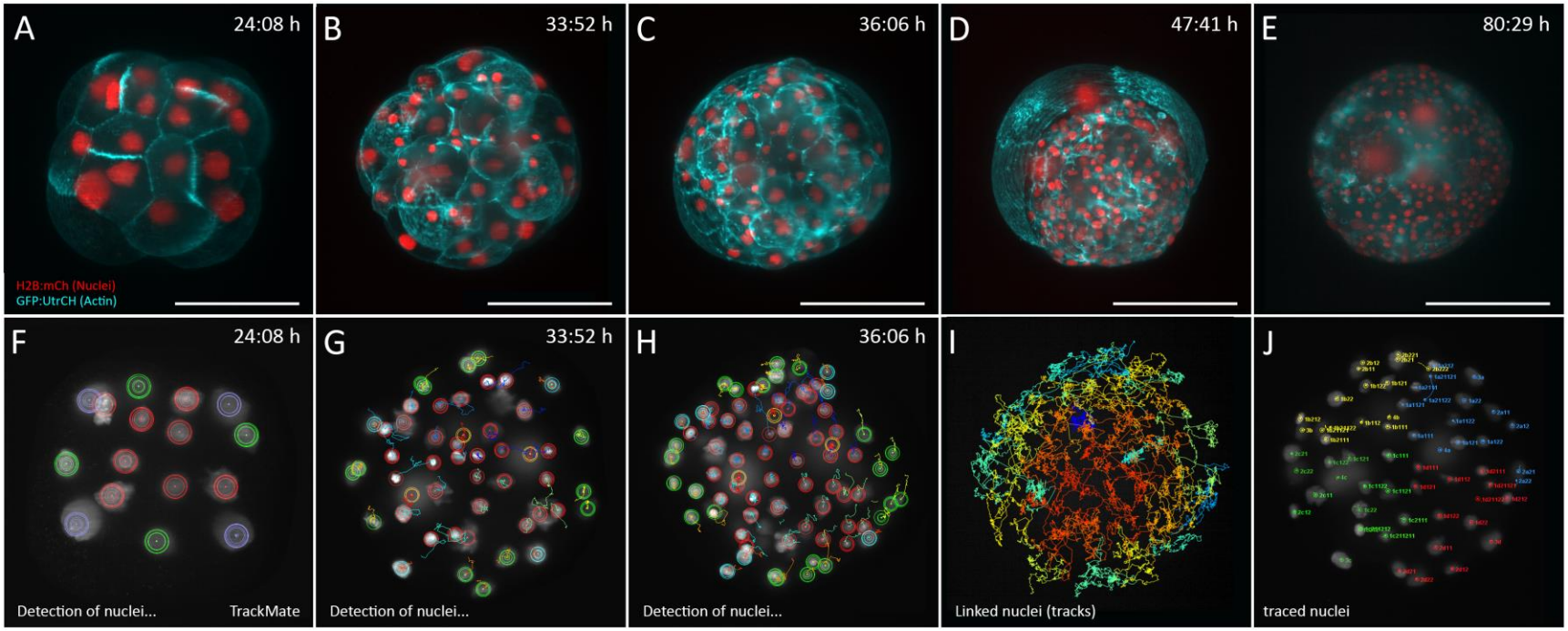


Figure 5.2 - Creating a cell lineage for the polyclad flatworm *M. crozieri*. **(A-E)** Shown are 5 days of OpenSPIM live-imaging of a single embryo. In this data, each nucleus can be detected **(F-H)** Detections and tracing of the individual nuclei with TrackMate **(I)**. After all nuclei have been detected, their trajectories can be visualized and further analysed as depicted in this panel. **(J)**. Embryo of which all nuclei have been traced and identified during development. The four quadrants are coloured as follows: A is blue, B is yellow, C is green and D is red. **(F-I)**. All scalebars are 100 µm.

A summary of the cell lineage can be seen in Figure 5.3. Due to image acquisition from an animal view, in both videos, the most vegetally-positioned macromeres of the fourth quartet remain undetected. However, these divisions are well known in polyclad flatworms and have been previously described in detail for *M. crozieri* (in this thesis, chapter IV and see Rawlinson (2010) and also in other polyclad flatworms (e.g. Malakhov and Trubitsina, 1998; Martin-Duran and Egger, 2012; Surface, 1907; Younossi-Hartenstein and Hartenstein, 2000). Small macromeres A-D can therefore be included as dashed lines in the lineage (Figure 5.3). For the same reason of fixed observation angle, the first two divisions of micromere 4d and its descendants could be detected in only one of the two embryos. These divisions have also already been described by us in detail for a different specimen of *M. crozieri* (see chapter IV).

We exported the tracking data into Fiji's 3D viewer. This allowed us to create a virtual 4-dimensional embryo that can be observed from any orientation during any recorded time-point, and to analyse specific cellular dynamics and spindle positions of interest in later embryonic stages where, for example, their laeotropic or dexiotropic nature is less pronounced.

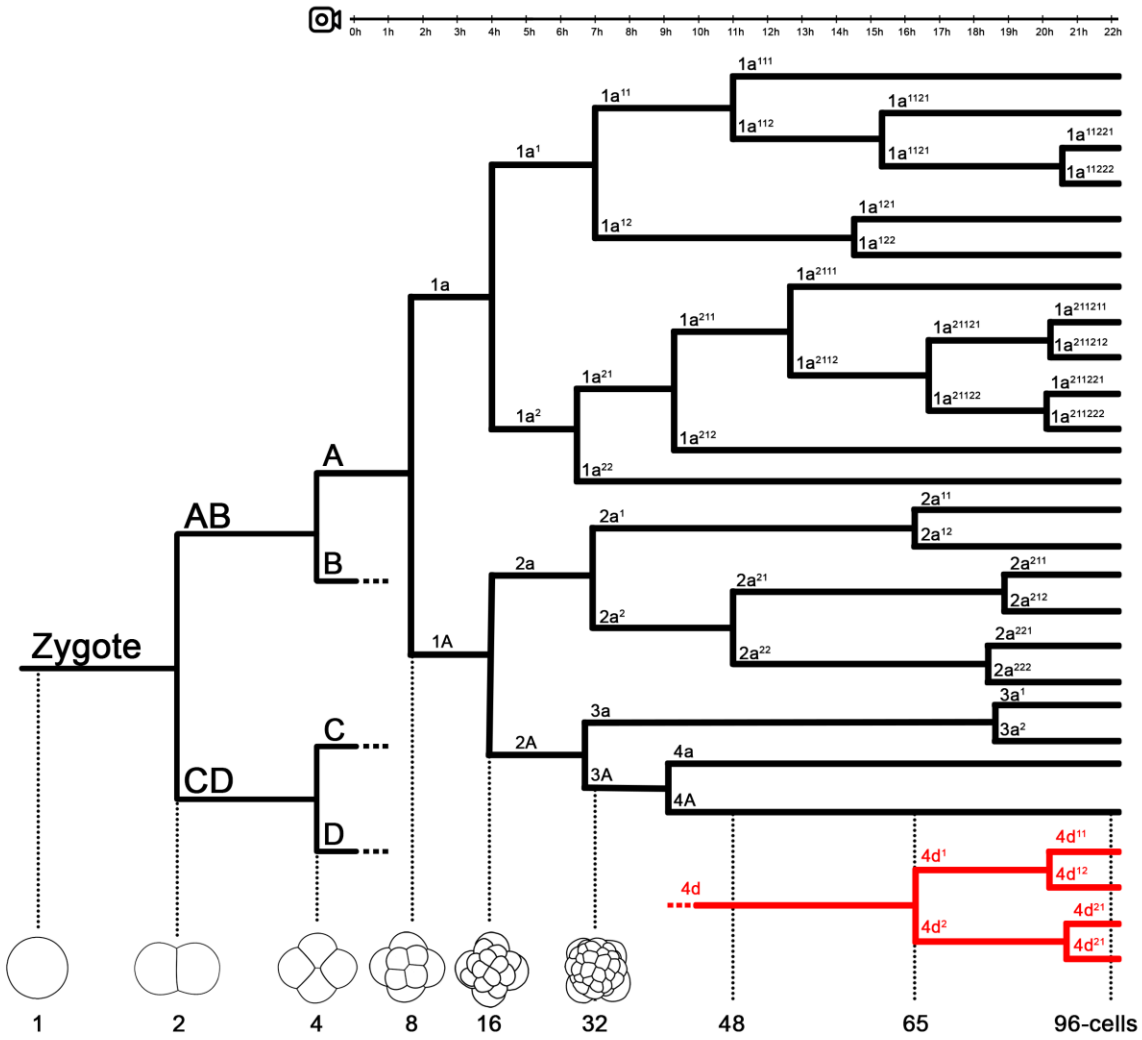


Figure 5.3 – Summary of the cell lineage of *Maritigrella crozieri* showing one of the quadrants starting at the 4-cell stage. The lineage is highly similar between the four quadrants with the exception of the D quadrant, where micromere 4d deviates from micromeres 3a-c (4d lineage shown as red lines). The timeline represents the hours of accurate time-lapse imaging starting at a 16-cell stage.

The data obtained were first used for a comparison with the cell lineage of *Hoploplana inquilina*, which is the only polyclad flatworm providing a comparable dataset of the early development based on detailed sagittal sections from fixed embryos (Surface 1907). We additionally describe in detail the apical cell mosaic in *M. crozieri* and performed long-term tracing of the apical rosette cell nuclei $1q^{111}$ for one of the presumed primary trochoblast cells $1c^{2}$.

### 5.1 Polyclad flatworms share a similar division timing pattern

A comparison of several different cell lineages can be challenging due to differences in data acquisition and its subsequent translation into a comparative and informative matrix. In any case the data must be summarised to facilitate the comparison. Since we are not investigating the phylogenetic relationship of lophotrochozoans on a large scale but are rather interested in how the relative timing of divisions varies between two polyclad species, we chose an approach that allowed us to graphically compare the summarised cell lineage data, which considerably facilitates the analysis. We first extracted the relative division timing information from *M. crozieri* based on the total number of cells and rearranged it into a temporal sequence according to each quadrant. The beginning of our sequence of quadrant A "2A, 2a, $1a^{2}$ etc." indicates that macromere 2A divides first (into daughter cells 3A and micromere 3a) followed by the division of micromere 2a (into $2a^{1}$ and $2a^{2}$), which is again followed by the division of micromere $1a^{2}$ (into $1a^{21}$ and $1a^{22}$) and so forth (see Figure 5.4) for the full A quadrant sequence of the two embryos).

| | | | | | | | | | | | | | | | | | | |
|---|---|---|---|---|---|---|---|---|---|---|---|---|---|---|---|---|---|---|
| Mc E2 Quad. A | $1a^2$ | 2A | 2a | $1a^1$ | X | $1a^{21}$ | $1a^{11}$ | $2a^2$ | $1a^{211}$ | $1a^{12}$ | $1a^{112}$ | $2a^1$ | $1a^{2112}$ | $2a^{22}$ | 3a | $2a^{21}$ | $1a^{21122}$ | $1a^{21121}$ | $1a^{1122}$ |
| Mc E1 Quad. A | 2A | 2a | $1a^2$ | $1a^1$ | 3A | $1a^{21}$ | $2a^2$ | $1a^{11}$ | $1a^{211}$ | $1a^{12}$ | $2a^1$ | $1a^{112}$ | $1a^{2112}$ | $2a^{22}$ | 3a | $1a^{21122}$ | $1a^{21121}$ | $1a^{121}$ | $1a^{1122}$ |

Figure 5.4 - An example of the relative division time sequence of the A quadrant of two *M. crozieri* embryos (E1 and E2). Both first quartet micromeres $1a^2$ (one from each embryo indicated in orange) are the only cells of the A quadrant separated by more than one cell division. Note that the division of macromere 3A was not detected in E2.

The first three cleavages do not show up in our cell lineage data as live imaging recordings of one embryo started between the 8- and 16-cell stage and therefore previous cleavage information is not included. The relative division timing sequences were visualised and compared by aligning corresponding quadrants and then by connecting the dividing blastomeres respectively by a simple line (Figure 5.4). In the example given below, both first quartet micromeres $1a^2$ (one from each embryo indicated in orange) are the only cells of the A quadrant separated by more than one cell division (see Figure 5.4). A line connecting both cells would need to cross macromere 2A and micromere 2a. The more similar two sequences are to each other, the less line crossing occurs. If a line crossed more than two other lines (>2) it indicates a deviation of the corresponding cell strong enough for us to highlight the line in red.

We compared the relative division timings between two *M. crozieri* embryos and then compared both embryos to the acotylean polyclad flatworm *H. inquilina,* the annelid *Hydroides elegans* (Arenas-Mena, 2007), and the gastropod mollusc *Crepidula fornicata* (Conklin, 1897), for which cell lineage data including relative division timing data was

readily accessible up to the 100-cell stage. A summary of the comparisons is given in Figure 5.5. A more detailed comparison of the data including all quadrants can be found within the supplementary files.

Unsurprisingly, yet supporting our chosen method of comparison, the closest resemblance regarding their relative division timing was determined between the two *M. crozieri* embryos (Figure 5.5, A). In general, this is also true for the relative division timings compared between the two *M. crozieri embryos* and *H. inquilina* (Figure 5.5, B). A significant difference is the preceding division of the first micromere descendants $1q^{21}$ in *M. crozieri*, while in *H. inquilina* $1q^{21}$ divide synchronously with micromeres $1q^{112}$. In the *M. crozieri* embryo where the 4d cleavage was recorded this division is clearly delayed until about the 64-cell stage (Figure 5.5). In *H. inquilina* Surface (1907) reported that these divisions already take place at the 45-cell stage.

When the relative division timings of the annelid *H. elegans* and the gastropod *C. fornicata* were compared to *M. crozieri,* a much denser crisscrossing pattern in terms of the relative division timing was noticed, indicating a much higher variation in division timing (Figure 5.5, C and D). This suggest that polyclad flatworms, even coming from different suborders (*H. inquilina* belongs to the Acotylea while *M. crozieri* belongs to the Cotylea), share a much more similar division timing pattern than members of other phyla. Some cells, however, seem to be more exposed to evolutionary change, with $1q^{21}$ (advanced in *M. crozieri* compared to *H. inquilina*) (Figure 5.5, B, highlighted in red) and micromere 4d (delayed in *M. crozieri* compared to *H. inquilina*) (Figure 5.6) being the most obvious examples. In Figure 5.6 A the accelerated divisions (compared to *H. inquilina*) of micromeres of the first

quartet (1q) are shown. These cells divide prior to the cleavage of 4d in *M. crozieri* (Figure 5.6, A, indicated by dashed red line and B, bottom) in contrast to *H. inquilina*, where – according to Surface (1907) – the same cells of the first quartet of micromeres divide after the cleavage of micromere 4d. Interestingly, the lineages of both $1q^2$ (which is strongly conserved in spiral cleaving embryos and gives rise to the prototroch cells) and the 4d cell are known to vary in their timing of appearance among other spiralian embryos; this variability has been shown in particular in molluscs (Guralnick and Lindberg, 2001; van den Biggelaar and Haszprunar, 1996).

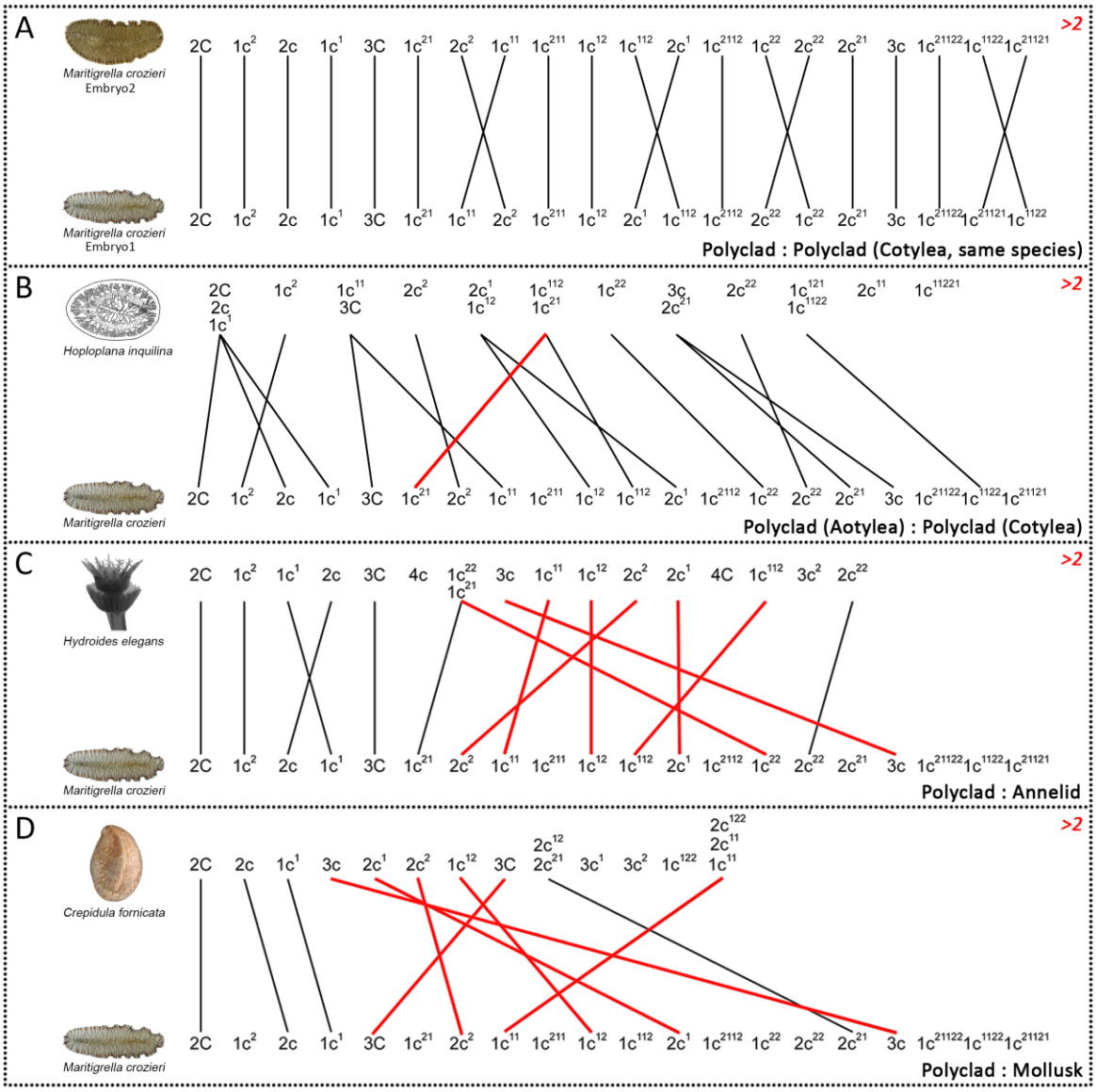


Figure 5.5 - A comparison of relative division timings (C quadrant lineage) between **(A)** two cotylean polyclad flatworm embryos of the species *Maritigrella crozieri* **(B)** the acotylean polyclad flatworm *Hoploplana inquilina* and *Maritigrella crozieri* **(C)** the annelid *Hydroides elegans* and *Maritigrella crozieri* and **(D)** the slipper snail *Crepidula fornicata* and *Maritigrella crozieri*. Cell divisions, which significantly deviate in their sequential cleavage pattern are highlighted in red. A much more synchronous division pattern is observed between polyclad flatworms compared to the annelid worm and the molluscan gastropod.

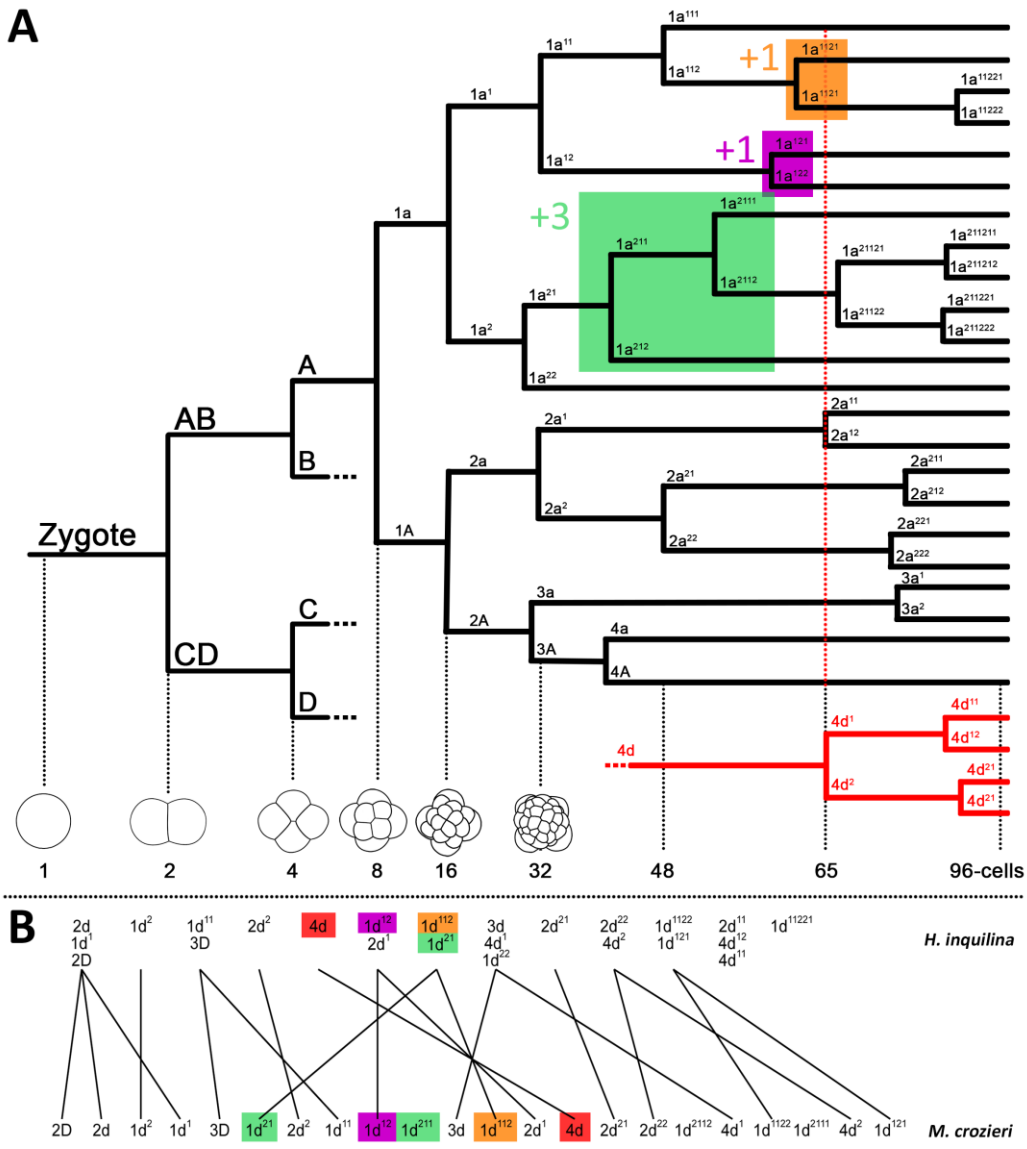


Figure 5.6 – Comparison of relative divisions timing between *M. crozieri* and *H. inquilina* **(A)** Cell lineage of *M. crozieri*. Compared to *H. inquilina* the daughter cells of micromeres with accelerated divisions are highlighted as follows: $1a^{21}$ (green), $1a^{12}$ (pink) and $1a^{112}$ (orange). These cells (and their counterparts of corresponding quadrants B, C, D; not shown) are present prior to the cleavage of micromere 4d (indicated by red dashed line). The coloured numbers refer to the formation of additional cells, which will be present in *M. crozieri* but not in *H. inquilina*. E.g. micromere $1a^{21}$ (green) will divide twice prior to the cleavage of 4d. Therefore, micromere 4d will cleave at a cell stage, that is postponed due to micromere $1a^{21}$ by +3 cells or, if all quadrant ($1q^{21}$) are considered, by +12 cells. **(B)** Comparison of the D quadrant between *H. inquilina* (top) and *M. crozieri* (bottom). The 4d cells are highlighted in red. In *H. inquilina* divisions of micromeres $1d^{12}$ (pink), $1d^{21}$ (green) and $1d^{112}$ divide after the cleavage of 4d. In. *M. crozieri* the opposite in corresponding micromeres is the case with $1d^{21}$ dividing twice before micromere 4d cleaves.

## 5.2 *Spindle positions during the early development appear similar in polyclad flatworms*

Mitotic spindle positions of individual cells were analysed by linking the cell lineage TrackMate data with Fijis 3D viewer (a plugin implemented in TrackMate). In this way, the laeotropic or dexiotropic nature of each division could be elucidated. The spindle orientation of most vegetally positioned macromeres 3A-D was determined to be slightly dexiotropic by looking at several embryos microinjected with a nuclear marker and captured *in-vivo* from a vegetal view (n = 4) during or shortly after the formation of the fourth quartet.

Afterwards, each spindle orientation was investigated for its spatial division pattern and then compared to its counterpart cells of the remaining quadrants (e.g. $1a^1$ to $1b^1$ to $1c^1$ to $1d^1$). The divisions of each dividing cell were captured from an animal view. The corresponding cells of all four quadrants were then merged into a single image, which allows us to recognise distinct laeotropic or dexiotropic quadrant divisions, if present, at a glance. Figure 5.7 shows spindle orientations of the early development obtained by this method for *M. crozieri.*

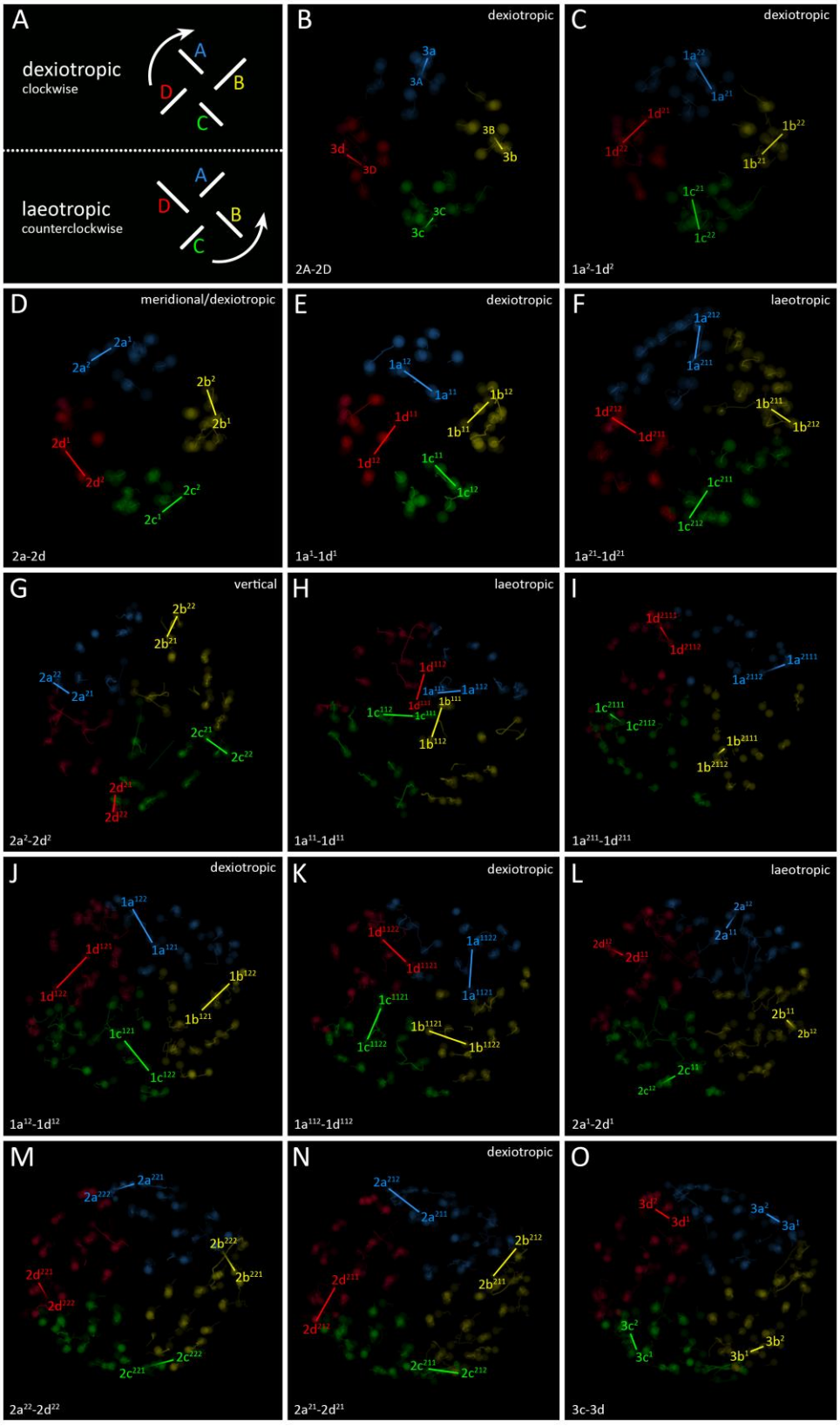


Figure 5.7 – see Figure legend on next page

Figure 5.7 - Spindle positions during the early cleavages of *M. crozieri* determined by OpenSPIM 4D microscopy recordings. The animal view is shown with the same cells of each quadrant (A in blue, B in yellow, C in green and D in red). In panel A an explanation is given how the laeotropic or dexiotropic divisions pattern can be determined. In this embryo panel C, E, J and K show obvious examples of dexiotropic divisions while B, F and H divide clearly laeotropically. Other divisions need closer examination from a lateral view of each individual cell and cell mates of the same tier can have a distinct division pattern or the division may take place in a vertical manner so that the pattern becomes ambiguous. Such an example can be seen in B, where during the division of the second quartet of macromeres (2Q) a false laeotropic impression is received when looking at the embryo from an animal view. The cleavage, however, is actually dexiotropic.

For the polyclad flatworm *H. inquilina*, Surface describes 19 early divisions (each consisting of four corresponding quadrant cells - 76 cells in total), as at least slightly laeotropic or slightly dexiotropic but mostly distinguishes a clear laeotropic or dexiotropic cleavage pattern (summarised in Table 5.1). For *M. crozieri* most laeotropic or dexiotropic divisions correspond to those found by Surface, however there are some differences.

In *M. crozieri* the second quartet micromere descendants $2a^2$-$2d^2$, which Surface describes as almost vertical but slightly dexiotropic in *H. inquilina,* also show a vertical division plane but spindle orientations are positioned in a slightly laeotropic pattern in *M. crozieri* in contrast to *H. inquilina* (see Table 5.1). The laeotropic or dexiotropic nature of $1a^{21}$-$1d^{21}$, $1a^{22}$-$1d^{22}$ is not clearly defined in *M. crozieri* and in some cases the spindle position of at least one of the two cells was reversed, like spindle position observations made in the slipper shell *C. fornicata* (Conklin 1807).

| Cells | *H. inquilina* | *M. crozieri* |
|---|---|---|
| **A-D** | dexiotropic | dexiotropic |
| **1a-1d** | laeotropic | laeotropic |
| **1A-1D** | laeotropic | laeotropic |
| **$1a^{1}$-$1d^{1}$** | dexiotropic | dexiotropic |
| **$1a^{2}$-$1d^{2}$** | dexiotropic | dexiotropic |
| **2a-2d** | meridional/dexiotropic | meridional/dexiotropic |
| **2A-2D** | dexiotropic | dexiotropic |
| **$1a^{11}$-$1d^{11}$** | laeotropic | laeotropic |
| **$1a^{12}$-$1d^{12}$** | dexiotropic | dexiotropic* |
| **$1a^{21}$-$1d^{21}$** | laeotropic | vertical/laeotropic |
| **$1a^{22}$-$1d^{22}$** | dexiotropic | irregular |
| **$2a^{1}$-$2d^{1}$** | laeotropic | laeotropic* |
| **$2a^{2}$-$2d^{2}$** | vertical/dexiotropic | vertical L |
| **3a-3d** | radial/sl. Dexiotropic | vertical |
| **3A-3D** | sl. dexiotropic | sl. dexiotropic |
| **$1a^{112}$-$1d^{112}$** | dexiotropic | dexiotropic* |
| **$1a^{121}$-$1d^{121}$** | laeotropic | laeotropic |
| **$2a^{21}$-$2d^{21}$** | dexiotropic | irregular |
| **$1a^{1122}$-$1d^{1122}$** | dexiotropic | dexiotropic |

Table 5.1 - A comparison of the laeotropic/dexiotropic spindle positions during cell divisions between *H. inquilina* (Surface, 1907) and *M. crozieri*. An asterisk was added whenever at least one of the four cells' spindle position in one embryo was found to be reversed but a clear laeotropic/dexiotropic trend for the overall four quadrants was still recognisable. The cells in green mark a strongly conserved spindle orientation pattern that all spiral cleavers follow.

## 5.3 The lineage of apical cells 1q$^{11}$ gives rise to a typical spiralian apical cell mosaic and could be involved in the formation of the central nervous system

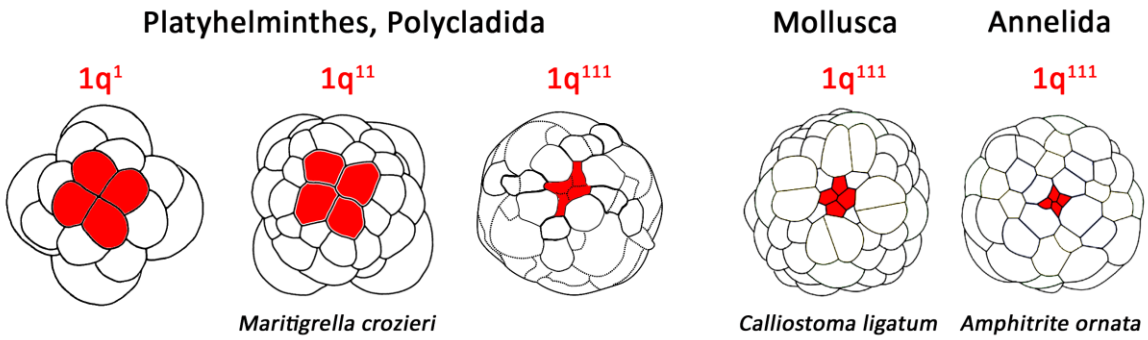


Figure 5.8 – The position of apical micromeres 1q$^{1}$ and 1q$^{11}$ and apical rosette cells 1q$^{111}$ are indicated in three schematic *Maritigrella crozieri* embryos. Additionally, the position of micromeres 1q$^{111}$ are also indicated in two other spiral cleavers: *Calliostoma ligatum*, Mollusca; *Amphitrite ornata*, Annelida). *Calliostoma* and *Amphitrite* are drawings after (Maslakova et al., 2004b).

In the following section, we will describe several cleavage patterns that arise from the 1q$^{11}$ lineage at the apical pole of *M. crozieri* embryos and later attempt to trace the apical rosette cells 1q$^{111}$, into an advanced gastrulating stage. This is of interest, as it could give rise to the apical organ in *M. crozieri*, as well as eyes.

Apical rosette cells from micromeres 1q$^{11}$ in *M. crozieri* divide in an obviously laeotropic fashion, as can be seen, for instance, from our previously described spindle position analysis (see Figure 5.7, H). This specific division builds the basis for a common pattern, which is often found in spiral cleaving lophotrochozoans: the so-called “annelid cross” (Figure 5.9 and Figure A. 1). Together with a few other cells, which form the so-called “molluscan cross”, an apical cell mosaic appears. Its shape is derived from the centralised apical rosette cells 1a$^{111}$-1d$^{111}$, surrounded by the “annelid cross” cells (1a$^{112}$-d$^{112}$) and

"molluscan cross" cells ($1a^{12}$-$1d^{12}$ and their descendants respectively). The latter are edged by the so-called "tips of the "molluscan cross""-cells ($2a^{11}$-$2d^{11}$). Because the division of first quartet micromeres $1a^{11}$-$1d^{11}$ in *M. crozieri* is highly asymmetric (i.e. the decendants are different sizes), the apical rosette cells (Figure 5.9, depicted in red) are much smaller than the "annelid cross" cells $1a^{112}$-$d^{112}$ (Figure 5.9, depicted in blue). The size of the "annelid cross" cells also slightly surpasses the size of the "molluscan cross" cells (Figure 5.9, depicted in yellow), which are connected by the tips of the "molluscan cross" cells $2a^{11}$-$2d^{11}$ (Figure 5.9, depicted in green).

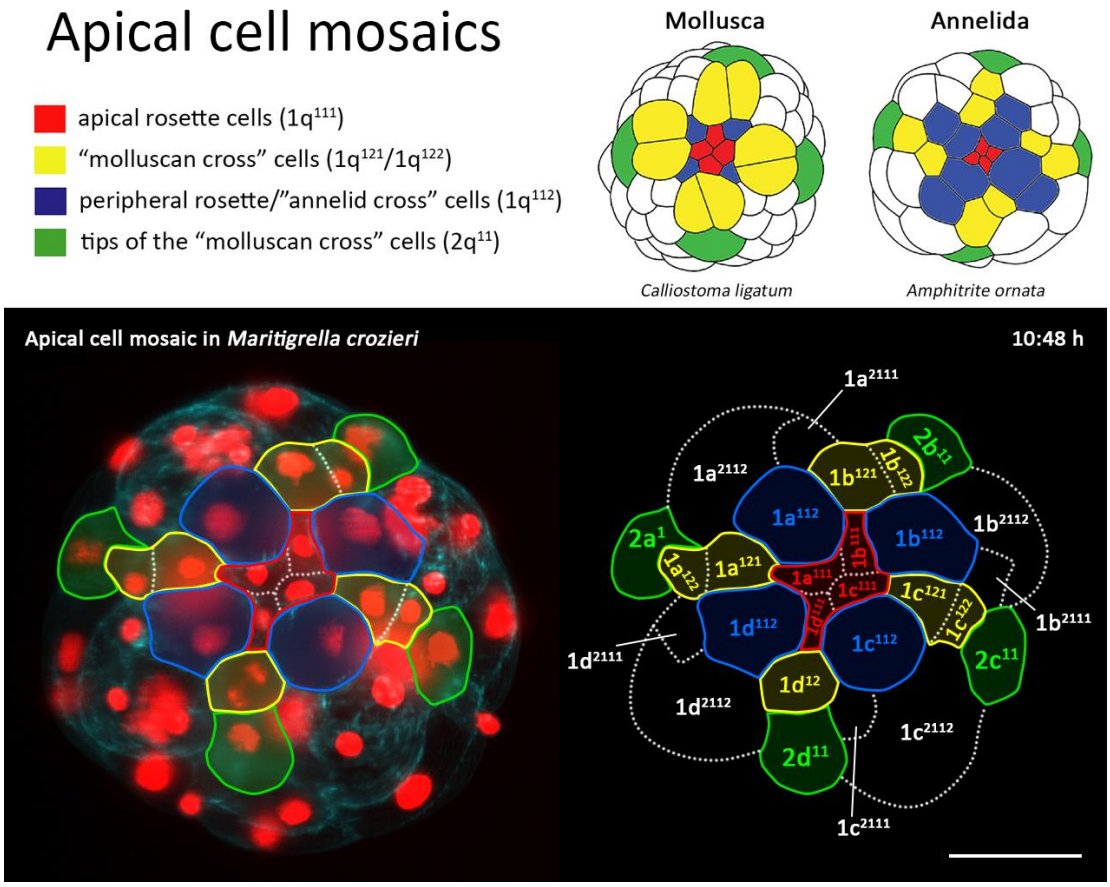


Figure 5.9 – Top: Apical cell mosaic which emerges after the formation of the apical rosette cells ($1q^{111}$) in two representative spiral cleavers (top, after Maslakova, (2004)) and bottom: *M. crozieri*. Individual cells in *M. crozieri* have been identified by cell lineage tracing. Scale bar = 50 µm.

### *5.3.1 The correct spatial arrangement of apical rosette cells 1q$^{111}$ in polyclad flatworms*

The division of cells 1a$^{11}$-1d$^{11}$ in *M. crozieri* closely follows the description of *H. inquilina* by Surface (1907) in detail (Figure 5.10, A-D). However, once the apical rosette cells 1q$^{111}$ and their sister cells 1q$^{112}$ are present in the embryo, Surface (1907) states that that apical rosette cells in *H. inquilina* lose connection to their sister cells during their formation (see Figure 5.10, G, H) because "the laeotropic direction of the spindle is so marked that the cell 1a$^{1.1.1}$ comes to lie in front of 1d$^{1.1.2}$ and 1b$^{1.1.1}$ in front of 1a$^{1.1.2}$ and so on, so that there is a rotation of 45 degrees". In this case, which becomes also clear from his figures, apical rosette cell 1a$^{111}$ comes to lie in between of 1c$^{112}$ and 1d$^{112}$ and 1b$^{111}$ in between 1a$^{112}$ and 1d$^{112}$ and so on (Figure 5.10, G, H). In *M. crozieri,* however (see Figure 5.10, A-F) this rotation of 45 degrees does not actually happen as all apical rosette cells clearly remain positioned in close contact to their sister cells (Figure 5.10, E, F). Thereby 1a$^{111}$ keeps contact with 1a$^{112}$ while lying next to 1d$^{112}$ and 1b$^{111}$ keeps contact with 1b$^{112}$ while lying next to 1a$^{112}$ and so on. A possible reason why Surface was convinced that a rotational event during the divisions of apical cells 1q$^{11}$ lead to a new, rotated arrangement of apical rosette cells 1q$^{111}$ can be seen in Video 9, which shows how 1q$^{111}$ are first displaced far off from their sister cells, but then retract to a closer position of their sister cells 1q$^{112}$.

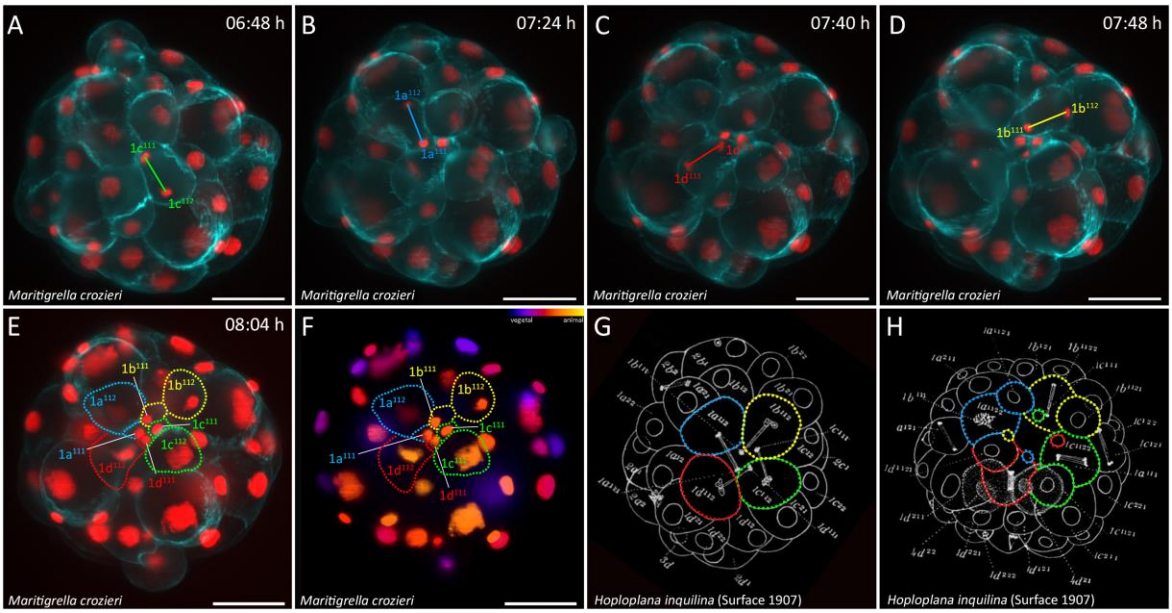


Figure 5.10 - Formation of the apical rosette cell 1q$^{111}$, in *M. crozieri* and *H. inquilina*, from an animal view. In a typical trochophore larvae these cells give rise to head structures such as eyes and apical "sensory" organs. **(A-D)** Laeotropic divisions of apical cells 1q$^{11}$ in a slightly asynchronous manner (1 hour in total). **(E)** Same embryo after all apical rosette cells 1q$^{111}$ have formed and showing that they remain in contact with their sister cells 1q$^{112}$. **(F)** Nuclei of same embryo with their depth coded as seen in top left part of the panel. **(G)** Embryo of *H. inquilina* during formation of the apical rosette cell 1q$^{111}$ also showing clearly a laeotropic division. **(H)** An embryo of *H. inquilina* at a later stage, where the sister cells (1q$^{112}$) of the apical rosette cells have already divided. Unlike in *M. crozieri*, the small apical rosette cells in the centre of the embryo (coloured accordingly) have clearly lost contact to their former sister cells. Drawing of G and H after Surface (1907). All scale bars are 50 µm.

### 5.3.2 *Descendants of peripheral rosette cells 1q$^{112}$ could be interpreted as cerebral ganglia cells*

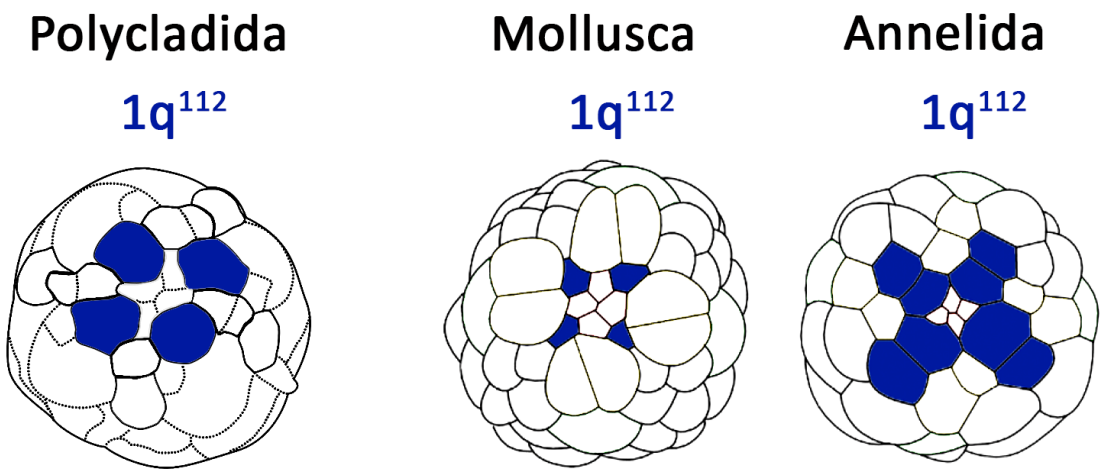


Figure 5.11 – The position of micromeres 1q$^{112}$ are indicated in three different spiral cleaving embryos (*Maritigrella crozieri*, Polycladida; *Calliostoma ligatum*, Mollusca; *Amphitrite ornata*, Annelida). Calliostoma and Amphitrite are drawings after (Maslakova et al., 2004b).

Another deviation from *H. inquilina* concerns the division of micromeres 1q$^{112}$, which derive from first quartet cells 1q$^{1}$. The latter are known to make – along with eyes and apical "sensory" structures - significant contributions to the central nervous system in spiralian embryos (e.g. cerebral ganglia, "brain"; see Chapter I). In a classical study of the annelid *Arenicola* the origin of the cerebral ganglion was claimed to derive exactly from blastomeres 1c$^{112112}$ and 1d$^{112112}$, and these cells were therefore designated as the "cephalic neuroblasts" (Child, 1900). According to Surface, the lineage of first quartet micromeres 1q$^{112}$ (or peripheral rosette cells/""annelid cross"" cells) also gives rise to the primitive ganglion in the polyclad *H. inquilina* (Surface, 1907). He first describes these cells

to divide in a very unequal manner with the smaller, upper cells ($1q^{1121}$) (see also Figure 5.10, F) lying on the surface of the embryo. Notably, the fate of micromeres $1q^{1121}$, which are not shown by Surface to divide again in *H. inquilina*, is not followed any further. Both daughter cells of $1q^{1122}$, however, are shown here in *M. crozieri* to divide again, first $1q^{11222}$ – in an unequal and slightly dexiotropic manner – followed a bit later by micromeres $1q^{11221}$. It is important to mention that, for Surface, micromeres $1q^{11221}$ are large and vegetally positioned cells compared to micromeres $1q^{11222}$, which are much smaller and animally positioned. This labelling of cells is slightly confusing as according to the nomenclature as most embryologists now use it, one would expect these cells to be named vice-versa, according to their animal/vegetal positioning, (which is what we do in *M.* crozieri) but in case of *H. inquilina* we decided to keep the original labelling by Surface.

Eventually Surface describes how the large and more vegetally positioned micromeres $1q^{11221}$ (corresponding to $1q^{11222}$ in *M. crozieri*) bud four comparatively large cells into the interior of the embryo, which he labels to be the "primitive ganglion cells".

In *M. crozieri,* we noticed in our OpenSPIM live imaging recordings used for this cell lineage study, some differences in comparison to *H. inquilina* during divisions of the corresponding peripheral rosette cells $1q^{112}$. First, the divisions of $1q^{112}$ appear as equal and almost horizontal divisions, and not as unequal divisions with animal/vegetal dispositions of both daughter cells. The daughter cells $1q^{1121}$ and $1q^{1122}$ then divide vertically and unequally in *M. crozieri*, with $1q^{1122}$ earlier than $1q^{1121}$, so that one of their more vegetally positioned daughter cells contribute to the deeper layer of cells, while the other, smaller cell remains on the surface. For $1q^{1122}$, these divisions are the same as described in *H. inquilina*, while

the division of $1q^{1121}$ is not mentioned. Cells $1q^{11211}$ and $1q^{11221}$ stay on the surface of the embryo for as long as we could trace these cells and show no further division during this time. The sub-epidermally positioned cells $1q^{11212}$ and $1q^{11222}$, which are now located below the most apical pole of the embryo, however, keep proliferating and it seems likely that some of their descendants will be involved in forming parts of the central nervous system such as cerebral ganglia as suggested also by Surface.

### 5.4 Tracing the apical rosette cells $1q^{111}$ suggest their possible role as apical organ founder cells.

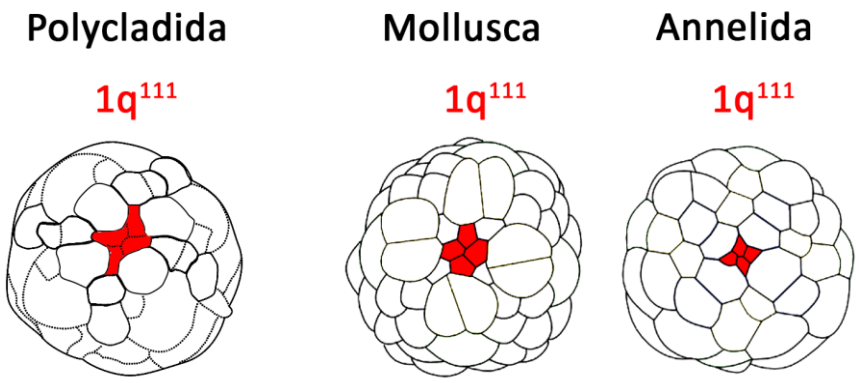


Figure 5.12 – The position of apical rosette cells $1q^{111}$ are indicated in a schematic *Maritigrella crozieri* embryo. Additionally, the position of micromeres $1q^{111}$ are also indicated in two other spiral cleavers: *Calliostoma ligatum*, Mollusca; *Amphitrite ornata*, Annelida). *Calliostoma* and *Amphitrite* are drawings after (Maslakova et al., 2004b).

We traced the apical lineage of *M. crozieri* for as long as possible during its embryonic development to locate their final position (Figure 5.14). While the peripheral rosette cells $1q^{112}$ proliferate, as we have just seen in the previous section, this is initially not the case for their sister cells, the apical rosette cells $1q^{111}$. Once these cells have formed (Figure

5.14, B), their division is arrested for about 20 hours before another round of divisions begins (Figure 5.13, Figure 5.14, B-E). The more vegetally positioned daughter cells of each individual quadrant $1q^{1112}$ stay initially in close contact with the animally positioned sister cells but they cannot be traced anymore with the necessary accuracy, and are therefore not shown in Figure 5.14. Descendants of the apical rosette cells, $1q^{1111}$, can still be located at the most apical pole of the embryo at > 50% epiboly (gastrulation) (Figure 5.14, H) and their final position is the most apical point of the embryo (Figure 5.14, I). This is the location where we expect the apical organ to form and we therefore suggest a likley involvement in the development of this structure or at least some of the traced descendants of apical rosette cells $1q^{111}$, similar to other lophotrochozoan spiral developers.

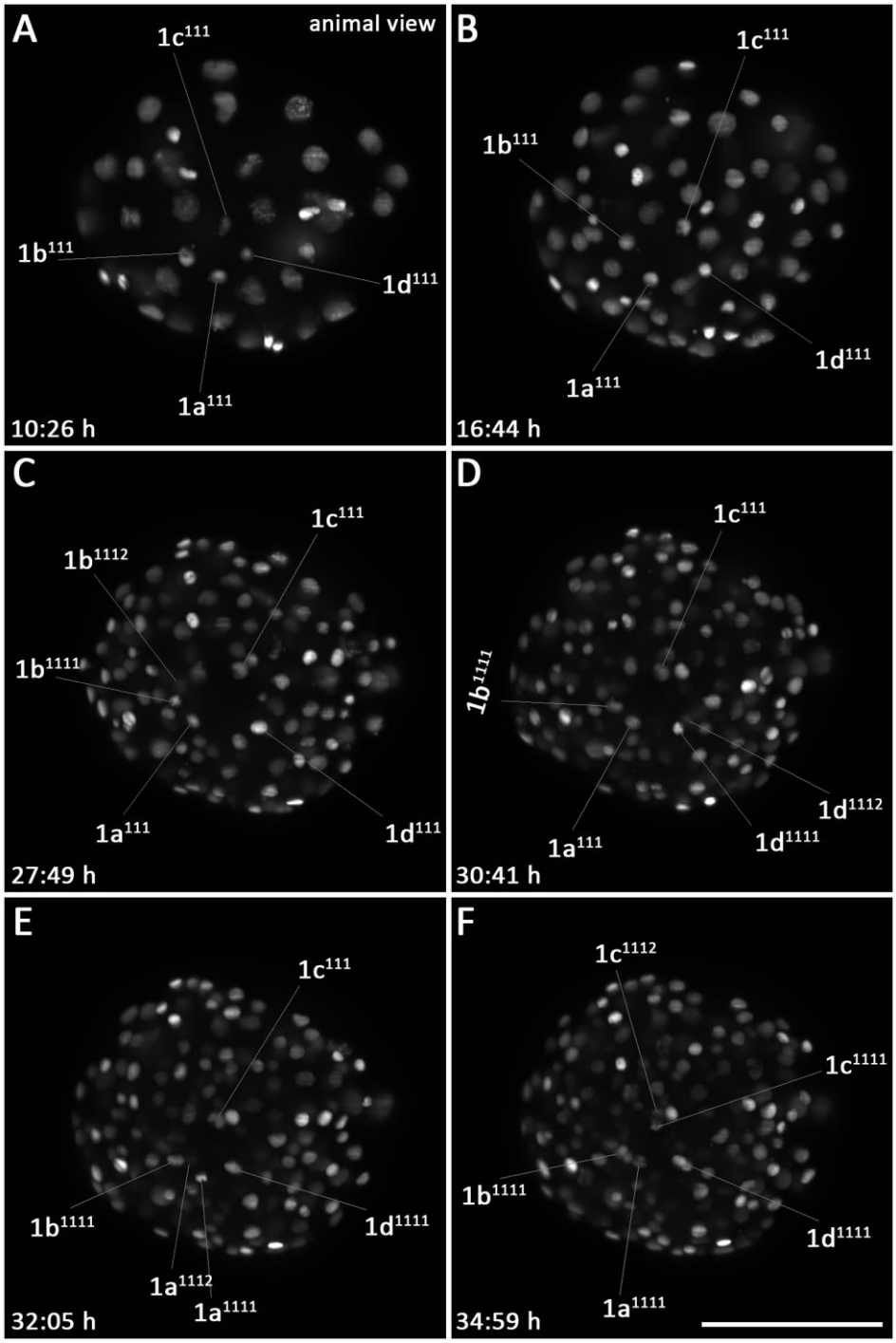


Figure 5.13 - Divisions of apical rosette cell $1q^{111}$ in a *M. crozieri* from the animal view **(A)** Embryo after the formation of apical rosette cells $1q^{111}$. **(B)** Same embryo more than six hours later. Apical rosette cells do not divide for almost a day. **(C-F)** The asynchronous divisions of each of the apical rosette cells $1q^{111}$ is shown. The first division can be observed more than 25 hours after their initial formation and it takes approximately 6-7 hours until all apical rosette cells have divided. Scale bar is 100 µm.

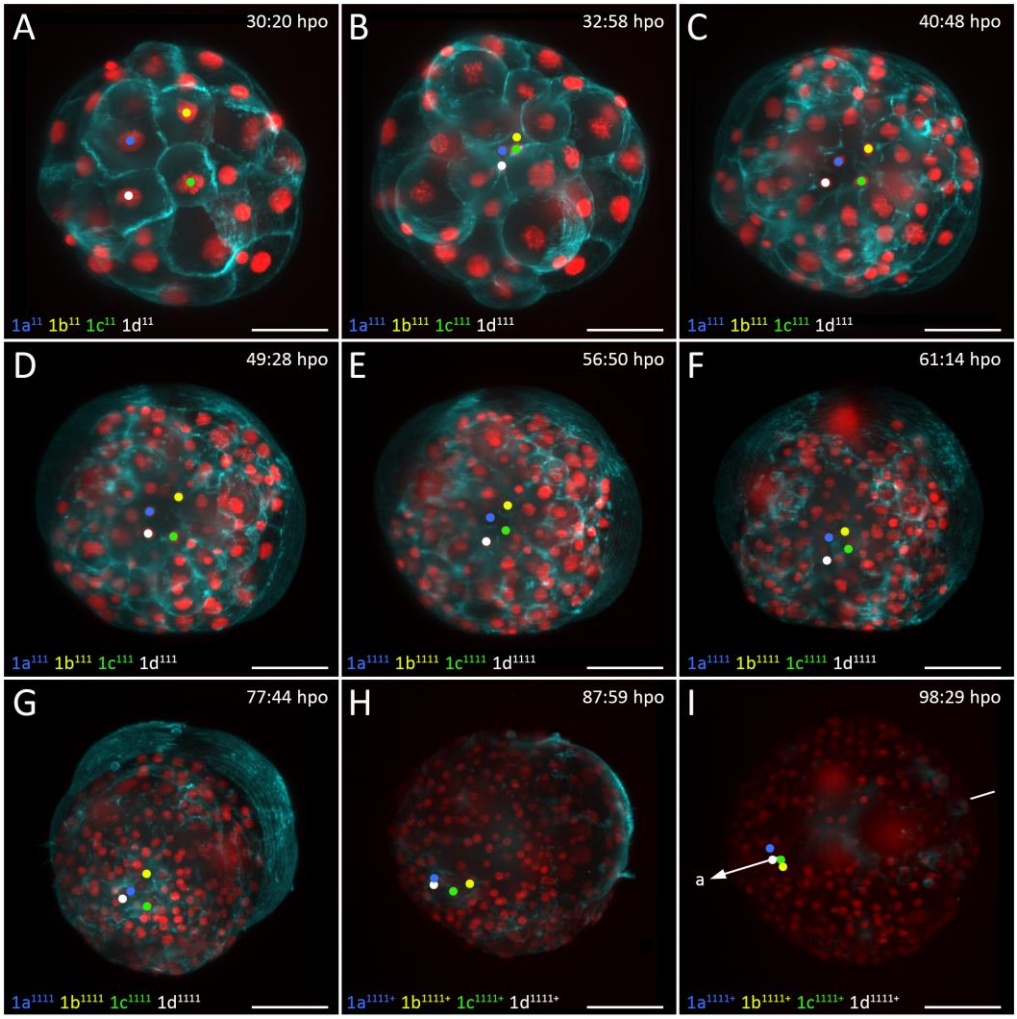


Figure 5.14 - Long term tracing (>75 hours) of nuclei in *M. crozieri* embryo with focus on the apical lineage. Traced cells are depicted as dots and coloured as follows: A quadrant cells in blue, B quadrant cells in yellow, C quadrant cells in green and D quadrant cells in white **(A)** Apical cells $1q^{11}$ are shown **(B-D)** Apical rosette cells $1q^{111}$ have formed and are shown at different time points **(E)** Apical rosette cells have divided at this timepoint and only $1q^{1111}$ are further traced. **(F)** Descendants of apical rosette cells $1q^{1111}$ are shown. Embryo is at the onset of epiboly **(G)** Epiboly has started and embryo becomes elongated and the animal tip slightly shifts to the left. **(H)** Embryo has reached more than 50% epiboly. At this timepoint tracking of cell becomes more difficult due to decreasing signal of fluorescently tagged nuclei. Another division of $1d^{1111}$ has been observed and the same is also likley for its counterpart cells $1a^{1111}$-$1c^{1111}$. Therefore, $1q^{1111}$ are now labelled as $1q^{1111+}$. **(I)**. The position of the traced nuclei marks most likely the place where the apical organ will form. Arrow marks the animal tip of the embryo. Scale bar = 50 µm

## *5.5* The lineage of micromeres $1q^2$: cleavage patterns and evidence for these cells being considered primary trochoblasts in *M. crozieri*

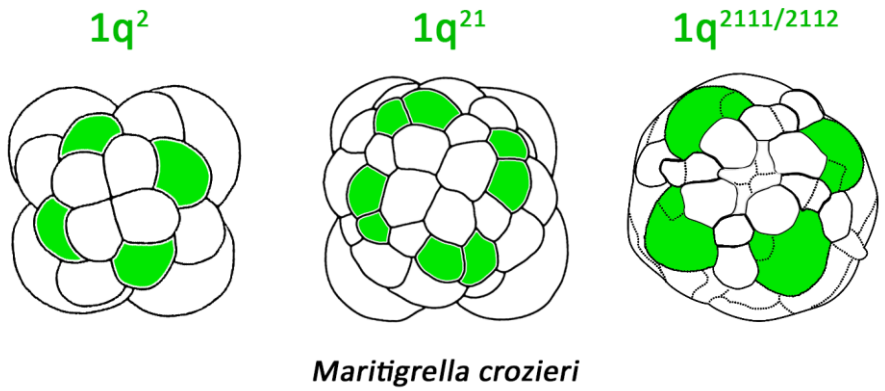


Figure 5.15 – The position of micromeres $1q^2$ and some of its descendants in two later embryonic stages. In most spiral cleaving lophotrochozoans micromeres of $1q^2$ are called the primary trochoblasts as they give rise major parts of the prototroch.

In essentially all investigations of spiral cleaving embryos that exhibit a ciliated trochophore larva, the so-called prototroch (the main ring of cilia used by the larva for locomotion and feeding) emerges, for the most part, from specific founder cells called primary trochoblasts (1a-1d) or more specifically from their descendants ($1a^2$-$1d^2$) (Henry et al. 2007, Nielsen 2004). This suggests a strong case for homology of these cells among lophotrochozoan phyla.

In *M. crozieri*, and polyclads in general, the fate of the cells that are homologous to the primary trochoblasts is entirely unknown and, due to early ciliation of epidermal cells causing rotational movements, we were unable to follow the fate of presumed primary trochoblasts up to a stage where the formation of the ciliary band has occured. We could, however, analyse the early cleavage pattern of micromeres $1a^2$-$1d^2$ and follow one of its

descendants from a 4-cell stage for almost 70 hours into a gastrulating embryo consisting of hundreds of cells to detect the number of divisions and where their progeny end up in order to see whether these observations support their ultimate fate as ciliary band cells.

During the sixth division round, almost simultaneously with the formation of the fourth quartet at the vegetal pole of the embryo (32- to 36-cell stage), micromere divisions commence with the advanced cleavage of $1a^{21}$-$1d^{21}$, which at this point have the largest cell nuclei of all micromeres. Conspicuously, their descendants $1a^{211}$-$1d^{211}$ also show the embryo's most rapid division rounds during these early cleavages (see Figure 5.3) and increase their cell volume until they obtain the largest size of all micromeres, most prominently seen at the stage where the annelid/"molluscan cross" is present. During these divisions, the enlarged cell nuclei of $1q^{21}$, $1q^{211}$, $1q^{2112}$, $1q^{21121}$ can be easily observed (Figure 5.16, Video 6 and Video 7). The rhythm of these divisions is very synchronous among all four quadrants and cleavage is highly asymmetrical with $1a^{212}$-$1d^{212}$ and $1a^{2111}$-$1d^{2111}$ being comparatively miniaturised. Furthermore, spindles become noticeably aligned along the a/v axis (see Figure 5.16) causing micromeres $1a^{2112}$-$1d^{2112}$ to become positioned slightly deeper in the embryo where they contribute significantly to the formation of an irregular double layer, described by Rawlinson (2010), forming at the animal pole of the embryo. In contrast to micromeres $1a^{211}$-$1d^{211}$ we noticed that the cleavage of $1a^{212}$-$1d^{212}$ is comparatively decelerated.

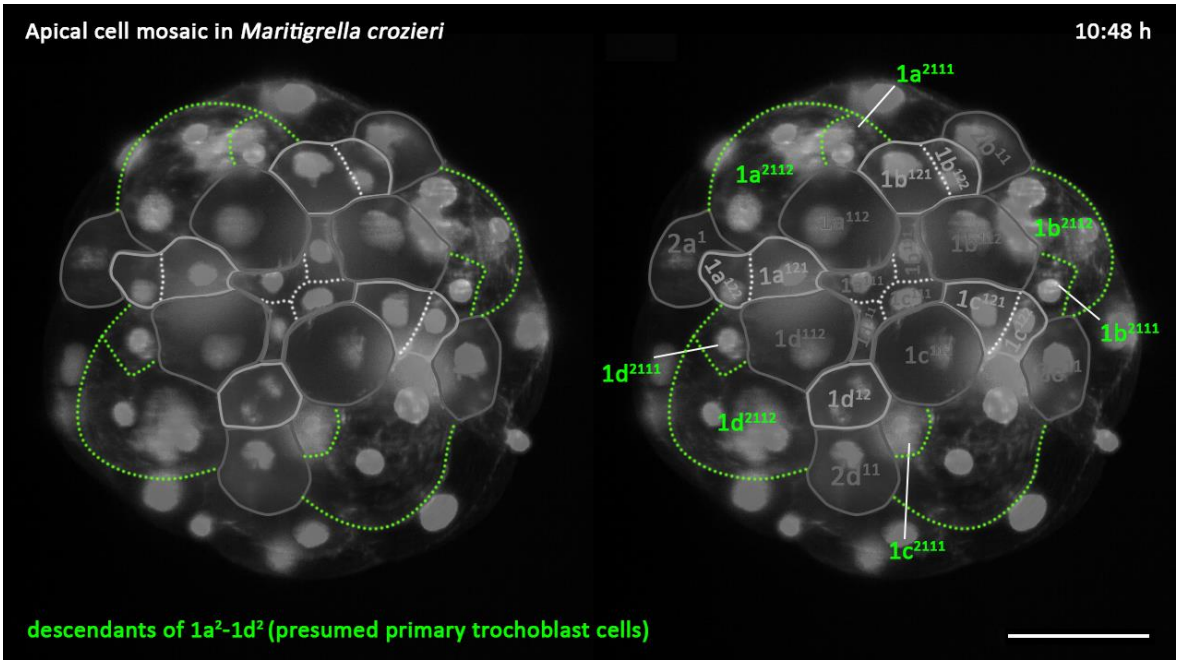


Figure 5.16 - Descendants of the putative primary trochoblast ($1q^2$) shown in green at the time where the annelid/"molluscan cross" forms. The cells $1q^{2112}$ and their nuclei are large and several highly asymmetric divisions can be observed around this stage and later. Scale bar is 50 µm.

Long-term cell-tracing shown in Figure 5.17 of blastomere $1c^2$ undertaken in one *M. crozieri* embryo from the 4-cell stage to gastrulation revealed that many of its descendants, including the descendants of $1c^{212}$, which show a decelerated division rate, line up at the embryo's surface in a well-ordered ring-like shape (Figure 5.16). Furthermore, descendants of $1d^{12}$ also contribute to this pattern (Figure 5.17, D). This specific spatial positioning is similar to embryonic SEM pictures of *M. crozieri* (see Figure 5.18) and to other spiral cleaving embryos (Nielsen, 2004; Henry et al. 2007) and suggests that a similar fate of $1q^2$ in the form of ciliary band precursors cells is a reasonable prediction. The most apical part of the embryo is marked by descendants of $1q^{111}$ (Figure 5.17, C and D).

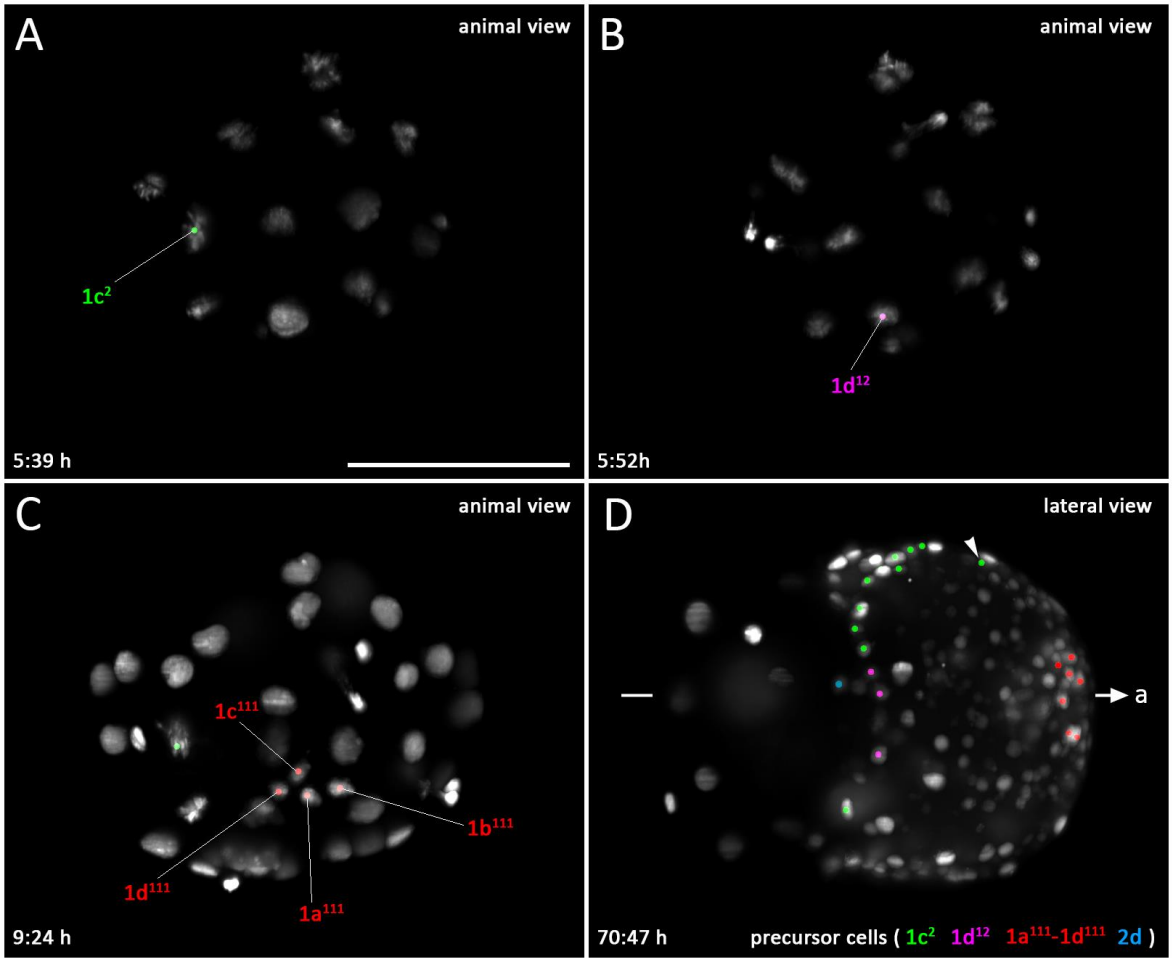


Figure 5.17 - Tracing of micromere $1c^2$, micromere $1d^{12}$ and of the apical rosette cells $1q^{111}$ for more than 70 h. **(A)** Identified nucleus of blastomere $1c^2$, which in other trochophore embryos becomes a major part of the prototroch **(B)** Identified nucleus of blastomere $1d^{12}$, which in other trochophore embryos sometimes becomes a minor part of the prototroch (accessory trochoblasts) **(C)** The four nuclei of the apical rosette cells are marked as red dots and indicate the most animal pole of the embryo. **(D)** Fate of the six nuclei almost 70 h later. White arrowhead indicates a traced nucleus descending from $1c^2$, which is located at the back site of the embryo. This figure is based on the original OpenSPIM files and therefore represents a mirror image. Arrowhead indicates the apical pole. Scale bar = 100 µm.

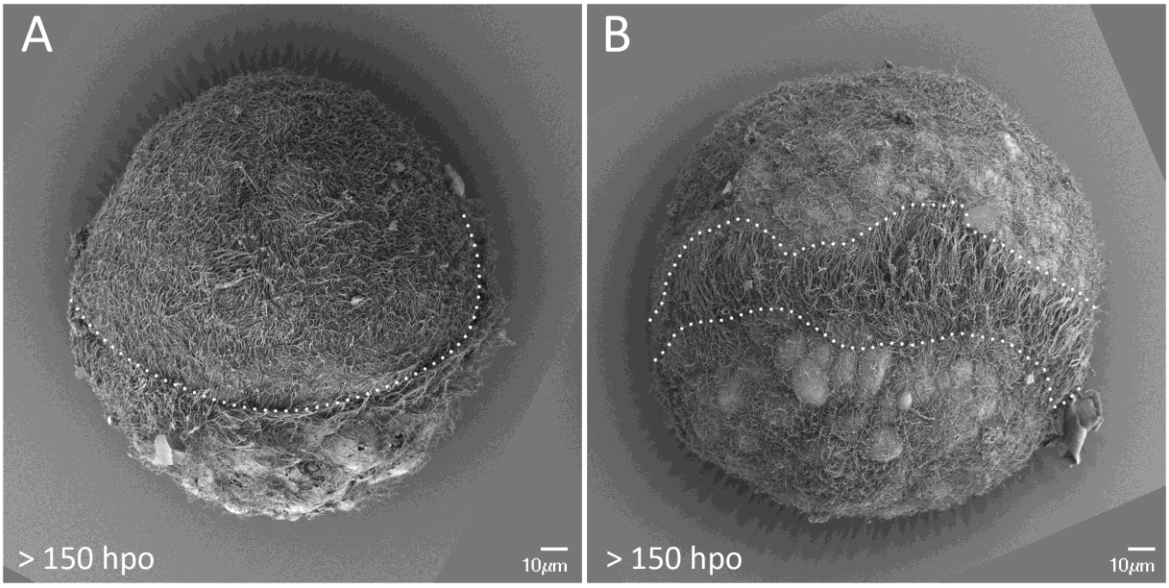


Figure 5.18 – Two examples (A and B) of SEM pictures of advanced embryos showing first signs of ciliary band cells.

### 5.6 FoxQ2 expression patterns in the apical pole of *M. crozieri* embryos and larvae makes a conserved cell-lineage of the apical organ more plausible

While a similar morphology of complex structures in marine larvae such as the apical organ could be interpreted as a product of convergent evolutionary forces (Strathmann, 2000), comparisons of cell lineages in the spiralian developmental program has been used to infer homology of larval organs such apical organs or ciliary bands (Henry et al., 2007; Nielsen, 2005). Further evidence for or against homology of these structures, useful to complement cell lineage data, can come by looking at conserved transcription profiles, e.g. in areas of larval organ formation during embryonic development and also in newly hatched larvae. Unfortunately, gene expression studies are still a difficult undertaking in polyclad flatworms

including *M. crozieri* (Lapraz et al., 2013). We were, however, able to investigate at least one expression pattern in more detail, namely of the apical marker gene FoxQ2, an important protagonist in the transcriptional patterning profile of the apical plate of many marine larvae (Santagata et al., 2012).

Both whole mount in situ hybridization (WISH) and immunocytochemistry methods revealed in embryos and larvae of *M. crozieri* that the apical marker FoxQ2 is expressed in hatched larvae within the apical plate region (Figure 5.19 A-B, white arrows and D) and also in the most apical region of earlier embryonic stages post gastrulation (Figure 5.19C). This expression pattern can be interpreted as a first sign of a molecularly conserved apical region in the head region of a Müller's larva but will remain uncertain until further gene expression patterns of the apical plate region can be revealed. For our cell lineage study regarding the fate of apical rosette cells $1q^{111}$ it is interesting that the expression of FoxQ2 in *M. crozieri* embryos is located at the tip of the apical pole (Figure 5.19, C), exactly at the same place where our cell lineage recordings of earlier gastrulating embryos end (Figure 5.14, I and Figure 5.17, D). Together with transcripts of FoxQ2 being expressed in hatched larvae in an area where an apical organ is to be expected (Figure 5.19, A-B, D) these expression patterns of FoxQ2 in embryo and larvae serve as a bridge, which connects descendants of apical rosette cells to the apical organ of Müller's larva in *M. crozieri*. This suggest a conservation of the cell lineage of the apical organ in *M. crozieri* with those of other spiral cleaving lophotrochozoa.

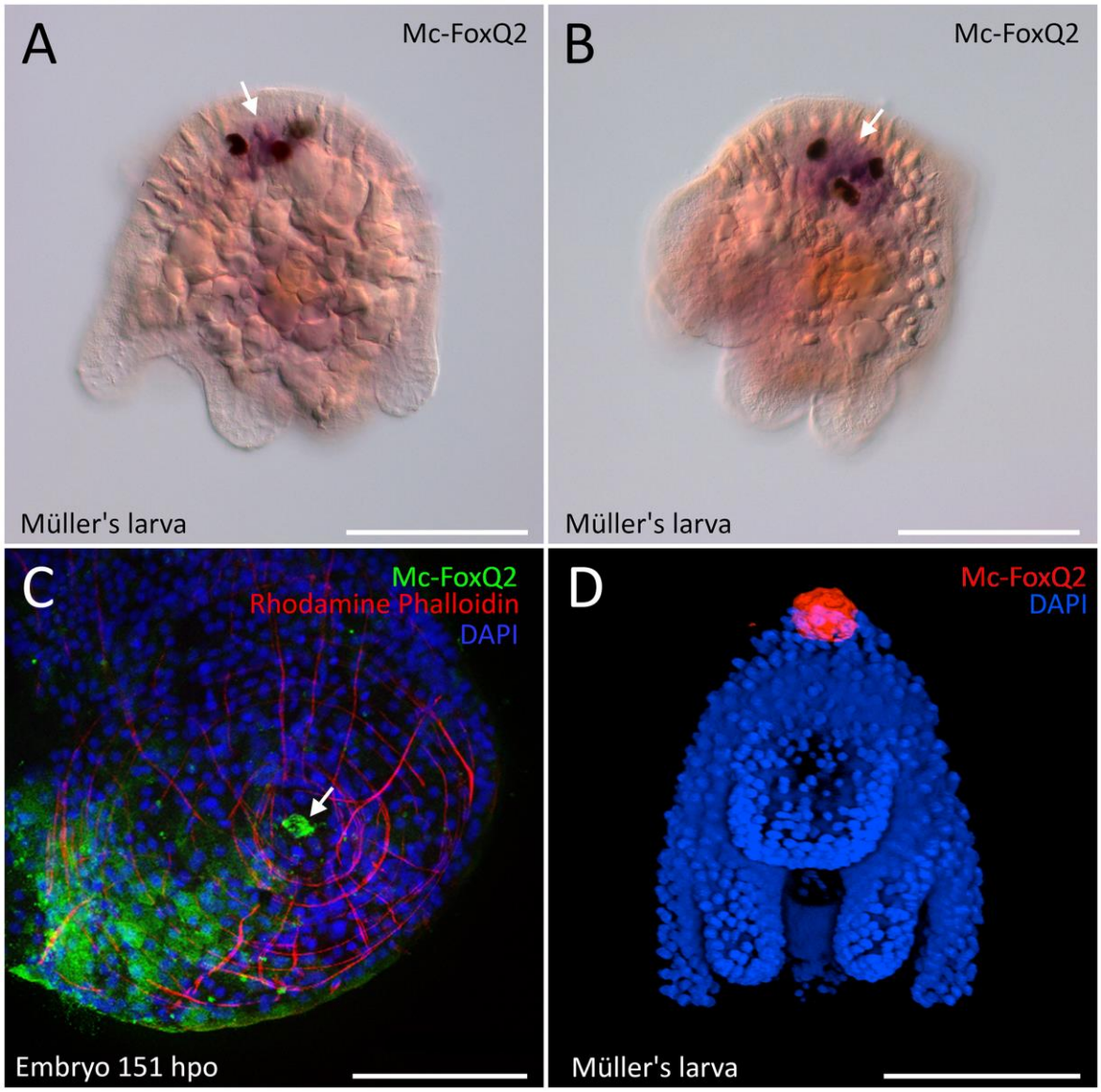


Figure 5.19 - WISH and immunocytochemistry of the apical plate marker FoxQ2 in *M. crozieri*. **(A-B)** indicates mRNA expression just underneath the epidermis (white arrowheads). **(C)** A squash preparation acquired using confocal scanning microscopy of a Mc-FoxQ2. immunohistochemistry staining in an advanced embryonic stage (151 hours post oviposition). **(D)** A rendering of a 3d reconstruction of a Mc-FoxQ2 immunohistochemistry staining in a 1-day old Müller's larva captured with a Zeiss Z.1 light-sheet microscope from 5 different angles. All scale bars are 100 µm.

# Discussion

## 5.7 Comparison of relative division timings and spindle positions found in *M. crozieri*

In general, during early spiral cleavage micromere quartets of embryos divide with similar geometry and timing. With increasing complexity of the developing embryo, the synchrony in the relative division timing decreases, often concomitant with a decrease in divisions that exhibit a spiral pattern. Variations of these patterns occur even among the same class of animals as is exemplified by the wide variety of relative division timings found among the gastropods (van den Biggelaar and Haszprunar, 1996). In theory, this information can be used in a comparative approach to infer phylogenetic relationships. One example of such an undertaking is given by Guralnick and Lindberg (2001), where cell timing information has been used to find a phylogenetic signal among spiral cleaving embryos. It is interesting that in this study Guralnick and Lindberg could highlight certain cleavage patterns such as the advanced formation of second quartet micromeres $2q^1$ already at the 24-cell stage in gastropods, while other spiral cleavers, including polyclads like *M. crozieri* (see Figure 5.3) and *H. inquilina* (Surface 1907), form $2q^1$ consistently at the 32-cell stage. Another example in the gastropods, where division timing has been used to infer evolutionary relationships among the major taxa, is the accelerated or decelerated formation of the 4d cell (the mesentoblast). In ancestral-like gastropod species micromere 4d forms last, while in more derived clades an acceleration to the 24-cell stage has taken place (van den Biggelaar and Haszprunar, 1996).

### *5.7.1 Similar relative division timings in the early cell lineage of cotylean and acotylean polyclad flatworms suggest that this pattern is conserved*

Using our cell-lineage data, we could investigate lineage specific cleavage patterns by graphically comparing the relative timing of specific divisions between two polyclad species and with two other members of the Lophotrochozoa up to the 100-cell stage. In *M. crozieri,* quartets form and cleave relatively synchronously up to the 64-cell stage and later, and lead to a specific relative division timing pattern (see Figure 4.8), which is very similar to the one described by Surface (1907) for the polyclad *H. inquilina* (Figure 5.5, B). This pattern can furthermore be easily distinguished from the two other lophotrochozoan phyla representatives, as we have shown for the annelid *Hydroides elegans* (Arenas-Mena, 2007) and the gastropod *Crepidula fornicata* (Conklin, 1897) (see Figure 5.5, B-D). Overall, we think that the similarity between the timing of blastomere cleavages of cotylean and acotylean polyclad flatworms shown in this work is significant enough to interpret as an overall conserved cleavage pattern.

### *5.7.2 The postponed cleavage of micromere 4d in M. crozieri can be explained by an accelerated cleavage pattern of the putative primary trochoblast 1q²*

The deviations between the two polyclad species are most pronounced in the significantly advanced cleavage of first quartet micromeres $1q^{21}$ and a concomitant "delay" of the division of micromere 4d to a stage of about 64 cells (see Figure 5.5). This could be interpreted as a cotylean - acotylean specific deviation, but this remains to be seen until more cell lineage data of other polyclad flatworms become available. Interestingly, both

the lineage of $1q^2$, which is strongly conserved in spiral cleaving embryos and gives rise to the prototroch cells, as well as the 4d blastomere, are known to vary in their timing of appearance among spiralian embryos, which has been shown in particular in molluscs (Guralnick and Lindberg, 2001; van den Biggelaar and Haszprunar, 1996).

Here we should mention that we have shown in chapter IV that the precise timing of the appearance of micromere 4d can vary slightly and it is possible that in some embryos of *M. crozieri* 4d already forms earlier than the 64-cell stage. On the other hand, divisions of $2q^1$ take place close to the cleavage of 4d as can be seen in our cell-lineage (Figure 5.6) and slight variations in division timing of these cells can therefore alter the cell-stage during which micromere 4d cleaves. The suggested 64 cells can therefore not be considered the definite cell-stage when 4d divides. That its division is postponed in *M. crozieri* embryos compared to *H. inquilina* is nonetheless clear.

In the two polyclad flatworms the "postponed" cleavage of micromere 4d and the putative primary trochoblast lineage $1q^2$ are linked. As we have shown, in *M. crozieri* micromeres $1q^{21}$ and even their daughter cells $1q^{211}$ divide before micromere 4d cleaves (at about the 64-cell stage) (Figure 5.6). This alone leads to an additional 12 cells, emerging entirely from $1q^2$ lineage, which cannot be present in *H. inquilina*, where $1q^{21}$ divides after micromere 4d cleaves (at the 45-cell stage) (Figure 5.6, B). These accelerated divisions of $1q^{21}$ in *M. crozieri* thus have knock-on effects on the precise cell stage when micromere 4d forms, which has to be consequently "delayed" (in case of $1q^{21}$ by 12 cells), postponing the 4d cleavage from cell-stage 45, as is the case in *H. inquilina*, to 57; but together with divisions of micromeres $1q^{112}$ and $1q^{12}$, results in a division at the 64-cell stage. Therefore, we suggest, that

micromere 4d is not necessarily "delayed" in *M. crozieri*, despite the significant difference of approximately 20-cells compared to *H. inquilina*. We would rather say that the first quartet of micromeres is significantly accelerated in *M. crozieri*, which is why 4d gets inevitably postponed to a later cell stage (from a 45-cell to about a 65-cell stage).

A more proliferative first quartet of micromeres, which most likely gives rise to the ectodermally derived tissue in the episphere of the Müller's larva could already reflect the formation of prominent ciliary band structures in *M. crozieri*. For instance, the highly prominent 8 lobes present in *M. crozieri* larvae comprise a great number of ciliary band cells (Lapraz et al., 2013; Rawlinson, 2010; Rawlinson, 2014) (we counted about 450 cells; student data) but is reduced in larvae of *H. inquilina,* where one pair of lateral lobes is entirely absent. Given that in most spiral developers the primary trochoblast $1q^2$ gives rise to ciliary band cells (Damen and Dictus, 1994; Henry et al., 2007; Maslakova et al., 2004a; Maslakova et al., 2004b), this supports a slightly accelerated and more proliferative $1q^2$ lineage in *M. crozieri*. This of course follows the idea that larval structures such as lobes and ciliary bands, in particular their presence/absence or reduction, are reflected in the early cell lineage of the developing embryo (discussed in more detail in chapter VI). This idea could be further tested by comparing relative division timings of direct developing polyclad flatworms to indirect developers. Could, for instance, the absence of ciliary bands in direct developing polyclads make a noticeable difference during early cleavage in comparison to *M. crozieri*? If so, we would expect a significant difference in the relative division timing and proliferation rate of the putative primary trochoblast lineage, $1q^2$.

### *5.7.3 Spindle positions during spiral cleavage in the polyclad flatworms H. inquilina and M. crozieri are conserved*

The comparison between dexiotropic/laeotropic cleavages summarized in Table 5.1 shows that spindle positions of individual cells are very similar between the two polyclad species. We marked in green the cleavages, which are basically the same in all dexiotropic spiral cleaving embryos. This indicates that up to the 100-cell stage early development is conserved between *M. crozieri* and *H. inquilina*. However, there were a few inconsistencies we noticed: In *M. crozieri* the division of $1a^{22}$-$1d^{22}$ did not show a clear dexiotropic division pattern as described by Surface for *H. inquilina*. Furthermore, whenever pronounced vertical divisions occur, the comparison is more difficult and more often leads to different observations e.g. the divisions of the second quartet micromeres $2a^{2}$-$2d^{2}$ are indicated by Surface as vertical but dexiotropic while we find these divisions to be more of laeotropic nature (see Table 5.1). We also recognised that occasionally one or even two spindles were reversed in *M. crozieri*, meaning that the spindle was oriented in the opposite direction in comparison to its counterpart cells of the other quadrants (see cells in see Table 5.1 indicated by an asterisk). Reversed spindle orientations are not easily spotted from an animal view and became clearer when spindle positions were individually observed from a lateral view, which is straight forward with the 4d virtual embryo. These reversed spindle positions are not mentioned by Surface but they occur for example quite commonly in the description of the slipper snail *Crepidula fornicata* (Conklin, 1897). We think that this is a general feature of spiralian embryos especially in later divisions (> 36-cell stages) after the formation of the four quartets.

### *5.7.4 Spiralian cross patterns as seen in the polyclad flatworm M. crozieri are most likely a by-product of the conserved spiral cleavage pattern*

The stereotypical spiral quartet cleavage leads to a conserved cleavage geometry of early blastomeres. This subsequently also affects the apical pole by forming two stereotypical cross-patterns, which both symmetrically surround the centrally positioned apical rosette cells ($1q^{111}$). The first pattern that can be distinguished is called the "annelid cross" which is formed by peripheral rosette cells $1q^{112}$ and $1q^{2}$ and their derivatives. The second pattern is the so-called the "molluscan cross" and is composed of blastomeres $1q^{12}$ ("molluscan cross" cells) and $2q^{11}$ (tip cells of the "molluscan cross") and their derivatives (Raven, 1966; Siewing, 1969; Verdonk and Van den Biggelaar, 1983). Regarding the sizes and relative division rates between molluscs, nemerteans, annelids and sipunculids the following can be summarised: molluscs tend to have smaller peripheral rosette cells ($1q^{112}$), nemerteans tend to have large apical rosette cells ($1q^{111}$) with an accelerated relative division rate and annelids have relatively large peripheral rosette cells ($1q^{112}$) with an accelerated relative division rate (Maslakova et al., 2004b). Such a comparison among spiral cleaving taxa is possible due the highly stereotypic geometry of the apical cell mosaic. The apical rosette cell formation appears to be a key event for the formation of the apical cell mosaic and we want to point out one more time the deviation found between *H. inquilina* (Surface, 1907) and *M. crozieri* regarding the formation of the apical rosette cells. As shown in the results section of this chapter and in contrast to our observations in *M. crozieri*, Surface describes a very unusual final positioning of the apical rosette cells ($1q^{111}$), whereby $1a^{111}$ becomes to lie in between of $1c^{112}$ and $1d^{112}$ but loses contact to its sister cell $1a^{112}$ (and respectively

for all other rosette cells). One possibility is that this observation was mistakenly made, as apical rosette formation is arguably one of the most conserved patterns of spiralian taxa displaying spiral quartet cleavage. The division of apical cell $1q^{11}$ in particular always proceeds in a very marked laeotropic division and represents the starting point of the apical cell mosaic comprising the annelid/"molluscan cross" pattern. This event is shared by polyclad flatworms as shown by us in detail for *M. crozieri* (see Figure 5.7, H and Figure 5.10). To our knowledge there is not a single case of any spiral cleaving embryo in which the laeotropical division of $1q^{11}$ results in two daughter cells (apical rosette cells + "annelid cross" cells) separated from each other. The only "deviation" of the highly conserved laeotropic division of apical cells $1q^{11}$ is found in its reversed form (dexiotropic division) if the embryos' spiral cleavage pattern is already hard-wired from the beginning to the sinistral (counter clockwise) cleavage mode instead to the more commonly found dexiotropic (clockwise) mode. In this case, embryos such as the bladder snail *Physa fontinalis* (Wierzejski, 1905) or the annelid *Hydroides elegans* (Arenas-Mena, 2007), display a laeotropic helical twist during the third cleavage (4-8 cell stage) and show a dexiotropic division pattern of $1q^{11}$.

In short, the clockwise and counterclockwise orientation of the first micromere quartet (1q) is fundamentally conserved as much as is the quartet formation by alternating spindle positions in macromeres.

Interestingly, it appears that spindle positions of $1q^{11}$ are not the only highly conserved feature in the apical plate. In most spiralian taxa the relative division timing of the resulting apical rosette cells $1q^{111}$ is, in comparison to its more vegetally positioned sister cells $1q^{112}$,

either significantly delayed for several rounds of cleavages, or these cells do not divide any further. An example for a complete arrest is given in the common pond snail *Lymnaea stagnalis* (Dettlaff and Vassetzky, 1991) for which the relative division timing of the first quartet of micromeres could be followed in detail for a prolonged period of time (Verdonk, 1965). The nemerteans provide an exception to this rule, as their apical rosette cells divide early on during the development (see Maslakova et al., 2004) and this might be linked to the uniquely large size of nemertean animal micromeres, which already at the 8-cell stage are either of equal size or exceed the size of the macromeres.

These typical cleavage patterns of the apical cell lineage $1q^{11}$, shared by many spiral cleaving taxa, allow to predict how the apical rosette cells and other cells organised around it form. This suggests two things: firstly, some apical cell mosaic patterns, in particular apical rosette cells and the "annelid cross", are intrinsically part of the spiral quartet cleavage mode; and secondly, the "annelid cross" must be a highly conserved geometric structure and always forms as the inevitable by-product of the highly spiral division apical cells $1q^{11}$.

It would be very much surprising if "annelid/molluscan cross" patterns would not be present in an embryo that follows the conserved spiral quartet cleavage, as its cleavage mode itself dictates the formation of cross-like patterns. As has been pointed out by Jenner (2003), this implies that cross-patterns can be found ubiquitously in spiral cleaving embryos. But, and this should be kept in mind, these patterns do not necessarily represent synapomorphies with phylogenetically relevant information, as they have been used in the past (see also Nielsen (2004) and citation therein; Jenner (2003) and citations therein).

However, we think it makes sense to predict that cross-like patterns are as old as the last common ancestor of the Lophotrochozoa (Merkel et al., 2012) assuming that the stereotypic spiral cleavage as we see it today was present.

### *5.7.5 A highly conserved cleavage pattern of the apical cell lineage 1q$^{11}$ indicates a strong conservation in the cell fate of apical rosette cells 1q$^{111}$, which in spiral cleavers give rise to the apical organ*

Spiral cleavers usually form the apical organ from descendants of the apical-most 1q1 micromeres (Nielsen, 2004; Nielsen, 2005). In *M. crozieri*, even though our cell lineage is limited to the time point of cilia formation during gastrulation, our preliminary tracing experiments suggest that descendants of apical rosette cells 1q$^{111}$ end up exactly at the place where the apical organ is expected to be formed (Figure 5.14, Figure 5.17, D). This is further supported by our gene expression patterns of the apical marker FoxQ2, which spatially link the embryo's most apical tip post-gastrulation to the apical plate of hatched larvae (Figure 5.19).

At the same time, we find it intriguing that the asymmetric, strictly spiral divisions of apical cells 1q$^{11}$ (laeotropic in dexiotropic species and vice versa) and the cleavage timing of their derivatives cells altogether appear to represent a shared trait that is highly conserved among different spiralian taxa, including the polyclad flatworms as shown in this chapter. Due to this high similarity of the cleavage pattern in the lineage of the apical cell 1q$^{11}$, we suggest that there are also likely few evolutionary changes in the final fate of these cells, including apical rosette cells 1q$^{111}$ could be more restricted. This also supports the idea of

a common history of the apical organ (derived from apical rosette cells $1q^{111}$), which is found in many planktonic trochophore-like larval stages, as a plausible scenario.

Recently however, a cell lineage study on the bryozoan species *Membranipora membranacea*, brought forward some evidence, which supports an alternative view. This lophotrochozoan member also has a planktonic larval stage, the cyphonautes larva, which comprises ciliated bands and an apical organ, but displays a unique developmental mode, very different from the typical spiral quartet cleavage, exhibiting a biradial cleavage symmetry. The cell lineage, including the apical organ, however, shows similarities to the fate map of other spiral cleaving embryos, despite the lack of the conserved spiral cleavage pattern. This fact prompts the authors to argue against a correlation of the stereotypic geometry of blastomeres with a specific cell fate (Vellutini et al., 2016) and would therefore diminish the idea that highly conserved cleavage patterns as seen in the lineage of apical cells $1q^{11}$ could indicate a more conserved cell fate across spiral cleaving lophotrochozoans. Instead these authors argue that the "underlying molecular pattering" is the main factor that drives cell fates and therefore explains much better its evolutionary conservation. In this regard, more cell lineage and gene expression studies in non-spiral cleaving lophotrochozoans are necessary to further clarify these seemingly opposing views.

## 5.8 The cell lineage of the putative primary trochoblast $1q^2$

### *5.8.1 Conservation of primary trochoblasts cell lineage in the spiralian developmental program*

Trochophores are primary marine larvae named after a highly characteristic feature they share: the prototroch. This structure is a belt of specialised, often elongated epidermal cells (called prototrochal cells) with long compound cilia, that usually encircles the whole body of the larva and acts as its primary locomotion system and is also used for feeding (Henry et al., 2007). Besides other types of ciliary structures that may be present in the trochophore the prototroch initially emerges in the developing embryo. Noticeably, in spiralian embryos with stereotypical blastomere arrangement during early cleavage it derives without exception from the first micromere quartet (1q). The larger portion of prototrochal cells is usually generated by primary trochoblast cells $1q^2$ and so-called accessory trochoblasts from apical micromeres $1q^{1222}$ may also contribute to the structure (Henry et al., 2007). Interestingly the timing of prototroch formation can vary during embryogenesis depending on the organism's developmental mode.

In polyclad flatworm larvae, hundreds of prototroch-like specialised epidermal cells are present, which follow the lobes of polyclad larvae and form multilayered bands of varying numbers (Figure 1.9 and Figure 1.10) (Lacalli, 1982; Ruppert, 1978) (see also chapter I). The resulting structure is called the ciliary band and, just like prototrochs of other marine larvae, it functions as a locomotory structure and is most likely additionally used for feeding. Ciliary bands can vary among different polyclad larvae (Rawlinson, 2014) and it was not shown yet if they consist of compound cilia (Nielsen, 2012b) as is usually the case

in prototrochs of other marine larvae (Jenner, 2003). The origin of ciliary bands amongst the early blastomeres has not been studied in detail but from a cell-lineage study performed on the acotylean polyclad *H. inquilina* it appears that the greater part of the ciliary band is derived from the first quartet and second quartet of micromeres, the latter more specifically from micromeres 2a and 2c. Surprisingly, fluorescent positive cells with long cilia and traced from the third quartet micromeres were also previously noted in *H. inquilina* (Boyer et al., 1998). Interestingly, the fact that the prototroch derives from first, second and third quartets of micromeres in *H. inquilina* resembles a study performed on the nemertean *Cerebratulus lacteus* (Henry and Martindale, 1998). Much earlier, Surface (1907) who looked in detail at the early embryogenesis of the polyclad *H. inquilina* also pointed out that blastomeres $1q^2$ correspond in mode and time of origin to cells found in annelids (the trochoblasts) and their molluscan equivalent (the turret cells). Given the strong conservation of primary trochoblasts among spiralian embryos (Henry et al., 2007) Surface's assumption does not sound unreasonable.

### *5.8.2 Lineage tracing in the polyclad flatworm M. crozieri supports the presence of a true primary trochoblast in M. crozieri*

The ubiquitous presence of primary trochoblasts $1q^2$ in spiral cleaving embryos, its unambiguous fate determined to give rise to major parts of the prototroch and its first acknowledgment in the polyclad flatworm *H. inquilina* (Boyer et al., 1998; Surface, 1907) prompted us to study if the homologous blastomere $1q^2$ would also give rise to ciliary band structures in the polyclad flatworm *M. crozieri*. Tracing one of the putative primary trochoblasts, $1c^2$, in *M. crozieri* showed that its descendants become arranged in a ring-like

pattern in gastrulating embryos located in an area where ciliary band cells would be expected to appear (Figure 5.17, Figure 5.18, see also Rawlinson 2010). Additionally, descendants of blastomere $1d^{12}$ fit into the pattern of this structure suggesting a putative fate as accessory trochoblasts (Figure 5.17, D). Both blastomeres, $1q^{2}$ and $1q^{12}$, could therefore be interpreted as precursor cells of the future ciliary band, fulfilling a cell-lineage fate as primary and accessory trochoblasts, which are typical for the spiralian developmental program.

## 5.9 Further evidence for the presence of a true primary trochoblast $1q^{2}$ in *M. crozieri*

### *5.9.1 Distinct developmental modes can be reflected in specific early cell lineages in primary marine larvae: A few examples*

There are several examples of marine larval adaptations being reflected in changes in the early development mode and thus early cell lineage. For example, in gastropods, free-spawners form the prototroch early on while in intracapsular developers the formation of a prototroch can be significantly postponed or may not form at all (Guralnick and Lindberg, 2001). In the latter case, trochal cells are sometimes delayed, presumably conditioned by this mode of development. Furthermore, the original prototroch in intracapsular developing larvae can be modified into another more efficient locomotory organ, the velum (Garstang, 1928), whose evolution was also recently argued to lead initially during early cleavage to a slower cleavage rhythm in trochal cell lines (van den Biggelaar and Haszprunar, 1996). A good example for such a scenario is the well-studied pond snail

*Lymnaea stagnalis*, which can be arguably considered almost a direct developer, in which the trochophore-stage has been greatly obscured by an advanced development into a veliger larva. In *L. stagnalis t*he four primary trochoblasts $1q^2$, after their division at stage 10, do not divide anymore for a long time (Dettlaff and Vassetzky, 1991). This restraint reflects the minor role given to prototrochal cells up to the point of an early veliger at stage 22,. The initially reduced development of prototrochal cells follows in principle an old idea, namely that larval adaptation may be reflected in the early embryonic stages (see Guralnick (2013).

Interestingly, a similar scenario has been suggested for echinoderm larvae. Usually, their planktotrophic larvae form prominent skeletal elements called spicules, which unmistakably define the shape of the pluteus stage. The larvae of echinoids can, however, be modified from a planktotrophic into lecithotrophic larvae, which completely gave up a planktotrophic life style. In this case, the skeletogenic cell lineage is affected, which leads to a reduced or absent skeleton in the larva. This loss of larval skeletal elements is reflected within the embryo's early cell lineage, where a characteristic unequal fourth cleavage, that gives rise to micromeres, from which skeletogenic cells arise in other lineages, is missing. This deviation in the cell lineage can be interpreted as an adaptation to a new life history as non-feeding larvae (Wray, 1994).

Another example from the late 19th century comes from Lillie, who suggested that discrepancies in the cell lineage of the freshwater clam *Unio* were adaptations to its modified larval stage, the glochidium larva (Lillie, 1898). Mead, in 1897, also argued that the cause of the delayed divisions of the first quartet of micromeres in the slipper snail

*Crepidula* compared to annelids is its relatively long protecting intracapsular stage (Mead, 1897).

If larval adaptation can alter the early cell lineage, as it seems to be the case for the seemingly more versatile primary trochoblasts, then more examples should be present in other taxa, such as polyclad flatworms. Therefore, if different developmental modes, as shown in the various examples of this section (we should also bear in mind direct versus indirect development), are reflected within different aspects of the early cell lineage (e.g. high proliferation rate, relative division timing), this information could be helpful to identify homologous founder blastomeres, which will give rise to specialised larval organs.

### *5.9.2 High proliferative rate and large size supports putative fate of primary trochoblasts in M. crozieri*

We investigated the cleavage pattern of descendants of the putative primary trochoblast to understand if the adaptation of *M. crozieri* to a planktotrophic lifestyle with eight lobes comprising a prominent ciliary and could be linked to the cleavage mode of cell $1q^2$ and perhaps even to the size of its direct descendants. The ciliary band in *M. crozieri* is made up of hundreds of cells in hatchlings, and should manifest itself in a higher proliferation rate in early blastomeres. Those are suspected to be part of the ciliary band lineage.

This fits well with our observations of rapid division rounds observed in descendants of cells $1q^{211}$ (Figure 5.3). We have shown in *M. crozieri* that these founder cells become very large around the formation of the apical cell mosaic, carrying enlarged prominent nuclei and undergoing highly asymmetric cell divisions (Figure 5.16). In this regard, we think that the

increased proliferation rate of putative trochoblast cells and their prominent size further supports the idea that in *M. crozieri* micromeres $1q^2$ represent true primary trochoblasts.

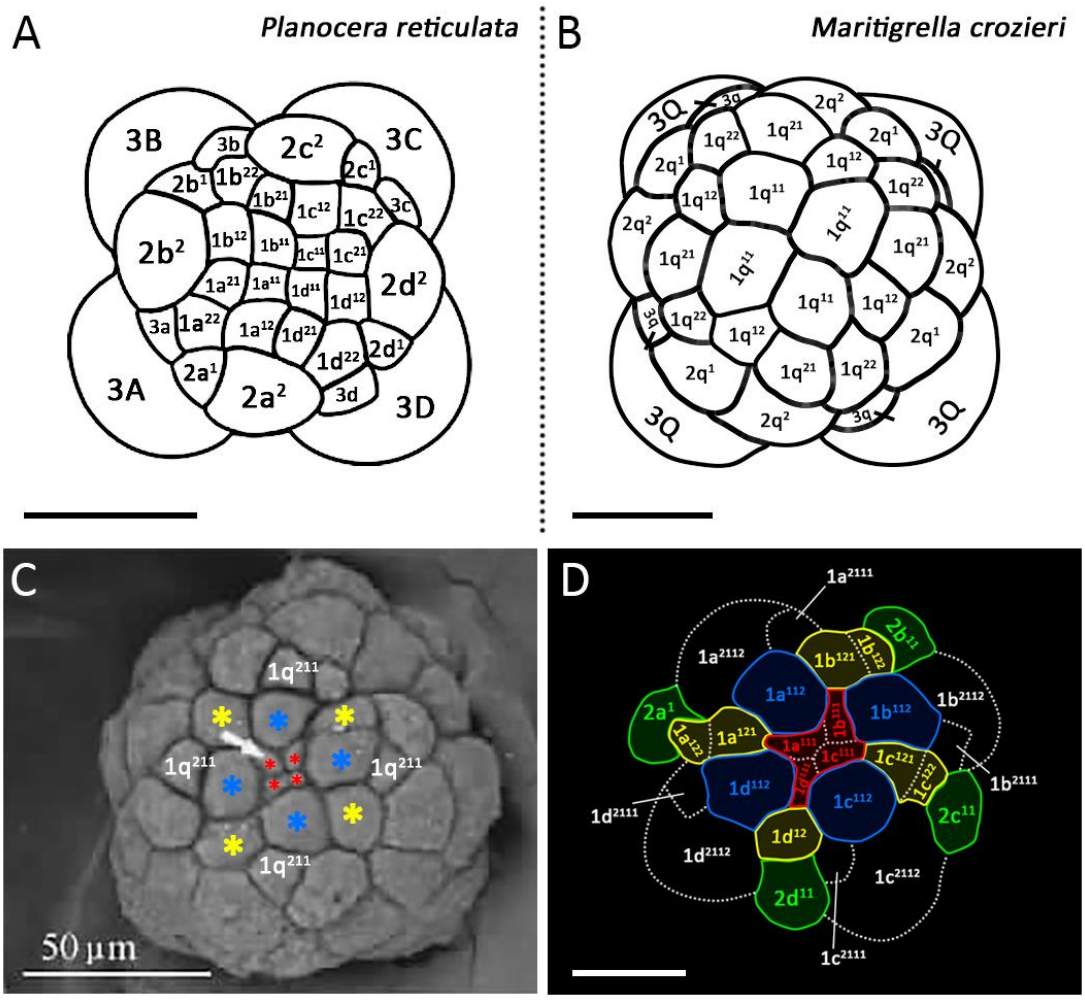


Figure 5.20 – A comparison between the acotylean polyclad flatworm *Planocera reticulata* and the cotylean polyclad flatworm *Maritigrella crozieri*. (A is drawn and C modified after (Tang et al., 2011).

### *5.9.3 Comparison of M. crozieri and direct developing polyclad flatworms could provide further evidence for the lineage of the primary trochoblast reflecting an indirect life style*

Consistently, the volume increase of rapidly dividing cells $1q^{211}$ as seen clearly in *M. crozieri* also appears to be a pronounced feature in other indirect developing polyclad species. For example, in the drawings of the indirect developing polyclad flatworm *Eurylepta cristata* (Selenka, 1881) after the formation of the apical rosette cells, large descendants of $1q^{2}$ (most likely $1q^{211}$), connected with the "annelid cross" cells, are recognisable. By contrast, descendants of the primary trochoblast in two direct developers (with no prototroch), *Leptoplana tremellaris* and *Leptoplana alcinoi*, remain small (Selenka, 1881). Additionally, a recent study on another direct developer, *Planocera reticulata,* shows the early development via SEM pictures and a transitional state before a juvenile, which the authors describe as a ciliated free-swimming planktonic larva, which then gradually reduces its cilia before turning into a juvenile with a pharyngeal mouth opening (Tang et al., 2011). In fact this peculiar larva, that resembles more a pre-juvenile stage with sometimes thin lobes, has been initially described by Kato (1940) and then in more detail by Teshirogi et al. (1981). Ciliary band cells, if present at all, are likely to be highly reduced. In this context, we find it notable that the 32-cell stage already shows obvious differences compared to *M. crozieri*. Micromeres of the second quartet in particular $2q^{2}$ are already significantly enlarged in *P. reticulata*, similar to the description by Selenka for direct developers, while first quartet micromeres are comparatively small (Selenka, 1881). However, *P. reticulata* forms an apical cell mosaic, with the typical peripheral rosette cells ($1q^{112}$) and much smaller apical rosette

cells ($1q^{111}$) similarly to *M. crozieri*. This allows one to identify ""molluscan cross"" cells ($1q^{121}$), nested between the "annelid cross" cells. In *M. crozieri* $1q^{2111}$ and $1q^{2112}$, the derivatives of putative primary trochoblasts $1q^2$, are directly connected to the annelid ross cells and the latter can be easily recognised by their large size. Interestingly, cells positioned around the "annelid cross" where $1q^2$ descendants are expected to lie in *P. reticulata* during this stage do not show any dramatically increased cell size (Figure 5.20).

It would be a plausible scenario for polyclad flatworms that cells of comparatively large size may reflect their provisions for a relatively increased proliferation rate. If correct, then in direct developers, or developers without a proper larval stage featuring a prominent ciliary band such as *P. reticulata*, the size of putative trochoblasts (1q) and micromeres forming lobes can be expected to be reduced because producing highly proliferative trochoblasts during early development would make little sense if they do not form proper ciliary band structures. Furthermore, In the polyclad *H. inquilina*, cells of the second quartet (2q) have been shown to give rise to the somatoblast (2b), which forms circular muscles and major parts of the stomodeum (Boyer et al., 1998). Stomodeum precursor cells might play a more crucial role for direct developers such as *L. tremellaris*, *L. alcinoi* and *P. reticulata*, which will much earlier on start feeding with a well formed pharyngeal structure, while indirect developers featuring a more primitive mouth, such as *M. crozieri* and *H. inquilina* are primarily planktotrophic and feeding depends on the ciliary bands until metamorphosis takes place. Based on these observations, we suggest that the different feeding mechanisms between juveniles and planktotrophic larvae may be reflected in cell size differences between 1q and its derivatives (larger and more proliferative if ciliary bands are

present) and perhaps even in micromere $2q^2$ (larger in direct developers where pharyngeal structures replace ciliary bands and a primitive mouth). Future comparisons of division time rhythms between direct and indirect developers could further strengthen this idea. If more evidence for a correlation between an advanced cell division timing of descendants $1q^2$ and formations of ciliary bands becomes obvious, this would further suggest that primary trochoblasts found in polyclad flatworms originate from the same blastomeres as found in other spiralians, which we think is likely to be the case.

# CHAPTER 6 Functional analysis of spiral cleavage mechanisms

## Introduction

In this short chapter, we investigate spiral cleavage by carrying out drug treatments similar to previous work in molluscs (Shibazaki et al., 2004). Shibazaki showed that the principle mechanism for spiral deformation of blastomeres depends on actin filaments rather than on spindle-forming microtubules. Spiral deformations could be driven in lophotrochozoan species as a product of the same cytoskeletal mechanism. We will test this hypothesis by the effect of two drugs on the spiral cleavage pattern in *M. crozieri*, in particular during the third division round (4- to 8-cell stage). We will interfere with the actomyosin cortex using the actin polymerisation inhibiting agent Latrunculin A, and with spindles using the microtubule polymerisation inhibiting agent Colchicine. This will test if the mechanism that drives the spiral cleavage pattern in snails is also present in polyclad flatworms.

# Results

## 6.1 Spindle inclination remains flexible and can be adjusted prior to anaphase in 4-cell stage embryos

In most spiral cleaving embryos, the third cleavage is highly characteristic for its unequal division into four larger macromeres (1Q) and four smaller micromeres (1q) accompanied by the iconic helical deformation of blastomeres (spiral deformation) (Figure 6.1, A-C). We observed that during metaphase, several minutes before anaphase starts, spindles still undergo dynamic movements and can change their inclination angle, yet formation of blastomeres appear to be unaffected (Figure 6.1, A-B). This observation is a clue suggesting that spindle inclination may have little effect on the helical deformations of the blastomeres.

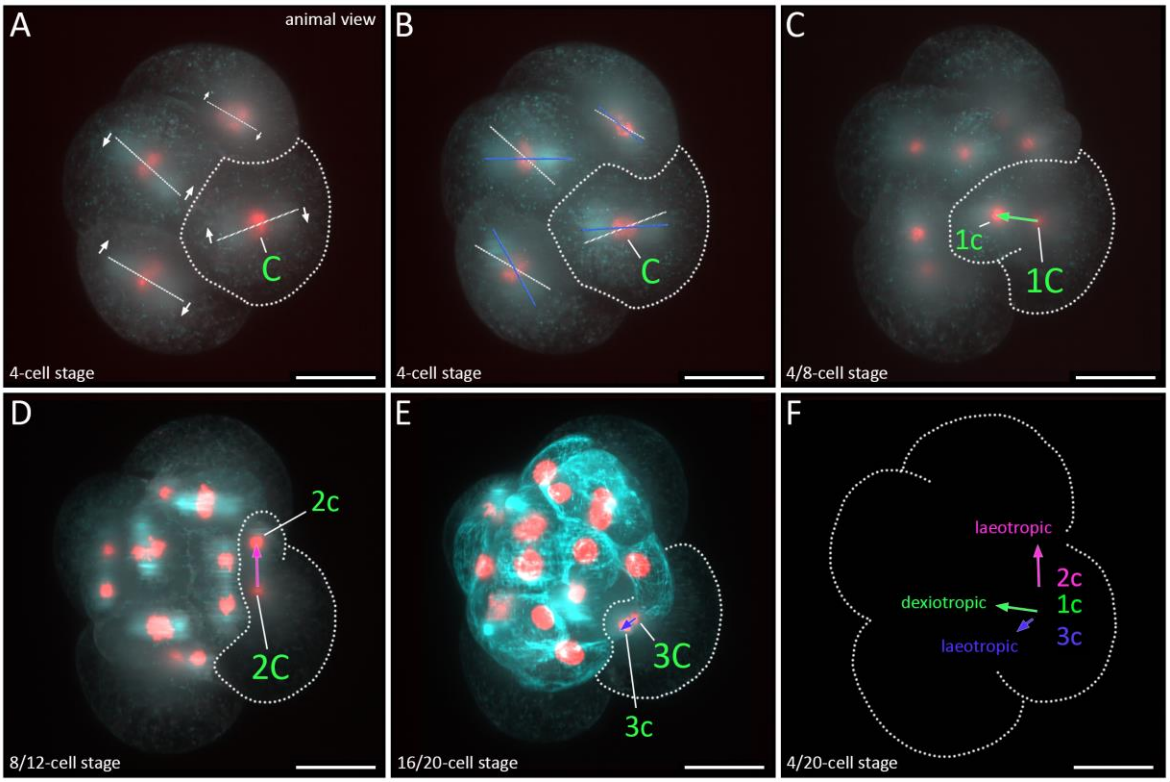


Figure 6.1 – Dynamic changes of spindle inclinations during the third cleavage in *M. crozieri* with a focus on the C blastomere **(A-C)** Transition from 4-cell stage into an 8-cell stage (3rd cleavage) with focus on the spindle inclinations. **(A)** 4-cell stage with sister chromatids of each blastomere during metaphase. The position of spindles is indicated with a white line. Arrows indicate their future inclination **(B)** Same embryo shown 13 min later with blastomeres still in metaphase just before separation of sister chromatids. The white line marks the previous position of the spindle. Blue line indicates the new inclination angle. **(C)** Blastomeres are now in late anaphase. **(D-F)** Embryo continues development into a 12-cell stage (D), 16-cell stage (E). **(F)** Spindle positions of the C-blastomere between third and fifth cleavages showing the alternating spindle positions from dexiotropic to laeotropic, to dexiotropic. 1q = first quartet, 2q = second quartet, 3q = third quartet. Scale bar = 50 µm.

## 6.2 F-Actin and spindle (alpha Tubulin) visualization during early cleavage

Prior to the drug treatment experiments we performed a series of antibody stainings to visualise the cell cortex of early blastomeres and the formation of the spindle apparatus during early cleavage (Figure 6.2). In one oocyte, F-Actin staining was already observed in form of two small rings closely associated with each of the microtubule organizing centers (MTOC) of the forming spindle apparatus (Figure 6.2, A). Otherwise F-Actin staining was observed as expected in the cell cortex of early blastomeres (Figure 6.2, B-F). Alpha Tubulin was detected either as a filamentous microtubule network, which can cover the whole blastomere (Figure 6.2, D and E) or as a distinct staining of the spindle apparatus (Figure 6.2, A and F). A transition of a filamentous network into a spindle apparatus can be seen in a 4/8-cell stage embryo showing prominent spiral deformations (Figure 6.2, C). Conspicuously, we occasionally observed embryos where an increased F-Actin staining was obvious in only one of the four quadrants. In one embryo, this was accompanied by a significant decrease in alpha Tubulin staining (Figure 6.2, E).

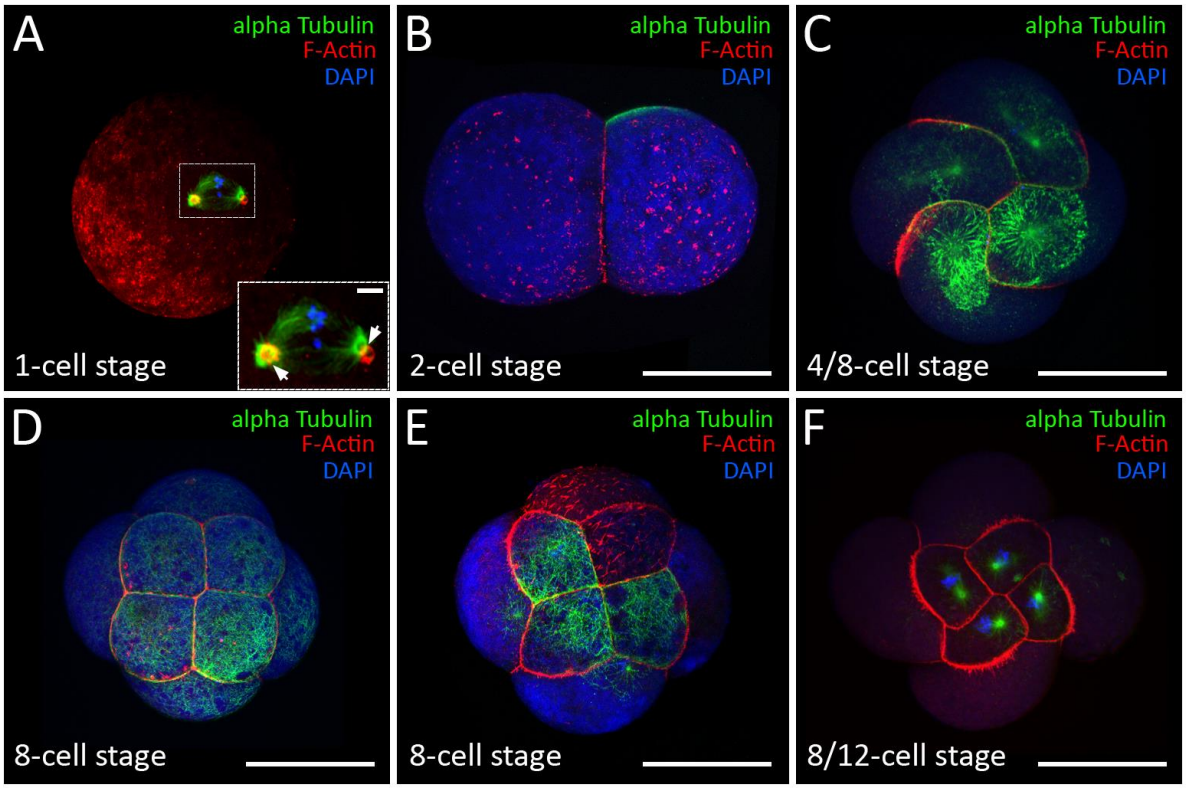


Figure 6.2 - Confocal laser scanning images of control embryos between the 1-cell and 8-cell stage stained with anti-alpha Tubulin antibodies (green), Alexa Fluor 568 Phalloidin (red) and DAPI (blue). Scale bars are 100 µm.

## 6.3 Effects of Colchicine and Latrunculin A treatments in embryos (4/8-cell stage) of *M. crozieri*

For the pharmacological treatment experiments, about 100 embryos at the 4-cell stage were collected, except for 0.05% Colchicine treated embryos (n = 22) and their controls (n = 6). Each drug condition consists of controls (incubated in the highest EtOH concentration used as drug solvent), low drug concentrations and high drug concentrations.

Colchicine is well known for its inhibitory effects during mitosis by disrupting microtubule polymerization and thereby severely affecting correct spindle formation (Dustin, 1984). The strongest concentration of 0.05% Colchicine led to embryos completely devoid of any spindle apparatus (n = 22). Only one embryo developed into a severely deformed 8-cell stage. Interestingly, drug treated embryos were found to arrest at the onset of metaphase where they showed clearly spiral deformations of blastomeres (14/22). All control embryos (n=6) made it into an 8-cell stage.

A similar result was obtained in embryos which were treated with Colchicine concentrations of 0.005%. In this case 48% of all embryos (41/85) displayed spiral deformations and no spindles were detected in any of the embryos selected for confocal imaging (n=8) (Figure 6.3, C; Figure 6.4). However, alpha Tubulin staining observed via confocal imaging was often present in the form of small spots close to the nuclei (7/8). By contrast, confocal imaging revealed that 13/15 control embryos did show normal spindle formations as seen in Figure 6.3,A . The lowest Colchicine concentrations (0.0005%) led to embryos of which 39% (n=27/70) showed spiral deformations (Figure 6.3, D; Figure 6.4) and from which all embryos used for confocal imaging (n=3) showed intact spindles indicating that this Colchicine treatment was not sufficient to inhibit spindle formation.

Latrunculin A is a drug commonly used to study cell functions due to its disrupting effect on F-Actin assembly (Spector et al., 1983). For this experiment two different concentrations were chosen. Both, 0.325 µM and 0.75 µM resulted in embryos completely devoid of any spiral deformations and none of the embryos (n=48) showed any sign of F-Actin around the cell periphery (Figure 6.3, F-G; Figure 6.4). Of all embryos treated with 0.325 µM Latrunculin

A, five had blastomeres carrying two nuclei and one embryo showed two blastomeres also carrying two nuclei. Most embryos treated with 0.75 µM Latrunculin A simply fell apart into four individual blastomeres (see Figure 6.3, H as an example). A similar although slightly less severe effect was observed in embryos treated with 0.325 µM Latrunculin A solution (Figure 6.3, F) and 5 embryos were found exhibiting an 8-cell stage.

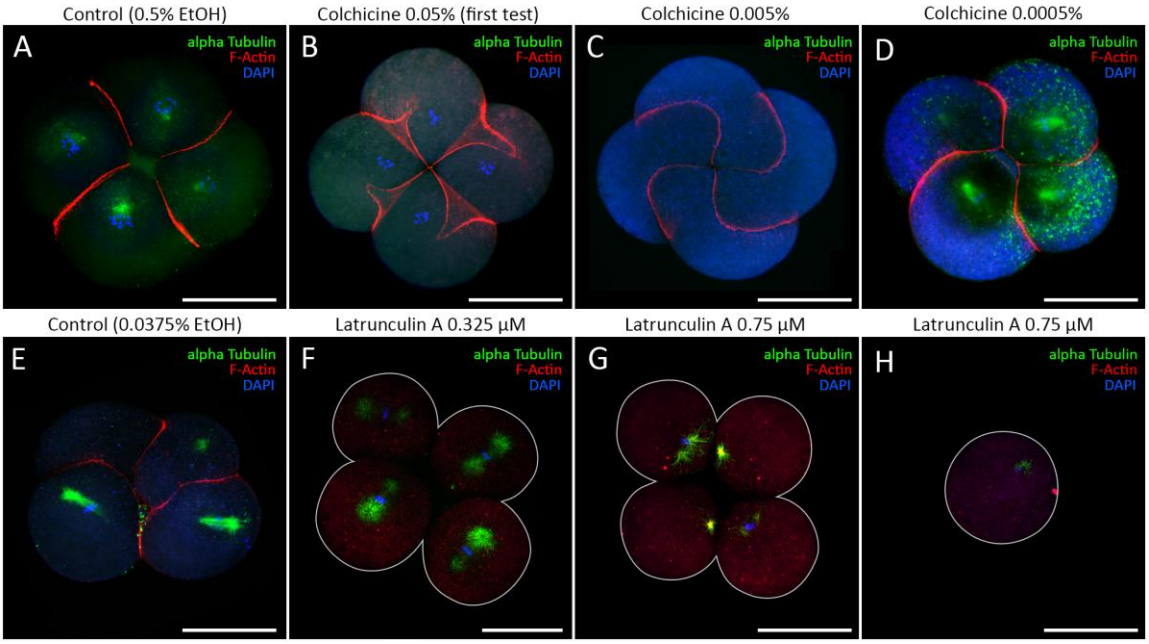


Figure 6.3 - Confocal laser scanning images of Colchicine **(A-D)** and Latrunculin A **(E-H)** treated embryos during the third cleavage. **(A)** Embryo used as a control for the Cholchicine treatment experiment. **(B-C)** Embryos exposed to 0.05% and 0.005% concentrations of Colchicine showing spiral arrangement of blastomeres but no spindle formations. **(D)** Embryo exposed to 0.0005% Colchicine showing spiral arrangement of blastomeres and spindle formation in each cell. **(E)** Embryo used as a control for the Latrunculin A treatment experiment. **(F)** Embryo exposed to 0.325 µM Latrunculin A showing no sign of spiral arrangement of blastomeres and no F-Actin cell cortex staining but the formation of spindles in each cell. **(G)** Embryo exposed to 0.75 µM Latrunculin A looking similar to G. **(H)** Single blastomere of an embryo, which lost attachment to other blastomeres after being exposed to 0.75 µM Latrunculin A. Scale bars = 100 µm.

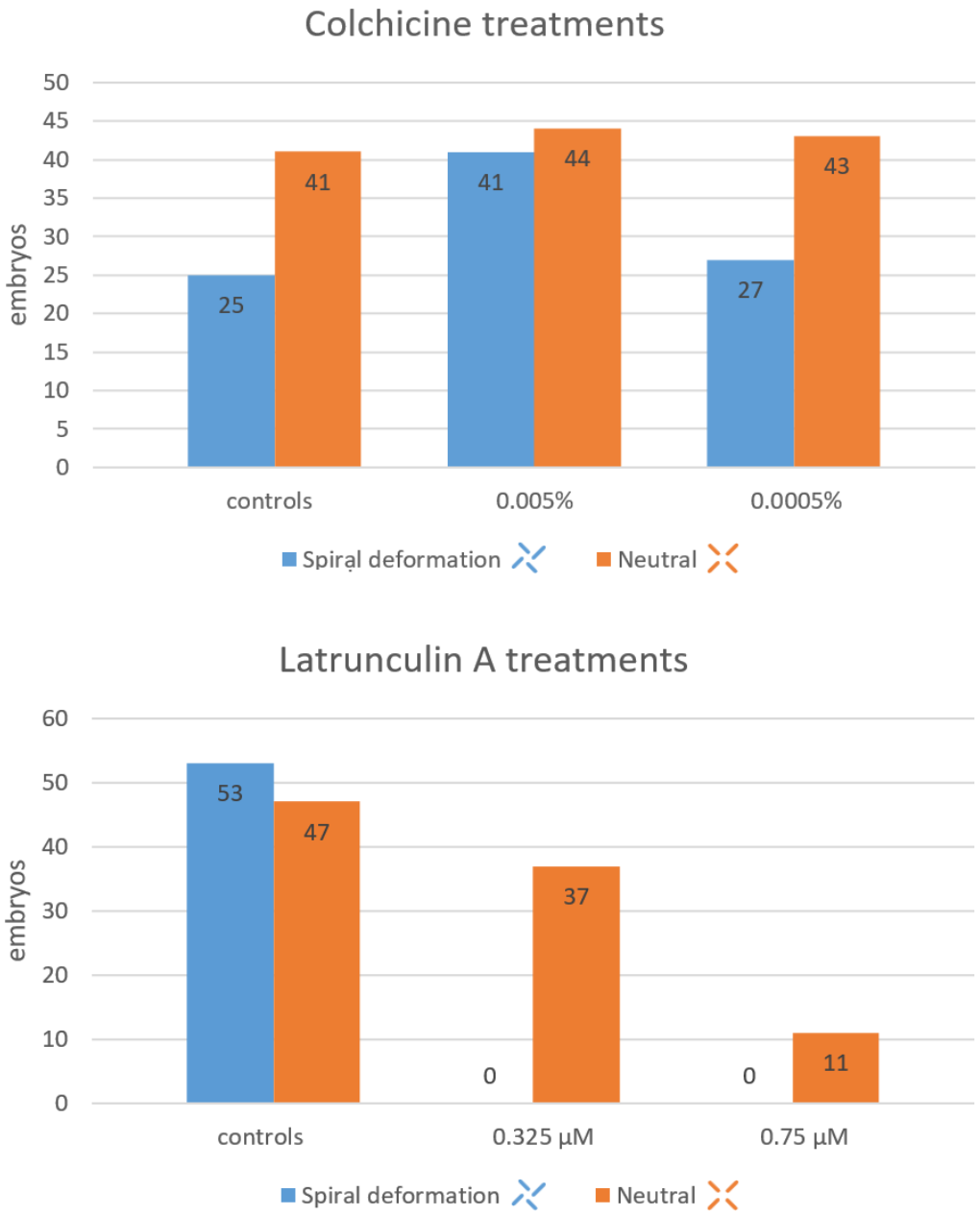


Figure 6.4 - Summary of Colchicine and Latrunculin A treatments during the transition from 4-cell stage into a 8-cell stage showing their effect on the helical deformation of blastomeres (spiral deformation). While the treatment of Colchicine has no obvious effect on spiral deformation the treatment (top) 0.325 µM and 0.75 µM Latrunculin A leads to its complete loss (bottom). The lower number of 0.325 µM and 0.75 µM Latrunculin A treated embryos is caused by their disintegration into single blastomeres during treatment or subsequent fixation.

# Discussion

## 6.4 A conserved mechanism of the spiral cleavage pattern can be demonstrated in *M. crozieri* embryos

Shibazaki et al. (2004) demonstrated that dextral cleaving metaphase/anaphase 4-cell stage embryos of the pond snail *L. stagnalis,* which were devoid of spindles due to treatments with the microtubule depolymerization agent Nocodazole, nonetheless showed the typical spiral deformation of blastomeres. In some embryos, spiral deformations were observed to be even slightly more prominent. This observation suggested the presence of a cross-talk between the spindle forming microtubules and actin. It also made clear that the iconic spiral twist depends not on spindle inclination, but rather on actin polymerization, which affects spiral deformation to which the spindle position prior to anaphase can adjust. We show a very similar finding in *M. crozieri* embryos treated with the microtubule depolarization agent Colchicine (which has the same effect as Nocodazole). Embryos with high Colchicine concentrations (0.05%, 0.005% and 0.0005%) were, as expected, devoid of spindles (Figure 6.3, B-C) but showed clear signs of spiral deformations similar to control embryos (Figure 6.2; Figure 6.3, A). On the other hand, in Latrunculin A treated embryos (which are expected to have reduced actin cytoskeleton), spiral deformations were absent (Figure 6.3, F-H), reflecting once more the result of similarly treated *L. stagnalis* embryos (Kuroda, 2015; Shibazaki Y, Shimizu M, 2004). Polyclad flatworms recapitulate the observation made in the snail *L. stagnalis,* that spiral

deformations depend on actin polymerization, which in turn influences spindle orientations and not vice versa.

This result is also in accordance with our observation that spindle positions remain relatively dynamic during the third cleavage and their inclination angle can be still adjusted in blastomeres to the point at which anaphase is initiated (Figure 6.1). We can also corroborate the suggested presence of a cross-talk between microtubules and actin during metaphase as we found in *M. crozieri*, like *L. stagnali*s, occasionally exceedingly prominent spiral deformations in Colchicine treated *M. crozieri* embryos (Figure 6.2, B), which are not seen in control embryos or pharmacologically untreated spiral cleaving embryos. Our drug treatment experiments on the polyclad flatworm *M. crozieri* suggest that the principle mechanism for spiral deformation of blastomeres in different lophotrochozoan phyla such as snails and polyclad flatworms depends on actin filaments and is independent of spindle forming microtubules. Microtubules interact with the actin filaments and must be present to accordingly initiate anaphase and subsequently blastomere cleavage in *M. crozieri*.

# CHAPTER 7 CONCLUSIONS

## 7.1 Summary of the findings

In the first part of this thesis I have described the design and assembly of a T-configuration OpenSPIM with twin lasers (Chapter III). I have shown that a home-built SPIM microscope can be used as a scientific instrument to study the embryonic development of the polyclad flatworm *M. crozieri* on fixed specimens and *in vivo*. With our microscope, we produced high-quality 3D images of fixed larvae and have captured in detail the early embryonic development up to the 128-cell stage in a series of 3D reconstructed time-points.

In the second part of this thesis I increased the current knowledge of the early development of the polyclad flatworm *M. crozieri*, which facilitates evolutionary comparisons of the development of different flatworms and lophotrochozoans more broadly (Chapter IV). I showed that the early cleavages in *M. crozieri* are accompanied by cytoplasmic perturbations, which are most pronounced in macromeres during the formation of the third and fourth quartets and during cleavage in the mesentoblast precursor 4d. Based on our live-imaging data we suggest that these perturbations are probably the product of dynamic cytoskeletal activity that may play an important role in normal development. Our description of the early embryonic development of the cotylean polyclad flatworm *M. crozieri* closely resembles what is known of the acotylean polyclad *H. inquilina*. Both species, *M. crozieri* and *H. inquilina,* share the same symmetry breaking mechanism resulting in animally and vegetally positioned pairs of daughter cells of 4d and both show a slight tendency to an increased size of the D-blastomere (determined to be one of the

vegetal cross-furrow cells) at the 4-cell stage, which we confirmed in *M. crozieri* by precise volume measurements. This finding is consistent with an unequal cleavage mechanism, that specifies the D-quadrant early on. This is surprising, as *M. crozieri* has previously been suggested to represent an equal cleaver, where animal/vegetal (micormere/macromere) interactions are thought to be crucial for the establishment of the D quadrant and thus for normal development. Despite of the fact that the first two cleavages result in a slightly unequal 4-cell stage, it should not be excluded that cell-cell interactions, which are thought to be the driving mechanism for specifying the D quadrant in equal cleavers, may still play a crucial role for the early development in polyclad flatworms.

The third part of this work our comparison of the relative division timing pattern, based on our cell-lineage study, revealed a high degree of conservation between the two polyclad species and a lower degree in two other lophotrochozoan animals (annelid and mollusc; Chapter V). Also spindle positions, which define an either laeotropic or dexiotropic cleavage pattern during early development, appear to be conserved, particularly in the micromere lineage of the first quartet (1q) that gives rise to head structures in polyclad larvae. We think that cross patterns of the apical cell mosaic in *M. crozieri*, that reliably appear in many spiral cleavers after the apical rosette cells ($1q^{111}$) have formed, reflect a particularly conserved cleavage pattern characteristic for the apical cell lineage of many spiral cleavers and could also mean that a more conserved cell fate of these blastomeres is possible.

Long term tracing of blastomeres with focus on apical rosette cells $1q^{111}$, and the putative primary trochoblasts $1q^{2}$, corroborates a conserved fate of, respectively, the apical organ

and also ciliary band cells in polyclad flatworms, which they seem to share with other lophotrochozoans (Chapter V).

Finally, drug treatment experiments on polyclad embryos suggest that the principle mechanisms for spiral deformation of blastomeres depends on the polymerization of actin filaments but takes place independently of spindle forming microtubules, which corroborates previous findings on snails (Chapter VI). Ultimately, although much remains to be done, this work adds new knowledge to our current understanding of spiral cleavage in the Lophotrochozoa by shedding light on the development of a poorly studied clade - the polyclad flatworms.

## 7.2 Long-term live imaging experiments: Current limitations and trials to overcome them

Here I will discuss the limitations and challenges of working on the polyclad *M. crozieri,* and the newly-established live-imaging setup that I used throughout this work. Addressing these challenges will facilitate future work on this exciting novel model for evo-devo, and is thus important to point out possible strategies to tackle these issues. One of my aims was to obtain live recordings of the embryonic development in *M. crozieri* for a duration that is long enough to determine the fate of functional larval organs such as the apical organ and the ciliary band among the early blastomeres of spiral cleaving embryos. In this section, I will summarise the main challenges of such an undertaking, which partly prevented me from achieving more robust results and how I envisage they could be addressed in future work.

### *7.2.1 A protocol for cryopreservation of M. crozieri embryos needs further elaboration*

In the case of *M. crozieri,* gravid adults are found in the Florida Keys, where animals are handpicked from *Ecteinascidia turbinata* colonies, but cannot be adequately fed once they are in laboratory culture. This limits the availability of oocytes and living embryonic material suitable for live recordings to a couple of weeks weeks, depending, for instance, on the size of specimens collected. Therefore, it is easy to understand that each individual animal, which arrives safely in London and contains enough eggs for poking and microinjections, is of considerable value for our research. For our live-imaging recordings at least two gravid adults poked simultaneously as this might help with normal fertilization of all eggs and allows to readily microinject up to 200 embryos, of which at least half will show fluorescent signal and are therefore available for each live-recording session. Our OpenSPIM set-up, however, currently allows us to acquire time-lapse recordings of only one individual embryo at a time. Only then accurate sample positioning by the 4D stage is guaranteed, that has to be precise enough to, for instance, allow tracing of fluorescently marked nuclei during embryonic development. While there is certainly still the possibility to further advance the OpenSPIM setup by implementing more sophisticated 4D-stages and mounting strategies, which allow for instance imaging of several embryos at a time, another idea was to use some of these embryos for cryopreservation either before or after microinjections, in a comparable manner as performed on human and mouse embryos. This would allow long-term storage and provide a convenient way to perform live-imaging studies even when adult animals are not in culture. While in human and mouse embryos

recent cryopreservation kits guarantee a very high success rate (Joyce Harper, UCL, personal communication), their solutions are unfortunately not optimised for oocytes kept in sea water, and embryos of *M. crozieri* are unable to withstand a normal procedure and solutions, which are clearly optimised for mouse and human eggs. We noticed this during a preliminary test on *M. crozieri* oocytes during a vitrification workshop at University College London (data not shown). Therefore, a more adapted protocol is certainly necessary, which would use more elaborated solutions, that can take salt water conditions needed for marine invertebrate oocytes (e.g. from *M. crozieri*), into account. Such a protocol would be of value, not only for research in living embryos in *M. crozieri* but also for many other marine lophotrochozoan non-model organisms, which are currently difficult to collect and cannot be cultured readily in the lab.

### *7.2.2 Using the CRISPR Cas9-knock out system to prevent rotational embryonic movements caused by ciliary beating*

Although the fluorescent signal starts to weaken over the days of *M. crozieri* embryonic development, as nuclei divide and shrink while cell density simultaneously increases, it is striking that the signal is sufficient to trace individual nuclei until gastrulation. However, there inevitably comes the time-point when the embryos start to form epidermal cilia at around 5 days post poking embryo when epidermal cells start covering the embryo during epiboly, which leads to its rotational movements (see video 9). This event marks a definitive break of any lineage tracing, that can be only achieved up to this point.

One approach to reduce rotational movements of gastrulating embryos was using the CRSIPR-Cas9 system to knock out a gene of the intraflagellar transport (IFT) machinery, IFT-

88, which is required for the correct assembly of eukaryotic cilia (Pazour et al., 2000). Therefore, we produced two sgRNAs targeting this gene, which were co-injected together with the Cas9 proteins into *M. crozieri* oocytes during a single microinjection session. Embryos were subsequently allowed to develop for several days. While OpenSPIM live-imaging and observations of these embryos gave the impression that the rotational movements of a few embryos were slightly delayed (data not shown), we also realised that all embryos were still eventually able to develop cilia and begin rotational movements or gave rise to larvae that clearly showed swimming behaviour indicating presence of cilia. Sequencing of individual microinjected embryos also did not show that the targeted area of IFT-88 was affected by the CRISPR-Cas9 system. Despite our unsuccessful first trial, more time and work clearly needs to be invested to make the CRISPR-Cas9 system readily usable in *M. crozieri*. This could be perhaps more efficiently tested on location in Florida, where *M. crozieri* animals can be collected almost all year long and a continuous supply of fresh material is available.

## 7.3 Future outlooks

Here, I want to summarise several interesting directions that this project could take on in future work.

### *7.3.1 Complete cell lineage until larva*

Further investigations of the apical rosette cell lineage ($1q^{111}$) and the primary trochoblast cell lineage ($1q^{2}$) into the larval stage of *M. crozieri* would strengthen my current findings, presented in this thesis, that these two lineages, which respectively give rise to the apical organ and the ciliary band cells, are homologous to the lineages found in other lophotrochozoan phyla.

One strategy could be to combine the live-imaging recordings of fluorescently tagged nuclei, as performed in this study, with fluorescent vital dyes that label the membrane of cells and are more commonly used for cell-lineage tracing (e.g. DiI) by a second round of microinjections specifically into blastomeres $1q^{11}$ or $1q^{2}$. Live imaging could then be interrupted at the point where the embryo starts rotating and the DiI fluorescently labelled cells investigated after the development into a larva is complete.

### *7.3.2 4d fate and mesentoblast*

According to Boyer (1998), Surface (1907) and this study, the 4d blastomere gives rise to mesodermal structures such as longitudinal, diagonal, and oral hood muscles as well as mesenchyme and some endoderm in polyclad larvae.

Surface described the more animally positioned daughter micromere $4d^{1}$ as the true mesentoblast (giving rise to mesoderm and some endoderm) and the larger daughter micromere $4d^{2}$ as the entoblast, giving solely rise to endoderm. This has to be

reinvestigated in more detail. A conclusive proof for $4d^1$ being the mesentoblast would be to directly inject $4d^1$ to follow its fate, which due to its central position and small size, as show in this work, is very difficult. Alternatively, indirect evidence could arise by injecting the large $4d^2$-blastomere to see if developed larvae contain labeled endoderm and/or mesoderm.

In the first case this would prove that blastomere $4d^1$ (or one of its daughter cells) is indeed the mesentoblast and that spiral cleavage in polyclad flatworms is in fact delayed by at least one cell cycle. The second scenario is that also $4d^2$ gives rise to some mesoderm. This second scenario is important, because it directly points to the 4d blastomeres to give rise to endomesoderm, which is more in accordance with the canonical spiral developmental program as seen in other lophotrochozoans. Additionally, a cell lineage, similar to our early cell-lineage created for *M. crozieri*, but with focus on the cleavage pattern of the 4d blastomere, could shed more light on the fate and behavior of this evolutionary important cell.

### *7.3.3 Investigating the MAPK pathway during early cleavage in M. crozieri*

As discussed in Chapter I, the MAPK signalling pathway may have an important role for the establishment of a dorsal "organizer" during early spiral cleavage. This might be also true for polyclad flatworms, where the temporal and spatial expression pattern of MAPK is completely unknown. Our preliminary immunohistochemistry stainings of MAPK showed a weak, but specific, expression pattern in one of the four quadrants of the first quartet of micromeres (1q) during early cleavage (8- to 16-cells) and then slightly stronger in one quadrant of the micromeres of $1q^1$ (Figure A. 2). A specific expression pattern in one of the four macromeres was not observed during these stages. This finding need of be thoroughly reinvestigated, as the role of this pathway in polyclads may provide new insights into evolutionary changes in the spiralian developmental program.

### *7.3.4 Investigating direct developers for a comparison study*

In this work, we have created an early cell lineage for *M. crozieri* that includes information of the relative division timing. As discussed in Chapter VI, we think that such information is likely to reflect adaptations to new developmental modes. A test case, to further strengthen this hypothesis, would be to compare the early cell lineage of the primary trochoblast $1q^2$, which typically gives rise to the future prototroch/ciliary bands between *M. crozieri* and any direct developing polyclad flatworm, which does not develop any lobes or ciliary band-like structures. The comparative study between direct versus indirect developing polyclad flatworms can of course uncover further evolutionary changes between these two different developmental modes.

# REFERENCES


**Ackermann, C., Dorresteijn, A. and Fischer, A.** (2005). Clonal domains in postlarval Platynereis dumerilii (Annelida: Polychaeta). *J. Morphol.* **266**, 258–280.

**Adoutte, A., Balavoine, G., Lartillot, N. and De Rosa, R.** (1999). Animal evolution - The end of the intermediate taxa? *Trends Genet.* **15**, 104–108.

**Aguinaldo, A. M. A., Turbeville, J. M., Linford, L. S., Rivera, M. C., Garey, J. R., Raff, R. A. and Lake, J. A.** (1997). Evidence for a clade of nematodes, arthropods and other moulting animals. *Nature* **387**, 489–493.

**Amat, F., Höckendorf, B., Wan, Y., Lemon, W. C., McDole, K. and Keller, P. J.** (2015). Efficient processing and analysis of large-scale light-sheet microscopy data. *Nat. Protoc.* **10**, 1679–96.

**Amiel, A. R., Henry, J. Q. and Seaver, E. C.** (2013). An organizing activity is required for head patterning and cell fate specification in the polychaete annelid Capitella teleta: New insights into cell-cell signaling in Lophotrochozoa. *Dev. Biol.* **379**, 107–122.

**Anderson, D. T.** (1973). *Embryology and Phylogeny in Annelids and Arthropods*. Pergamon Press.

**Anderson, D. T.** (1977). The embyonic and laval development of the turbellarian Notoplana australis (Schmarda, 1859) (Polycladida : Leptoplanidae). *Mar. Freshw. Res.* **28**, 303–310.

**Arenas-Mena, C.** (2007). Sinistral equal-size spiral cleavage of the indirectly developing polychaete hydroides elegans. *Dev. Dyn.* **236**, 1611–1622.

**Asadulina, A., Panzera, A., Verasztó, C., Liebig, C. and Jékely, G.** (2012). Whole-body gene expression pattern registration in Platynereis larvae. *Evodevo* **3**, 27.

**Baguñà, J.** (1976). Mitosis in the intact and regenerating planarian Dugesia mediterranea n.sp. II. Mitotic studies during regeneration, and a possible mechanism of blastema formation. *J. Exp. Zool.* **195**, 65–79.

**Boyer, B. C.** (1986). Experimental evidence for the origins of determinative development in the polyclad turbellarians. *Hydrobiologia* **132**, 117–119.

**Boyer, B. C.** (1987). Development of in vitro fertilized embryos of the polyclad flatworm, Hoploplana inquilina, following blastomere separation and deletion. *Roux's Arch. Dev. Biol.* **196**, 158–164.

**Boyer, B. C.** (1989). The Role of the First Quartet Micromeres in the Development of the Polyclad Hoploplana inquilina. *Biol. Bull.* **177**, 338–343.

**Boyer, B. C., Henry, J. Q. and Martindale, M. Q.** (1996). Dual origins of mesoderm in a basal spiralian: cell lineage analyses in the polyclad turbellarian Hoploplana inquilina. *Dev. Biol.* **179**, 329–338.

**Boyer, B. C., Henry, J. Q. and Martindale, M. Q.** (1998). The cell lineage of a polyclad turbellarian embryo reveals close similarity to coelomate spiralians. *Dev. Biol.* **204**, 111–123.

**Burkel, B. M., Von Dassow, G. and Bement, W. M.** (2007). Versatile Fluorescent Probes for Actin Filaments Based on the Actin-Binding Domain of Utrophin. *Cell Motil Cytoskelet.* **64**, 822–832.

**Cannon, L. R. G.** (2003). Marine flatworms: the world of polyclads. *CSIRO Publ.*

**Chan, X. Y. and Lambert, J. D.** (2014). Development of blastomere clones in the Ilyanassa embryo: Transformation of the spiralian blastula into the larval body plan. *Dev. Genes Evol.* **224**, 159–174.

**Child, C. M.** (1900). The early development of Arenicola and Sternaspis. *Arch. für Entwicklungsmechanik der Org.* **9**, 587–723.

**Clement, A. C.** (1962). Development of Ilyanassa following removal of the D macromere at successive cleavage stages. *J. Exp. Zool.* **149**, 193–215.

**Conklin, E.** (1897). The embryology of Crepidula. *J. Morphol.* **XIII**, 1–205.

**Conzelmann, M., Williams, E. A., Tunaru, S., Randel, N., Shahidi, R., Asadulina, A., Berger, J., Offermanns, S. and Jékely, G.** (2013). Conserved MIP receptor-ligand pair regulates Platynereis larval settlement. *Proc. Natl. Acad. Sci. U. S. A.* **110**, 8224–9.

**Costello, D. P.** (1945). Experimental studies of germinal localization in Nereis. I. The development of isolated blastomeres. *J. Exp. Zool. Part A Ecol. Genet. Physiol.* **100**, 19–66.

**Damen, P.** (1994). Cell lineage, and specification of developmental fate and dorso- ventral organization in the mollusc Patella vulgata. *Den Haag; Thesis Univ. Utrecht, Cip-Data K. Bibliotheek*.

**Damen, P. and Dictus, W. J. a. G.** (1994). Cell-lineage analysis of the prototroch of the gastropod mollusc Patella vulgata shows conditional specification of some trochoblasts. *Roux's Arch. Dev. Biol.* **203**, 187–198.

**Dettlaff, T. A. and Vassetzky, S. G.** (1991). *Animal species for developmental studies (Invertebrates)*. 1st ed. Springer.

**Dohmen, M. R. and Van de Mast, J. M. A.** (1978). Electron microscopical study of RNA-containing cytoplasmic localizations and intercellular contacts in early cleavage stages of eggs of Lymnaea stagnalis (Gastropoda, Pulmonata). **81**, 403–414.

**Dorresteijn, A. W. C.** (1990). Quantitative analysis of cellular differentiation during early embryogenesis of Platynereis dumerilii. *Dev. Biol.* **199**, 14–30.

**Dorresteijn, A. W. C. and Fischer, A.** (1988). The process of early development. *Mikrofauna Mar.* **4**, 335–352.

**Dorresteijn, A. W. C., Bornewasser, H. and Fischer, A.** (1987). A correlative study of experimentally changed first cleavage and Janus development in the trunk of Platynereis dumerilii (Annelida, Polychaeta). *Dev. Genes Evol.* **196**, 51–58.

**Drobysheva, I. M.** (1988). An autoradiographic study of the replacement of epidermis in polyclad turbellarians. *Prog. Zool.* **36**, 97–101.

**Drobysheva, I. M. and Yurij, V. M.** (2001). On mitosis in embryos and larvae of polyclads (Platyhelminthes). *Belgian J. Zool.* **131**, 65–66.

**Dunn, C. W., Hejnol, A., Matus, D. Q., Pang, K., Browne, W. E., Smith, S. A., Seaver, E., Rouse, G. W., Obst, M., Edgecombe, G. D., et al.** (2008). Broad phylogenomic sampling improves resolution of the animal tree of life. *Nature* **452**, 745–749.

**Dustin, P.** (1984). Microtubules. *Springer-Verlag* 171–189.

**Egger, B., Steinke, D., Tarui, H., De Mulder, K., Arendt, D., Borgonie, G., Funayama, N., Gschwentner, R., Hartenstein, V., Hobmayer, B., et al.** (2009). To be or not to be a flatworm: The Acoel controversy. *PLoS One* **4**, (5):e5502.

**Egger, B., Lapraz, F., Tomiczek, B., Müller, S., Dessimoz, C., Girstmair, J., Škunca, N.,**

**Rawlinson, K. A., Cameron, C. B., Beli, E., et al.** (2015). A transcriptomic-phylogenomic analysis of the evolutionary relationships of flatworms. *Curr. Biol.* **25**, 1347–1353.

**Ehlers, U.** (1985). Das Phylogenetische System der Plathelminthes. *Gustav Fischer Verlag*.

**Fahrbach, F. and Rohrbach, A.** (2010). A line scanned light-sheet microscope with phase shaped self-reconstructing beams. *Opt. Express* **18**, 2608–2610.

**Fischer, A. H. L. and Arendt, D.** (2013). Mesoteloblast-like mesodermal stem cells in the polychaete annelid Platynereis dumerilii (Nereididae). *J. Exp. Zool. Part B Mol. Dev. Evol.* **320**, 94–104.

**Freeman, G. and Lundelius, W. J.** (1992). Evolutionary implications of the mode of D quadrant specification in coelomates with spiral cleavage. *J. Evol. Biol.* **5**, 205–247.

**Gammoudi, M., Noreña, C., Tekaya, S., Prantl, V. and Egger, B.** (2012). Insemination and embryonic development of some Mediterranean polyclad flatworms. *Invertebr. Reprod. Dev.* **56**, 272–286.

**Garstang, W.** (1928). The origin and evolution of larval forms. *Nature* **122**, 366.

**Giesa, S.** (1966). Die Embryonalentwicklung von Monocelis fusca oersted (Turbellaria, Proseriata). *Z. Morph. Oekol. Tiere* **57**, 137–230.

**Girard, C.** (1854). Researches upon nemerteans and planarians. *Merrihew and Thompson*.

**Gualda, E. J., Vale, T., Almada, P., Feijó, J. A., Martins, G. G. and Moreno, N.** (2013). OpenSpinMicroscopy: an open-source integrated microscopy platform. *Nat. Methods* **10**, 599–600.

**Guralnick, R.** (2002). A recapitulation of the rise and fall of the cell lineage research program: the evolutionary-developmental relationship of cleavage to homology, body

plans and life history. *J. Hist. Biol.* **35**, 537–567.

**Guralnick, R. P. and Lindberg, D. R.** (2001). Reconnecting cell and animal lineages: what do cell lineages tell us about the evolution and development of Spiralia? *Evolution (N. Y).* **55**, 1501–1519.

**Gustafsson, M. K.** (1976). Studies on cytodifferentiation in the neck region of Diphyllobothrium dendriticum Nitzsch, 1824 (Cestoda, Pseudophyllidea). *Zeitschrift für Parasitenkd.* **50**, 323–329.

**Hadfield, M. G., Meleshkevitch, E. A. and Boudko, D. Y.** (2000). The apical sensory organ of a gastropod veliger is a receptor for settlement cues. *Biol. Bull.* **198**, 67–76.

**Halanych, K. M., Bacheller, J. D., Aguinaldo, a M., Liva, S. M., Hillis, D. M. and Lake, J. a** (1995). Evidence from 18S ribosomal DNA that the lophophorates are protostome animals. *Science* **267**, 1641–1643.

**Hall, B. K. and Wake, M. H.** (1999). The origin and evolution of larval forms. *Gulf Prof. Publ.*

**Hallez, P. P.** (1879). Contributions à l'histoire naturelle des Turbellariés. *Danel* **2**, 1–213.

**Hara, K.** (1971). Cinematographic observation of "surface contraction waves" (SCW) during the early cleavage of axolotl eggs. *Wilhelm Roux. Arch. Entwickl. Mech. Org.* **167**, 183–186.

**Hejnol, A.** (2010). A twist in time-the evolution of spiral cleavage in the light of animal phylogeny. *Integr. Comp. Biol.* **50**, 695–706.

**Hejnol, A., Martindale, M. Q. and Henry, J. Q.** (2007). High-resolution fate map of the snail Crepidula fornicata: The origins of ciliary bands, nervous system, and muscular elements. *Dev. Biol.* **305**, 63–76.

**Hejnol, A., Obst, M., Stamatakis, A., Ott, M., Rouse, G. W., Edgecombe, G. D., Martinez, P., Baguñà, J., Bailly, X., Jondelius, U., et al.** (2009). Assessing the root of bilaterian animals with scalable phylogenomic methods. *Proc. Biol. Sci.* **276**, 4261–4270.

**Henry, J.** (2002). Conserved mechanism of dorsoventral axis determination in equal-cleaving spiralians. *Dev. Biol.* **248**, 343–355.

**Henry, J. Q.** (2014). Spiralian model systems. *Int. J. Dev. Biol.* **58**, 389–401.

**Henry, J. Q. and Martindale, M. Q.** (1987). The organizing role of the D quadrant as revealed through the phenomenon of twinning in the polycheate Chætopterus variopedatus. *Roux's Arch. Dev. Biol.* **196**, 499–510.

**Henry, J. Q. and Martindale, M. Q.** (1994). Establishment of the dorsoventral axis in nemertean embryos: Evolutionary considerations of spiralian development. *Dev. Genet.* **15**, 64–78.

**Henry, J. Q. and Martindale, M. Q.** (1998). Conservation of the spiralian developmental program: cell lineage of the nemertean, Cerebratulus lacteus. *Dev. Biol.* **201**, 253–269.

**Henry, J. J. and Martindale, M. Q.** (1999). Conservation and innovation in spiralian development. *Hydrobiologia* **402**, 255–265.

**Henry, J. J. and Perry, K. J.** (2008). MAPK activation and the specification of the D quadrant in the gastropod mollusc, Crepidula fornicata. *Dev. Biol.* **313**, 181–195.

**Henry, J. Q., Perry, K. J. and Martindale, M. Q.** (2006). Cell specification and the role of the polar lobe in the gastropod mollusc Crepidula fornicata. *Dev. Biol.* **297**, 295–307.

**Henry, J. Q., Hejnol, A., Perry, K. J. and Martindale, M. Q.** (2007). Homology of ciliary bands in Spiralian Trochophores. *Integr. Comp. Biol.* **47**, 865–871.

**Huisken, J.** (2012). Slicing embryos gently with laser light sheets. *BioEssays* **34**, 406–411.

**Huisken, J. and Stainier, D. Y. R.** (2007). Even fluorescence excitation by multidirectional selective plane illumination microscopy (mSPIM). *Opt. Lett.* **32**, 2608–2610.

**Huisken, J., Swoger, J., Del Bene, F., Wittbrodt, J. and Stelzer, E. H. K.** (2004). Optical sectioning deep inside live embryos by selective plane illumination microscopy. *Science* **305**, 1007–1009.

**Jägersten, G.** (1972). Evolution of the Metazoan life cycle. *Acad. Press*.

**Jenner, R. A.** (2003). Unleashing the force of cladistics? Metazoan phylogenetics and hypothesis testing. *Integr. Comp. Biol.* **43**, 207–218.

**Kato, K.** (1940). On the development of some Japanese polyclads. *Japanese J. Zool.* **8**, 537–574.

**Kaufmann, a., Mickoleit, M., Weber, M. and Huisken, J.** (2012). Multilayer mounting enables long-term imaging of zebrafish development in a light sheet microscope. *Development* **139**, 3242–3247.

**Keferstein, W.** (1868). Beiträge zur Anatomie und Entwicklungsgeschichte einiger Seeplanarien von St. Malo. *Dieterichsche Buchhandlung* **14**,.

**Keller, P. J., Schmidt, A. D., Wittbrodt, J. and Stelzer, E. H. K.** (2008). Reconstruction of zebrafish early embryonic development by scanned light sheet microscopy. *Science* **322**, 1065–1069.

**Koop, D., Richards, G. S., Wanninger, A., Gunter, H. M. and Degnan, B. M.** (2007). The role of MAPK signaling in patterning and establishing axial symmetry in the gastropod Haliotis asinina. *Dev. Biol.* **311**, 200–212.

**Kühn, A.** (1971). Lectures on developmental physiology. *Springer Sci. Bus. Medi*.

**Kuroda, R.** (2015). A twisting story: how a single gene twists a snail? Mechanogenetics. *Q. Rev. Biophys.* **48**, 445–452.

**Kuroda, R., Endo, B., Abe, M. and Shimizu, M.** (2009). Chiral blastomere arrangement dictates zygotic left-right asymmetry pathway in snails. *Nature* **462**, 790–794.

**Kwan, K. M., Fujimoto, E., Grabher, C., Mangum, B. D., Hardy, M. E., Campbell, D. S., Parant, J. M., Yost, H. J., Kanki, J. P. and Chien, C.-B.** (2007). The Tol2kit: A multisite gateway-based construction kit forTol2 transposon transgenesis constructs. *Dev. Dyn.* **236**, 3088–3099.

**Lacalli, T. C.** (1982). The nervous system and ciliary band of Müller's larva. *Proc. R. Soc. Lond. B. Biol. Sci.* **217**, 37–58.

**Ladurner, P., Rieger, R. and Baguñà, J.** (2000). Spatial distribution and differentiation potential of stem cells in hatchlings and adults in the marine platyhelminth macrostomum sp.: a bromodeoxyuridine analysis. *Dev. Biol.* **226**, 231–241.

**Lambert, J. D.** (2009). Patterning the spiralian embryo: insights from Ilyanassa. *Curr. Top. Dev. Biol.* **86**, 107–133.

**Lambert, J. D.** (2010). Developmental Patterns in Spiralian Embryos. *Curr. Biol.* **20**, R72–R77.

**Lambert, J. D. and Nagy, L. M.** (2001). MAPK signaling by the D quadrant embryonic organizer of the mollusc Ilyanassa obsoleta. *Development* **128**, 45–56.

**Lambert, J. D. and Nagy, L. M.** (2003). The MAPK cascade in equally cleaving spiralian embryos. *Dev. Biol.* **263**, 231–241.

**Lang, A.** (1884). Die Polycladen (Seeplanarien) des Golfes von Neapel: und der angrenzenden Meeres-Abschnitte: eine Monographie. *Wilhelm Engelmann*.

**Lapraz, F., Rawlinson, K. A., Girstmair, J., Tomiczek, B., Berger, J., Jékely, G., Telford, M. J. and Egger, B.** (2013). Put a tiger in your tank: the polyclad flatworm Maritigrella crozieri as a proposed model for evo-devo. *Evodevo* **4**, 29.

**Laumer, C. E., Bekkouche, N., Kerbl, A., Goetz, F., Neves, R. C., Sørensen, M. V., Kristensen, R. M., Hejnol, A., Dunn, C. W., Giribet, G., et al.** (2015a). Spiralian Phylogeny Informs the Evolution of Microscopic Lineages. *Curr. Biol.* **25**, 1–6.

**Laumer, C. E., Hejnol, A. and Giribet, G.** (2015b). Nuclear genomic signals of the "microturbellarian" roots of platyhelminth evolutionary innovation. *Elife* **4**, 1–31.

**Lehmann, F. E. and Hadorn, H.** (1946). Vergleichende Wirkungsanalyse von zwei antimitotischen Stoffen, Colchicin und Benzochinon, am Tubifex-Ei. *Helv. Physiol. Pharmacol. Acta* **4**, 11–42.

**Li, R. and Albertini, D. F.** (2013). The road to maturation: somatic cell interaction and self-organization of the mammalian oocyte. *Nat Rev Mol Cell Biol* **14**, 141–152.

**Lillie, F. R.** (1898). Adaptation in cleavage. *Biol. Lect. Mar. Biol. Lab. Woods Hole, Mass.* 43–67.

**Lyons, D. C. and Henry, J. Q.** (2014). Ins and outs of spiralian gastrulation. *Int. J. Dev. Biol.* **58**, 413–428.

**MacKinnon, B. M., Burt, M. D. B. and Pike, A. W.** (1981). Ultrastructure of the epidermis of adult and embryonic Paravortex species (Turbellaria, Eulecithophora). *Hydrobiologia* **84**, 241–252.

**Malakhov, V. V. and Trubitsina, N. V.** (1998). Embryonic development of the polyclad turbellarian Pseudoceros japonicus from the sea of Japan. *Russ. J. Mar. Biol.* **24**, 106–113.

**Martín-Durán, J. M. and Egger, B.** (2012). Developmental diversity in free-living flatworms. *Evodevo* **3**, 7.

**Maslakova, S. A., Martindale, M. Q. and Norenburg, J. L.** (2004a). Vestigial prototroch in a basal nemertean Carinoma tremaphoros (Palaeonemertea, Nemertea). *Evol. Dev.* **226**, 219–226.

**Maslakova, S. A., Martindale, M. Q. and Norenburg, J. L.** (2004b). Fundamental properties of the spiralian developmental program are displayed by the basal nemertean Carinoma tremaphoros (Palaeonemertea, Nemertea). *Dev. Biol.* **267**, 342–360.

**Mead, A. D.** (1897). The Early Development of Marine annelids. *J. Morphol.* **XIII**, 228–326.

**Merkel, J., Wollesen, T., Lieb, B. and Wanninger, A.** (2012). Spiral cleavage and early embryology of a loxosomatid entoproct and the usefulness of spiralian apical cross patterns for phylogenetic inferences. *BMC Dev. Biol.* **12**, 11.

**Meyer, N. P. and Seaver, E. C.** (2010). Cell lineage and fate map of the primary somatoblast of the polychaete annelid capitella teleta. *Integr. Comp. Biol.* **50**, 756–767.

**Miller, A. L. and Bement, W. M.** (2009). Regulation of cytokinesis by Rho GTPase flux. *Nat. Cell Biol.* **11**, 71–77.

**Morris, J., Nallur, R., Ladurner, P., Egger, B., Rieger, R. and Hartenstein, V.** (2004). The embryonic development of the flatworm Macrostomum sp. *Dev. Genes Evol.* **214**, 220–239.

**Müller, J.** (1850). Archiv für Anatomie, Physiologie und wissenschaftliche Medicin. *Verlag von Veit Comp. Berlin.* 485–500.

**Newman, L. J. and Cannon, L. R. G.** (1998). Pseudoceros (Platyhelmintes: Polycladida) from Indo-Pacific with twelve new species from Austraslia and Papua, New Guinea. *Raffles Bull. Zool.* **46**, 293–323.

**Newman, L. J., Norenburg, J. L. and Reed, S.** (2000). Taxonomic and biological observations on the tiger flatworm, Maritigrella crozieri (Hyman, 1939), new combination (Platyhelminthes, Polycladida, Euryleptidae) from Florida waters. *J. Nat. Hist.* **34**, 799–808.

**Newmark, P. a and Sánchez Alvarado, a** (2000). Bromodeoxyuridine specifically labels the regenerative stem cells of planarians. *Dev. Biol.* **220**, 142–53.

**Nielsen, C.** (2004). Trochophora larvae: Cell-lineages, ciliary bands, and body regions. 1. Annelida and Mollusca. *J. Exp. Zool. Part B Mol. Dev. Evol.* **302**, 35–68.

**Nielsen, C.** (2005). Trochophora larvae: cell-lineages, ciliary bands and body regions. 2. Other groups and general discussion. *J. Exp. Zool. Part B Mol. Dev. Evol.* **304**, 401–447.

**Nielsen, C.** (2012a). How to make a protostome. *Invertebr. Syst.* **26**, 25–40.

**Nielsen, C.** (2012b). Animal evolution: interrelationships of the living phyla. *Oxford Univ. Press Demand*.

**Pazour, G. J., Dickert, B. L., Vucica, Y., Seeley, E. S., Rosenbaum, J. L., Witman, G. B. and Cole, D. G.** (2000). Chlamydomonas IFT88 and its mouse homologue, polycystic kidney disease gene tg737, are required for assembly of cilia and flagella. *J. Cell Biol.* **151**, 709–718.

**Peng, H., Bria, A., Zhou, Z., Iannello, G. and Long, F.** (2014). Extensible visualization and analysis for multidimensional images using Vaa3D. *Nat. Protoc.* **9**, 193–208.

**Pfeifer, K., Schaub, C., Domsch, K., Dorresteijn, A. and Wolfstetter, G.** (2014). Maternal inheritance of twist and analysis of MAPK activation in embryos of the polychaete annelid Platynereis dumerilii. *PLoS One* **9**, :e96702.

**Pick, K. S., Philippe, H., Schreiber, F., Erpenbeck, D., Jackson, D. J., Wrede, P., Wiens, M., Alié, A., Morgenstern, B., Manuel, M., et al.** (2010). Improved phylogenomic taxon sampling noticeably affects nonbilaterian relationships. *Mol. Biol. Evol.* **27**, 1983–1987.

**Pietzsch, T., Saalfeld, S., Preibisch, S. and Tomancak, P.** (2015). BigDataViewer: visualization and processing for large image data sets. *Nat. Methods* **12**, 481–483.

**Pitrone, P., Schindelin, J., Stuyvenberg, L., Weber, M., Eliceiri, K. W. and Huisken, J.** (2013). OpenSPIM - an open access platform for light sheet microscopy. *Nat. Methods* **10**, 598–599.

**Preibisch, S., Saalfeld, S., Schindelin, J. and Tomancak, P.** (2010). Software for bead-based registration of selective plane illumination microscopy data. *Nat. Methods* **7**, 418–419.

**Preibisch, S., Amat, F., Stamataki, E., Sarov, M., Singer, R. H., Myers, E. and Tomancak, P.** (2014). Efficient Bayesian-based multiview deconvolution. *Nat. Methods* **11**, 645–648.

**Raff, R. a and Love, A. C.** (2004). Kowalevsky, comparative evolutionary embryology, and the intellectual lineage of evo-devo. *J. Exp. Zool. B. Mol. Dev. Evol.* **302**, 19–34.

**Raven, C. P.** (1966). Morphogenesis : the analysis of molluscan development. *Pergamon Press*.

**Rawlinson, K. A.** (2010). Embryonic and post-embryonic development of the polyclad flatworm Maritigrella crozieri; implications for the evolution of spiralian life history traits. *Front. Zool.* **7**, 12.

**Rawlinson, K. A.** (2014). The diversity, development and evolution of polyclad flatworm larvae. *Evodevo* **5**, 9.

**Reisinger, V. E. and Cichocki, I.** (1974). Ontogenetische Studien an Turbellarien: ein Beitrag zur Evolution der Dotterverarbeitung im ektolecitalen Ei I. Teil. *J. Zool. Syst. Evol. Res.* **12**, 161–195.

**Render, J. A.** (1989). Development of Ilyanassa obsoleta embryos after equal distribution of polar lobe material at first cleavage. *Dev. Biol.* **132**, 241–250.

**Richter, S., Loesel, R., Purschke, G., Schmidt-Rhaesa, A., Scholtz, G., Stach, T., Vogt, L., Wanninger, A., Brenneis, G., Döring, C., et al.** (2010). Invertebrate neurophylogeny: suggested terms and definitions for a neuroanatomical glossary. *Front. Zool.* **7**, 29.

**Rieger, R. M.** (1994). The biphasic life cycle - a central theme of metazoan evolution. *Integr. Comp. Biol.* **34**, 484–491.

**Rieger, R. M., Salvenmoser, W., Legniti, A. and Tyler, S.** (1994). Phalloidin-rhodamine preparations of Macrostomum hystricinum marinum (Plathelminthes): morphology and postembryonic development of the musculature. *Zoomorphology* **114**, 133–147.

**Robert, H.** (1902). Recherches sur le développement des Troques. *Arch Zool Exper Gen* **3**, 18–538.

**Ruppert, E. E.** (1978). A review of metamorphosis of turbellarian larvae. In “Settlement and Metamorphosis of Marine Invertebrate Larvae.” *Settl. Metamorph. Mar. Invertebr.*

*larvae. Elsevier, New York* **65**, 65–81.

**Santagata, S., Resh, C., Hejnol, A., Martindale, M. Q. and Passamaneck, Y. J.** (2012). Development of the larval anterior neurogenic domains of Terebratalia transversa (Brachiopoda) provides insights into the diversification of larval apical organs and the spiralian nervous system. *Evodevo* **3**, 3.

**Schindelin, J., Arganda-Carreras, I., Frise, E., Kaynig, V., Longair, M., Pietzsch, T., Preibisch, S., Rueden, C., Saalfeld, S., Schmid, B., et al.** (2012). Fiji: an open-source platform for biological-image analysis. *Nat. Methods* **9**, 676–682.

**Schmidt-Rhaesa, A., Harzsch, S. and Purschke, G.** (2016). Structure and Evolution of Invertebrate Nervous System.

**Schmied, C., Stamataki, E. and Tomancak, P.** (2014). Open-source solutions for SPIMage processing. *Methods Cell Biol.* **123**, 505–29.

**Schmied, C., Steinbach, P., Pietzsch, T., Preibisch, S. and Tomancak, P.** (2015). An automated workflow for parallel processing of large multiview SPIM recordings. *Bioinformatics* **32**, 1112–1114.

**Selchow, O. and Huisken, J.** (2013). Light sheet fluorescence microscopy and revolutionary 3D analyses of live specimens. *Photonik Int.* 3–6.

**Selenka, E.** (1881). Zoologische Studien: Zur Entwickelungsgeschichte der Seeplanarien. *Wilhelm Engelmann* **2**, 1–36.

**Shibazaki Y, Shimizu M, K. R.** (2004). Body Handedness Is Directed by Genetically Determined Cytoskeletal Dynamics in the Early Embryo. *Curr. Biol.* **14**, 1462–1467.

**Siewing, R.** (1969). Lehrbuch der vergleichenden Entwicklungsgeschichte der Tiere. *Parey*.

**Smith, J., Tyler, S., Thomas, M. B., Rieger, R. M., Iii, J. S., Tyler, S., Thomas, M. B. and Rieger, R. M.** (1982). The morphology of turbellarian rhabdites: phylogenetic implications. *Trans. Am. Microsc. Soc.* **101**, 209–228.

**Smith, J. P. S., Teyler, S. and Rieger, R. M.** (1986). Is the Turbellaria polyphyletic? *Hydrobiologia* **132**, 13–21.

**Spector, I., Shochet, N. R., Kashman, Y. and Groweiss, A.** (1983). Latrunculins: novel marine toxins that disrupt microfilament organization in cultured cells. *Science.* **219**, 493–495.

**Spek, J.** (1918). Die amöboiden Bewegungen und Strömungen in den Eizellen einiger Nematoden während der Vereinigung der Vorkerne. *Arch. für Entwicklungsmechanik der Org.* **44**, 217–255.

**Stegmaier, J., Amat, F., Lemon, W. C., Teodoro, G., Mikut, R. and Keller, P. J.** (2016). Real-time three-dimensional cell segmentation in large-scale microscopy data of developing embryos. *Dev. Cell* **36**, 225–240.

**Strathmann, R. R.** (2000). Functional design in the evolution of embryos and larvae. *Semin. Cell Dev. Biol.* **11**, 395–402.

**Struck, T. H., Wey-Fabrizius, A. R., Golombek, A., Hering, L., Weigert, A., Bleidorn, C., Klebow, S., Iakovenko, N., Hausdorf, B., Petersen, M., et al.** (2014). Platyzoan paraphyly based on phylogenomic data supports a noncoelomate ancestry of Spiralia. *Mol. Biol. Evol.* **31**, 1833–1849.

**Surface, F. M.** (1907). The early development of a polyclad, Planocera inquilina. *Proc. Acad. Nat. Sci. Philadelphia* **59**, 514–559.

**Tang, Q., Wang, Y.-J. and Wang, X.-A.** (2011). Early Embryo and Larva of Planocera reticulata in Vitro Fertilization and SEM Observation. *Chines J. Zool.* **46**, 66–71.

**Telford, M. J., Herniou, E. A., Russell, R. B. and Littlewood, D. T.** (2000). Changes in mitochondrial genetic codes as phylogenetic characters: two examples from the flatworms. *Proc. Natl. Acad. Sci. United S.tates Am.* **97**, 11359–11364.

**Teshirogi, W., Sachiko, I. and Jatani, K.** (1981). On the Early Development of Some Japanese Polyclads. *Rep. Fukaura Mar. Biol. Lab* 2–31.

**Tinevez, J.-Y., Perry, N., Schindelin, J., Hoopes, G. M., Reynolds, G. D., Laplantine, E., Bednarek, S. Y., Shorte, S. L. and Eliceiri, K. W.** (2016). TrackMate: an open and extensible platform for single-particle tracking. *Methods* **115**, 80–90.

**Tomer, R., Denes, A. S., Tessmar-Raible, K. and Arendt, D.** (2010). Profiling by Image Registration Reveals Common Origin of Annelid Mushroom Bodies and Vertebrate Pallium. *Cell* **142**, 800–809.

**van den Biggelaar, J. A. M.** (1976). Development of dorsoventral polarity preceding the formation of mesentoblast in Lymnaea stagnalis. *Proc. K. Ned. Akad. van Wet. Ser. C Biol. Med. Sci.* **79**, 112–126.

**van den Biggelaar, J. A. M.** (1996). Cleavage pattern and mesentoblast formation in Acanthochiton crinitus (Polyplacophora, Mollusca). *Dev. Biol.* **174**, 423–430.

**van den Biggelaar, J. A. M. and Haszprunar, G.** (1996). Cleavage Patterns and Mesentoblast Formation in the Gastropoda : An Evolutionary Perspective. **50**, 1520–1540.

**van den Biggelaar, J. A. M., Dictus, W. J. A. G. and van Loon, A. E.** (1997). Cleavage patterns, cell-lineages and cell specification are clues to phyletic lineages in Spiralia.

*Semin. Cell Dev. Biol.* **8**, 367–378.

**Vellutini, B. C., Martín-durán, J. M. and Hejnol, A.** (2016). Conserved traits of spiralian development in the bryozoan Membranipora membranacea. *bioRxiv* : 068783.

**Verdonk, N. H.** (1965). Morphogenesis of the head region in Limnaea stagnalis L. *Thoben offset*.

**Verdonk, N. H. and Van den Biggelaar, J. A. M.** (1983). Early development and the formation of the germ layers. *The mollusca* **3**, 91–122.

**Wagner, D. E., Wang, I. E. and Reddien, P. W.** (2011). Clonogenic Neoblasts Are Pluripotent Adult Stem Cells That Underlie Planarian Regeneration. *Science (80-. ).* **332**, 811–816.

**Wall, R.** (1990). *This side up: spatial determination in the early development of animals*. first pape. Cambridge University Press.

**Wang, X.-A. and YU, M.** (2008). Embryonic Development of the Polyclad Notoplana humilis. *Chines J. Zool.* **43**,.

**Westheide, W. and Rieger, R.** (2013). Spezielle Zoologie. Teil 1: Einzeller und Wirbellose Tiere. 3. Auflage. *Springer-Verlag*.

**Wierzejski, A.** (1905). Embryologie von Physa fontinalis L. *Zeitschrift für wissenschaftliche Zool.* **83**, 502–706.

**Willems, M., Egger, B., Wolff, C., Mouton, S., Houthoofd, W., Fonderie, P., Couvreur, M., Artois, T. and Borgonie, G.** (2009). Embryonic origins of hull cells in the flatworm Macrostomum lignano through cell lineage analysis: Developmental and phylogenetic implications. *Dev. Genes Evol.* **219**, 409–417.

**Wilson, E. B.** (1892). The cell-lineage of Nereis. *J. Mor* **VI**, 361–480.

**Wilson, E. B.** (1897). Considerations on cell-lineage and ancestral reminiscence, based on a re-axamination of some points in the early development of annelids and polyclades. *Ann. N. Y. Acad. Sci.* **11**, 1–27.

**Wilson, E. B.** (1904). Experimental studies on germinal localization. *J. Exp. Zool. Part A Ecol. Genet. Physiol.* **1**, 1–72.

**Wray, G. A.** (1994). The Evolution of Cell Lineage in Echinoderms. **34**, 353–363.

**Yoneda, M., Kobayakawa, Y., Kubota, H. Y. and Sakai, M.** (1982). Surface contraction waves in amphibian eggs. *J. Cell Sci.* **54**, 35–46.

**Younossi-Hartenstein, A. and Hartenstein, V.** (2000). The embryonic development of the polyclad flatworm Imogine mcgrathi. *Dev. Genes Evol.* **210**, 383–398.

APPENDIX

**ADDITIONAL FIGURES**

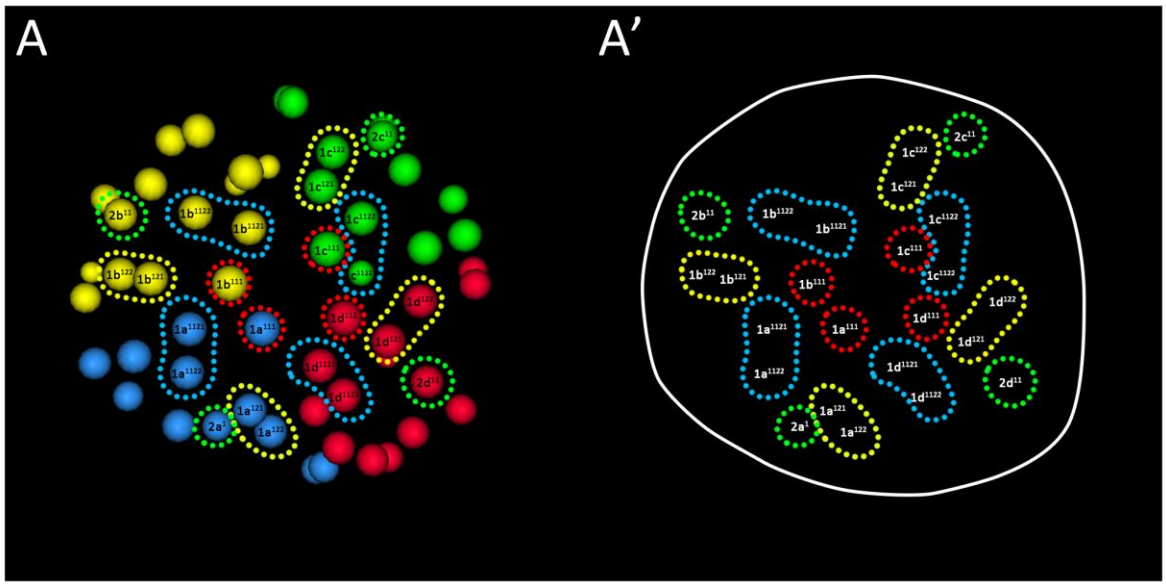


Figure A. 1 Apical cell mosaic in 3d reconstructed *M. crozieri* embryo based on nuclei information. Shown are apical rosette cells ($1q^{111}$), peripheral rosette cells ($1q^{112}$), ““molluscan cross”” cells ($1q^{121}/^{122}$) and tips of the ““molluscan cross”” cells ($2q^{11}$). Individual cells in *M. crozieri* have been identified by cell lineage tracing and different colors indicate quadrant affiliation (blue is for A quadrant, yellow is for B quadrant, green is for C quadrant and red is for D quadrant). The dotes lines indicate cell forming the apical cell mosaic: Red dotted cells represent the apical cell mosaic ($1q^{111}$), yellow dotted cells the “molluscan cross” cells ($1q^{121}/1q^{122}$), blue dotted cells the “annelid cross” cells ($1q^{112}$) and the green cells the tips of the “molluscan cross” cells ($2q^{11}$).

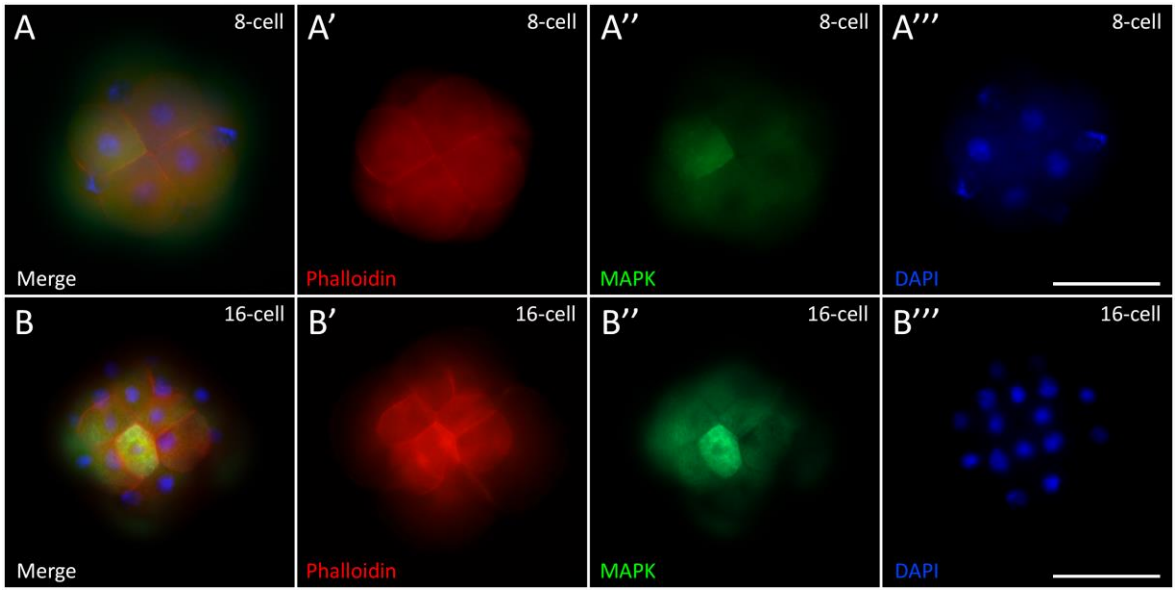


Figure A. 2 – Immunohistochemistry against MAPK diphosphorylated ERK-1/2 (Sigma) in two *M. crozieri* embryos. (A) Very weak, asymmetric MAPK signal was observed in one of the micromeres at the 8-cell stage (B) Slightly stronger signal of MAPK activity in one of the vegetal cross furrow micromeres ($1q^1$) at the 16-cell stage. These observations are preliminary and therefore need to be reinvestigated in more detail in *M. crozieri* embryos.

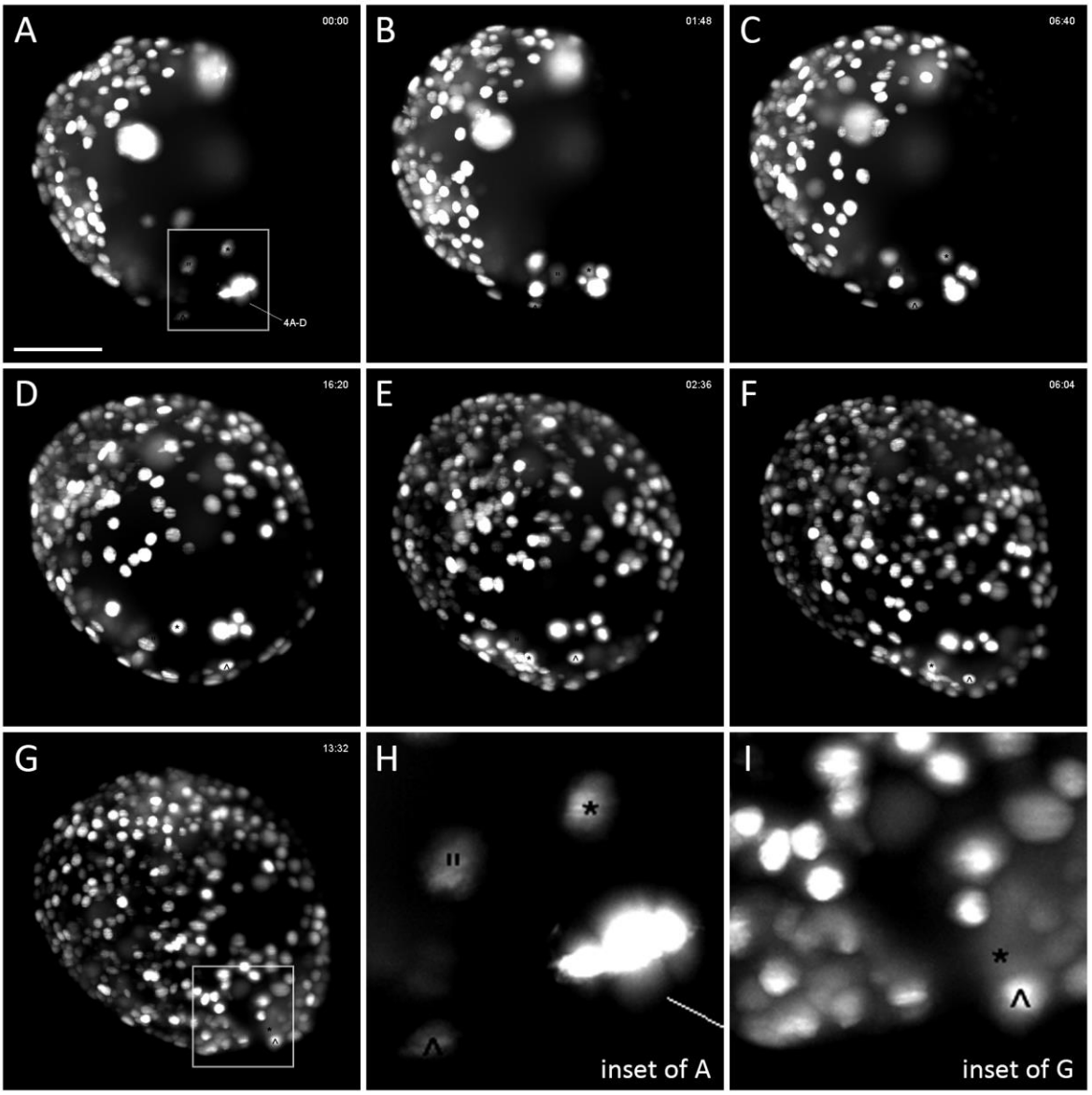


Figure A. 3 – Vegetal view of a gastrulating *M. crozieri* embryo, where putative descendants of $4d^2$ have been identified and marked (depicted here with three different symbols; see A and its inset H) and then traced for thirteen hours (B-G).The cell marked with an asterisk (and potentially also the cell indicated with ">") contacts macromeres 4Q (depicted in C), then seemingly loses contact again (D-F). In I, the final position of two of the three cells is shown at a location where first signs of invagination seemingly occur. Scale bar is 50 µm.

**ADDITIONAL TABLES**

Table A. 1 - List of OpenSPIM parts

| **OpenSPIM parts** | | |
|---|---|---|
| **LASER2000** | | |
| **ref** | **part** | **qty** |
| Stradus VersaLase™ | VersaLase 488/561 | 1 |
| n.a. | Heat sink (special modification) | 1 |
| **Pieter Fourie Design and Engineering CC** | | |
| ref | part | qty |
| 2 | RC1 vertical slit stilt | 2 |
| 3 | RC1 Ø1/2" lens stilt | 11 |
| 8 | Metal objective holder ring | 3 |
| 9 | Detection axis holder, base | 1 |
| 10 | Detection axis holder, top | 1 |
| 11 | Infinity space tube | 1 |
| 12 | Ø1"/Ø25.4 mm microscopy fluorescence emission filter holder, base | 2 |
| 13 | Ø1"/Ø25.4 mm microscopy fluorescence emission filter holder, top | 2 |
| 18 | RAIL CARRIER 15.4 mm, MOD ONLY | 8 |
| 23 | Acrylic sample chamber T, OLYMPUS | 1 |
| 24 | Metal chamber holder T, OLYMPUS | 1 |
| 25 | INSERT FOR RAIL CARRIER 15.4 mm (RC1 MODIFIED) | 8 |
| 27 | RC1 MOD, Ø1/2" lens stilt | 2 |
| 37 | RC1 Iris stilt | 2 |
| 38 | RC1 Ø1/2" mirror stilt | 5 |
| **AHF Fluorescent filters** | | |
| **ref** | **part** | **qty** |
| F72-866 | 446/523/600/677 HC Quadband Filter (Emission Filter) | 1 |
| F59-486 | Dual Line Laser Clean-up ZET 488/561 | 1 |
| **Picard Industries** | | |
| **ref** | **part** | **qty** |
| USB-4D-STAGE | 4D stage | 1 |
| **Thorlabs** | | |
| **ref** | **part** | **qty** |

| | | |
|---|---|---|
| DG05-1500-H1-MD | Ø1/2" SM05-Mounted Frosted Glass Alignment Disk w/Ø1 mm Hole | 2 |
| NE20A-A | Ø25 mm AR-Coated Absorptive Neutral Density Filter, SM1-Threaded Mount, 350-700 nm, OD: 2.0 | 2 |
| TRF90/M | 90° Flip Mount for Ø1" Filters and Optics, Metric | 5 |
| VA100/M | Adjustable Mechanical Slit, Metric | 2 |
| LMR05/M | Lens Mount for Ø1/2" Optics, One Retaining Ring Included, M4 Tap | 10 |
| KM05/M | Kinematic Mount for Ø12.7 mm Optics, Metric | 5 |
| GM100/M | Ø25.4 mm Gimbal Mirror Mount, Metric, One Retaining Ring Included | 2 |
| RSP1X15/M | Metric Rotation Mount, 360° Continuous or 15° Indexed Rotation | 2 |
| BB1-E02 | Ø1" Broadband Dielectric Mirror, 400-750 nm | 2 |
| BB05-E02 | Ø1/2" Broadband Dielectric Mirror, 400-750 nm | 5 |
| AC127-050-A-ML | f=50 mm, Ø1/2" Achromatic Doublet, SM05-Threaded Mount, ARC: 400-700 nm | 2 |
| AC127-025-A-ML | f=25 mm, Ø1/2" Achromatic Doublet, SM05-Threaded Mount, ARC: 400-700 nm | 2 |
| AC127-019-A-ML | f=19 mm, Ø1/2" Achromatic Doublet, SM05-Threaded Mount, ARC: 400-700 nm | 2 |
| AC127-075-A-ML | f=75 mm, Ø1/2" Achromatic Doublet, SM05-Threaded Mount, ARC: 400-700 nm | 2 |
| ACY254-050-A | f = 50 mm, Ø1" Cylindrical Achromat, AR Coating: 350 - 700 nm | 2 |
| RC1 | Rail Carrier, 1" x 1", 1/4" (M6) Counterbored Mounting Hole | 24 |
| LMR1/M | Lens Mount for Ø1" Optics, One Retaining Ring Included, M4 Tap | 2 |
| SM1D12D | Ring-Activated SM1 Iris Diaphragm | 2 |
| MB6090/M | Aluminum Breadboard, 600 mm x 900 mm x 12.7 mm, M6 Taps | 1 |
| AV2/M | Sorbothane Feet, M6 Thread, 20 - 32 kg (44 - 70.4 lb) Load, 4 Pieces | 3 |
| RLA300/M | Dovetail Optical Rail, 300 mm, Metric | 3 |
| RLA150/M | Dovetail Optical Rail, 150 mm, Metric | 5 |
| HW-KIT1/M | M4 Cap Screw and Hardware Kit | 2 |
| HW-KIT2/M | M6 Cap Screw and Hardware Kit | 1 |
| SPW602 | SM1 Spanner Wrench, Graduated, Length = 3.88" | 1 |
| BS004 | 50:50 Non-Polarizing Beamsplitter Cube, 400 - 700 nm, 1/2" | 1 |
| BS127CAM | 12.7 mm (0.50") Beamsplitter Cube Adapter for Compact 30 mm Cage Cube | 1 |
| CM1-4ER/M | Compact Clamping 4-Port Prism/Mirror 30 mm Cage Cube, M4 Tap | 1 |
| CL3/M | Compact Variable Height Clamp, M6 Tapped | 3 |
| PH30/M | Post Holder with Spring-Loaded Hex-Locking Thumbscrew, L = 30 mm | 1 |
| TR40/M | Ø12.7 mm x 40 mm Stainless Steel Optical Post, M4 Stud, M6-Tapped Hole | 1 |
| **Olympus** | | |
| objectives | | |
| **ref** | **part** | **qty** |
| N2667500 | UMPLFLN10XW | 2 |

| | | |
|---|---|---|
| N2667700 | LUMPLFLN40XW | 1 |
| **video camera mounts & adapters** | | |
| U-TLU | single port tube with lens | 1 |
| U-TV1x | video camera adapter (projection lens) | 1 |
| U-CMAD3 | video camera mount adapter | 1 |
| **www.esimagingsolutions.com** | | |
| Controller Box | ESio TTL Controller | |
| Andor | | |
| Camera | Zyla 5.5 3 Tap ex-demo model | |
| HP | | |
| **ref** | | **qty** |
| HP Z230 Workstation | Acquisition computer | 1 |
| HP Z820 Workstation | Processing computer | 1 |
| **Misco.co.uk** | | |
| **ref** | **part** | **qty** |
| LN47340 | Drobo 5D 5 Bays DAS Thunderbold x2 (10Gbs x2) | 1 |
| LN46168 | Red WD30EFRX 3TB HDD | 5 |

Table A. 2 - Acquisition and processing computer information

| |
|---|
| Product: HP Z820 Workstation |
| Processor: 2x Xeon E5-2630 v2 2.60Ghz |
| Drives: 1x 256GB SSD; 3x 3 TB Hard drives |
| Graphics: 2x Nvidia Quadro K4000 graphic cards |
| Memory: 128GB RAM |